Sirindhorn International Institute of Technology
Thammasat University

Thesis BF-PhD-2007-01

FILLING ABILITY PREDICTION MODEL AND USE OF INDUSTRIAL WASTES FOR SELF-COMPACTING CONCRETE

Ratchayut Kasemchaisiri

FILLING ABILITY PREDICTION MODEL AND USE OF INDUSTRIAL WASTES FOR SELF-COMPACTING CONCRETE

A Thesis Presented

by

Ratchayut Kasemchaisiri

Doctor of Philosophy
Building Facilities Engineering Program
Sirindhorn International Institute of Technology
Thammasat University
October 2007

FILLING ABILITY PREDICTION MODEL AND USE OF INDUSTRIAL WASTES FOR SELF-COMPACTING CONCRETE

A Thesis Presented

By

Ratchayut Kasemchaisiri

Submitted to

Sirindhorn International Institute of Technology

Thammasat University

In partial fulfillment of the requirement for the degree of

DOCTOR OF PHILOSOPHY IN ENGINEERING

Approved as to style and content by the Thesis Committee:

Chair and Advisor

_____

Prof. Somnuk Tangtermsirikul, D.Eng.

Co-Advisor

_____

Assoc. Prof. Amorn Pimammas, Ph.D.

Member

_____

Assoc. Prof. Krishna Murari Neaupane, D.Eng.

Member

_____

Assoc. Prof. Boonchai Satitmannaitham, D.Eng.

October 2007

Acknowledgement

The author wishes to express his gratitude and sincere appreciation to his advisor, Prof. Dr. Somnuk Tangtermsirikul, for his invaluable guidance, patience and encouragement throughout the duration of this study. His indefatigable and strong intention is mostly appreciated. The author also truly thanks Mr. Annop Tekajarin, Managing Director of the Concrete Products and Aggregate Co., Ltd. (CPAC) for offering the opportunity to pursue his doctoral degree at Sirindhorn International Institute of Technology (SIIT), Thammasat University and would like to acknowledge the research fund supported by the Metal and Material Technology Center (MTEC), National Science and Technology Development Agency (NSTDA), Thailand.

Sincere appreciation and gratitude are contributed to Assoc. Prof. Dr. Amorn Pimanmas, Assoc. Prof. Dr. Krishna Murari Neaupane, and Assoc. Prof. Dr. Boonchai Satitmannaitham for devoting their valuable time to serve as members of the thesis committee. A special thank is conveyed to Prof. Dr. Yin-Wen Chan of National Taiwan University for serving as an external examiner for this thesis.

Grateful acknowledgements are made to Dr. Pitisan Krammart, Dr. Taweechai Sumranwanich and Dr. Jittbodee Khunthongkeaw, former doctoral students of SIIT, and to Mr. Kulanan Thumasujarit, a master degree's graduate of SIIT, and to Mr. Sarawuth Charoensirisatien, a former colleague at CPAC, for their numerous information and suggestions for completing his thesis.

Special thanks are given to all secretaries of the School of Civil Engineering and Technology, Sirindhorn International Institute of Technology and all colleagues at CPAC for their kind services and supports throughout his study.

Finally, the author sincerely dedicates this work to his beloved wife and parents for their tenderness and encouragement during his study and best support in all of his life.

Abstract

The models for predicting three functional requirements of filling ability of self-compacting concrete (SCC) i.e. deformability, segregation and passing ability through narrow spaces were proposed. Deformability was defined to include deformation capacity indicated by slump flow and velocity of deformation measured by 50-cm slump flow time (T_{50}). Models for predicting slump flow and T_{50} were developed based on the concepts of free water, water retainability of solid particles, and inter-particle forces in the concrete. It was found that slump flow and T_{50} varied mainly with free water content and were also affected by volume ratio of paste to void of compacted aggregate phase (γ), water retainability of solid particles, and efficiency and dosage of superplasticizer (SP). The dispersion effect of SP was considered to reduce water retainability of powders as well as friction and cohesion among solid particles. Since static segregation has relationship with bleeding, a model for predicting bleeding capacity which was formulated as a function of free water content, effective surface area of solid particles, and average degree of reactions of binders was adopted. It was found that the increases of w/b and γ increased bleeding due to the larger free water amount. Bleeding of the mixtures with naphthalene and melamine based SPs increased with the increase of water reducing efficiency when all other mix proportion parameters were kept constant. However, polycarboxylate based SP showed lower bleeding though having higher water reducing efficiency than the others. The bleeding capacity of 0 % was specified as the minimum requirement for SCC to avoid static segregation. A model for predicting volume of aggregate blocking through bridging at narrow openings was extended from the previously proposed one. The parameters considered in the previous model are size distribution and volumetric ratio of aggregates, and clear spacing and size of the reinforcements. The effects of aggregate shape and viscosity of the concrete were introduced into the model in this study. It was observed that the maximum L-box passing ability and width of the optimum range of T_{50} for achieving the highest passing ability were smaller in cases of higher irregularity and larger volume of aggregates. The verification tests confirmed that the proposed models could be used to predict slump flow, T_{50} and bleeding capacity with satisfactory accuracies. However, the accuracy of model for predicting blocking conditions of SCC and the prediction of bleeding of SCC using polycarboxylate based SP should be further verified.

This study is also aimed to investigate the effects on properties of SCC of bottom ash and very fine sand as partial replacement of normal fine aggregate. When using bottom ash in concrete, water retainability is more practical for being used in mix proportioning than water absorption of the aggregate. A test method for determining water retainability was therefore proposed. Test results of SCC mixtures with bottom ash show that slump flow and L-box passing ability reduced, while T_{50} increased with the increase of bottom ash contents. The use of bottom ash resulted in the reduction of compressive and splitting tensile strengths and caused the increase of porosity. However, these properties were improved in long term by pore refinement due to pozzolanic reaction when 10 % bottom ash content was used. Chloride penetration, carbonation depth, shrinkage in drying environment of the bottom ash mixtures except for the mixture with 10 % bottom ash were larger than those of the control SCC, mainly due to higher porosity. On the other hand, the resistance to sodium sulfate was enhanced with the increase of bottom ash content. It was found that at 10 % very fine sand content, slump flow and L-box passing ability were slightly higher than that of the control SCC due to the compatibility between void content and specific surface area of aggregates and reduced with the increase of very fine sand content when very fine sand content were over 10 %. The increase of very fine sand content increased T_{50} due to the higher effective surface area of the aggregates. As a result, it can be concluded that the optimum replacements for the tested bottom ash and very fine sand are about 10 % by weight of total fine aggregate.

Table of Contents

List of Figures

List of Tables

List of Symbols and Notations

a, b	Constants encountering different unit and method of consistency measurement.
A, B	Weight of oven-dry aggregate sample and weight of the sample after test, respectively (g)
$\alpha_{ave}(t_o)$	Average degree of reaction at 30 min after mixing (%)
$\alpha_{C_3S}(t)$	Degree of hydration of C_3S without replacement of fly ash (%)
$\alpha_{C_3S,poz}(t)$	Degree of hydration of C_3S with replacement of fly ash (%)
α_{FTS}	Slope of flow table spread vs. free water content curve (mm/kg/m^3 of mortar)
α_{SF}	Secant slope of slump flow vs. free water content curve (cm/kg/m^3 of concrete)
α_{SL}	Slope of slump value vs. free water content curve (cm/kg/m^3 of concrete)
$\alpha_{hy}(t)$	Average degree of hydration reaction of paste at the considered age (%)
$\alpha_k(t)$	Degree of hydration of each oxide compound in cement at the considered age (%)
$\alpha_{poz}(t)$	Degree of pozzolanic reaction of fly ash at the considered age (%)
$\alpha_{poz}(365)$	Degree of pozzolanic reaction of fly ash at 365 days (%)
$\alpha_{react}(t)$	Average degree of reactions (including hydration and pozzolanic reaction) (%)
α_{VB}	Slope of Vebe time vs. free water content curve (sec/kg/m^3 of concrete)
α_x	Slope of deformation of fresh concrete or mortar vs. free water content curve
BR(t)	Bleeding rate of concrete at the considered time (cc/min)
BV(t)	Bleeding volume of the concrete at the considered time (ASTM C232 Method A: Sample consolidated by tamping) (cc)
$BV(t_o)$	Initial bleeding volume of concrete (cc)
BV_T	Bleeding capacity of concrete with water reducing admixture (cc)
BV_{To}	Bleeding capacity of the mixture without water reducing admixture (cc)
β_{agg}'	Surface water retainability coefficient (excluding absorption) of total aggregates (g/g of SSD aggregate)
β_g'	Surface water retainability coefficients (excluding absorption) of coarse aggregates (g/g of SSD aggregate)
β_s'	Surface water retainability coefficient of fine aggregate (g/g of SSD aggregate)
$\beta_c(t_o)$	Water retainability coefficient of cement at 30 min after mixing (g/g of dried weight)
$\beta_f(t_o)$	Water retainability coefficient of fly ash at 30 min after mixing (g/g of dried weight)
β_p	Water retainability coefficient of powder without application of water reducing admixture (g/g of dried weight)
β_{pi}	Water retainability coefficient of powder material type i (g/g of dried weight)
β_p'	Water retainability coefficient of powders with water reducing admixture
c	Clear spacing of the reinforcements (mm)
$\%CaO_c$	Calcium oxide content in cement (% by weight)
$\%CaO_f$	Calcium oxide content in fly ash (% by weight)
CaO_{eff}	Effective unit calcium oxide content in paste (kg/m^3)
CVC	Conventional concrete

D_{af}	Three-quarter dimension of each aggregate fraction (mm)
D_{av}	Average diameter of the aggregate particles (cm)
D_{ca}	Ratio between reinforcement clear spacing and three-quarter dimension of each aggregate fraction
D_{max}	Maximum size of aggregate (mm)
D_i	Average dimension between the upper sieve and the sieve i on which aggregate particles are retained (cm)
Δ_m	Difference of moisture content of the tested aggregate (%)
F	Filling coefficient
F_f	Fineness of fly ash (cm^2/g)
FTS	Flow table spread of mortar (mm)
η_a	Effective contact area ratio of aggregate
η_p	Effective contact area ratio of powder
Φ	Reinforcement diameter (mm)
ϕ_{bvt}	Bleeding capacity factor due to the application of water reducing admixtures (excluding polycarboxylate based superplasticizer)
ϕ_{rb}	Reduction factor for water retainability coefficient of powders due to the application of water reducing admixture
ϕ_{dps}	Dispersion factor due to the application of water reducing admixture for modifying the slope of consistency vs. free water content of fresh concrete or mortar, encountering different unit and method of consistency measurement
ϕ_{rn}	Reduction factor for the effective surface area of powder materials due to the application of water reducing admixture
ϕ_{vis}	Viscosity factor for the aggregate blocking volume.
φ	Dosage of water reducing admixture (% by weight of powder)
φ'	Water reducing efficiency of water reducing admixture
ε_f	Effectiveness of calcium oxide in fly ash
ε	Void content in the loose state of a single-size group of the solid particles
ζ_{tTc}	Time and temperature factor for the specific surface area of cement
ζ_{tTf}	Time and temperature factor for the specific surface area of fly ash
ζ_{tTp}	Time and temperature factor for the specific surface of powder materials
G_b	Weight ratio of coarse aggregate to total concrete of the bottom concrete portion (%)
G_t	Weight ratio of coarse aggregate to total concrete of the top concrete portion (%)
γ	Ratio of volume of paste to volume of voids in the compacted aggregate phase
γ'	Modified ratio of volume of paste to volume of voids in the compacted aggregate phase due to the use of a few of very fine sand to replace fine aggregates
γ_o	Ratio of volume of paste to volume of voids in the compacted aggregate phase without very fine sand
γ_{vfs}	Ratio of additional volume of paste to volume of voids in the compacted aggregate phase due to the use of a few percent of very fine sand to replace fine aggregates.
k	Oxide compound of cement (C_3A, C_4AF, C_3S, C_2S).
K	Ratio between reinforcement diameter and maximum size of aggregate.
L	Lubrification coefficient
LOI	Loss on ignition (%)
m_i	Moisture content of aggregate (%)

m_k	Mass of each mineral compound of cement per cubic meter of cement paste at any water to binder ratio (kg/m^3)
m_t	Moisture content of the top portion of the tested porous fine aggregate sample (%)
m_b	Moisture content of the bottom portion of the tested porous fine aggregate sample (%)
M_i	Weight percentage of aggregate retained on the corresponding sieve of the aggregate size group i (%)
M_i	Upper sieve dimension of aggregate group i (mm)
M_{i-1}	Lower sieve dimension of aggregate group i (mm)
n	Total number of types of powder materials used in the concrete
n	Number of aggregate size groups
n_a	Volume ratio of total aggregates to total concrete
n_{ai}	Volume ratio of aggregate group i to total concrete.
n_{abi}	Blocking volume ratio of aggregate group i to total concrete.
n_{abi}'	Blocking volume ratio of aggregate group i with the effects of particle shape of the coarse aggregate and viscosity of the mixture
N_{ga}	Volume ratio of coarse aggregate to total aggregates in the concrete (m^3 of concrete)
ρ	Specific gravity of the aggregate
ρ_p	Specific gravity of powder
ρ_w	Specific gravity of water
r	Replacement ratio by weight of powder to total powders
r	Replacement ratio of the lubricating powder in the total powder materials
%rFA	Replacement percentage of fly ash in total binders, % by weight
R	Specific surface area ratio of filling powder to cement
R′	Normalized ratio of specific surface area of filling powder to surface area of cement
S_o	Specific surface area of aggregate on spherical shape basis (cm^2/kg)
S_{agg}	Specific surface area of aggregate (cm^2/kg)
S_c	Specific surface area of cement (cm^2/g)
S_p	Specific surface area of filling powder (cm^2/g)
S_{eff}	Effective surface area solid particles in the concrete without the application of water reducing admixture (cm^2/m^3 of concrete)
S_{eff}'	Effective surface area of solid particles in the concrete with the application of water reducing admixture (cm^2/m^3 of concrete)
$S_{eff}'(t_o)$	Effective surface area of solid particles with the application of water reducing admixture at 30 min after mixing (cm^2/m^3 of concrete)
SCC	Self-compacting concrete
SF	Slump flow of SCC (cm)
SF_{woa}	Slump flow of SCC mixture without water reducing admixture (cm)
SF_{wa}	Slump flow of SCC mixture with water reducing admixture (cm)
S_g	Specific surface area of coarse aggregate (cm^2/kg)
S_s	Specific surface area of fine aggregate (cm^2/kg)
S_{so}	Specific surface area of the assumed spherical fine aggregate (cm^2/g)
S_{go}	Specific surface area of the assumed spherical coarse aggregate (cm^2/g)
S_G	Difference of coarse aggregate weight ratio to total concrete between the top and the bottom concrete portions (%)
SiO_2	Silicon dioxide content in paste (kg/m^3)
SiO_{2c}	Silicon dioxide content in cement (% by weight)

SiO_{2f}	Silicon dioxide content in fly ash (% by weight)
SL	Slump value of fresh conventional concrete (cm)
SP	Superplasticizer
S_p	Specific surface area of powder (cm^2/kg)
S_{pi}	Specific surface area of powder material type i (cm^2/g)
S_p'	Specific surface area of binders with the effect of elapsed time and temperature (cm^2/g)
S_s	Specific surface area of fine aggregate (cm^2/g)
S_{ta}'	Effective surface area of aggregates in the concrete (cm^2/m^3 of concrete)
S_{ta}	Surface area of total aggregates in the concrete (cm^2/m^3 of concrete)
S_{tp}	Surface area of total powder materials in the concrete (cm^2/m^3 of concrete)
S_{tp}'	Effective surface area of powder materials in the concrete with application of water reducing admixture (cm^2/m^3 of concrete)
t_o	Starting time of bleeding (min)
t	Considered time (min)
t	Considered time (day)
t_s	Initial setting time of cement with the water reducing admixture
T_{50}	50-cm slump flow time (sec)
T	Environmental temperature (^oC)
T_c	Concrete temperature (^oC)
V_a	Volume of total aggregates in the concrete (m^3 of the mix)
V_{abi}	Blocking volume of aggregate group i (m^3 of the mix)
V_{ai}	Volume of aggregate group i in the concrete (m^3 of the mix)
V_{atmax}	Maximum total aggregate volume (m^3 of the mix)
VB	Vebe time of roller-compacted concrete (sec)
V_c	Volume of cement in the concrete (m^3 of the mix)
V_{fill}	Volume of the filling particles in the voids among cement (m^3 of the mix)
V_g	Volume of coarse aggregate in the concrete (m^3 of the mix)
V_p	Volume of other powder materials in the concrete (m^3 of the mix)
V_{paste}	Volume of paste in a unit volume of fresh concrete (m^3 of the mix)
V_s	Volume of fine aggregate in the concrete (m^3 of the mix)
V_t	Total volume of the concrete mixture (m^3)
V_{ta}	Total volume of aggregates (m^3/m^3 of concrete)
V_{tp}	Total volume of powders (m^3/m^3 of concrete)
V_{vfs}	Volume of very fine sand (m^3 of the mix)
$V_{vfs\text{-}fill}$	Volume of the filling particles of very fine sand in the voids among compacted aggregates (m^3 of the mix)
V_{void}	Volume of void in the densely compacted total aggregate phase (fine and coarse aggregate) in a unit bulk volume of the aggregate (m^3 of the mix)
V_w	Volume of water in the concrete (m^3 of the mix)
w_g'	Saturated surface-dried weight of coarse aggregate (kg/m^3 of concrete)
w_s'	Saturated surface-dried weight of fine aggregate (kg/m^3 of concrete)
w_{pi}	Absolutely dry weight of powder material type i (kg/m^3 of concrete)
w/b	Water to binder ratio
w/p	Water to powder ratio
W_{aa}	Additional free water due to filling effect of ultra-fine particles (kg/m^3 of concrete)
W_c	Cement content in paste (kg/m^3)
W_f	Fly ash content in paste (kg/m^3)
W_{fr}	Free water content of fresh concrete (kg/m^3 of concrete)

$W_{fr}(t_o)$	Free water content at 30 min after mixing (kg/ m^3 of concrete)
W_o	Minimum free water content required for initiating deformation (kg/m^3 of concrete)
W_{ra}'	Restricted water at the surface of aggregates (kg/m^3 of concrete)
W_{rp}	Water restricted by powder materials (kg/m^3 of concrete)
W_u	Unit water content of the mixture (kg/m^3 of concrete)
W_{wa}	Quantity of water required, to attain a flow diameter of 180$\pm$5 mm with 0.5% dosage of water reducing admixture
W_{woa}	Quantity of water required, to attain a flow diameter of 180$\pm$5 mm without water reducing admixture
WRA	Water reducing admixtures
Ω	Filling factor due to the use of very fine sand
X	Deformability measuring value of fresh concrete
ψ	Angularity factor
ψ_s	Angularity factors for the irregularity of the particles of fine aggregates
ψ_g	Angularity factors for the irregularity of the particles of coarse aggregate

Chapter 1

Introduction

1.1 General

Durability of concrete structures, a major problem of civil engineering, has become a common interest and seriously focused during the past several decades. To make durable concrete structures, sufficient compaction by skilled workers is one of the requirements. In the last few decades, self-compacting concrete that can be compacted into every corner of a formwork, purely by means of its own weight without the need of compaction has been studied. Self-compacting concrete was firstly developed by Okamura, Ozawa and Maekawa at the University of Tokyo in 1986 (Okamura, et al., 1993). As the concrete during casting is not subjected to any external energy input from vibrators, tampering or the similar actions, the concrete can be described as "self-compacting". A widely adopted acronym for Self-Compacting Concrete is SCC. The term "Self-Consolidating Concrete" is frequently used in North America. It is stated that SCC can be used in most applications where traditionally vibrated concrete is used. SCC is suitable for high performance, densely reinforced structures as well as for less demanding unreinforced applications for instance in backfill. SCC can be fiber reinforced and is equally applicable for in situ construction as well as in pre-casting (Skarendahl, 2000).

A major motivation for the development of self-compacting concrete was to solve the problem of low durability caused by inadequate homogeneity of the cast concrete (Okamura, H., et al., 1995). One of the main reasons for the difficulties of compaction relates to the trend of increased congestion of the reinforcement in many structures. Increasing structural performance has led to increased reinforcement volumes. Furthermore, there is a tendency to use smaller bar diameters to limit cracking. As a result, the quality assurance of concrete construction aims at the improvement of homogeneity of concrete, which is an important objective of the development of SCC for structures with congested reinforcement.

SCC has been proven for not only improved durability but also increased reliability of structures (Domone, 2000, and Tangtermsirikul, et al., 2000). Complete elimination of the compacting work through the use of self-compacting concrete increases speed and simultaneously reduces cost, which thus improves the productivity. Increased speed is not only important as a mean of reducing cost of placement but can also lead to shortening of the total time of construction. With fresh concrete requiring no external compaction, and having predictable filling ability, increased degree of automation and industrialization of the concrete construction process is possible. The use of SCC thus plays an important role in increasing the competitiveness of concrete construction through reducing cost and increasing performance (Skarendahl, 2000).

Moreover, the working environment loading is high in concrete construction. One of the most severe loads is from the vibration process causing the noise, either from handhold vibrators, or form surface vibrators. Elimination of vibrators is thus one of the goals toward desirable working environment. Improvement of the working condition

increases the well being of the workers, and at the same time reduces the society cost for health care. As a result, the reductions of noise and vibration are advantages for both the working environment of the construction workers as well as the disturbance for building site neighbors.

Additionally, there exist numerous situations when access of vibrators is difficult due to the formwork configuration or production process constraints for examples inclined components with double-sided formwork, confined and enclosed spaces and very high casting heights. One typical situation is such as repair of the bottom side of a horizontal slab or beam. The use of SCC improves the possibilities of solving these situations in a rational way.

1.2 Statement of Problem

Due to the above mentioned benefits, SCC is currently a potential concrete used in many countries. However, due to the relatively short history of SCC, efficient methods for mix proportioning are essential for promoting the use of SCC. A method, developed at the University of Tokyo, is the prototype method that has been extensively employed in the first period of development. This simple method assumes that SCC is generally supplied from ready-mixed concrete plants, in which the coarse and fine aggregate contents are fixed, so that good filling ability can be achieved by adjusting only the water to powder ratio and superplasticizer dosage (Okamura, et al., 1995). Some subsequent researchers have modified the method with the aims of producing more efficient mixes from a wider range of materials such as the methods of Delft University, University College London, and Ouchi et al. etc. (Domone, 2000).

Desirably, a good mix design method should cover a wide range of concrete performances and be applicable to various available materials. Based on several different approaches, a number of SCC mix design methods have been proposed with some inherent limitations, either in the materials or in the range of concrete performances. In addition, traditional mix design methods requires making a large number of trial mixing batches as the main process to choose suitable ingredients of concrete and determine their relative quantities and to check the calculated mix proportions for the required properties such as the workability, strength, and durability. For SCC, it is not possible to attain this purpose from such the traditional method of mix proportioning. A prediction model of concrete properties is adopted as a mean of minimizing the mix proportioning process by reducing the number of trial mixes. And it could be a useful approach to establish the rational mix design method.

Even though popularity of self-compacting concrete (SCC) in concrete construction has increased in many countries, its use is still limited in Thailand due to the main reason of its high cost. Industrial wastes and by-products have been introduced in Thai concrete industry to conserve natural resources and environment as well as to reduce the cost of concrete. As an example, fly ash, a by-product from thermal power plants, has been widely used in concrete as a pozzolanic material for replacing a part of cement due to its main benefits on workability and durability (Tangtermsirikul, 1998). The idea of using available industrial wastes and by products to replace natural aggregates is another alternative solution to obtain a reasonable concrete cost, since about 60 to 80 % of concrete volume is occupied by aggregates.

1.3 Objectives and Scope of the Study

Main objectives of this study are to develop models for predicting filling ability of self-compacting concrete and to provide basic information for using some available waste materials in SCC mixtures in order to promote more application of SCC in Thailand's construction.

To achieve self-compaction of fresh concrete, SCC has to be designed to have good filling ability that is defined as the ability to fill formwork and encapsulate reinforcing bars only through the self-weight with ensured homogeneity. It can be simply described by three functional requirements, including deformability, resistance to segregation, and passing ability. Hence, the models for predicting deformability, segregation and passing ability through narrow spaces are developed, which are considered as the useful tool for establishing a rational mix design method of SCC. The development scheme is illustrated as in Fig. 1.1. The model for predicting deformability is developed based on the concepts of free water content and inter-particle forces in the concrete. It includes prediction models for deformation capacity and for velocity of deformation. Segregation is considered to have relationship with bleeding, so a prediction model for bleeding is adopted in this study. Passing ability can be simulated by adopting a model for predicting aggregate blocking during SCC flow through narrow spaces. The parameters considered in the model are size distribution, volumetric ratio, shape and maximum size of aggregates, as well as the effect of viscosity of the concrete, clear spacing and size of the reinforcement. It is noted here that the proposed models are limited for self-compacting concrete without static segregation and containing no viscosity agents.

Moreover, the locally available materials shall be applied with the achievement of required performances and effective concrete cost for expanding the use of SCC in Thailand. Therefore, this study also focuses on the use of some industrial wastes in SCC. Effects of bottom ash and very fine sand on properties of SCC are thus studied to compare the properties of SCC mixed with either bottom ash or very-fine sand as partial replacement of fine aggregate with the properties of the control SCC made from river sand. Test methods for slump flow, 50-cm slump flow time and L-box passing ability are performed to assess the filling ability. Some properties of hardened concrete i.e. porosity, pore size distribution and compressive strength are investigated. To assess the durability, chloride penetration, carbonation depth, drying shrinkage, and expansion in sodium sulfate solution are also observed.

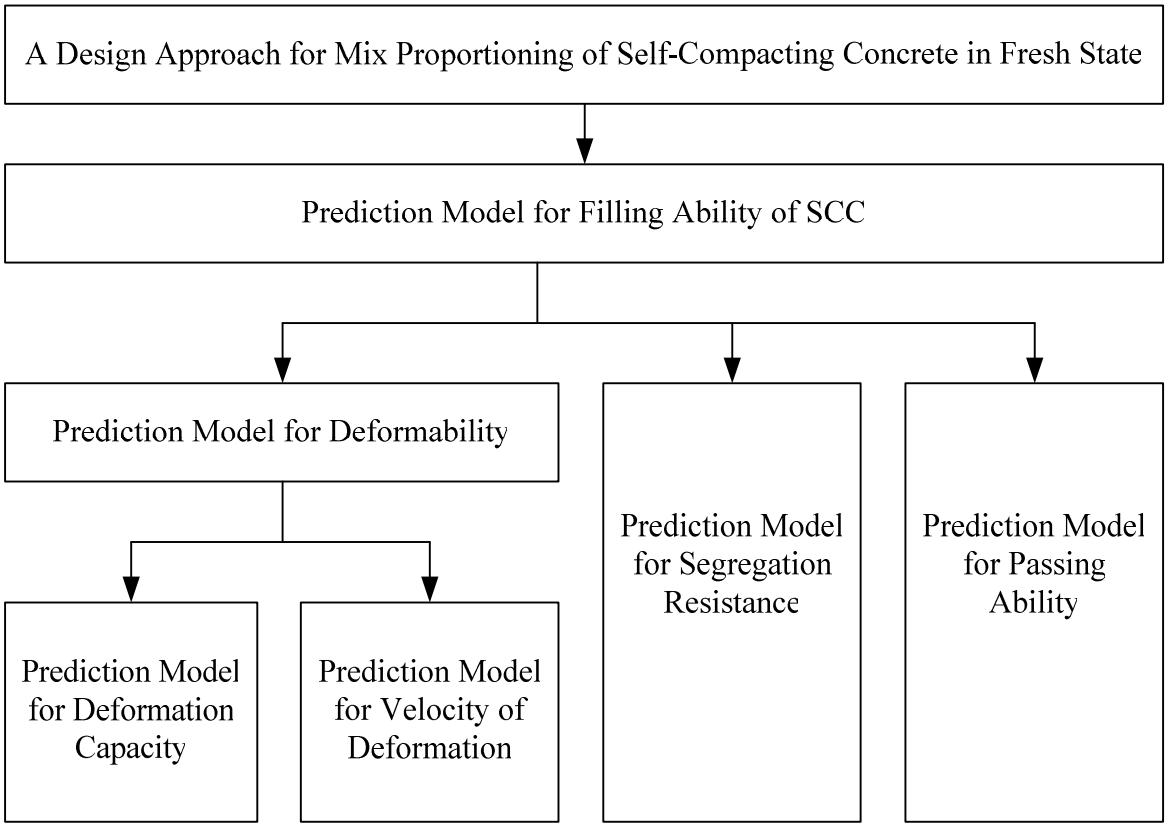

Fig 1.1 Diagrammatic illustration of a design approach for mix proportioning of SCC based on filling ability prediction models

Chapter 2

Theoretical Background and Literature Review

2.1 General

This study concentrates on the formulation of model for predicting filling ability and the application of bottom ash and very fine sand for self-compacting concrete. Many researchers have studied fresh properties of SCC and use of some industrial wastes in concrete, as well as proposed design approaches for mix proportioning of SCC. The followings are summaries of such studies.

2.2 Filling ability of SCC

According to the report of RILEM technical committee SCC-174, self-compaction of fresh concrete is achieved by designing the concrete to have suitable inherent filling ability that is defined as the ability to fill formwork and encapsulate reinforcing bars only through the self-weight of the concrete with required performances and uniform-quality. As a fresh state, filling ability can be characterized in relation to the functional requirements which are deformability, resistance to segregation, and passing ability (Tangtermsirikul, et al., 2000).

2.2.1 Deformability of SCC

Under its self-weight, self-compacting concrete must be able to deform or change its shape very well. The meaning of the deformability includes both the flow, in terms of how far from the discharge the concrete can flow, or deformation capacity, and the speed with which it flows, or called velocity of deformation. An ideal SCC should have as large as possible the deformation capacity and velocity of deformation. However, too large deformation capacity and velocity of deformation will result in segregation. So, to attain the preferred deformability, SCC should be designed to have proper values of deformation capacity and velocity of deformation. With the slump flow measurement, the deformation capacity can be evaluated as the final flow diameter of the concrete measured after the concrete has completely stopped deforming. By the same method, the velocity of deformation can be evaluated as the time the concrete takes to reach a certain deformation such as the flow diameter of 50 cm (Tangtermsirikul, et al., 1992).

2.2.2 Resistance to Segregation of SCC

Self-compacting concrete has to have enough deformability and at the same time enough resistance to segregation to perform its filling ability efficiently. Resistance to segregation means the ability of the particle suspension to maintain homogeneity throughout the mixing, transportation and casting process (Skarendahl, 2000). SCC should not have excessive segregation in neither static nor dynamic states: bleeding, segregation between paste and aggregate, and segregation of coarse aggregate leading to blocking. To

avoid the segregation between water and solid, it is essential to reduce the amount of movable water in the mixture.

2.2.3 Passing Ability of SCC

In cases where there are narrow openings or spaces in the formwork or where the reinforcement is congested, an extra requirement has to be fulfilled namely passing ability or the avoidance of blocking of coarse aggregates through bridging. So, passing ability is defined as the ability of the concrete to pass obstacles like narrow sections in formwork, closely space reinforcing bars etc. without getting blocked by interlocking of aggregate particles (Skarendahl, 2000). There must be a compatibility between the size and amount of large solid particles in the self-compacting concrete and the clear spacing between reinforcing bars and formwork openings that the concrete must flow through.

2.3 Researches on Deformability of SCC

Tangtermsirikul, et al. (1992) studied the velocity of deformation of SCC and proposed a method for evaluation of velocity of deformation by adopting the slump flow test. The velocity of deformation was defined as the average velocity of deformation measured from 40 cm to 60 cm of the concrete flow. It was found that the velocity of deformation decreased with the increase of amount of viscosity agent even though the amount of superplasticizer was increased to obtain mixtures with the maximum filling ability for each content of viscosity agent. In addition, the velocity of deformation decreased with the increase of time after mixing. There were a correlation between velocity of deformation of the concrete and viscosity of the corresponding mortar and a good linear correlation between the v50, which was defined as the secant velocity of deformation at slump flow of 50 cm and the average velocity of deformation. Therefore, the v50 was utilized as the simple parameter for evaluating velocity of deformation.

Ouchi, et al. (1996) investigated the effect of superplasticizer on the balance between flowability and viscosity of mortar in self-compacting concrete. From his experimental results, the ratio of funnel speed to flow area of mortar with a fixed amount of superplasticizer was found to be almost constant, independent of the water-powder ratio. A higher amount of superplasticizer resulted in a lower ratio of funnel speed to flow area. The ratio was proposed as an index for the effect of superplasticizer on mortar flowability and viscosity from the viewpoint of achieving self-compactability. This index was convenient for evaluating the amount of superplasticizer for proper flowability and viscosity of mortar using only one set of experimental results. The relationship between superplasticizer amount and its effect was found to differ depending on the type of powder or superplasticizer. The difference could be indicated quantitatively by the proposed index.

Domone, et al. (1999) focused on properties of mortar for SCC. The results reported that many of the important parameters that influence the performance of SCC could be assessed by test on mortars, on which the workability and workability retention depends on a combination of factors, including the powder composition and the dosage and type of superplasticizer. In addition, it was found that ternary blends of powder had potentially very useful properties in this respect. They also reported that the two most commonly used single point tests, the spread and V-funnel flow time, had been shown to be closely related to the Bingham constants of yield stress and plastic viscosity respectively, and therefore the

use of either of these individually did not give a satisfactory indication of the mortar's performance.

Saak, et al. (1999) investigated the influence of various admixtures on the rheology of cement paste for being used in self-compacting concrete. It was reported that the viscosity of cement paste was dependent on the shear history of the sample. The results showed that at the same yield stress, the melamine-based superplasticizer had a lower equilibrium viscosity than the naphthalene superplasticizer. Also, the yield stress and equilibrium viscosity increased significantly for paste containing 30 % silica fume by volume as the superplasticizer dosage was decreased. Yield stress and viscosity increased in a similar manner due to small additions of surface coated cellulose powder. At zero yield stress, replacement of cement by 30 % silica fume by volume led to a 36 % reduction in equilibrium viscosity compared to cement paste containing only superplasticizer, which could be attributed to an increase in the solid packing density and spherical morphology of the silica fume particles. Additionally, at the same yield stress, a lower viscosity was possible through adjustment of superplasticizer dosage or cellulose content.

Yahia, et al. (1999) investigated an effect of rheological parameters on self-compactability of concrete containing various mineral admixtures. It was found that when incorporated at a fixed coarse aggregate volume of 30 %, by unit volume of concrete, in mixtures made with 45 % sand by volume of mortar, and prepared with a w/c ranging between 0.83 and 1.03, by volume, high deformability was achieved. Also, the fresh properties of concrete were in good agreement with those of the matrix of mortar. On the other hand, rheological properties of the matrix of mortar, sampled form concrete mixer before adding coarse aggregate, were lower than those obtained with original mortar mixed with Hobart mixer. Moreover, self-compactability of concrete was roughly related to the couple value of yield stress and plastic viscosity of the matrix of mortar. Low yield stress and optimum plastic viscosity were required to achieve accurate deformability. And suitable range values for rheological properties of the matrix of mortar that could be used to proportion self-compacting concrete were established for a given range of materials and mixture proportioning. Additionally, fly ash could secure higher viscosity and lower yield stress than limestone powder for mixtures prepared with a w/c ranging between 0.83 and 1.03, by volume.

Golaszewski, et al. (2002) presented the influence of chemically different superplasticizers on the rheological properties of standard mortars. The rheological parameters of mortars, yield value and plastic viscosity, were determined using rotational rheometer. The influence of the performance of superplasticizers was investigated taking into account following factors: chemical base of superplasticizers (i.e. naphthalene sulfonic acid, polycarboxylate acid, policarboxylate ester), superplasticizer dosage, w/c ratio, cement type, cement physical and chemical properties and temperature. The results presented that by testing rheological parameters of mortars with rotational viscometer, it was possible to precisely determine the performance of superplasticizers.

Wallevik (2006) concluded that a relationship between the yield stress and slump depended on the concrete mixture proportions. More precisely, a particular trend line between the yield stress and slump seemed to depend on volume fraction of matrix used in the concrete. The study showed a low correlation between the slump and plastic viscosity.

Felekoğlu, et al. (2006) studied the selection of amount and type of powders from the viewpoint of fresh state rheology. The influence of powder materials on self-compactability, viscosity, and strength were compared with a properly designed set of test methods (mini-slump, V-funnel tests, viscosity measurements, and compressive strength tests). It may be advised that, for each cement–powder–plasticizer mixture, a series of test methods could be used to determine the optimum content and type of materials for a specified workability.

Sahmaran, et al. (2006) showed that the use of mineral admixtures such as fly ash improved the workability properties of SCC. Replacing part of the binder with fly ash not only caused a reduction in the dosage of cement and superplasticizer. Properties in the fresh state of SCC with high volumes of high-lime and low-lime fly ash replacements were investigated. The fresh properties of the concretes were observed through slump flow and diameter, V-funnel time, L-box, GTM sieve stability, setting times and the rheological parameters relative yield stress and relative plastic viscosity. It was observed that the geometry and surface characteristics of the fly ash affected the workability properties of SCC mixtures. As a result, it was possible to produce SCC incorporating fly ash replacement volumes of up to 70 % with sufficient strength.

2.4 Researches on Bleeding and Segregation of Fresh Concrete

Soshiroda (1981) studied the segregation tendency of concrete containing a high-range water-reducing admixture and its effects on the homogeneity of the concrete after hardening. Segregation during placing was investigated by means of a modified remolding test. Segregation during and after placing, including bleeding, was investigated by examining the variation of internal structure of hardened concrete caused by segregation and bleeding. The anisotropy in the direction of casting and the heterogeneity relative to the depth were examined as the variation on 150-mm cube specimens and 150- by 150- by 450-mm columns, respectively. For the former, the tensile anisotropies were determined by the splitting test changing the loading direction. For the latter, splitting tensile strengths, unit weights and coefficients of water absorption relative to the depth as well as coarse aggregate contents of both the top and the bottom portions were determined. There was no great difference in the resistance to segregation during placing and the effects of segregation on the homogeneity after hardening between the concrete containing the admixture and the conventional air entrained concrete without the admixture when slump, water to cement ratio and fine aggregate percentage are held constant. Excessive dosage of the high-range water-reducing admixture tended to promote segregation of fresh concrete and subsequently tended to increase the heterogeneity of hardened concrete with the depth.

Hoshino (1989) investigated the relationship between bleeding, coarse aggregate, and specimen height of concrete. The coarse aggregate in concrete had a slight effect on bleeding water. This was based on assumption that bleeding water was affected directly by the surface area of the particles and the surface area per unit weight of aggregate particles was far smaller than that of the cement and fine aggregate particles, the influence of the cement on the amount of bleeding was thus greater. It was found that, the amount of bleeding water decreased with the increase of the size of the coarse aggregate. The influence of the shape of coarse aggregate on the bleeding water was that irregular aggregate caused more seepage water to be retained within the concrete than spherical aggregate does, so lower bleeding was achieved.

Tangtermsirikul (1989) studied the influencing factors which are surface area of solid particles, water to cement ratio, air content on bleeding rate and bleeding capacity and found that the larger the total surface area of solid particles in the fresh concrete mixture was, the lower permeability of the fresh concrete mixture is. Therefore, smaller bleeding rate could be expected. For effect of water to cement ratio w/c, cement pastes with higher w/c ratio gave higher value of bleeding rate for cement pastes made from same cement and it could be expected that the cement paste with higher w/c ratio gave higher bleeding capacity than that with lower w/c ratio since cement paste with higher w/c ratio contains larger amount of water in the mixture. For effect of sample height, the higher sample gave rise to larger bleeding capacity.

Whiting, et al. (1992) reported that the effects of water reducers on bleeding depended on the chemical composition of the admixture. A reduction of bleeding could result in the difficulties for finishing the flat surfaces when rapid drying conditions were present. The effectiveness of water reducers on concrete was a function of their chemical composition, concrete temperature, cement composition and fineness, cement content, and the presence of other admixtures.

Nabil (1999) studied the effect of blended fly ash cement on the bleeding of fresh mortars. It was reported that when using a ground fly ash in mortar, the bleeding of fresh mortar depended on the original fineness of the fly ash and decreased significantly with an increase in the fineness of the fly ash.

Assaad, et al. (2004) proposed test methods to assess the resistance to segregation and surface settlement during the plastic stage of SCC. The methods included evaluating surface settlement, aggregate segregation, and monitoring in-place changes in electrical conductivity. The surface settlement test is appropriate to assess the stability over the dormant period. The column segregation test is useful for determining the distribution of coarse aggregate throughout a column of fresh concrete and can be adopted for testing SCC at the batching plant or at the job site. The segregation index from this test could be related to the apparent yield value g and torque plastic viscosity h determined using a concrete rheometer. SCC was found to possess a suitable segregation index of 2 to 4% when the g and h parameters ranged from 0.3 to 1.7 N.m and 17 to 30 N.m.s, respectively. An electrical conductivity test was shown to offer a more precise way to monitor the in-place stability of mortar taken from the SCC. Sensitive indexes deducted from the conductivity curves could help to interpret the overall stability of the system and provided relevant information on internal water migration and segregation of solid particles in the plastic system.

Fumoto (2004) studied an evaluation index for segregation resistance and the qualities of powder relating to the index. The indication was proposed as the ratio between coarse aggregate weight in concrete contained in the lower part of cylindrical vessel and that in upper part after tamping by a steel rod. This index more accurately expressed the segregation potential under construction. Plastic viscosity of mortar and volumetric percentage of coarse aggregate in concrete mainly influenced the index. The influence of fly ash, Blast-furnace slag powder, limestone powder, crushed stone powder, and recycled concrete powder on properties of a mortar was investigated. It was found that the flow of mortar mixed with powder having rough surface largely decreased with increasing plastic viscosity due to the increase of quantity of powder.

Safawi, et al. (2004) studied the effect of vibration on segregation tendency of high fluidity concrete. It was reported that the viscosity of concrete must be enhanced to balance the flowability of concrete and the coarse aggregate distribution at the same time. Concrete flowability and viscosity were quantified by the standard slump test and V-funnel test, respectively. Despite being flowable, the study concluded that concrete viscosity was an important parameter in determining the tendency for coarse aggregates to segregate. Large-sized coarse aggregates were affected more by the vibration process than the small-sized ones.

El-Chabib, et al. (2006) presented an extensive experimental program to evaluate the segregation potential of a wide range of SCC mixtures. A simple test method for quantitatively evaluating the segregation of SCC was proposed and its results were compared to that of other test methods in the literature. The large created experimental database was also used to train an artificial neural network (ANN) that was able to accurately predict the segregation resistance of new SCC mixtures unfamiliar to the model. ANN response in simulating the effect of basic mixture ingredients of SCC on its resistance to segregation were compared to those obtained using actual experimental results.

Thumasujarit (2006) conducted comprehensive experiments to clarify the mechanisms of bleeding of fly ash concrete. The mix proportion of concrete was designed based on variation of ratio of paste volume to void volume of aggregate phase, water to binder ratio, type and replacement percentage of fly ash and limestone powder, type and dosage of water reducing admixtures, height of specimen and concrete temperature in order to investigate the effect of these parameters on bleeding. Moreover, as the analytical parameters, the amount of free water, effective surface area of solid particles, average degree of reaction, and water retainability coefficient of powder materials were computed and investigated for their effects on bleeding. It was found that the increasing of replacement percentage of fly ash, water to binder ratio, ratio of paste volume to void volume, dosage of admixture caused increasing of bleeding. Fly ash with lower water retainability also caused increasing of bleeding.

2.5 Researches on Passing ability and Aggregate Blocking

Noguchi, et al. (1999) investigated the rheological approach for passing ability between reinforcing bars of SCC. It was found that when fresh concrete passed through narrow spaces, the reduction of relative excess paste thickness due to the increase of the volume fraction of aggregate increased the rheological constants. The behavior of fresh concrete passing through narrow spaces could be macroscopically interpreted as changes in its rheological properties. By using a box-shaped passing ability tester, the experimental equations determining volume fraction of aggregate in concrete were obtained as a function of the altered volume fraction of aggregate in concrete when passing through a space, ratio of relative clearance between reinforcing bars, and plastic viscosity.

Ouchi, et al. (1999) proposed a simple evaluation method for interaction between coarse aggregate and mortar particles in SCC. The V-funnel speed of mortar with coarse aggregate and that without coarse aggregate were compared. To avoid the blocking occurrence, glass bead with the diameter of 10 mm was adopted as the model coarse aggregate with the 20 % content in total volume of mortar. As a result, the index for the interaction was proposed as the ratio of the funnel speed of mortar with glass beads (R_{mb})

to that without glass beads (R_m). It was found that the index R_{mb}/R_m was constant on condition that the deformability or viscosity of mortar itself was in the range for achieving self-compactability of fresh concrete, as well as proposed evaluation method by examining the sand content in mortar to determine the self-compactability.

Petersson, et al. (1999) investigated the blocking of self-compacting concrete with different maximum aggregate size and use of viscosity agent instead of filler. The investigation showed that the L-box was sensitive to blocking. It also showed that the blocking was more severe when using more that 3 bars in the L-box, which concluded that the greatest influence was the number of bars. When using aggregate with smaller maximum sizes the blocking was more severe in the experiments compared to the calculations in the blocking model. This led to the recommendation to keep the amount of reinforcement constant (3 bars) and to use 1.4 times the gap to the wall. The relative concrete area constant should be constant e.g. gap/relative area = 0.21. With respects to concrete properties, reduction of filler by using a viscosity agent indicated that up to about 10 % of filler could be replaced. The investigation also showed that when using viscosity agent the workability by elapsed time decreased compared to mixes with only fillers. This is a difficulty when using viscosity agent for self-compacting concrete. Also, the use of viscosity agent thus gives better stability but can not replace the filler in the model. When blocking is not the main problem then the viscosity agent can be used with of without extra filler to keep the stability.

Tangtermsirikul, et al. (2002) studied on the optimum aggregate phase based on deformability and blocking criteria of SCC. It was reported that to attain the minimum paste volume of SCC mixture, the concept of maximum aggregate particle distance based on the void ratio-total surface area of the aggregate phase could be employed. Additionally, they also proposed the blocking criteria which related the aggregate blocking volume ratio to the ratio between reinforcement clear spacing and diameter of aggregate particle fraction and the ratio between reinforcement diameter and maximum size of aggregate particle, as well as coarse aggregate type. This was based on the facts that blocking was easier to occur when coarse aggregate content was larger, maximum size of coarse aggregate was larger, clear spacing of steel was smaller, size of steel was larger and aggregate shape was more angular. It was also evident that the proposed blocking criteria could be used to obtain SCC which had minimum paste and had no blocking.

McBride, et al. (2006) examined the effect of aggregate content and gradation on passing ability of SCC. The tested mixtures ranged over two uniform aggregate sizes, two aggregate contents, two different mixture design philosophies, and a well-graded aggregate mixture. Passing ability tests, slump flow tests, horizontal flow tests, and stereology tests were performed on these mixtures. Stereology is a statistical counting technique used primarily by natural scientists. Concrete researchers have used this to describe bubble size and distribution in concrete. A vertical flow box was developed by McBride to determine the passing ability of the various mixtures. Various bar spacing were tested. It was reported that two stereology parameters could be correlated to the minimum bar spacing that allowed SCC to pass. These parameters were the ratio of maximum aggregate size to mean aggregate free distance and the ratio of maximum aggregate size to mean aggregate random spacing.

2.6 Prediction Models for Workability

Kitticharoenkiat (1998) proposed a slump prediction model based on water retainability and free water concepts and modified the model proposed by Pongcorncharoen for predicting the workability of fresh concrete. The major parameters utilized for predicting the slump value of fresh concrete were the free water content (W_{fr}), ratio of paste volume to void content of aggregate phase (γ), surface area of aggregate phase (S_{agg}) and surface area of powder material (S_{pow}). The volume of free water was obtained by deducting the water retained in and on the surface of the powder materials and the aggregates from the unit water content of the concrete mix. It was confirmed that the slump of fresh concrete varied linearly with free water content (W_{fr}) in the mixture when the γ is constant. The verification of the model with the actual results obtained from various researchers showed that the model could be used to predict the slump of fresh concrete with satisfactory accuracy.

Khunthongkeaw (2001) modified the model proposed by Kitticharoenkiat (1998) for predicting workability of fresh concrete. It was found that the factors influencing the four analytical factors (viz. W_{fr}, γ, S_{agg} and S_{pow}) for predicting the workability of fresh concrete were not adequate to cover all physical mechanisms. The major additional physical mechanisms introduced into the model were the filling effect of ultra-fine particles, the lubrication ability of spherical powder particles, effect of porosity, shape and gradation of powder on water retainability of powder and environmental temperatures. The filling effect of the fillable powder releases the water trapped in the voids among cement particles and increases the free water content of the mixture. The amount of minimum free water required to initiate slump was considered as the result of inter-particular surface forces among solid particles in the mixtures and then formulated to have relationship with of the effective surface area of the solid particles in the mixture. Moreover, the lubricating effect of the spherical powder particles reduces the inter-particular friction amongst the larger particles and this reduces the amount of minimum free water required to initiate slump. It was confirmed that the slump of fresh concrete varied linearly with free water content in the mixture and non-linearly with the ratio of paste volume to void content of aggregate phase. He thus proposed a model for predicting workability of concrete and mortar with and without mineral and chemical admixture, in which the relationship between free water content in mixture and slump value was extended to relate free water content and other quantitative workability measuring methods, such as flow spread, slump flow, and Vebe time. It was found that flow spread and slump flow varied linearly with free water content, but Vebe time of roller-compacted concrete has non-linear relationship with free water content.

Wangchuk (2003) proposed the model for predicting initial slump of fresh concrete to consider the effect of water reducing admixtures and the slump loss of fresh concrete. The water reducing efficiency had been introduced as the indicator to categorize the water reducing effectiveness of water reducing admixtures. It was considered that the water reducing admixtures increased the slope of slump-free water content curves, reduced the water retainability coefficient of the powder materials and reduced the effective surface area of the powder materials. It is beneficial if the slump of concrete mixture at various times after mixing can be predicted so that the workability leading to uniformity of concrete can be achieved. It was found that with the elapse of time after mixing, the water retainability of the powder materials increased and this was considered to reduce the free water content in the mixture. It was also considered that the effective surface area of the

powder materials increased with time and caused the free water content required for initiating slump to increase.

Bui, et al. (2002) proposed a rheological model for SCC, developed based on the paste rheology criteria that include minimum apparent viscosity, minimum flow, and optimum flow-viscosity ratio. The rheology criteria of the cement paste matrix are related to the average aggregate diameter and aggregate spacing, which are influenced by physical properties and content of aggregates. The properties of SCC were characterized by quantitative measures of segregation and flow. The proposed model was developed by testing more than 70 concrete mixtures.

2.7 Mix Design Approaches of SCC

Okamura and Ozawa (1995) proposed the first original mix design method of SCC, which was developed at the University of Tokyo. The main features of the method included the determinations of air content, coarse aggregate content, fine aggregate content, water to powder ratio, and dosage of superplasticizer. The coarse aggregate content was set as 50 % of the dry rodded weight in the concrete. The fine aggregate content was fixed at 50 % of the resulting mortar volume. All particles larger than 0.09 mm were considered as aggregate, while all equal to and smaller than 0.09 mm as powder. The ratio of water to powder and dosage of superplasticizer were determined by testing mortar with the spread and V-funnel tests. The measurement of spread and flow time were converted to relative area (Γ_m) and relative flow time (R_m). The superplasticizer dosage and water to powder ratio were adjusted until Γ_m=5 and R_m is between 0.9 and 0.11. These proportions were then used as the starting point for trial mixes of the concrete. A slump flow of 65 cm was considered adequate. Since this prototype method was applicable to mixtures containing a limited range of Japanese materials, it had been subsequently modified and developed by many researchers for achieving more efficient mixes from a wider range of materials.

Ouchi, et al. (1998) proposed the method of determining a satisfactory combination of water to powder ratio and superplasticizer dosage, which was modified from the original method. Each parameter used in the method was determined independently, resulting in the reduction of the number of the required tests. Similar to the original method, the main concept involved the spread and V-funnel tests of mortar, expressed in the forms of relative area (Γ_m) and relative flow time (R_m), respectively. Test results showed that the relationship between Γ_m and R_m was linear for any particular value of superplasticizer dosage by weight of powder (S_p/P) and was of the form $R_m = A\Gamma_m^{0.4}$ for any particular value of water to power ratio by volume (V_w/V_p). This resulted in a single combination of water to power ratio (V_w/V_p) and dosage of superplasticizer (S_p/P) for any particular combination of Γ_m and R_m.

Skarendahl (1998) summarized that the mix design method of SCC used in Sweden was developed based on the mix proportioning and tests of mortar, similar to the original method proposed by Okamura and Ozawa (1995). The method consisted of the fallowing steps: identification of design criteria, determination of the fine mortar volume, formulation of the fine mortar composition, and formulation of the concrete composition, respectively. Deformability, spacing between steel bars, strength and durability of SCC mixture were considered as the design criteria. The volume of fine mortar was determined by using the tested void content of compacted aggregates and analyzing blocking criteria of SCC. The composition of fine mortar was formulated by determining water to powder ratio and

measuring the rheology of the tested fine mortar. The targeted properties of SCC mixture was verified and modified by doing trial mix batches. The deformability of SCC mixtures was achieved by using fines and superplasticizer. Viscosity agents were rarely used, but might be considered as a way to obtain SCC with less sensitive to variations, e.g. in moisture content of aggregates.

Walrawen (1998) reported that the original method of the University of Tokyo was adopted to be employed with Dutch circumstances and materials in particular a maximum aggregate particle size of 16 mm, which was intended to be applied to powder-typed SCC. The mix proportion according to the general approach was determined by the steps of determination of air content (A), coarse aggregate volume (G), fine aggregate volume (S), water to powder ratio, and dosage of superplasticizer, respectively. The coarse aggregate volume (G) was fixed at 50 % of total aggregates volume in the concrete. The fine aggregate volume (S) was determined at 40 % of the mortar volume. The water to powder volume ratio (V_w/V_p) was determined from the test of relative mortar flow and relative mortar V-funnel flow time. The adequate dosage of superplasticizer was estimated by tests on concrete with a slump flow of 65±5 cm. It was also found that the quantity of coarse aggregate could be increased to 60 % of the dry rodded bulk density, which corresponded to the maximum packing degree of the aggregate mixture. At this aggregate content, the required paste content was about 10 % less than that obtained by using the original method.

Chan, et al. (1998) developed a self-compacting engineered cementitious composite (ECC) by optimizing the micromechanical parameters, which control composite properties in the hardened state, and the processing parameters, which control the rheological properties in the fresh state. In the development concept of self-compacting ECC, micromechanics was adopted to properly select the matrix, fiber, and interface properties to exhibit strain hardening and multiple cracking behavior in the composites. With the selected ingredient materials, the self-compactability of ECC was realized by the controlled rheological properties of fresh matrix and the uniform dispersion of fibers. The controlled rheological properties of fresh matrix, including deformability, flow rate, and self-compactability, was a result of adopting an optimal combination of a superplasticizer and a viscosity agent. According to the measurements of slump flow and the result of self-placing test, the developed ECC was proven to be self-compacting. Flexural test demonstrated that the mechanical performance of self-compacting ECC was insensitive to the externally applied consolidation during placing, which confirmed the effectiveness of the self-compactability in maintaining the quality of the structural elements.

Domone (1999) also extended the original method of the University of Tokyo to apply with U.K. materials. The main differences to the original method were the increased sand contents of mortar. A maximum ratio of water to powder for segregation resistance was obtained from powder characteristics measured with the spread test. The method was applicable for SCC mixtures containing fly ash, GGBFS and/or limestone powder. Dosage of superplasticizer was obtained from mortar tests, as in the original method. Trial mix process of the resulting concrete was still required for adjusting mix proportion to obtain the specified values of slump flow, V-funnel time and U-box height.

Edamatsu, et al. (1999) proposed the mix-design method for SCC considering interaction between coarse aggregate and mortar particles by means of the relationship between filling height of fresh concrete and ratio of relative funnel speed of mortar with glass beads (R_{mb}) to that without glass beads (R_m), R_{mb}/R_m, obtained by a simple evaluation method, and the influence of the physical properties of particles in mortar on R_{mb}/R_m. The

results were summarized that it was possible to employ the simple evaluation method for the mix proportioning of self-compacting concrete because there was a close correlation between filling height and R_{mb}/R_m. Also, it was found that R_{mb}/R_m with the same volumetric ratio of fine aggregate to mortar volume excluding air (V_s/V_m) was affected by the physical properties of the fine aggregate or powder. Whereas, the tendency for R_{mb}/R_m to decrease with increasing V_s/V_m over a certain value and then decrease sharply was not affected by the physical properties of the materials used. And the certain material properties, which are the particle shape and the average particle diameter of the fine aggregate, had an influence on R_{mb}/R_m with the same V_s/V_m in the case of the same powder used. On the other hand, in the case of the same fine aggregate, these influencing properties were particle size distribution, powder particle shape, and coarse particles in the powder. In order to establish a rational mix design method for self-compacting concrete, it was necessary to quantify the relationship between R_{mb}/R_m and V_s/V_m by using these physical material properties.

Su (2001) proposed a mix design method for SCC. By the proposed method, the amount of aggregates required was determined, and the paste of binders was then filled into the voids of aggregates to ensure that the obtained concrete had flowability, self-compacting ability and other desired SCC properties. The amount of aggregates, binders and mixing water, as well as type and dosage of superplasticizer (SP) to be used are the major factors influencing the properties of SCC. Slump flow, V-funnel, L-flow, U-box and compressive strength tests were carried out to examine the performance of SCC, and the results indicated that the proposed method could produce successfully SCC of high quality. It was also reported that compared to the method developed by the Japanese Ready-Mixed Concrete Association (JRMCA), this method was simpler, easier for implementation and less time-consuming, requires a smaller amount of binders and saves cost.

Saak, et al. (2003) introduced a segregation-controlled design methodology for SCC. According to the theoretical assumption of this study, aggregate segregation is governed by the yield stress, viscosity, and density of the cement paste matrix. The concept of a rheological self-flow zone (SFZ) for concrete was introduced where aggregate segregation was avoided, yet the concrete had a high workability. The applicability of the theory was studied by systematically changing the rheology of the cement paste matrix of fresh concrete. The yield stress and viscosity of three different types of pastes incorporating silica fume and a cellulose thickening agent were measured as a function of density. A U-tube apparatus was then used to determine the SFZ for concrete made with the different cement paste compositions. The results suggested that the new segregation control design theory could be used to produce SCC. The slump of concrete produced using this methodology was 29 cm, with no segregation of coarse aggregate even at the periphery of the slumped material.

Sonebi (2004) reviewed statistical models obtained from a factorial design that was carried out to determine the influence of four key parameters on deformability, passing ability, segregation, and compressive strength. These parameters are important for the successful development of medium-strength SCC. The parameters considered in the study were the contents of cement and pulverized-fuel ash, water-powder ratio, and dosage of HRWRA. The responses of the derived statistical models were slump flow, fluidity loss, rheological parameters, Orimet time, V-funnel time, L-box, JRing combined with Orimet, JRing combined with cone, fresh segregation, and compressive strength at 7, 28, and 90

days. The models were valid for mixtures made with 0.38 to 0.72 w/p, 60 to 216 kg/m^3 of cement content, 183 to 317 kg/ m^3 of PFA, and 0 to 1 % of HRWRA, by mass of powder.

Kampmann, et al. (2006) proposed theoretical mix design methodology for SCC based on minimizing the water quantities and using new generation superplasticizers. The mix design took into consideration basic raw material properties and required water content for surface-saturating individual concrete ingredients. A case study was performed using locally available limestone material in Florida for validating the mix design methodology. The rheological properties of fresh concrete were evaluated using specific SCC test procedures. The hardened concrete engineering properties were also evaluated for representative mix designs.

2.8 Use of Industrial Wastes as Concrete Aggregate

Kourd (1989) studied the influence of natural and crushed stone very fine sand (finer than 75 micron) on the performance of fresh and hardened concrete. The study indicated that the water demand increased rapidly when the VFS replacement was more than 5 % in natural sand concrete and more than 15 % in crushed stone sand concrete. Data of bleeding water indicated a definite beneficial effect from the incorporation of more VFS in the fine aggregate. Furthermore, the compressive strength of constant slump concrete decreased linearly with increasing percentage of VFS replacement; the flexural and bond strength were similarly affected. For concretes with constant water to cement ratio, incorporation of VFS resulted in significant reduction in slump. Although the compressive strength of natural sand concrete was not significantly affected by the incorporation of VFS, crushed stone sand concrete indicated an increase in strength.

Baguant (1995) investigated the properties of concrete with bagasse ash as fine aggregate. Bagasse is the fibrous residue of sugar cane, which is burned for energy leaving various types of ashes as waste residue, of which grate ash was found to be the most suitable for use in concrete. Grate ash showed poor chemical reactivity with portland cement, making it not very effective as a pozzolanic material. It can, however, be used as a fine aggregate of concrete. The use of only the ash as fine aggregate gave harsh concrete with low workability and poor cohesion. This was improved by blending about 25 % normal sand with the ash. Bleeding was less than and comparable with that of normal concrete. Grate ash concrete, in particular the lower strength mixes, had 10 to 18 % higher initial drying shrinkage, which require more stringent curing precautions than normal concrete. For a given strength, the grate ash concrete required more cement than normal concrete. In comparison with normal concrete, grate ash concrete had similar strength development and shrinkage, slightly lower modulus of elasticity, and about 40 % lower creep deformations. Grate ash concrete also showed similar durability properties to normal concrete, in terms of their resistances to mechanical abrasion, water absorption, chloride diffusion, and carbonation. However, due to the porosity of the grate ash particles, the concrete had a much better resistance to freezing and thawing attack than normal concrete, even though all concretes were non-air-entrained.

Ghafoori, et al. (1997) studied the use of lignite-based bottom ash as a fine aggregate in structural grade concrete. Bottom ash concrete was combined with portland cement, crushed limestone coarse aggregate, and water to produce concretes with cement contents ranging from 297 to 475 kg/m^3 and uniform slump of 100 mm. The engineering characteristics of mixtures made with bottom ash were compared with those of

conventional concretes in order to evaluate the effectiveness and suitability of bottom ash as a possible fine aggregate in portland cement-based mixtures. It was concluded that the use of bottom ash increased the demand for mixing water in obtaining the required workability. As a consequence, both fresh and hardened properties were impacted, particularly for mixtures with low cement content. When a water reducing admixture was used, the engineering properties of bottom ash concretes were similar, and in most cases superior, to those of control concretes.

Bakoshi (1998) studied the strength and durability of concrete using bottom ash, an industrial by-products discharged from coal-fired thermal power stations, as replacement of fine aggregate. The concrete mixed with bottom ash from 0 to 40 % in volume for fine aggregate was investigated. The test results of the concrete strength indicated that the compressive strength and tensile strength of bottom ash concrete generally increased with the increase of replacement ratio of fine aggregate and curing age. The freezing and thawing resistance of concrete using bottom ash was lower than that of ordinary concrete and the abrasion resistance of bottom ash concrete was higher than that of ordinary concrete. The use of bottom ash in amounts of 10 to 40 % as replacement for fine aggregate was effective in improving the concrete properties except for the freezing and thawing resistance.

Uchikawa, et al. (1998) examined the workability, strength development, hydration of cement, composition and structure, and harmful elements of High Volume Waste Concrete (HVWC). Incineration ash of urban refuse and sintered coal ash were used as the substitution for fine aggregates, while sintered sewage sludge and glass cullet were used as the substitution for coarse aggregates. It was determined that HVWC could keep good workability without segregation and developed higher strength than ordinary concrete even though the amounts of waste-derived aggregates in concrete exceeded 600 kg/m^3. Increase in combined water in hardened HVWC and the production of cement hydrates i.e. C-S-H with age was normal and the influence of trace elements contained in waste-derived aggregates on the cement hydration was negligible. Decrease in the amounts of $Ca(OH)_2$ and increase in C-S-H, which was estimated from the pore volume of 3 to 6 nm in diameter, was recognized in later age in the case when blast-furnace slag or fly ash was used as a binder. Non-uniformity in distribution of aggregate, large pore and microgroove between aggregate and cement paste which might occur by the use of large amounts of waste-derived aggregate was not observed. There was no remarkable difference in type and quantities of elements between HVWC and ordinary concrete dissolved from them.

Ghafoori, et al. (1998) reported the behavior of laboratory-made roller compacted concretes (RCC) containing pulverized coal combustion high-calcium dry bottom ash as a fine aggregate. Different RCC mixtures with cement contents ranging from 9 to 15 %, and coarse aggregate contents of 50, 55, and 60 % by mass of total dry solids were prepared at the optimum moisture content and were consolidated and water-cured at different ages for six months. It was concluded from test results that RCC samples containing dry bottom ash offered excellent strength, stiffness, and deformation properties, considering the range of the used cement factors. In term of durability of bottom ash RCC, resistance to sulfate attack, rapid freezing and thawing, and wear were improved with increases in cement and/or coarse aggregate contents.

Jianxiong, et al. (1999) studied on SCC mixed with superfine sand and pozzolanic materials. It was found that it was feasible to make self-compacting high performance

concrete with superfine sand which fulfils the requirements for strength, durability and construction work in which SCC with a slump of 180 to 250 mm, slump flow 400 to 680 mm, and 28 day strength 50 to 68 MPa were made in the laboratory by using superfine sand in combination with 30 to 60 % slag and fly ash. Thus the cement content in the concrete could be reduced by 30 to 60 %. Also, the ground pozzolanic materials and suitable superplasticizers played important roles in making self-compacting high performance concrete with superfine sand with satisfied sulfate resistance.

Jaturapitakkul, et al. (2003) studied the potential of using bottom ash from the Mae Moh power plant in Thailand as a pozzolanic material. The bottom ash samples were improved its pozzolanic property by grinding until the particle size retained on sieve # 325 was less than 5 % by weight and were used to replace Portland cement type I in mortar and concrete mixtures. The results indicated that the particle of bottom ash was large, porous, and irregular shapes. The grinding process reduced the particle size as well as porosity of the bottom ash. Compressive strengths of mortar containing 20 to 3 % of bottom ash as cement replacement were much less than that of cement mortar at all ages, but the use of ground bottom ash produced higher compressive strength than the cement mortar after 60 days. When ground bottom ash was used at a 2 % replacement of cement to make concrete, the concrete with higher cement content produced higher percentage compressive strength as well as a higher development rate than those of the low cement content concretes. With the cement content in ground bottom ash concrete of 440 and 260 kg/m^3, the concrete needed 14 and 60 days, respectively, to develop higher compressive strength than that of the concrete without bottom ash. As a result of the compressive strengths, it was concluded that ground bottom ash could be used as a good pozzolanic material.

Naik, et al. (2004) studied the use of high volumes of fly ash, bottom ash, and used foundry sand in the manufacture of pre-cast concrete products such as wet-cast concrete bricks and paving stones. ASTM Class F fly ash was used as a partial replacement for 0 (reference), 25, and 35 % of Portland cement. Bottom ash combined with used foundry sand replaced 0 (reference), 50, and 70 % of natural sand. Tests for compressive strength, freezing-and-thawing resistance, drying shrinkage, and abrasion resistance were conducted on the wet-cast concrete masonry units manufactured at a commercial manufacturing plant. It was concluded that all wet-cast bricks could be used for both exterior and interior walls in regions where freezing and thawing is not a concern, and for interior walls in regions where freezing and thawing is a concern. None of the wet-cast paving-stone mixtures, including the reference mixture, satisfied all the ASTM requirements for paving stones.

Bai, et al. (2005) investigated the strength and drying shrinkage of concrete with the natural sand replaced with furnace bottom ash (FBA) at 0, 30, 50, 70, and 100 % by mass, at fixed water to cement ratios and fixed slump ranges. The results showed that, at fixed water to cement ratios, the compressive strength and the drying shrinkage decreased with the increase of the FBA content. However, at fixed workability, the compressive strength was comparable with that of the control concrete, while the drying shrinkage increased with the increase of the FBA sand content beyond 30 % replacement level. Nevertheless, 30% of the natural sand could be beneficially replaced with the FBA sand to produce concrete in the compressive strength range from 40 to 60 N/mm^2 without detrimentally affecting drying shrinkage properties of the concrete.

Chapter 3

Experimental Program

3.1 General

Generally, development of models to predict deformability, segregation, and passing ability of SCC requires understanding of all related mechanisms and relationships between various influencing parameters.

Various parameters considered, in the model, to influence deformability of fresh SCC are ratio of paste volume to void content of densely compacted aggregate phase (γ), free water content, water retainability of aggregates and powder materials, surface area of aggregate and powder materials, type and dosage of superplasticizer, and water reducing efficiency of superplasticizers. Prediction model for bleeding is formulated based on concept of free water, surface area of solid particles in concrete and degree of reaction of binders. The parameters considered in model for predicting passing ability are size distribution, volumetric ratio and shape of aggregates. The effect of viscosity of the concrete, clear spacing and size of the reinforcement are also considered for passing ability through narrow openings.

In formulation of models for predicting slump flow, 50-cm slump flow time and bleeding, the constituents of the tested SCC mixtures were proportioned by varying water to powder ratio, ratio of paste volume to void content of aggregate phase, replacement ratio of fly ash and limestone powder, type and dosage of superplasticizer. Shape and size of coarse aggregate, and diameter of steel bars were varied to study their effects on L-box passing ability of the tested SCC mixtures to formulate a prediction model for passing ability.

To study effects on properties of SCC of bottom ash and very fine sand as partial replacement of total fine aggregate, the mix proportion of SCC was determined by fixing the ratio of paste volume to void content of densely compacted aggregate phase and the water to powder ratio. The mixture using only river sand as fine aggregate was considered as the control concrete. Bottom ash and very fine sand were used to replace fine aggregate at various percentages.

3.2 Materials Used

3.2.1 Cement

Ordinary Portland cement Type 1, Elephant Brand, conforming to ASTM C150-92 Type 1, and manufactured by the Siam Cement (Kaeng Koi) Co., Ltd., Thailand was used throughout the study.

3.2.2 Fly ash

Lignite fly ash collected from Mae Moh Lignite Power Plant in Lampang Province was used.

3.2.3 Limestone Powder

Limestone powder from the Siam Mortar Co. Ltd., Thailand was used.

The chemical compositions and physical properties of cement, fly ash, and lime stone powder used in this study are summarized in Table A-1 of Appendix A.

3.2.4 Bottom Ash

Bottom ash I collected from the power plant of Thai Acrylic Fiber Co., Ltd. in Saraburi province of Thailand was used to study the effects of bottom ash on properties of SCC. Bottom ash II collected from Mae Moh power plant in Lampang province and expanded clay lightweight aggregate imported from Arika Co., Ltd. of Spain were used to confirm the reliability of the test method developed in this study for water retainability of porous fine aggregate. The chemical compositions and physical properties of both bottom ashes and expanded clay used in this study are listed in Table A-2 of Appendix A.

3.2.5 Fine Aggregate

Fine aggregates were categorized into two types as follows.

1) Normal sand was used as the control fine aggregate. It is natural river sand passing sieve no. 4 and has the fineness modulus, specific gravity, and absorption of 2.78, 2.65, and 0.7 %, respectively. Its properties comply with ASTM C33-92a..

2) Very fine sand was used as partial replacement of total fine aggregate to study its effects on the filling ability of SCC. It is also natural river sand but having the fineness modulus 1.2 to 1.7, which is normally employed in plastering or decorated purposes. It is a by-product from the production process of normal sand used in concrete industry. The gradation of normal sand and very fine sand used in this study is shown in Table A-4. Specific gravity and absorption of very fine sand are 2.65 and 0.8 %, respectively.

3.2.6 Coarse Aggregate

Crushed limestone with maximum sizes of 12, 19, and 25 mm from a single source were used. The coarse aggregate was washed to remove dirt and subsequently stored in clean and sealed buckets. Gradations of crushed limestone are summarized in Table A-6 and its specific gravity and absorption are 2.70 and 0.5 %, respectively.

3.2.7 Mixing Water

Ordinary tap water was used throughout the study.

3.2.8 Superplasticizer

Four bases of water reducing admixture and superplasticizers from different sources and different lots as shown in the Table 3.1 were used. The properties of water reducing admixture and superplasticizers are shown in Table A-7 in Appendix A.

Table 3.1 Type and source of water reducing admixtures

Base	ASTM Type	Trade Name	Source	Designated as in this study
Lignosulfonate	D	Daratard 500	W R Grace (Thailand)	Retarder
Naphthalene	F	Mighty MX	Kao Industry (Thailand)	Naphthalene (I)
	F	Sikament FF	Sika (Thailand).	Naphthalene (II)
Melamine	F	Sikament F6	Sika (Thailand)	Melamine
Polycarboxylate	F	ABVA 105	W R Grace (Thailand)	Polycarboxylate

3.3 Determination of Material Properties

3.3.1 Cementitious and Powder Materials

Chemical compositions of cement were analyzed in accordance with ASTM C 114-88. The specific gravity and specific surface area of cement and limestone powder were analyzed in accordance with ASTM C 188 and ASTM C 204-92, respectively. The chemical compositions and physical properties of fly ash and bottom ash were analyzed in accordance with ASTM C 311-98b.

3.3.2 Aggregates

The specific gravity of fine aggregate and coarse aggregate were tested in accordance with ASTM C 128-97 and ASTM C 127-88, respectively. Sieve analysis was carried out according to ASTM C136. Compacted void content of mixture of fine and coarse aggregates was performed following ASTM C29/C29M-91a.

Since there is still no standard test to directly measure the specific surface area of aggregates, the specific surface area was calculated from the gradation curve by assuming that the aggregate has a spherical shape and then applying a shape factor to account for the irregularity of the particles (Kitticharoenkiat, 1998, Khunthongkeaw, 2001, and Wangchuk, 2003).

3.4 Determination of Mix Proportions

Mix proportion of the investigated SCC mixtures in this study was determined by varying the ratio of paste volume to void volume of densely compacted aggregate phase (γ) which is defined as

$$\gamma = \frac{V_{paste}}{V_{void}} \tag{3.1}$$

where

γ is ratio of paste volume to void volume of densely compacted aggregate phase.

V_{paste} is volume of paste, including volume of air voids, in a unit volume of fresh concrete, m^3.

V_{void} is volume of void in the densely compacted total aggregate phase (fine and coarse aggregate) in a unit boundary volume of the aggregate, m^3.

The volume of paste can be derived as,

$$V_{paste} = V_c + V_f + V_w + V_{air} \quad (3.1a)$$

where

V_c, V_f , V_w, V_{air} are volumes of cement, fly ash, water, and air, respectively.

All mixtures of concrete tested in this study were designed to have γ values in the range from 1.4 to 1.8 and water to powder ratio (w/p) varying from 0.25 to 0.45. It is noted here that the mixtures with high w/p were intentionally determined to study the behaviors of bleeding and aggregate blocking. Sand to total aggregate ratio by weight (s/a) was controlled at 0.50 which was a little higher than the ratio giving the minimum void content of the densely compacted aggregate phase was selected to minimize paste content of the mixture and to control the amount of coarse aggregate. Fly ash was used to replace total powders at the ratios of 0 %, 30 % and 50 %. Limestone powder was used to replace total powders at 10 %. To investigate the effect of type and dosage of superplasticizer on deformability and segregation, the amount of each type of superplasticizer was varied with the dosage from 0 % to 2.0 % by weight of powder.

3.5 Determination of Water Retainability of Powder Materials

Tangtermsirikul and Kitticharoenkiat (1999) introduced an easy method for estimating the water retainability of powder materials by finding a point of lowest water to powder material ratio by weight that initiates slump of paste using a mini-slump test.

A metal mold, in the form of a frustum of a cone with dimensions as follows: 40$\pm$3 mm inside diameter at the top, 90$\pm$3 mm inside diameter at the bottom and 75$\pm$3 mm in height, and a metal tamper, weighing 340$\pm$15 g and having a flat circular tamping face 25$\pm$3 mm in diameter, are used in the mini slump test.

The test is conducted by mixing the powder paste with a guessed value of water to powder material ratio starting from low ratio so that the mixture has no slump. The mixture, approximately one third of the volume of the mold, is placed in the mold and tamped 25 times with the tamper. The other two portions of mixture are placed and tamped until the mold is full. The excess is struck off and the mold is immediately removed by raising it carefully in the vertical direction. The slump of the mixture is measured. The entire process is repeated by increasing the water to powder material ratio until slump is

initiated. The water to powder material ratio, which initiates slump, is the water retainability coefficient (β) of that powder material.

3.6 Determination of Water Reducing Efficiency of Superplasticiser

The water reducing efficiency of water reducing admixtures is tested on powder paste i.e. cement, fly ash, and lime stone powder pastes. Test method developed by Wangchuk (2003) was adopted to obtain water reducing efficiency of superplasticizers in this study. It is determined by using a metal mold in the form of a frustum of a cone with dimensions as follows: 40±3 mm inside diameter at the top, 90±3 mm inside diameter at the bottom and 75±3 mm in height.

A similar method for determining the water reducing efficiency of admixtures has been described by Meyer and Perenchio (1979) using the mini-slump technique that was developed by Kantro at the Portland Cement Association.

The test is performed as follows: Powder paste, with a guessed value of water to powder ratio that would give a flow diameter about 180±5 mm is placed in the mold. After filling, the mold is removed immediately by raising it carefully in the vertical direction and the diameter of the flow of the cement paste is measured. The water to powder ratio is varied till the required flow diameter of 180±5 mm is obtained. This is firstly tested for control mixture without water reducing 1admixtures. Then for a given dosage of water reducing admixture (the value of 0.5 % was recommended by Wangchuk (2003)), the quantity of water is varied and the test repeated till the required flow diameter as that of the control mix is obtained.

Fig. 3.1 Measurement of flow diameter of powder paste in the determination of water reducing efficiency of superplasticizer

The water reducing efficiency (φ′) of superplasticizer is subsequently given by (Wangchuk, 2003) :

$$\varphi' = 1 - \frac{W_{wa}}{W_{woa}} \tag{3.2}$$

where

φ' is the water reducing efficiency of water reducing admixtures.

W_{woa}, W_{wa} are the quantities of water required to attain a flow diameter of 80±5 mm for paste without water reducing admixture and for paste with 0.5 % dosage of water reducing admixture, respectively.

3.7 Determination of Dispersion Factor Due to Superplasticizer for SCC

By introducing superplasticisers into the concrete, powder particles are dispersed. This dispersion force improves deformation of mixture and is considered in the model by introducing a factor called dispersion factor. The dispersion factor (ϕ_{dps}) is introduced to account for the effect of dispersion due to the use of superplasticizers on water retainability of powders and inter-particle contacts in concrete. From slump flow test, this factor can be determined by the ratio of slump flow value of SCC mixture with superplasticizer and that of the same mix proportion without superplasticizer, as the following expression.

$$\phi_{dps} = \frac{SF_{woa}}{SF_{wa}} \tag{3.4}$$

where

ϕ_{dps} is the dispersion factor

SF_{woa} is the slump flow of SCC mixture without water reducing admixture, cm.

SF_{wa} is the slump flow of SCC mixture with water reducing admixture, cm.

The effects of influencing factors on the dispersion factor, i.e. ratio of paste volume to void content of densely compacted aggregate phase , water to powder ratio, type and dosage of superplasticizer, and water reducing efficiency of the superplasticizers, was investigated and discussed in section 4.4.4 in chapter 4.

3.8 Determination of Filling Ability of SCC

In this study, the quantitative deformability of SCC can be measured by slump flow test. Measurements of bleeding water and static segregation were performed to study segregation of SCC. Passing ability of SCC through narrow openings was measured by using L-box apparatus.

3.8.1 Determination of Deformability

Deformability was defined and represented in this study by two terms which are deformation capacity and velocity of deformation. By the slump flow test, the slump flow value, measured from the final flow diameter of the concrete, is a useful index to evaluate the deformation capacity. Unlike the value of slump test measured in the vertical direction, the slump flow value is however determined from the diameter of mixture after stop flowing. The velocity of deformation can be measured by the 50-cm slump flow time (T_{50}), simply obtained by recording the time the concrete takes to reach the flow diameter of 50

cm after lifting the cone. The tests for slump flow and 50 cm-slump flow time were carried out conforming to the standard method of RILEM Technical Committee-174, which was based upon the original study of Tangtermsirikul, et al. (1992).

3.8.2 Determination of Bleeding and Static Segregation

Measurement of bleeding water was performed following ASTM C232-99 Method A (sample consolidated by tamping). A cylindrical container of 14.16 liters in capacity, having an inside diameter of 254 mm and inside height of 279.4 mm was used in this test. After casting concrete into the container, draw off (with pipette or similar instrument) the water that had accumulated on the surface, at 10 minutes intervals during the first 40 minutes and at 30 minutes intervals thereafter until cessation of bleeding.

Since there is no standard test to directly measure the segregation of fresh concrete, both visual inspection test and the test method used by Assaad, et al. (2004) were adopted and modified to assess the static segregation in this study.

Test for segregation by visual inspection was conducted by examining the appeared condition of fresh concrete during the slump flow test, compared with the criteria of degree of segregation as prescribed in the Table. 3.2.

Table 3.2 Criteria of degree of segregation by visual inspection test

Degree of Segregation	Concrete Condition	
Non-Segregation		- Coarse aggregate particles are well dispersed thorough the concrete flow area, especially at the edge of the flow spread - No bleeding water
Slight Segregation		- Coarse aggregate slightly gathers at the center of the concrete flow - Appearance of a little bleeding water at the edge of the concrete flow

Degree of Segregation	Concrete Condition
Segregation	 - Coarse aggregate significantly gathers at the center of the concrete flow and having very little or no coarse aggregate particles at the edge of the flow spread - Significant bleeding water

The modified method based on the study of Assaad, et al. (2004) is another method used in this study. It was conducted by examining the variation of coarse aggregate along the height of sample caused by static segregation. By this concept, the volumetric percentage of coarse aggregate in concrete mainly influences the indication of static segregation; therefore the distribution of coarse aggregate throughout the sample height is investigated. The test was performed following the below procedure:

After finishing bleeding water measurement (approximately 4 hrs.), the concrete sample of the bleeding test was removed from the container and equally separated into three portions along the height of container i.e. top, middle, and bottom. The concrete weights of top and bottom portions were measured. Basically, the segregated concrete showed different coarse aggregate contents between the upper and lower parts of the container as illustrated in Figs. 3.2 and 3.3.

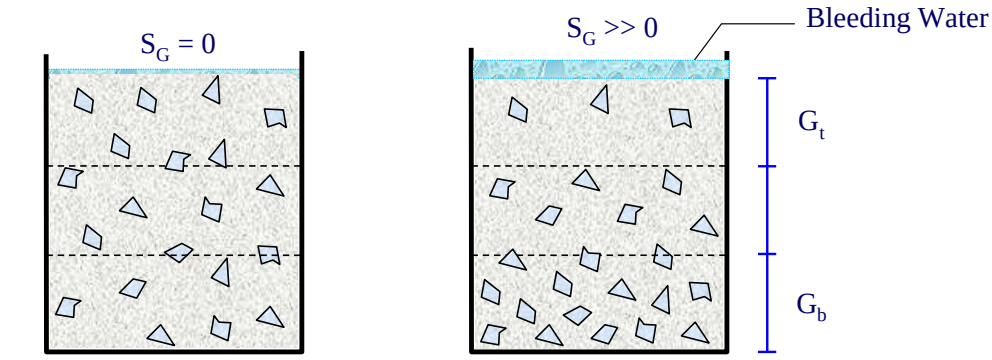

a) Homogenous Concrete b) Segregated Concrete

Fig. 3.2 Distribution of coarse aggregate along the height of concrete sample after finished bleeding test

a) Top portion of concrete sample b) Bottom portion of concrete sample

Fig. 3.3 Conditions of the top and bottom portion of concrete sample removed from the container

Subsequently, these two portions of the sample were sieved by using sieve no. 4 to separate coarse aggregate from the other components of the concrete. The weights of the separated coarse aggregate are recorded. Then, the ratio of coarse aggregate to total concrete by weight of the top and bottom concrete portions (G_t and G_b) were calculated in percentage. Finally, the difference of coarse aggregate weight ratio to total concrete between the top and the bottom concrete portions (S_G) was employed to indicate the degree of static segregation. The zero value of S_G indicated no static segregation of the tested concrete, while the acceptable resistance to segregation was defined in this study by the S_G value of not more than 10 % which was assessed by L-box passing ability with 20-mm steel bars and 33-mm clear spacing to provide good passing ability through narrow openings (more than 60 %). It can be calculated by the following equation.

$$S_G = G_b - G_t \quad (3.3)$$

where

S_G is difference of coarse aggregate weight ratio to total concrete between the top and the bottom concrete portions, %

G_b is weight ratio of coarse aggregate to total concrete of the bottom concrete portion, %

G_t is weight ratio of coarse aggregate to total concrete of the top concrete portion, %

3.8.3 Determination of Passing Ability through Narrow Openings

The L-box apparatus was used to measure the passing ability of SCC through narrow openings. It was installed with the vertical bars to provide three narrow openings of 33 mm as seen in Fig. 3.4.

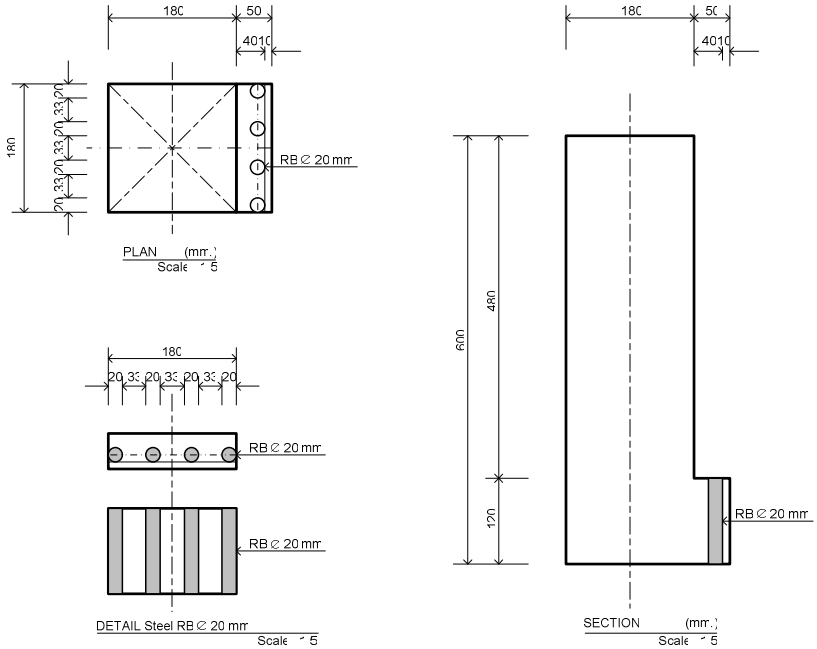

Fig. 3.4 L-box test apparatus used to evaluate the passing ability through narrow openings

The test was commenced by filling the concrete into the apparatus. After 1 to 2 minutes to let the concrete undergo static segregation if there was, the gate was lifted in order to allow the concrete to flow through the reinforcing bars.

Its test result is expressed in percentage of passing ability calculated from the ratio of the drop height (h) at the end of flow to the original height before the flow. A larger value of h, the descent of the sample head, indicates a better narrow-opening passing ability of the tested concrete. In this study, the judgment of "not pass" or "blocking" for the L-box test was defined by the passing ability value of less than 60 % (Tangtermsirikul, et al., 1995).

3.9 Experimental Programs

The experimental programs in this study were designed to explore the influencing factors and their mechanisms and effects on filling ability of SCC for formulating the prediction models, as well as the effects of bottom ash and very fine sand on properties of SCC. It is noted here that the amount of water in superplasticizer was also used to adjust the unit water content and included in the calculations of concrete volume and mixture parameters such as w/p and aggregate-to-paste ratios based on 50 percent solid content of SP. The solid content in the superplasticizer was ignored in volume calculation and was considered to have no effect on concrete properties due to its small quantity.

3.9.1 Effects of Free Water on Deformability

Various mix proportions used for studying the effect of free water on the slump flow and 50-cm slump flow of SCC were designed to have γ values varying from 1.4 to 1.8 and water to powder ratio (w/p) varying from 0.25 to 0.45. Fly ash was used to replace cement at the ratios of 0 %, 30 % and 50 %. The dosage of superplasticizers was varied from 0 % to 2.0 % by weight of powder. The tested mix proportions of concrete are summarized in Table B-1.

3.9.2 Effects of Superplasticizer on Deformability

By introducing superplasticizers into the concrete, powder particles are dispersed. This dispersion force improves deformation of mixture and is considered in the model by introducing a factor called dispersion factor. The dispersion factor (ϕ_{dps}) for modifying the slope of deformation vs. free water content curves is introduced to account for the effect of dispersion due to the use of superplasticizers on water retainability of powders and inter-particle contacts in concrete.

An experimental program was designed to investigate the effects of the influencing factors including the ratio of paste volume to void content of densely compacted aggregate phase , water to powder ratio, type and dosage of superplasticizer, and the water reducing efficiency of the superplasticizers on the dispersion effect. The tested mix proportions of concrete are summarized in Table B-1 in Appendix B.

3.9.3 Effects of Free Water on Bleeding and Static Segregation

Test results of bleeding and static segregation of the mixtures were carried out, for formulating the relationship between free water, water retainability of powders, effective surface area of solid particles and rate of hydration vs. bleeding and segregation. The SCC mixtures tested for this objective were designed by varying the γ value, water to powder ratio, replacement of fly ash, type and dosage of superplasticizers as shown in Table B-2. To study the effect of concrete temperature on bleeding, the tests were performed at various concrete temperatures i.e. 25, 35, and 45 ^{o}C.

3.9.4 Effects of Characteristics of Coarse Aggregate and Size of Reinforcements on Passing Ability through Narrow Openings

A test program was designed to investigate the effects of maximum size and shape of coarse aggregate particles, and clear spacing and size of the reinforcement as well as viscosity of the concrete on L-box passing ability. The slump flow of the tested mixtures was controlled in the range of 65 - 70 cm without visual segregation by varying dosage of superplasticizer. The mix proportions are summarized in Table B-3. Crushed limestone with maximum sizes of 12, 19, and 25 mm from a single source were used for this purpose. In this study, angularity factor proposed by Powers (1968) is used to account for the effect of particle shape of aggregates {see Eq. (4.7) for determination of the angularity factor}. The coarse aggregate having the maximum size of 19 mm with various particle shapes were incorporated in the SCC mixtures for investigating its effects on passing ability through narrow openings. The particle shapes of the coarse aggregate prepared for the study include various shapes such as general, almost rounded, flaky, and elongated with the angularity factor of 1.31, 1.13, 1.51 and 1.55, respectively, as shown in Fig. 3.5.

Almost Rounded ,
ψ = 1.13

Flaky,
ψ = 1.51

General crushed limestone ,
ψ = 1.31

Elongated ,
ψ = 1.55

Fig. 3.5 Crushed limestone coarse aggregate with various particle shapes

Moreover, size of the steel bars installed in L-box passing ability tester is varied to observe its influences on the aggregate bridging at the vicinity of clear spacing between steel bars. The L-box testers equipped with the gates made from the steel bars with diameters of 12, 20 and 25 mm and clear spacing of 33 mm were used (see Fig. 3.6).

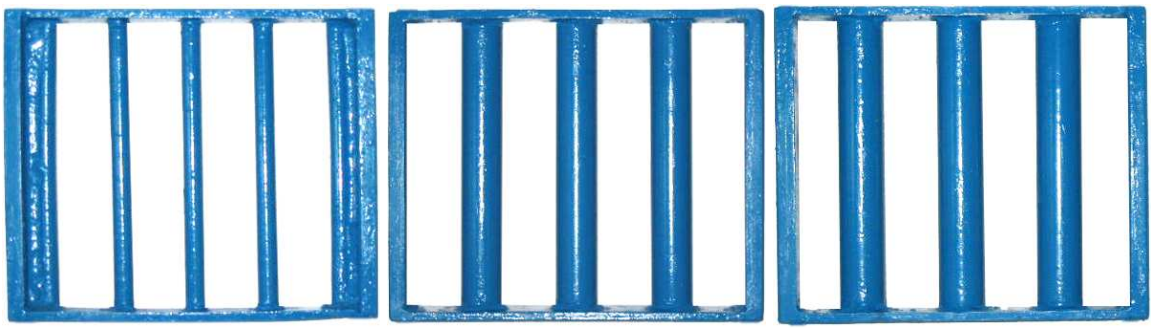

a) Steel Diameter of 12 mm b) Steel Diameter of 20 mm c) Steel Diameter of 25 mm

Fig. 3.6 Various diameters of the steel bars equipped in the L-box apparatus

3.9.5 Development of the Proposed Test Method for Water Retainability of Porous Fine Aggregate

As a porous fine aggregate, bottom ash was used in the SCC mixture in this study. Two main problems for the use of porous aggregate are the moisture property of the aggregate which is usually higher than that of the normal aggregate and the difficulty to measure the true moisture properties. In this study, a new test method to determine water

retainability of porous fine aggregates is developed with the acceptable reliability within reasonable time of testing.

Consistency of test results obtained from the proposed test method was evaluated by comparing the standard deviation values of water retainability from the proposed method within a group of four test results carried out by four different persons with those of the water absorption according to ASTM C 128. Three fine porous aggregates, i.e. bottom ashes I and II (BA-I and BA-II) collected from two sources in Thailand i.e. Saraburi and Mae Moh Power Plant, and an expanded clay lightweight aggregate (EC) were used. Chemical compositions and physical properties of the materials are shown in Table A-2. Figure 3.7 shows the enlarged pictures of these aggregates' particles. River sand was used as the control aggregate. The ASTM C 128 test method was performed to obtain the absorption of the fine aggregates to compare with the water retainability achieved by the proposed method. To prepare test samples, the water was prepared from 3 % to 60 % of dry aggregate weight to mix with the oven-dried porous aggregate.

In order to find the optimum test period, the periods of 6, 12, and 24 hours were tested for the static method and the periods of 6, 12, 24, and 36 minutes were performed for the accelerated (vibration) method.

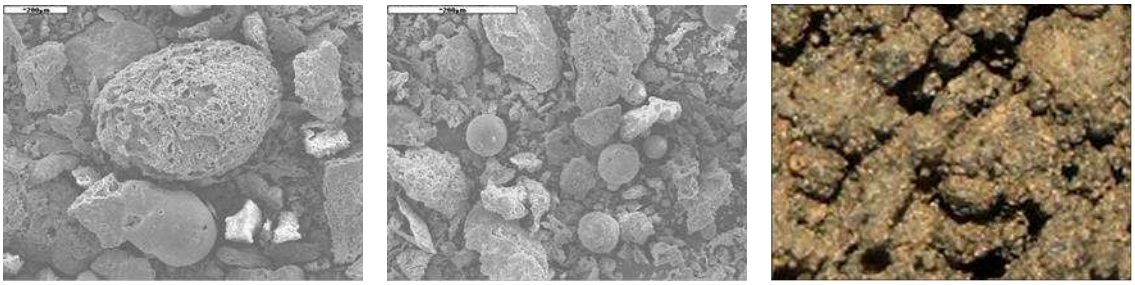

a) Bottom ash I (Saraburi) b) Bottom ash II (Mae Moh) c) Fine expanded clay

Fig. 3.7 Bottom ash I (BA-I, Saraburi), Bottom ash II (BA-II, Mae Moh) and Fine expanded clay (EC)

3.9.6 Application of the Proposed Test Method for Water Retainability of Porous Fine Aggregate

Reliability of the developed test method was confirmed by comparing the concrete properties of the mixtures proportioned by using water retainability obtained from the proposed test method with those prepared using the water absorption from ASTM C 128 method. Two types of bottom ash (BA-I and BA-II) and an expanded clay lightweight aggregate (EC) were used as partial replacement for fine aggregates of conventional concrete (CVC) and self-compacting concrete (SCC). The river sand concrete was regarded as the control concrete. To eliminate effects of the aggregate gradation on fresh concrete properties, each gradation of river sand used for the control mix were modified to be identical to those of the combined river sand with each porous aggregate and the replacement levels (10 % and 20 %). CVC was designed to have the γ values of 1.2 and 1.3, while SCC had the γ values of 1.5 and 1.7. Three porous materials were used to replace fine aggregate at the ratios of 0 %, 10 %, and 20 %. The dosage of superplasticizer was fixed at the same percentage of binder content. The tested mixture proportions of concrete are summarized in Table B-4 in Appendix B.

Tested properties of CVC and SCC proportioned by using the ASTM C 128 test method and the proposed test method are slump of CVC, slump flow of SCC, and compressive strength conducted according to BS 1881: Part 116.

3.9.7 Effects of Bottom Ash as Partial Replacement of Fine Aggregate on Properties of SCC

The effects of bottom ash on properties of SCC were investigated by comparing the test results of SCC mixed with bottom ash with those of the control SCC made of river sand. Mix proportion was determined by fixing the γ value at 1.5 and the water to powder ratio at 0.31 in order to maintain the same paste content. The mixture using normal river sand as fine aggregate was considered as the control concrete and was prepared to have the minimum slump flow of 65 cm without visual segregation and the minimum L-box passing ability of 60 %. Bottom ash was used to replace fine aggregate at the ratios of 0 %, 10 %, 20 %, and 30 % and the notations of mixtures were specified as SCC-BA 0% (control), SCC-BA 10 %, SCC-BA 20 %, and SCC-BA 30 %, respectively. The dosage of superplasticizer was fixed at the same percentage of binder content. The tested mixture proportions are summarized in Table B-5.

Tests for slump flow, 50-cm slump flow time, and L-box passing ability were performed to assess the filling ability. Segregation of SCC was observed by visual inspection during the slump flow test.

Some physical and mechanical properties i.e. porosity and pore size distribution, compressive strength, tensile strength and modulus of rupture were measured. Total porosity and pore size distribution in hardened concrete were tested using mercury intrusion method at the concrete ages of 28 and 56 days. Compressive strength and splitting tensile strength of SCC were tested according to BS 1881: Part 116 and ASTM C 496-96, respectively. Modulus of rupture was obtained from test of beams with third point loading arrangement, prepared and cured in accordance with ASTM C 78-94.

In term of durability, chloride penetration, carbonation depth, drying shrinkage, and expansion in sodium sulfate solution were also observed. The test method of rapid chloride permeability was performed following ASTM C 1202 at the concrete ages of 7, 28, and 56 days. Each measured value was obtained from the averaged chloride charge pass of three specimens for each mixture. For measuring carbonation depth, the accelerated test method was conducted in accordance with the recommendation of RILEM Committee CPC-18, TC14-CPC. The concrete specimens were moist-cured for 28 and 56 days before carbonated in the accelerated carbonation chamber for periods of 2 and 4 weeks. The temperature and relative humidity in the carbonation chamber with carbon dioxide concentration of 4% (40,000 ppm) were controlled at 40°C and 55%, respectively. Shrinkage in drying environment of specimens was measured accordingly to ASTM C 387-99. The specimens were cured in water for 1 day and then put in the control room with the condition of 55 % relative humidity and 30°C, and then the length change of specimens was measured at the drying ages of 1, 2, 3, 4, 7, 14, 28, 56, 91, 182, and 356 days by using the length comparator. Concrete deterioration subjected to sodium sulfate (Na_2SO_4, NS) is usually exhibited in term of concrete expansion leading to cracking. Therefore, the test method for expansion of concrete specimens submerged in sodium sulfate solution was performed according to ASTM C1012. Sodium sulfate solution (Na_2SO_4) which contains 50g of Na_2SO_4 (SO_4^{2-} of 33,800 ppm) in 1.0 liter of solution was prepared for sulfate

expansion test. The initial length of the specimens was obtained by using the length comparator in accordance with the ASTM C 490 after 28 days of curing in saturated limewater. After that they were placed in the sodium sulfate solution and the length change was measured at 2, 3, 4, 8, 13, and 16 weeks of sodium sulfate exposure. After 16 weeks, the subsequent measurements were made every two months of sodium sulfate exposure. Each expansion test result was obtained from the average of three specimens.

3.9.8 Effects of Very fine Sand as Partial Replacement of Fine Aggregate on Properties of SCC

This study focused on the effects of very fine sand as partial replacement of normal river sand on filling ability of the SCC mixtures. The gradation of very fine sand compared with that of normal sand is shown in Table A-5 in Appendix A. The tested mixtures incorporate very fine sand by replacing total fine aggregate at the ratios of 0 %, 10 %, 20 %, and 30 %, with the mixture notations of SCC-VFS 0% (control), SCC-VFS 10 %, SCC-VFS 20 %, and SCC-VFS 30 %, respectively. Gradations of the normal sand mixed with various very fine sand contents are shown in Table A-5 in Appendix A. Mix proportion was determined by fixing the powder contents at 520 and 540 kg/m^3 and the ratio of sand to total aggregate (s/a) of 0.45 that gives the minimum void content of the combined mixture of fine and coarse aggregates, as shown in Table B-6 in Appendix B.

Void content of the compacted mixtures of fine and coarse aggregates was tested according to the ASTM C29/C29M-91a to investigate the effect of very fine sand on the void content of the combined aggregates phase. For the SCC mixtures with very fine sand, slump flow, 50-cm slump flow time, and L-box passing ability were measured.

Chapter 4

Model for Predicting Deformability

4.1 General

Deformability of SCC is described as the ability of fresh concrete to deform or change its shape under its self-weight. In this study, it was defined and represented by two terms which are deformation capacity and velocity of deformation. Deformation capacity indicates how far the concrete can flow from the point of discharge, while velocity of deformation represents the flowing speed. An ideal SCC should have as large as possible the deformation capacity and velocity of deformation. However, segregation is often found, if SCC has too large deformation capacity and velocity of deformation. So, to achieve the preferred deformability, proper values of deformation capacity and velocity of deformation should be considered for mix proportioning of SCC mixture (Tangtermsirikul, et al., 2000). Using the slump flow test, the slump flow value, measured from the final flow diameter of the concrete, is a useful index to evaluate the deformation capacity whereas velocity of deformation can be measured by the 50 cm-slump flow time (T_{50}), simply obtained by recording the time the concrete takes to reach the average flow diameter of 50 cm after lifting the cone (Tangtermsirikul, et al., 1992)

Prediction models for deformation capacity and velocity of deformation were developed based on the concepts of free water content, water retainability of solid particles, and inter-particle forces among the solid particles in the concrete. Various parameters considered to influence the deformability of fresh SCC are ratio of paste volume to void content of densely compacted aggregate phase (γ), free water content, water retainability of aggregates and powder materials, surface area of aggregate and powder materials, and type, dosage and water reducing efficiency of superplasticizer. A model for predicting deformability of SCC was proposed as one of the three prediction models for the functional requirements of filling ability of SCC. However, it is noted here that the proposed model is limited to powder-typed self-compacting concrete without viscosity agents, which is the type of SCC mainly used in Thailand.

4.2 Model Formulation

The main factor affecting consistency of concrete in fresh state is free water content of the mixture, since by adding water beyond the water retainability of all solid particles into the mixture, the inter-particle distance of solid and the lubrication among solid particles are increased. It has been confirmed by many studies that free water content has a unique relationship with various types of consistency measurement (Ozawa, et al. 1992, Malier, 1992, Tangtermsirikul, et al., 2001, Khunthongkeaw, et al., 2001, 2003, and Wangchuk, et al., 2003). As an example, the relationship between initial slump and free water content of conventional concrete had been proposed by Tangtermsirikul, et al. (2001) and is shown in Fig. 4.1.

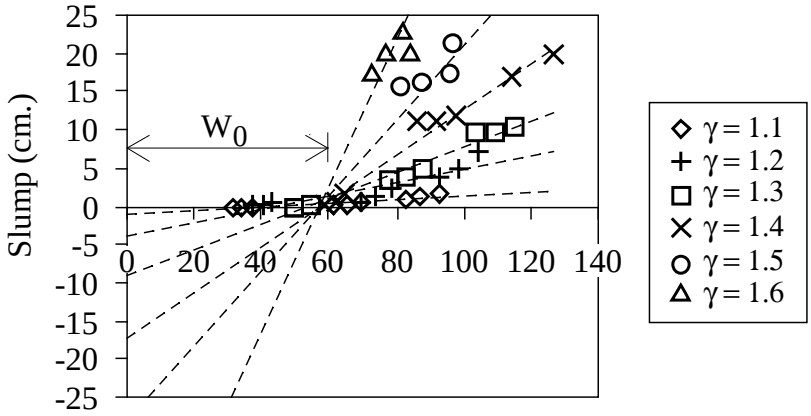

Free Water Content, W_{fr} (kg./m.^{3} of concrete)

Fig. 4.1 Relationship between slump of normal concrete and volume of free water in the mixtures (Tangtermsirikul, et al., 2001)

Consequently, an equation has been introduced to relate consistency of those concrete with free water content by considering difference in unit and method of consistency measurement as in the following equation:

$$X = \alpha_x.(W_{fr} - W_o)^a + b \quad (4.1)$$

where

- X is deformability measuring value of fresh concrete (different unit according to method of consistency measurement).
- α_x is slope of deformation of fresh concrete or mortar vs. free water content curve.
- W_{fr} is volume of free water in the mixture, kg/m^3 of the mix.
- W_o is minimum free water content required for initiating deformation, kg/m^3 of the mix.
- a, b are the constants encountering different unit and method of consistency measurement.

It is noted here that this relationship is limited for no-segregation fresh concrete and mortar.

From previous studies, this equation had been adopted for predicting various types of deformability. The linear equations for predicting slump value of conventional concrete and flow table spread of mortar, which were developed by Tangtermsirikul, et al. (2001) and Wangchuk, et al. (2003), are expressed in Eqs. (4.2) and (4.3), respectively while non-linear equation for predicting Vebe time of roller compacted concrete proposed by Khunthongkeaw, et al. (2003) is shown in Eq. (4.4).

$$SL = \phi_{dps}.\alpha_{SL}.(W_{fr} - W_o) \quad (4.2)$$

$$FTS = \phi_{dps}.\alpha_{FTS}.(W_{fr} - W_o) + 45 \quad (4.3)$$

$$VB = \alpha_{VB}.(W_{fr} - W_o)^{-0.82} - 2.7 \quad (4.4)$$

where

SL is slump value of conventional concrete, cm.
FTS is flow table spread of mortar, mm.
VB is Vebe time of roller-compacted concrete, sec.
α_{FTS} is slope of flow spread vs. free water content curve, mm/kg/m^3 of mortar.
α_{SL} is slope of slump value vs. free water content curve, cm/kg/m^3 of concrete.
α_{VB} is slope of Vebe time vs. free water content curve, sec/kg/m^3 of concrete.
ϕ_{dps} is dispersion factor due to the use of water reducing admixture for modifying the slope of consistency vs. free water content of fresh concrete or mortar, encountering different unit and method of consistency measurement.

It is known that introduction of the water reducing admixtures into the mixture causes a force system, resulting in dispersion of powder particles in the matrix (Neville, 1995). The action of the water reducing admixtures on the powder particles reduces the water retainability of powder materials and the number of possible contacts amongst the particles, as well as changes the slope of consistency vs. free water content curves in Eq. (4.1). These effects cause additional deformation to concrete mixtures. Therefore, in model formulation for predicting consistency of fresh mortar and concrete with the use of the water reducing admixture, three parameters considered in this study i.e. water retainability coefficient, effective surface area of the powder materials, and slope of consistency vs. free water content curves were modified to include these effects by incorporating the reduction factors for the water retainability coefficient (ϕ_{rb}) and for the effective surface area (ϕ_{rn}) of powder materials and the dispersion factor (ϕ_{dps}) for the slope of consistency vs. free water content curves in the model. The details of these parameters will be discussed in section 4.3.

In this study, Eq. (4.1) was adopted and extended for predicting deformation capacity of SCC. It was also found that free water content in mixture had relationship with 50-cm slump flow time of SCC. As a result, it is reasonable to formulate the model for predicting velocity of deformation based on the concept of free water content too. Flow charts showing the process for predicting deformation capacity (slump flow) and velocity of deformation (50-cm slump flow time) proposed in this study are shown in Figs. 4.2 and 4.3, respectively.

Fig. 4.2 Flow chart for predicting deformation capacity (slump flow)

Fig. 4.3 Flow chart for predicting velocity of deformation (50-cm slump flow time)

4.3 Parameters Used in Model Formulation

According to the studies on workability of fresh concrete by Tangtermsirikul (1989 to 2003), major mechanisms and concepts considered in formulation of the model include water retainability of solid particles, free water content and inter-particle forces among solid particles in the concrete. The below mentioned concepts and parameters had been proven by Tangtermsirikul, et al. (1989, 2001, 2003), Khunthongkeaw, et al. (2001, 2003), and Wangchuk, et al. (2003) to be applicable for various types of deformability and therefore were used to formulate the model for predicting SCC's deformability in this study.

4.3.1 Free Water Content in Fresh Concrete

Free water means the amount of water that is free from being restricted by all solid particles and can travel independently from the solid particles in the fresh concrete (Ozawa, 1992 and Tangtermsirikul, 2001). It consists of the part of water excluding water absorbed in and adsorbed on the surface of the solid particles. Some very fine powder particles can fill in the voids among cement particles. They replace and drive out the water that is initially entrapped in those voids. This driven-out water is considered as the extra amount of free water and consequently reduces water requirement of the mixture. Free water is considered to affect the consistency of fresh concrete and it can be obtained from the equation proposed by Tangtermsirikul, et al. (2001) and Khunthongkeaw, et al. (2003) as follows

$$W_{fr} = W_u - W_{rp} - W_{ra}' + W_{aa} \tag{4.5}$$

where

W_{fr} is free water content of the mixture, kg/m^3 of concrete.
W_u is unit water content of the mixture, kg/m^3 of concrete.
W_{rp} is water restricted by powder materials, kg/m^3 of concrete.
W_{ra}' is restricted water on the surface of aggregates, kg/m^3 of concrete.
W_{aa} is extra free water due to filling effect of ultra-fine particles, kg/m^3 of concrete.

4.3.2 Water Retainability of Powder Materials

Water retainability of powder is the water restricted by powder material which includes water absorbed inside the powder particles and water retained on their surfaces. It depends on many parameters, such as porosity, surface condition, shape, size distribution and loss on ignition of the powder (Tangtermsirikul, et al., , 2001 and Khunthongkeaw, et al., 2003). The total amount of water restricted by all powders (W_{rp}) can be obtained from the summation of the product of weight of each powder and its water retainability as:

$$W_{rp} = \sum_{i=1}^{n} \beta_{pi} w_{pi} \tag{4.6}$$

where

W_{rp} is water restricted by powder materials, kg/m^3 of concrete.
β_{pi} is water retainability coefficient of powder material type i, g/g of dried weight.

w_{pi} is absolutely dried weight of powder material type i, kg/m^3 of concrete.

n is total number of powder types in the mixture.

Regarding particle shape of powders and aggregates, an irregular particle has greater amount of restricted water than the spherical one. In this study, angularity factor proposed by Powers (1968) is used to account for the effect of particle shape on water retainability and other physical properties of powders and aggregates. The angularity factor of a certain size group is related to the void content of particles as expressed by the following equation (Tangtermsirikul, et al. 2001):

$$\psi = 1 + 4.44 \cdot (\varepsilon - 0.42) \tag{4.7}$$

where

ψ is angularity factor of powder or aggregate particles.

ε is void content in the loose state of a single-size group of the solid particles.

The approximate values of angularity factor for various types of powder materials and aggregates had been recommended by Tangtermsirikul, et al. (2001), Khunthongkeaw (2001), and Wangchuk (2003) as follows

ψ = 1.0 for spherical materials, such as spherical fly ash and silica fume.

ψ = 1.1 for near spherical materials, such as river gravel and river sand.

ψ = 1.2 – 1.3 for semi-round or semi-granular powder and aggregate.

ψ = 1.4 for granular powder and aggregate, such as crushed limestone aggregate and powder, and ground granulated blast furnace slag.

Specific surface area is another parameter affecting water retainability of powder. The effect of specific area of powder on water retainability had been investigated by Khunthongkeaw, (2003) and it was found that the water retainability coefficient varied with specific surface area of powders and type of powder as shown in Fig. 4.4.

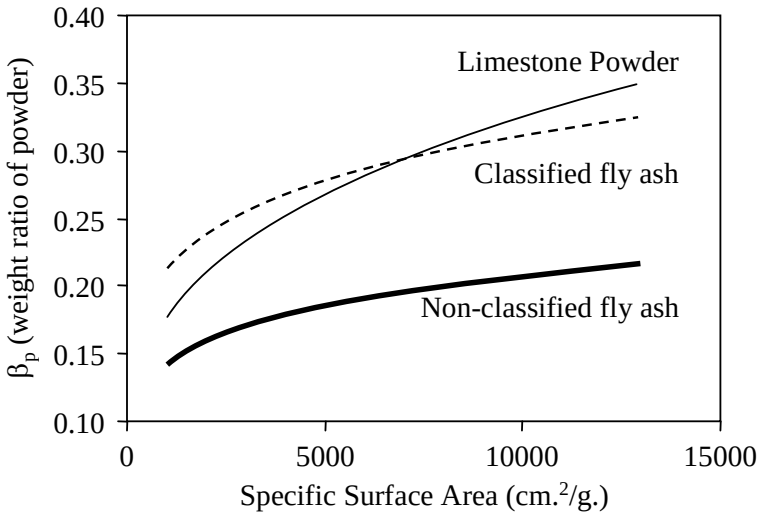

Fig. 4.4 Relationship between computed water retainability of several types of powder and their specific surface area at same specific gravity (Khunthongkeaw, 2003)

As a result, the water retainability coefficient of cement, fly ash and limestone powder has been separately formulated to have relationship with angularity factor, specific gravity, specific surface area, and loss on ignition, as in the following empirical equations (Khunthongkeaw, et al., 2003).

$$\beta_p = 0.004.\psi^{0.74}.S_p^{0.55} / \rho_p^{0.49} \quad \text{for cement} \quad (4.8a)$$

$$\beta_p = 0.028.S_p^{0.16}(2.98 + LOI)^{0.74} / \rho_p^{0.34} \quad \text{for fly ash} \quad (4.8b)$$

$$\beta_p = 0.045.S_p^{0.26} / \rho_p^{0.52} \quad \text{for limestone powder} \quad (4.8c)$$

where

β_p is water retainability coefficient of powder, g/g of dried weight.
ρ_p is specific gravity of powder.
S_p is specific surface area of powder, cm^2/g.
ψ is angularity factor.
LOI is loss on ignition of fly ash, %.

The action of water reducing admixtures, causing dispersion of powder particles, affects the system of forces inducing fresh concrete deformation. As a result, the deformation of fresh concrete is increased by reducing inter-particle forces due to the larger distance between powder particles and by increasing free water content due to the reduction of water retainability of powder materials. A reduction factor is introduced to incorporate the effect of water reducing admixture on the water retainability of powder materials. It was found by Wangchuk (2003) that this reduction factor varies as a function of the dosage and the water reducing efficiency of the admixtures as seen in Fig.4.5.

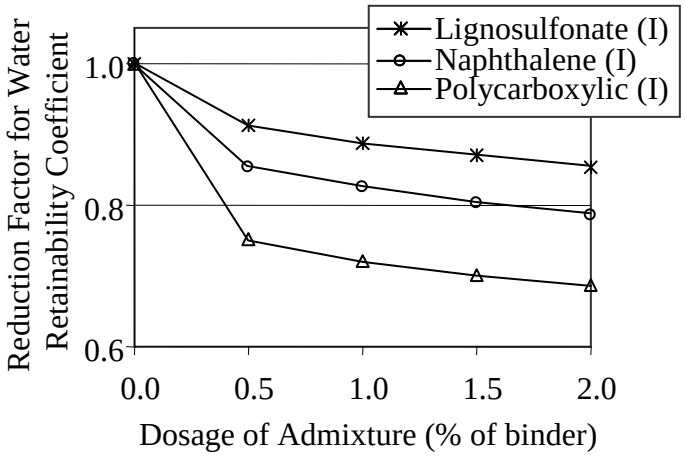

Fig. 4.5 Reduction factor for water retainability coefficient of cement due to the application of water reducing admixture (Wangchuk, 2003)

The reduction factor for the water retainability coefficient of powders (ϕ_{rb}) due to the application of water reducing admixture can be determined by the following expression.

$$\beta_p' = \phi_{rb}.\beta_p \quad (4.9)$$

where

β_p' is water retainability coefficient of powders with water reducing admixture, g/g of dried weight.

β_p is water retainability coefficient of powder without application of water reducing admixture, g/g of dried weight.

ϕ_{rb} is reduction factor for the water retainability coefficient of powders due to the application of water reducing admixture.

Since the effects of water reducing admixtures on different types of powder material are different, the reduction factor had been separately proposed by Wangchuk (2003) for cement, fly ash and limestone powder as given in the following equations.

$$\phi_{rb} = 1 - (0.08 + 0.73\ \varphi'^{\,1.9})\ \varphi^{\,(0.51 - 0.69\ \varphi')} \quad \text{for cement} \qquad (4.10a)$$

$$\phi_{rb} = 1 - (0.06 + 0.75\ \varphi'^{\,3.3})\ \varphi^{\,(0.36 - 0.43\ \varphi')} \quad \text{for fly ash} \qquad (4.10b)$$

$$\phi_{rb} = 1 - (0.24\ \varphi' - 0.014)\ \varphi^{\,(0.00004)} \quad \text{for limestone powder} \qquad (4.10c)$$

where

ϕ_{rb} is reduction factor for water retainabilty coefficient of powder materials due to the application of water reducing admixtures.

φ' is water reducing efficiency of water reducing admixtures, which can be obtained by the test explained in section 3.6 of chapter 3.

φ is dosage of water reducing admixtures, % by weight of powder.

4.3.3 Surface Water Retainability of Aggregates

Since standard condition of aggregate for mix proportioning is saturated surface-dried, the restricted water in addition to the absorbed water in the aggregate particles is considered as surface water retainability of aggregates (W_{ra}'), which can be determined from the following equation (Tangtermsirikul, et al., 2001 and Khunthongkeaw, et al. 2001, 2003):

$$W_{ra}' = \beta_s'\ w_s' + \beta_g'\ w_g' \qquad (4.11)$$

where

β_s' is surface water retainability coefficient of fine aggregate , g/g of SSD aggregate.

β_g' is surface water retainability coefficient of coarse aggregate, g/g of SSD aggregate.

w_s' is saturated surface-dried weight of fine aggregate, kg/m^3 of concrete.

w_g' is saturated surface-dried weight of coarse aggregate, kg/m^3 of concrete.

It had been reported by Tangtermsirikul, et al. (2001) and Khunthongkeaw, et al. (2001, 2003) that the surface water retainability coefficient varies with specific surface area

of aggregate. It is assumed that the water retainability of aggregates depends on irregularity and size of the particles so that specific surface area can be considered as an appropriate parameter. As a result, the derived surface water retainability coefficients of aggregates including fine and coarse aggregates are as follows (Tangtermsirikul, et al., 2001):

$$\beta_s' = 2 \times 10^{-6} (S_s)^{0.9} \quad (4.12)$$

$$\beta_g' = 2 \times 10^{-6} (S_g)^{0.9} \quad (4.13)$$

where

β_s', β_g' are surface water retainability coefficients (excluding absorption) of fine and coarse aggregates, respectively, g/g of SSD aggregate.

S_s, S_g are specific surface area of fine and coarse aggregates, respectively, cm^2/kg.

4.3.4 Additional Free Water Due to Filling Effect of Ultra-Fine Particles

If very fine powder is used in the concrete, some of these particles can fill in the voids among cement particles. This filling powder can drive away the water that is entrapped in those voids. The driven-out water is considered as the extra amount of free water (Malier, 1992). The volume of additional free water (W_{aa}) is equal to the volume of the filling particles in the voids among cement particles. Then, the mass of this extra free water content due to filling effect is determined as (Tangtermsirikul, et al., 2001 and Khunthongkeaw, et al., 2001, 2003):

$$W_{aa} = V_{fill} \times \rho_w \quad (4.14)$$

where

W_{aa} is additional free water due to filling effect of ultra-fine particles, kg/m^3 of concrete.

V_{fill} is volume of the filling particles in the voids among cement, m^3

ρ_w is specific gravity of water.

Amount of filling powder depends mainly on amount of cement, because higher cement content provides more voids to be filled by the finer powder. Therefore, the volume of the filling particles in the voids among cement (V_{fill}) can be derived as the product between solid volume of cement and a coefficient of filling, as shown in the following equation proposed by Khunthongkeaw, et al., (2001, 2003):

$$V_{fill} = F \times V_c \quad (4.15)$$

where

F is filling coefficient.

V_c is volume of cement, m^3 of the mix.

The filling coefficient (F) is affected by the ratio between size of filler particles and size of cement particles, indirectly represented by the ratio of specific surface area of the filling powder to that of cement (R), and also by the amount of the filling powder,

represented by replacement ratio (r), as shown in Fig. 4.6 (Khunthongkeaw, et al., 2001, 2003):

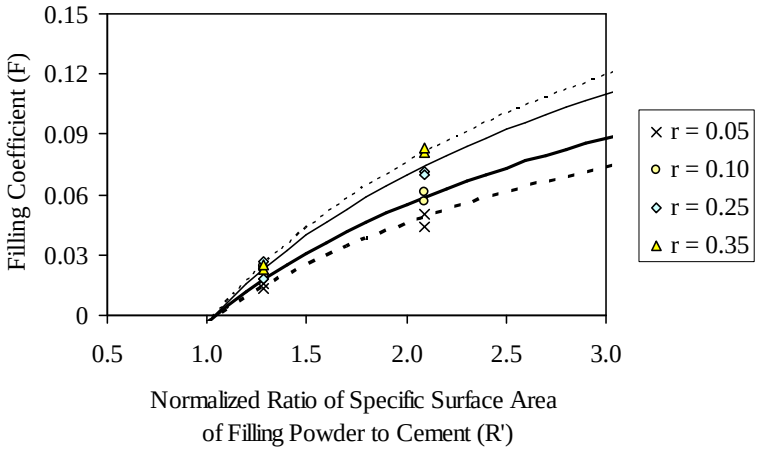

Fig. 4.6 Relationship between filling coefficient and normalized ratio of specific surface area of filling powder to cement (Tangtermsirikul, et al., 2001)

According to the shape of fine powder materials, spherical fine powder is considered to have higher ability to fill voids than non-spherical fine powder for the same specific surface area. Therefore, specific surface area ratio of filling powder to cement (R) had been modified to be the normalized specific surface area ratio of filling powder to cement (R′), by incorporating angularity factor of powder (ψ) to take into account the effect of particle shape. The mentioned factors can be obtained from the following equations, which were proposed by Khunthongkeaw (2001, 2003):

$$F = 0.25 - 0.69 / \exp(R')^{a} \quad (4.16)$$

where

$$a = 0.6\,(r)^{0.25} \quad (4.16a)$$
$$R' = 1 + 3.0(R - 1) / \psi^{3.3} \quad (4.16b)$$
$$R = S_p / S_c \quad (4.16c)$$

where

R is specific surface area ratio of filling powder to cement.
R′ is normalized ratio of specific surface area of filling powder to surface area of cement.
r is replacement ratio by weight of powder to total powders.
S_p, S_c are specific surface areas of filling powder and cement, respectively, cm^2/g.
ψ is angularity factor.

4.3.5 Minimum Free Water Content Required for Initiating Deformation

A certain amount of free water is required for overcoming inter-particle forces to initiate deformation of the fresh concrete. The forces vary with the number of feasible contact among the solids. Particles with larger surface area result in more contacts. Hence,

the inter-particle surface forces vary with surface area of the solids. Then, the amount of water for overcoming these inter-particle surface forces (W_o) had been formulated by Tangtermsirikul, et al. (2001) and Khunthongkeaw, et al. (2001, 2003) as a function of the effective surface area of solid particles as shown in Fig. 4.7.

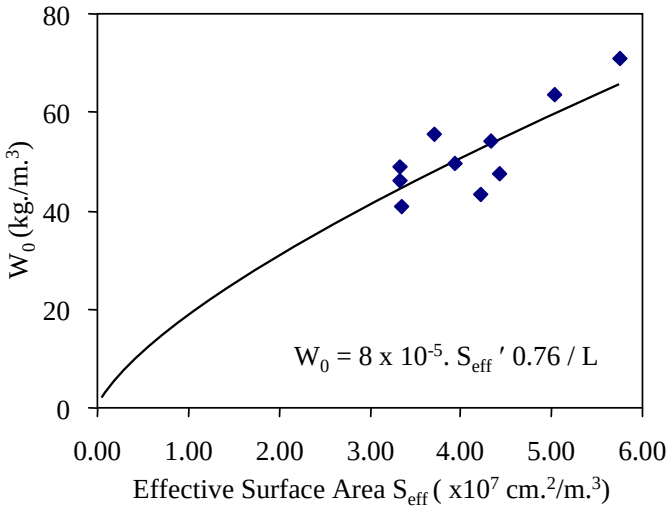

Fig. 4.7 Relationship between amounts of free water required for initiating deformation and effective surface area of solid particles (Tangtermsirikul, et al., 2001 and Khunthongkeaw, et al., 2001, 2003).

The empirical equation for the amount of water for balancing the inter-particle surface forces among solid particles is given by the following equation which was proposed by Tangtermsirikul, et al. (2001) and Khunthongkeaw, et al. (2001, 2003):

$$W_o = 8 \times 10^{-5}. S_{eff}{}' ^{0.76} / L \qquad (4.17)$$

where

W_o is the minimum free water content required for initiating deformation, kg/m^3 of concrete.
$S_{eff}{}'$ is effective surface area of solid particles, cm^2/m^3 of concrete.
L is lubrication coefficient.

Furthermore, fine fillers and spherical fillers can reduce inter-particle friction among larger particles, known as lubrication effect (Lane, 1983, Tangtermsirikul, et al., 2001 and Khunthongkeaw, et al., 2001, 2003). So, lubrication coefficient (L) is introduced to account for the lubrication effect of the fine fillers (lubricating powders). Figure 4.8 shows that the lubrication coefficient is influenced by the ratio of specific surface area of the lubricating powder to that of cement for different ratio of total powder replacement by lubricating powder (r).

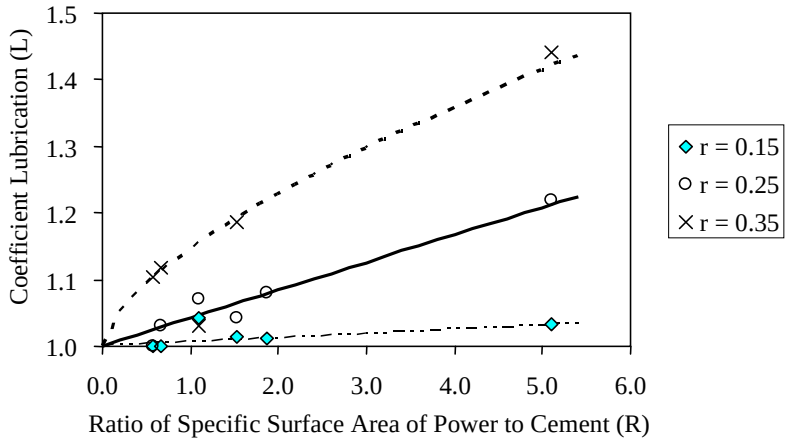

Fig. 4.8 Relationship between lubrication coefficient and ratio of specific surface area of powder to cement for different ratio of powder to total powders (Tangtermsirikul, et al., 2001 and Khunthongkeaw, et al., 2001, 2003)

So, it can be expressed as in a function of the ratio of specific surface area of the lubricating powder to that of cement, the replacement ratio of the lubricating powder in the total powder materials, and the angularity factor, as follows (Tangtermsirikul, et al., 2001 and Khunthongkeaw, et al., 2001, 2003):

$$L = 1 + (1.4 - \psi)\,(2.27\, r^{1.79})\, R^{(0.98 - 0.93\, r)} \tag{4.18}$$

where

L is lubrication coefficient.
R is ratio of specific surface area of the lubricating powder to that of cement.
r is replacement ratio of the lubricating powder in the total powder materials.
ψ is angularity factor.

4.3.6 Specific surface area of solid particles

Specific surface area, which is the surface area per unit mass, of cement and other powder materials is here determined by Blaine specific surface area technique whereas the specific surface area of aggregates (sand and gravel) is calculated from their gradation curves. The surface area of solid particles in mixtures can be derived as (Tangtermsirikul, et al., 2001 and Khunthongkeaw, et al., 2001, 2003):

$$S_{tp} = 1000 \sum_{i=1}^{n} S_{pi}\, w_{pi} \tag{4.19}$$

$$S_{ta} = 1000\,(S_s\, w_s' + S_g\, w_g') \tag{4.20}$$

where

$$S_s = \psi_s \cdot S_{so} \tag{4.20a}$$

$$S_g = \psi_g \cdot S_{go} \tag{4.20b}$$

where

S_{tp} is surface area of total powder materials in the mix, cm^2/m^3 of the mix.
S_{ta} is surface area of total aggregates in the mix, cm^2/m^3 of the mix.
w_{pi} is absolutely dry weight of powder material type i, kg/m^3 of the mix.
w_s', w_g' are saturated surface-dry weight of fine aggregate and coarse aggregate, respectively, kg/m^3 of the mix.
S_{pi} is specific surface area of powder material type i, cm^2/g.
S_s,S_g are specific surface areas of fine aggregate and coarse aggregate, respectively, cm^2/g.
n is total number of types of powder materials used in the mix
ψ_s, ψ_g are angularity factors applied to account for the irregularity of the particles of fine and coarse aggregates, respectively.
S_{so},S_{go} are specific surface area of the assumed spherical fine and coarse aggregates, respectively, cm^2/g, which can be derived from :

$$S_o = \frac{6000}{D_{av} \times \rho} \tag{4.21}$$

where

$$D_{av} = \frac{\sum D_i M_i}{\sum M_i} \tag{4.21a}$$

where

S_o is specific surface area of aggregate on spherical shape basis, cm^2/g.
D_{av} is average diameter of the aggregate particles, cm.
D_i is average dimension between the upper sieve and the sieve i on which aggregate particles are retained, cm.
M_i is weight percentage of aggregate retained on the corresponding sieve of the aggregate size group i, %.
ρ is specific gravity of the aggregate.

It is noted here that the water retainability of coarse aggregate can be practically neglected due to its small value when compared to that of the fine aggregate.

4.3.7 Effective Surface Area of Solid Particles

Effective surface area of solid particles indirectly indicates the number of feasible inter-particle contacts among the fine aggregates, coarse aggregate and powders; consequently it is related to inter-particle surface forces including friction and cohesion among solid particles in fresh concrete. It had been proposed by Tangtermsirikul (1992) and confirmed by Khayat (1999) that mixture having higher calculated effective surface area required more amount of water for initiating deformation. The effective surface area of solid particles (S_{eff}') can be determined from the summation of surface area of aggregates and surface area of powder materials that effectively contact around the aggregate as in the following equations which were proposed by Tangtermsirikul, et al. (2001) and Khunthongkeaw, et al. (2001, 2003).

$$S_{eff}' = S_{ta}' + S_{tp}' \tag{4.22}$$

where

$$S_{ta}' = \eta_a . S_{ta} \quad (4.22a)$$

$$S_{tp}' = \eta_p . \phi_{rn} . S_{tp} \quad (4.22b)$$

where

S_{eff}' is effective surface area of solid particles in the mixture, cm^2/m^3 of the mix.

S_{ta}' is effective surface area of aggregates in the mixture, cm^2/m^3 of the mix.

S_{tp}' is effective surface area of powder materials in the mixture with application of water reducing admixture, cm^2/m^3 of the mix.

S_{ta}, S_{tp} are surface area of total aggregates and total powder materials in the mix, respectively, cm^2/m^3 of the mix.

η_a, η_p are effective contact areas ratio of aggregate and powder, respectively, which can be obtained from Eqs. (4.23) and (4.24), respectively.

ϕ_{rn} is reduction factor for the effective surface area of powder materials due to the application of water reducing admixture, which can be determined from Eq. (4.25).

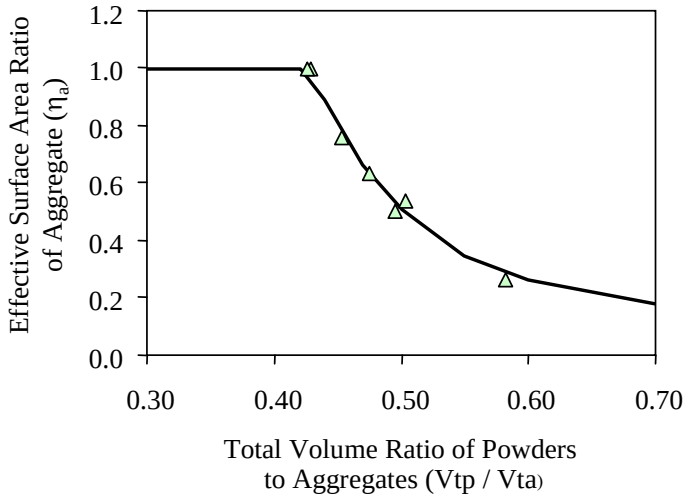

Fig. 4.9 Relationship between the effective contact area ratio of aggregates and total volume ratio of powders to aggregates in concrete (Khunthongkeaw, 2001)

The effective contact area ratio of aggregate (η_a) indicates the degree of effectiveness of surface area of aggregates, which is effectively contactable among the aggregates and it had been found to have relationship with volume ratio of powder to aggregate as shown in Fig. 4.9 and can be derived from the following equation (Khunthongkeaw, et al., 2001, 2003).

$$\eta_a = 0.01\left(\frac{V_{tp}}{V_{ta}}\right)^{-5.31} + 0.11 \qquad \leq 1.0 \quad (4.23)$$

where

η_a is effective contact area ratio of aggregate.
V_{tp} is total volume of powder, m^3/m^3 of concrete.
V_{ta} is total volume of aggregate, m^3/m^3 of concrete.

The effective contact area ratio of powder materials (η_p) indicates the ratio of surface area of powder material contacting effectively with aggregates to the total surface area of powder materials. It had been formulated by Khunthongkeaw, (2001) to have relationship with total surface area of aggregate as shown in Fig. 4.8 and in the following equation.

$$\eta_p = 0.026e^{-3\times10^{-8}\,(S_{ta})} \tag{4.24}$$

where

η_p is effective contact area ratio of powder.
S_{ta} is surface area of total aggregates in the mix, cm^2/m^3 of the mix.

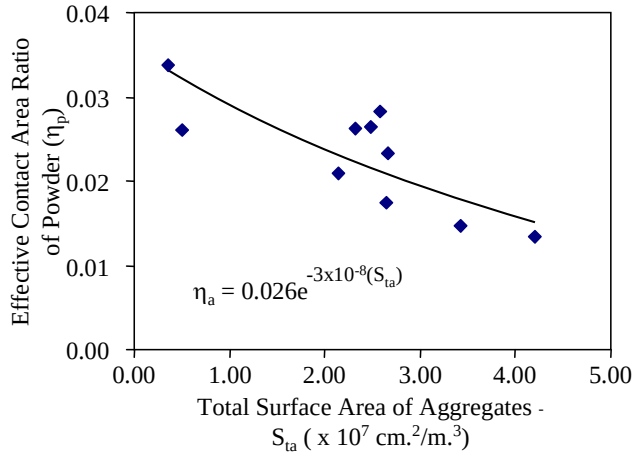

Fig. 4.10 Relationship between the effective contact area ratio of powders and total surface area of aggregates in concrete (Khunthongkeaw, 2001)

Powder particles are well dispersed and the close approach of the particles to one another is prevented when incorporating water reducing admixtures (Neville, 1995). This dispersion effect causes not only the reduction of water retainability of the powders but also the reduction of friction and cohesion among solid particles. It results in the reduction of possible powder to powder and powder to aggregates contacts, in other words, the effective surface area of solid particles, associated with powders, is reduced. A reduction factor (ϕ_{rn}) is therefore introduced to incorporate the reduction in the effective surface area of the powder due to the application of water reducing admixtures and is considered applicable only to the effective surface area of powder particles, as the dispersion force due to water reducers is not effective for dispersing the aggregate particles. The reduction factor for the effective surface area (ϕ_{rn}) was formulated by Wangchuk (2003) from the analysis of test results shown in Fig. 4.11 and could be obtained from:

$$\phi_{rn} = 1 - (0.2 + 2\,\varphi').\varphi \qquad \geq 0.4 \tag{4.25}$$

where

ϕ_{rn} is reduction factor for the effective surface area of powder materials due to the application of water reducing admixture and its value is limited between 0.4 and 1.0.

φ' is water reducing efficiency of water reducing admixtures.

φ is dosage of water reducing admixtures, % by weight of powder.

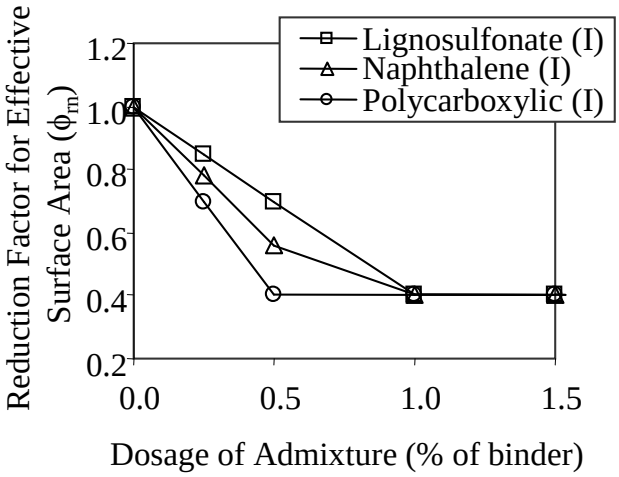

Fig. 4.11 Reduction factor for effective surface area of powder particles due to the application of water reducing admixture (Wangchuk, 2003)

4.3.8 Dispersion Factor due to the Use of Water Reducing Admixtures

The system of forces in the mixture is altered by the action of water reducing admixtures, resulting in the dispersion of powder particles. The dispersion effect improves deformation by increasing free water content due to the reduction of water retainability of powder materials and reducing inter-particle forces due to the larger distance between powder particles. This dispersion effect on the slope of consistency vs. free water content curves of fresh concrete in Eq. (4.1) is considered by introducing a factor called dispersion factor (ϕ_{dps}) in the model.

Since the dispersion effects due to the application of water reducing admixtures on different types of concrete are different due to the differences in unit and method of consistency measurement, the dispersion factor required for modifying the slope of consistency vs. free water content curves for each particular type of concrete is separately derived. Also, types of superplasticizers with different effectiveness are considered in the formulation of dispersion factor due to the differences of their mechanisms. For examples, the dispersion factors for modifying the slope of slump value vs. free water content curves of conventional concrete (α_{SL}) and that of flow table spread vs. free water content curves of mortar (α_{FTS}) in Eqs. (4.2) and (4.3), repectively, were proposed by Wangchuk (2003), which are applicable for all types of powder materials and for all types of water reducing admixtures, as shown in the following equations.

For slump value of conventional concrete with the use of lignosulfonate and naphthalene based WRA;

$$\phi_{dps} = 1 + 83.9 \cdot \varphi^{0.5} \cdot \varphi'^{0.4} \cdot \gamma^{2.79} \cdot (w/p)^{4.9} \quad (4.26a)$$

For slump value of conventional concrete with the use of polycarboxylate based WRA;

$$\phi_{dps} = 1 + 2 \times 10^3 \cdot \frac{\varphi^{3.9} \cdot \varphi'^{1.9} \cdot \gamma^{3.1}}{\exp(5.35 \cdot \varphi)} \cdot \exp\left(\frac{0.003}{(w/p)^{5.26}} \right) \quad (4.26b)$$

For flow table spread of fresh mortar;

$$\phi_{dps} = 1 + 1.274\ \varphi'^{\,0.334}\ \varphi^{\,0.24} \quad (4.26c)$$

where

ϕ_{dps} is dispersion factor for modifying the slope of consistency (with consideration of the difference in unit and method of measurement) vs. free water content of fresh mortar or concrete.
φ' is water reducing efficiency of water reducing admixtures.
φ is dosage of water reducing admixtures, % by weight of powder.
γ is ratio of volume of paste to volume of voids in the compacted aggregate phase and its value is limited from 1.1 to 1.3.
w/p is water to powder ratio.

4.3.9 Water-Reducing Efficiency of Admixtures

Water reducing admixtures are surface-active agents and are adsorbed on the powder particles causing dispersion of the powder particles. Therefore, the powder particles have greater mobility and the water trapped in the flocculated system is freed. Superplasticizer or high range water reducing admixtures are commonly used in production of SCC. Melamine sulphonate, naphthalene sulphonate, and polycarboxylate acid are examples of popular types of superplasticizer which render different dispersion mechanisms and effectiveness. The water reducing efficiency (φ') of water reducing admixtures is therefore introduced to account for their effectiveness in this study and can be obtained by the test method and from Eq. (3.2), which is explained in section 3.6 in Chapter 3.

4.4 Effects of Superplasticizer on Deformability of SCC

4.4.1 Effect of Type and Dosage of Superplasticizer on Deformability

It was confirmed from Figs. 4.12 to 4.17 that, when introducing superplasticizer into the mixtures, the dispersion of powder particles altered deformation capacity due to the increase of the mobility of powder particles. It can be seen that slump flow of all tested mixtures increased with the increase of dosage of superplasticizers. It was because the actions of the higher dosage of superplasticizers resulted in the increase of the free water content in the mixtures by reducing the water retainability of powder materials, as well as caused the reduction of the minimum free water content required for initiating deformation by altering the number of possible contacts amongst the particles including friction and cohesion forces among solid particles.

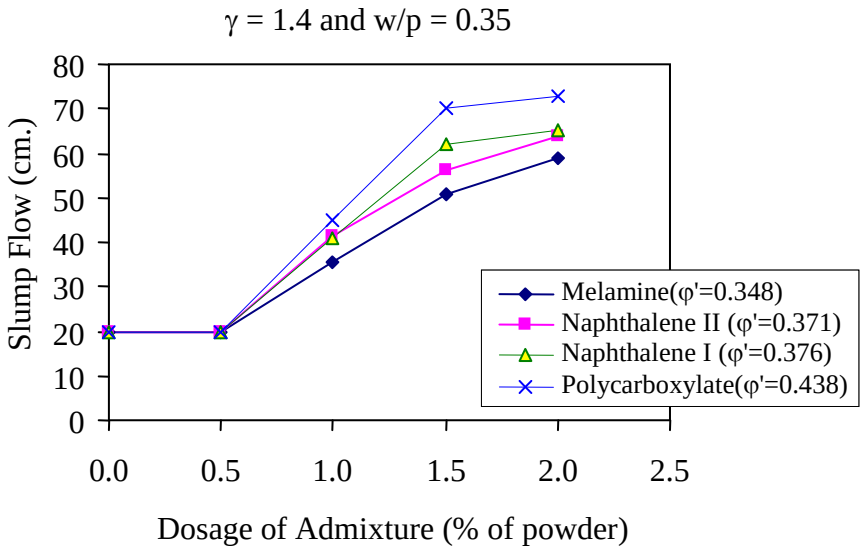

Fig. 4.12 Relationship between dosage of admixture and slump flow for different types of superplasticizer of the mixtures with γ = 1.4 and w/p = 0.35

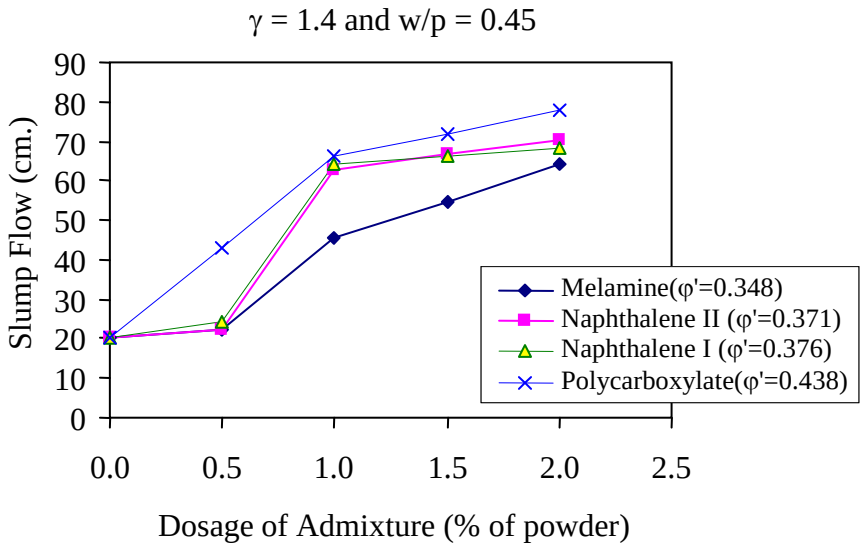

Fig. 4.13 Relationship between dosage of admixture and slump flow for different types of superplasticizer of the mixtures with γ = 1.4 and w/p = 0.45

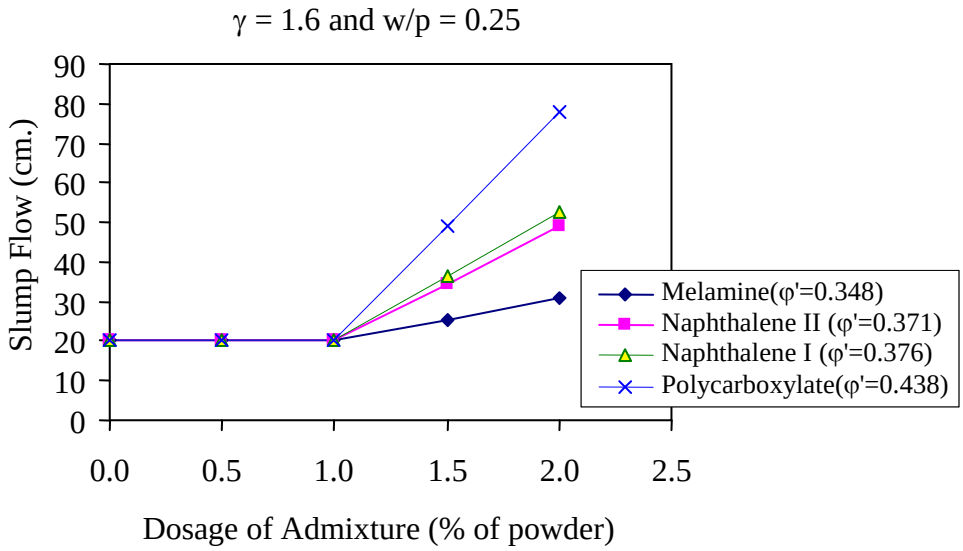

Fig. 4.14 Relationship between dosage of admixture and slump flow for different types of superplasticizer of the mixtures with γ = 1.6 and w/p = 0.25

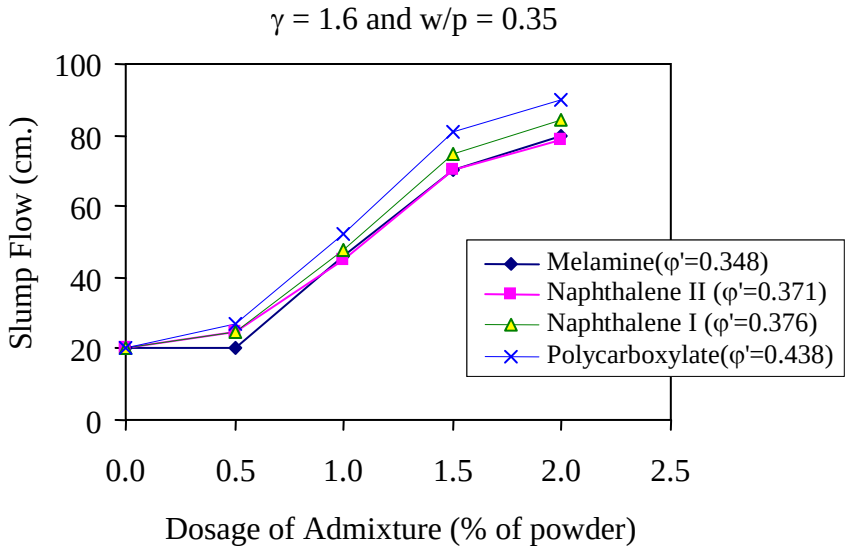

Fig. 4.15 Relationship between dosage of admixture and slump flow for different types of superplasticizer of the mixtures with γ = 1.6 and w/p = 0.35

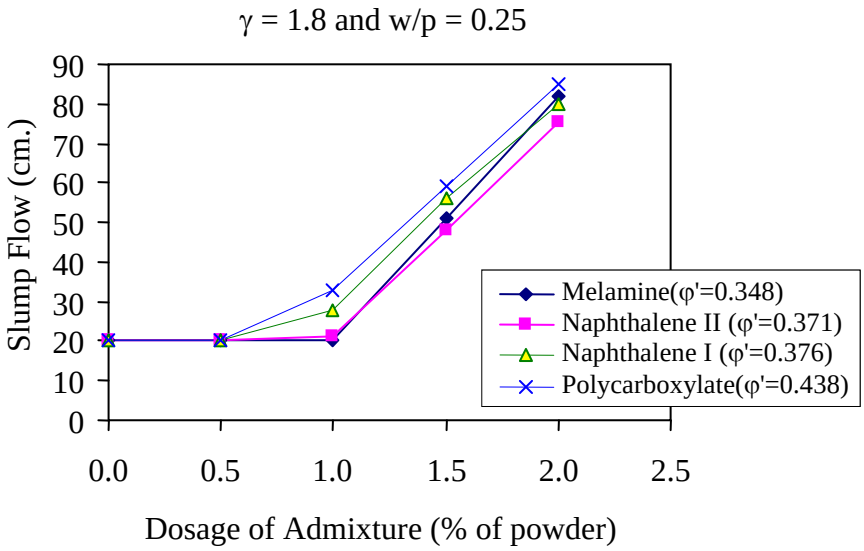

Fig. 4.16 Relationship between dosage of admixture and slump flow for different types of superplasticizer of the mixtures with γ = 1.8 and w/p = 0.25

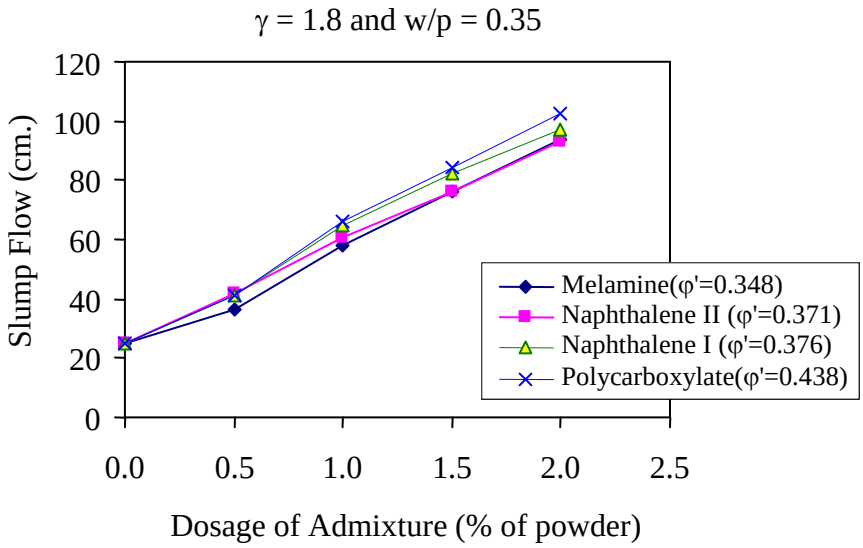

Fig. 4.17 Relationship between dosage of admixture and slump flow for different types of superplasticizer of the mixtures with γ = 1.8 and w/p = 0.35

On the other hand, Figs. 4.18 to 4.22 revealed that T_{50} of all tested mixtures reduced with the increase of dosage of superplasticizers. This was again due to the dispersion effects from the presence of superplasticizers on the water retainability of powders and the number of possible contacts amongst the particles (friction and cohesion forces among particles).

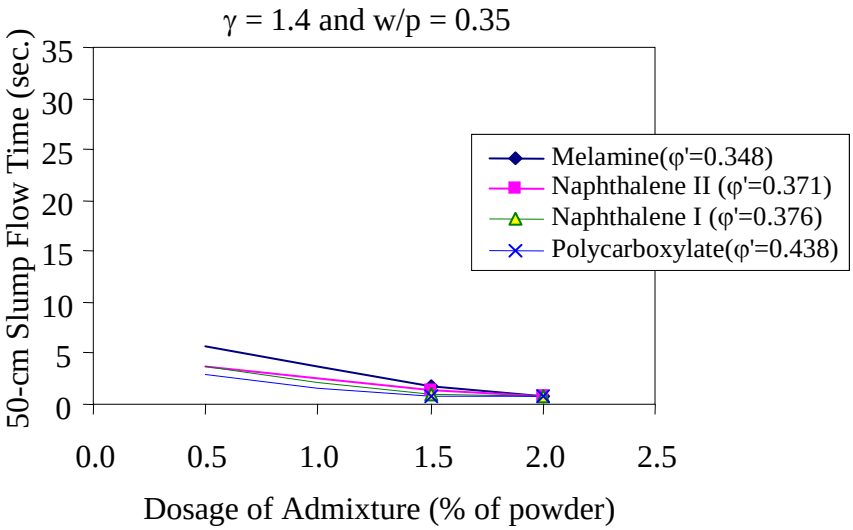

Fig. 4.18 Relationship between dosage of admixture and 50-cm slump flow time for different types of superplasticizer of the mixtures with γ = 1.4 and w/p = 0.35

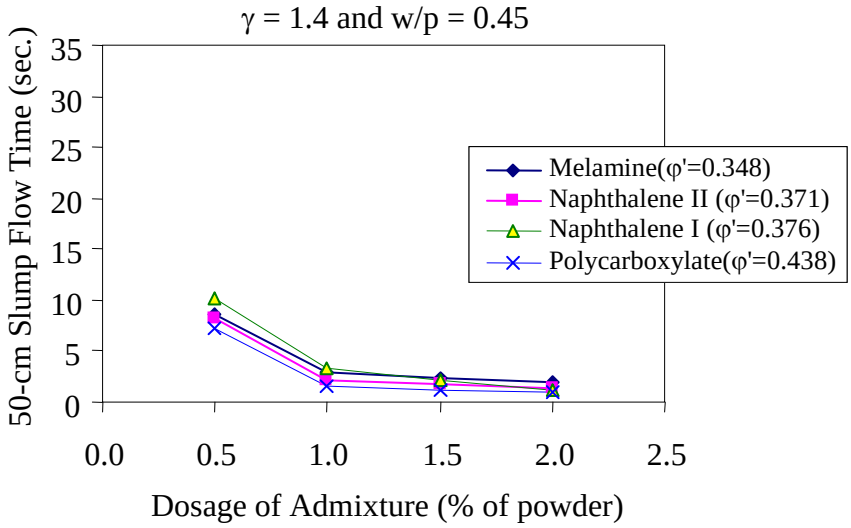

Fig. 4.19 Relationship between dosage of admixture and 50-cm slump flow time for different types of superplasticizer of the mixtures with γ = 1.4 and w/p = 0.45

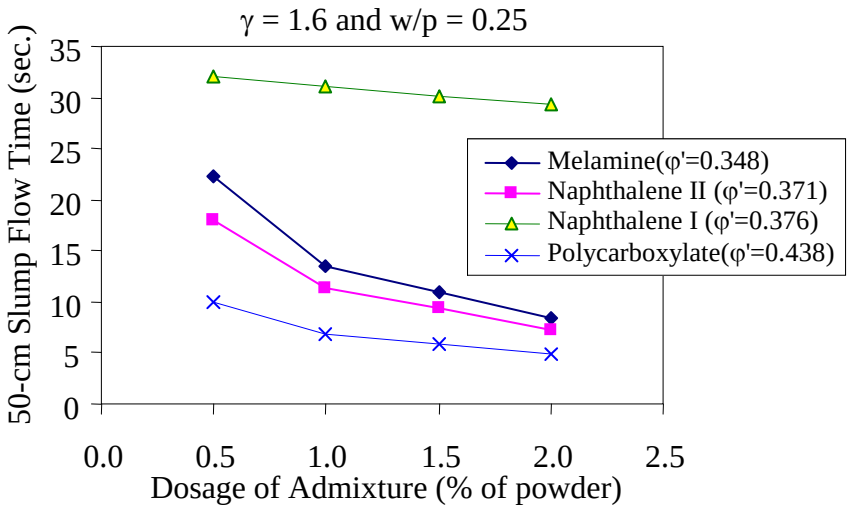

Fig. 4.20 Relationship between dosage of admixture and 50-cm slump flow time for different types of superplasticizer of the mixtures with γ = 1.6 and w/p = 0.25

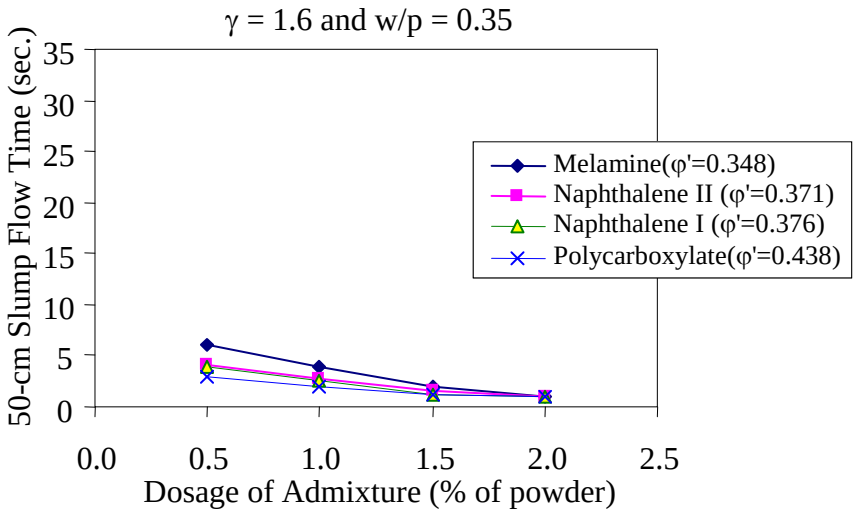

Fig. 4.21 Relationship between dosage of admixture and 50-cm slump flow time for different types of superplasticizer of the mixtures with γ = 1.6 and w/p = 0.35

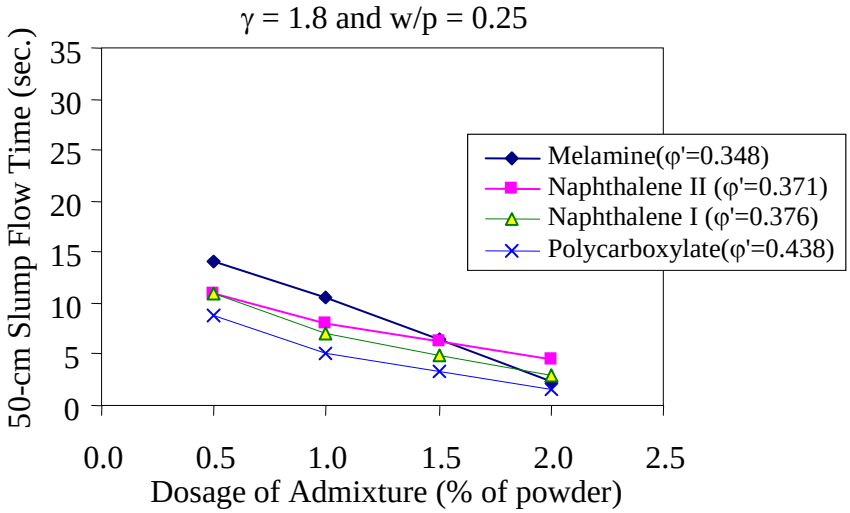

Fig. 4.22 Relationship between dosage of admixture and 50-cm slump flow time for different types of superplasticizer of the mixtures with γ = 1.8 and w/p = 0.35

Clearly, it can be seen from Figs 4.12 to 4.22 that the polycarboxylate superplasticizer is more effective than the naphthalene and melamine based superplasticizers. It is known that the mechanisms to cause dispersion of polycarboxylate typed superplasticizer are different from the others, i.e. steric hindrance and electrostatic repulsion.

4.4.2 Effect of Water to Powder Ratio on Deformability

In mix proportioning of the powder-typed SCC, low water to powder ratio (w/p) is normally recommended to enhance cohesiveness and to minimize bleeding for eventually achieving resistance to segregation and passing ability (Okamura, et al., 1995, Tangtermsirikul, et al., 2000, and Domone, 2000). By considering the mixtures with low to medium w/p ratio (0.25 to 0.45 as tested in this study), Figs. 4.23 to 4.26 indicated that at the similar ratio of volume of paste to volume of voids in the compacted aggregate phase (γ) and dosage of superplasticizer, all types of superplasticizer were more effective at the higher water to powder ratio.

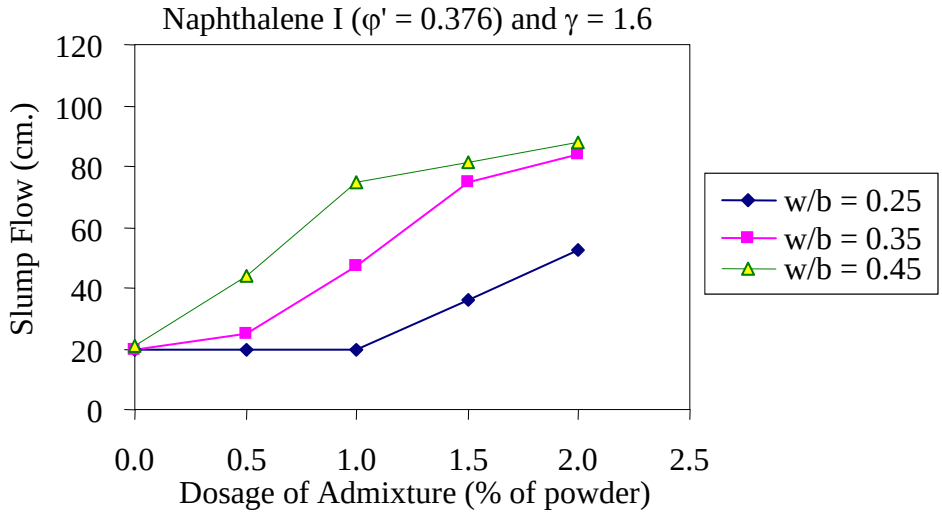

Fig. 4.23 Relationship between dosage of naphthalene-I based superplasticizer and slump flow for different ratio of water to powder (w/p)

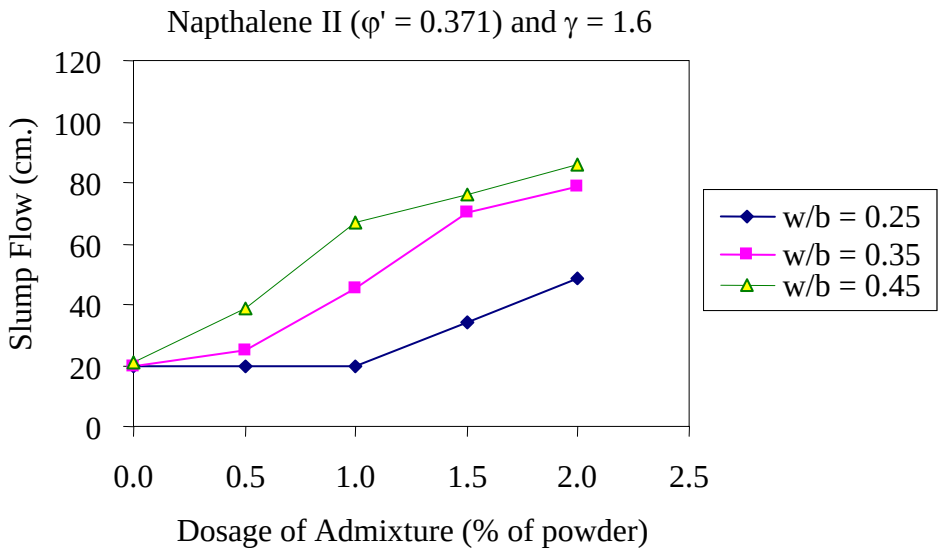

Fig. 4.24 Relationship between dosage of naphthalene-II based superplasticizer and slump flow for different ratio of water to powder (w/p)

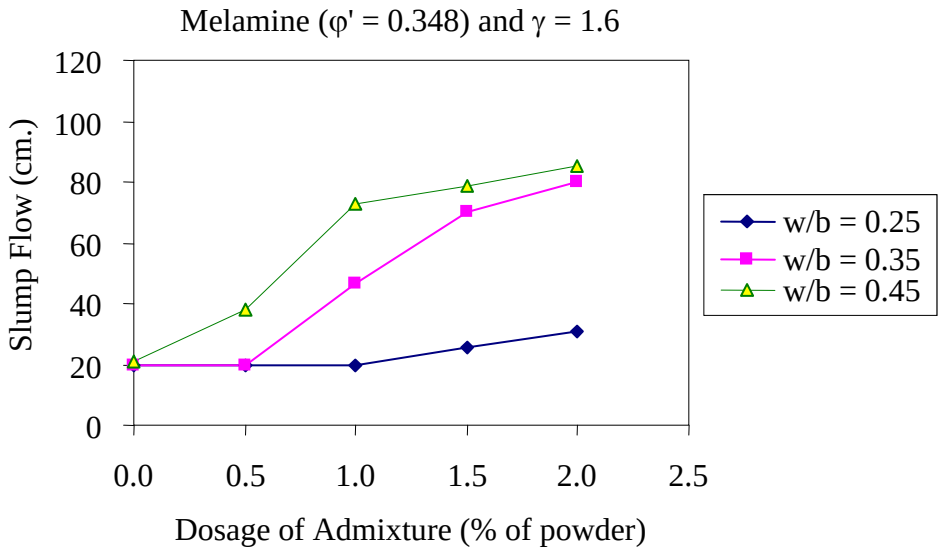

Fig. 4.25 Relationship between dosage of melamine based superplasticizer and slump flow for different ratio of water to powder (w/p)

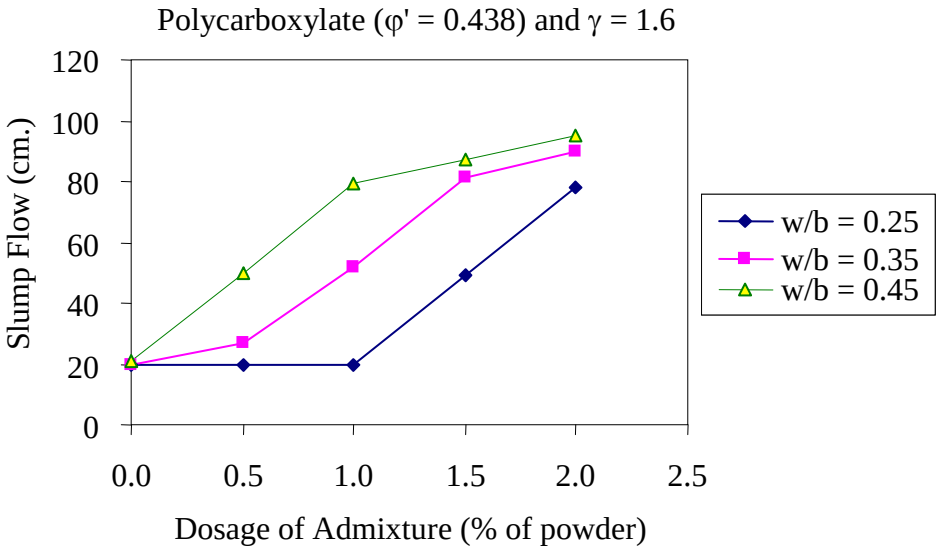

Fig. 4.26 Relationship between dosage of polycarboxylate based superplasticizer and slump flow for different ratio of water to powder (w/p)

Test results in Figs. 4.27 to 4.30 also revealed that at the similar γ value and dosage of superplasticizer, T_{50} reduced with the increase of the water to powder ratio due to the higher free water and the lower content of the minimum free water for initiating deformation in the mixtures caused by the dispersion effect due to superplasticizers on powder materials. However, the differences of T_{50} of the mixtures with different w/p ratios became smaller at high superplasticizer dosage.

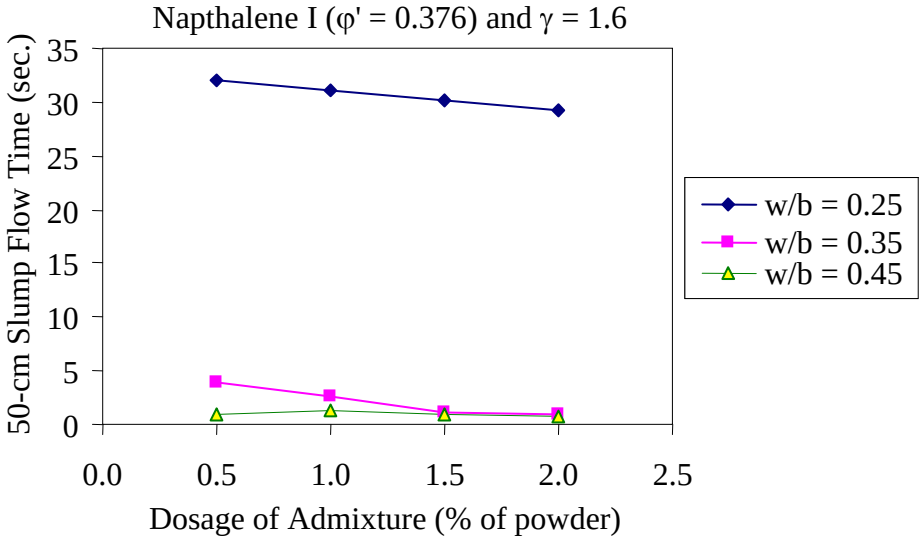

Fig. 4.27 Relationship between dosage of naphthalene-I based superplasticizer and 50-cm slump flow time for different ratio of water to powder (w/p)

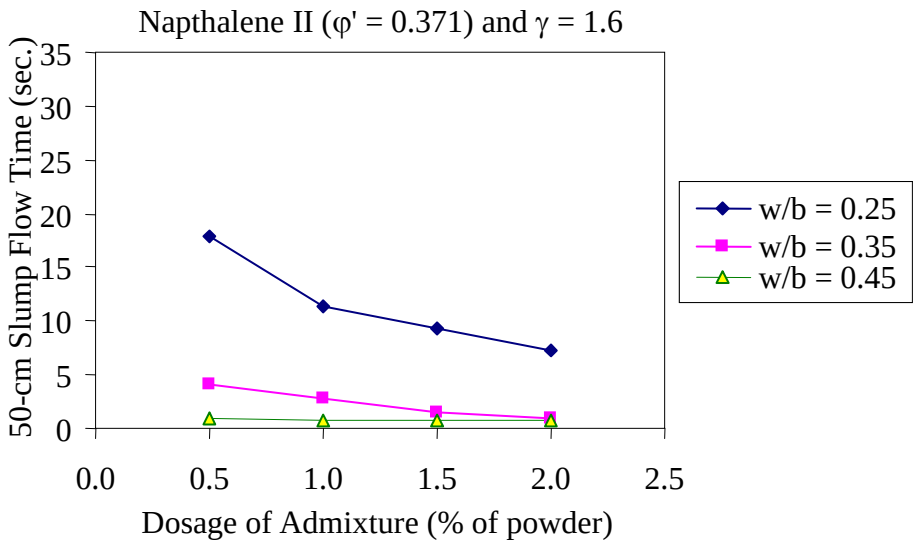

Fig. 4.28 Relationship between dosage of naphthalene-II based superplasticizer and 50-cm slump flow time for different ratio of water to powder (w/p)

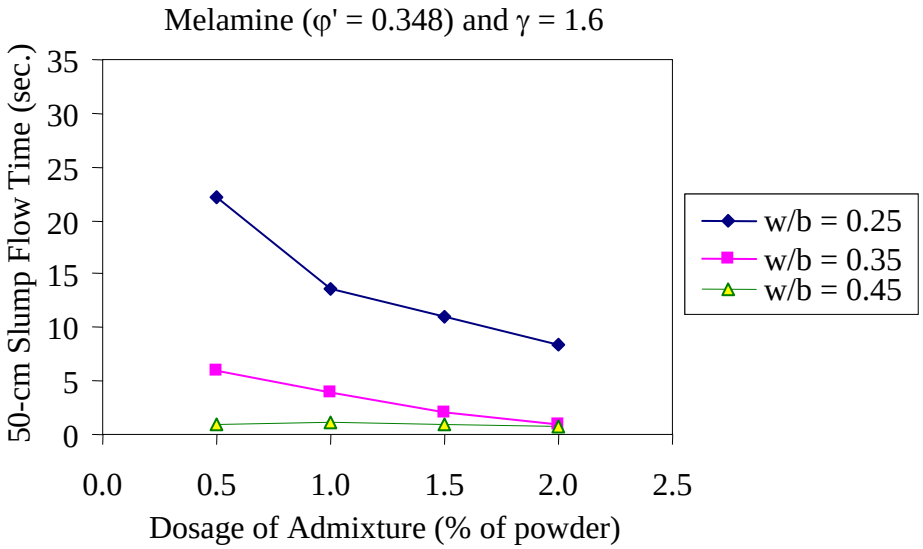

Fig. 4.29 Relationship between dosage of melamine based superplasticizer and 50-cm slump flow time for different ratio of water to powder (w/p)

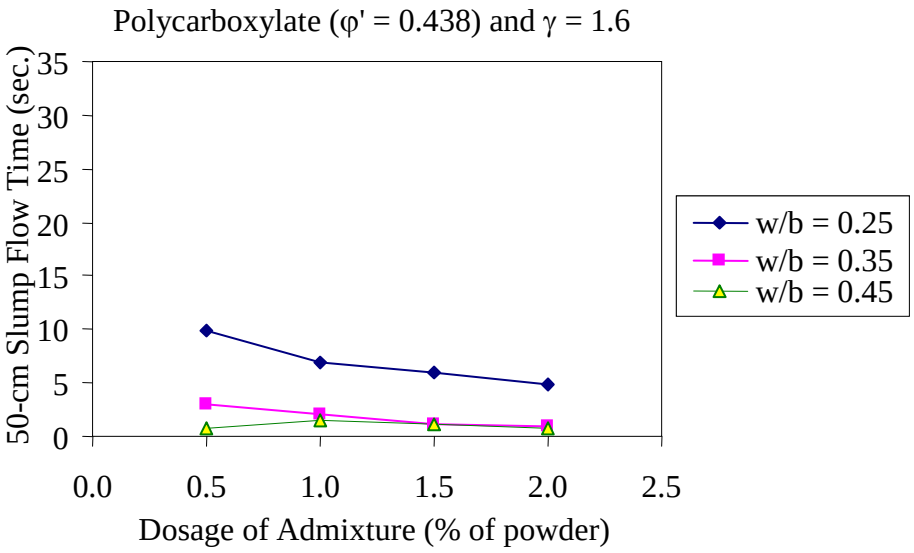

Fig. 4.30 Relationship between dosage of polycarboxylate based superplasticizer and 50-cm slump flow time for different ratio of water to powder (w/p)

4.4.3 Effect of Ratio of Paste Volume to Void Content of Compacted Aggregate Phase on Deformability

It was found from Figs. 4.31 to 4.33 that at the similar water to powder ratio and dosage of each type of superplasticizer, mixtures having larger paste content encountered larger superplasticizer effect. This was because the mixtures containing larger paste content had better deformability in nature.

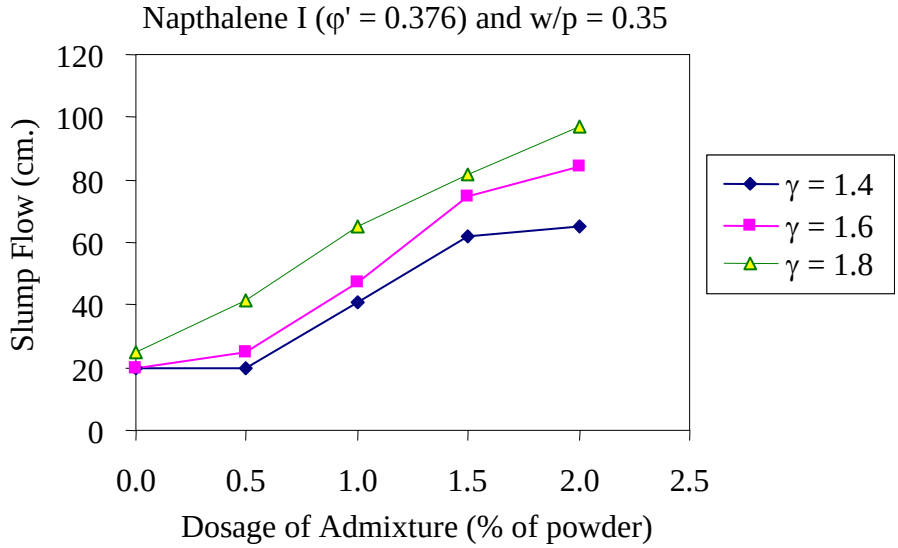

Fig. 4.31 Relationship between dosage of naphthalene-I based superplasticizer and slump flow for different ratio of paste volume to void content of compacted aggregate phase (γ)

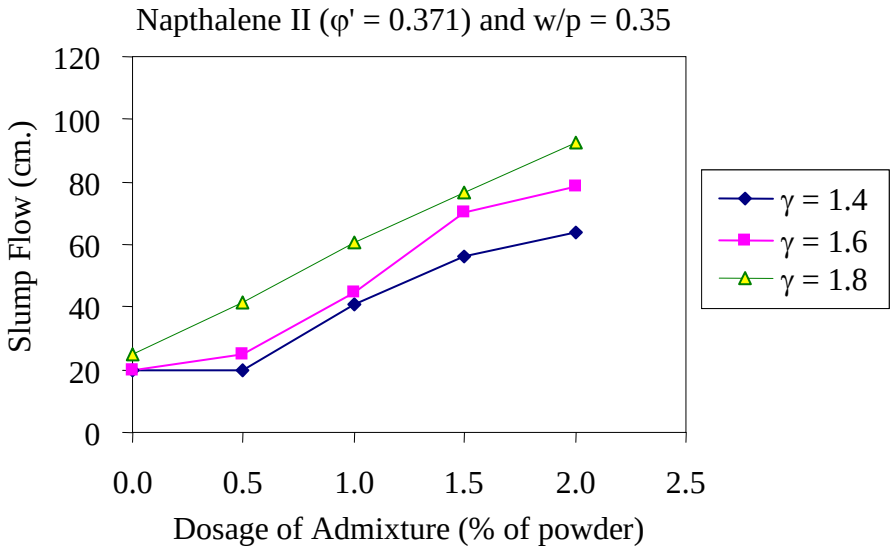

Fig. 4.32 Relationship between dosage of naphthalene-II based superplasticizer and slump flow for different ratio of paste volume to void content of compacted aggregate phase (γ)

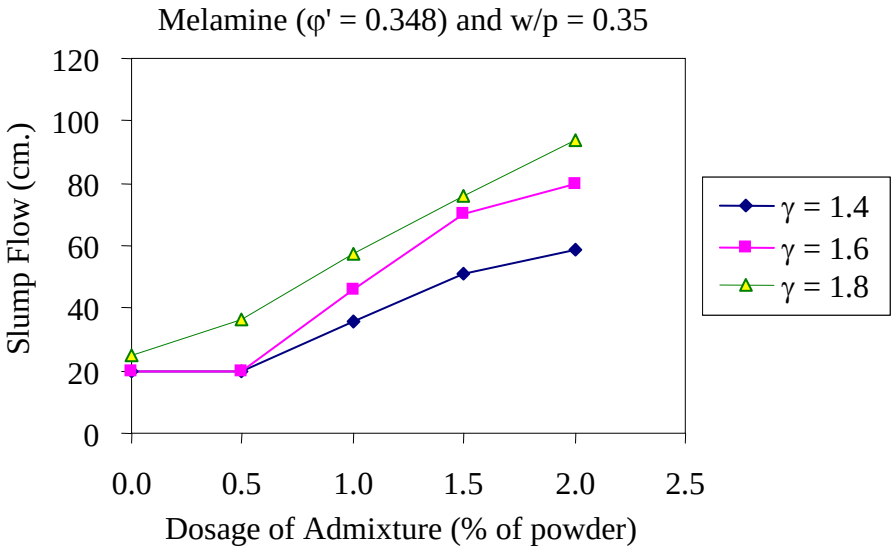

Fig. 4.33 Relationship between dosage of melamine based superplasticizer and slump flow for different ratio of paste volume to void content of compacted aggregate phase (γ)

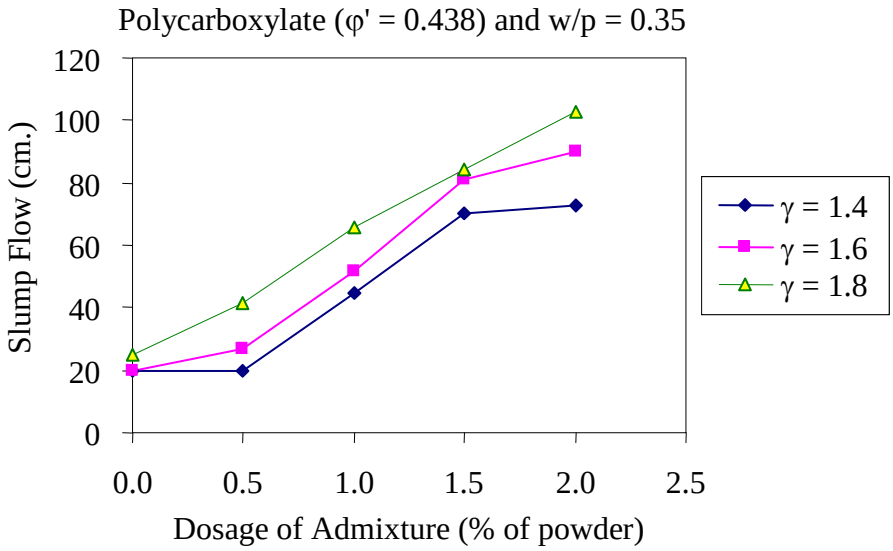

Fig. 4.34 Relationship between dosage of polycarboxylate based superplasticizer and slump flow for different ratio of paste volume to void content of compacted aggregate phase (γ)

Figs. 4.35 to 4.38 revealed that at the similar w/p ratio and dosage of superplasticizer, T_{50} reduced with the increase of the ratio of volume of paste to volume of void in the compacted aggregate phase. The difference also became smaller at higher superplasticizer dosages. This is because, at the same free water content, the increase of paste content reduces the number of possible contacts between aggregate particles, so the aggregate-to-aggregate frictions are reduced.

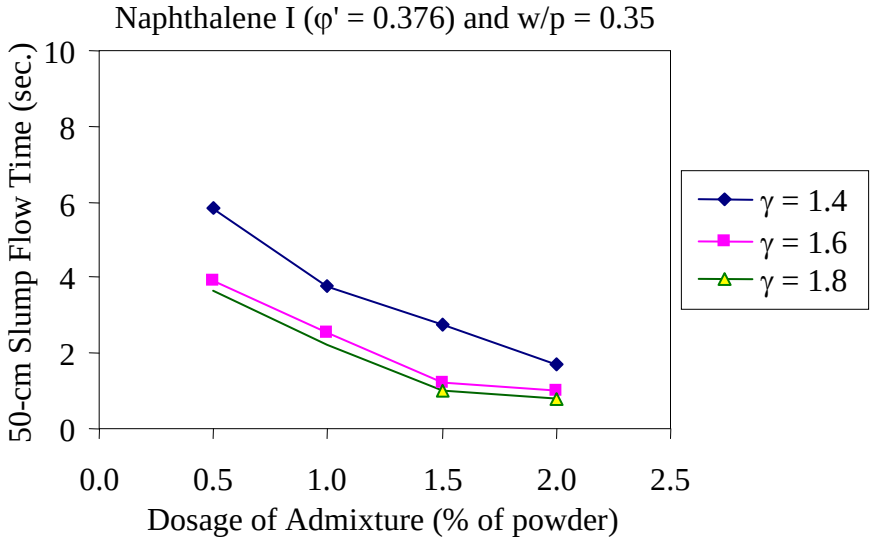

Fig. 4.35 Relationship between dosage of naphthalene-I based superplasticizer and 50-cm slump flow time for different ratio of paste volume to void content of compacted aggregate phase (γ)

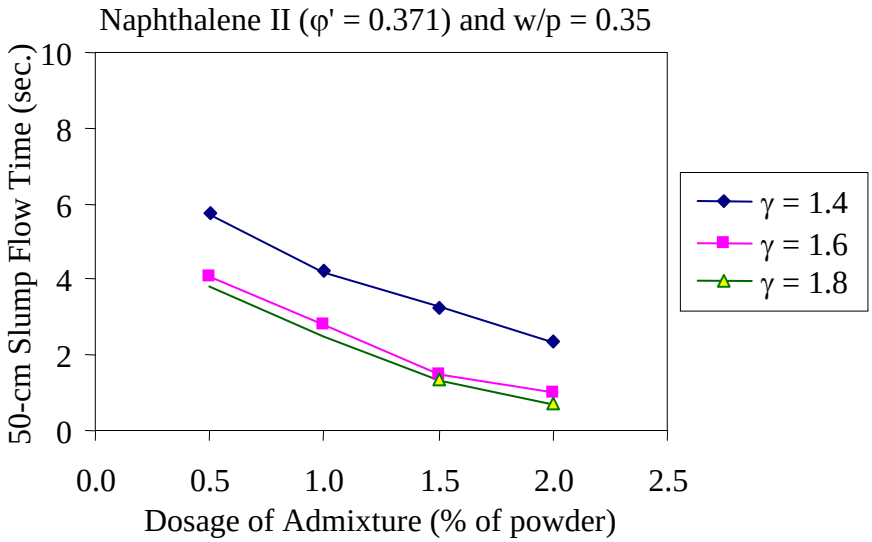

Fig. 4.36 Relationship between dosage of naphthalene-II based superplasticizer and 50-cm slump flow time for different ratio of paste volume to void content of compacted aggregate phase (γ)

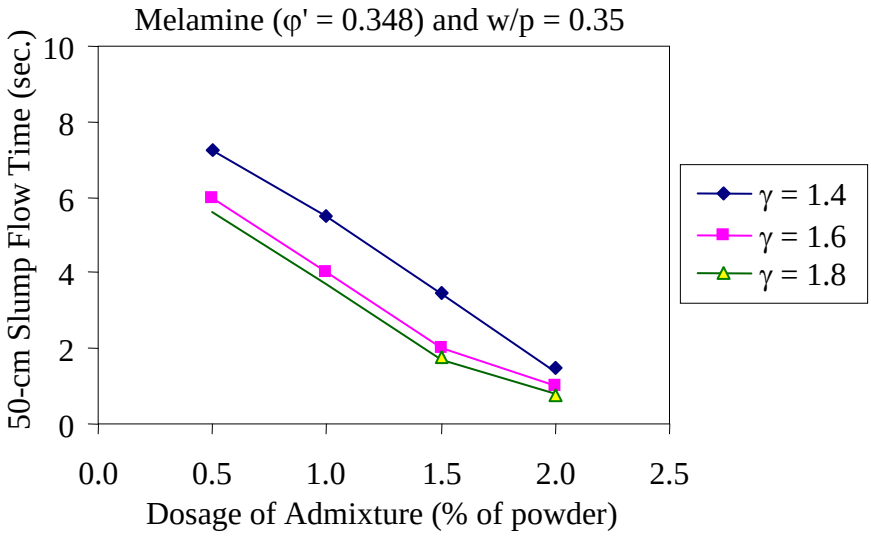

Fig. 4.37 Relationship between dosage of melamine based superplasticizer and 50-cm slump flow time for different ratio of paste volume to void content of compacted aggregate phase (γ)

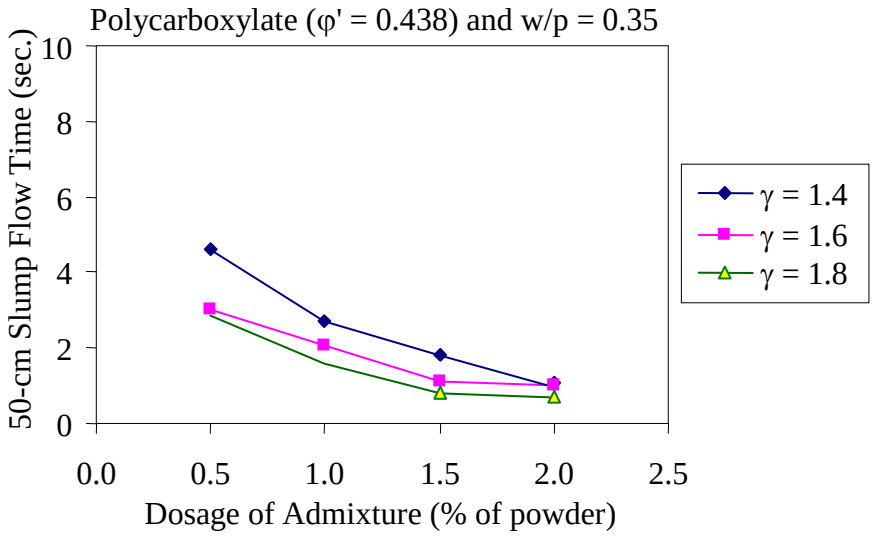

Fig. 4.38 Relationship between dosage of polycarboxylate based superplasticizer and 50-cm slump flow time for different ratio of paste volume to void content of compacted aggregate phase (γ)

4.4.4 Dispersion Factor

In this study, the dispersion effect due to the action of superplasticizer on powder materials was considered by introducing a parameter namely dispersion factor to modify the slope of deformation vs. free water content curves in the model formulation. The dispersion factor of each particular type of superplasticizer (ϕ_{dps}) was formulated from the analysis of the experimental data in Table B-1 as a function of ratio of paste volume to void volume of the compacted aggregate phase (γ), water to powder ratio, water reducing efficiency and dosage of superplasticizer as in the Eqs. (4.27) and (4.28).

For SCC mixture with the use of the naphthalene and melamine based superplasticizer;

$$\phi_{dps} = 1 + \{13.9 \cdot \varphi^{0.68} \cdot \varphi'^{1.41} \cdot \gamma^{1.03} \cdot (w/p)^{1.13} - 0.44\} \qquad (4.27)$$

For SCC mixture with the use of the polycarboxylate based superplasticizer;

$$\phi_{dps} = 1 + \left\{ \frac{2.98 \cdot \varphi^{0.86} \cdot \varphi'^{1.9} \cdot \gamma^{1.04} \cdot \exp(2.07 \cdot (w/p))}{\exp(0.03 \cdot \varphi)} - 0.9 \right\} \qquad (4.28)$$

where

ϕ_{dps} is dispersion factor for modifying the slope of deformation vs. free water content relationship.
φ' is water reducing efficiency of water reducing admixtures.
φ is dosage of superplasticizer, % by weight of powder.
γ is ratio of volume of paste to volume of voids in the compacted aggregate phase and its value is limited from 1.4 to 1.8.
w/p is water to powder ratio.

Eq. (4.27a) is for naphthalene and melamine based superplasticizers in which the dispersion mechanism is electrostatic repulsion whereas Eq. (4.27b) is for polycarboxylate based superplasticizer with the steric hindrance mechanism. It is noted here that there is no guarantee that Eq. (4.27a) will be good for all superplasticizers with the electrostatic repulsion mechanism or that Eq. (4.27b) will be good for all superplasticizers with the steric hindrance mechanism.

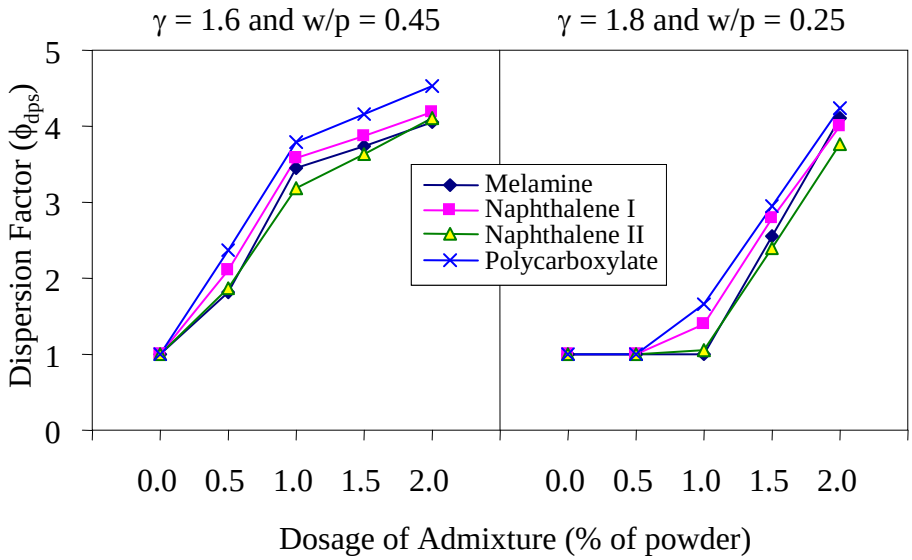

Fig. 4.39 Dispersion factor (ϕ_{dps}) of different types of superplasticizers for SCC

Fig. 4.39 shows the relationship between the dispersion factor and dosage for different types of superplasticizer. It was confirmed that polycarboxylate based superplasticizer has the highest dispersion factor followed by naphthalene based and others.

The dispersion factor will be used in the equations for predicting slump flow value (Eq. (4.28)) and 50-cm slump flow time (Eq. (4.29)) in sections 4.5 and 4.6, respectively. It is noted here that although the values of dispersion factor, ϕ_{dps}), one of the main parameters in the proposed model, was obtained from back analysis of the experimental data of the author's own test results, the verification tests by using test results from other researchers showed that the proposed models could be used to predict the of slump flow and T_{50} with satisfactory accuracies (see details in the section of Verification). This shows that the dispersion factor, ϕ_{dps}) can be applied not only for the SCC mixtures tested by the author.

4.4.5 Modifications for Ratio of Volume of Paste to Volume of Voids in the Compacted Aggregate Phase Due to the Filling Effect of Very Fine Sand Particles

Test results of the effect of very fine sand on deformation capacity of SCC in section 7.4.2 in Chapter 7 indicate that the replacement of normal sand with a few percent of very fine sand (for example 10 %) increases slump flow due to filling ability of the finer particles among the aggregate particles. In addition, it was found in section 4.5.1 that the larger paste content results in the larger slump flow. It was therefore assumed that when very fine sand is used to partially replace total fine aggregates at small percentage by weight, the slump flow is improved by the additional paste volume as very fine sand can be a part of the paste. The ratio of volume of paste to volume of voids in compacted aggregate

phase (γ) has to be modified to incorporate this filling effect and is determined in Eqs. (4.29) and (4.30).

$$\gamma' = \gamma_o + \gamma_{vfs} \tag{4.29}$$

where

$$\gamma_{vfs} = \frac{V_{p-vfs}}{V_{void}} \tag{4.30}$$

where

γ' is the modified ratio of volume of paste to volume of voids in the compacted aggregate phase due to the use of a few of very fine sand to replace fine aggregates.

γ_o is ratio of volume of paste to volume of voids in the compacted aggregate phase of the mixture without very fine sand.

γ_{vfs} is ratio of additional volume of paste to volume of voids in the compacted aggregate phase due to the use of a few percent of very fine sand to replace fine aggregates.

$V_{p\text{-}vfs}$ is additional volume of paste due to the use of a few percent of very fine sand to replace fine aggregates, m^3 of the mix.

V_{void} is volume of void in the densely compacted total aggregate phase (fine and coarse aggregate) in a unit boundary volume of the aggregate, m^3 of the mix.

The volume of additional paste due to the use of very fine sand ($V_{p\text{-}vfs}$) was assumed to be equal to the volume of very fine sand that has the abilities to fill in the voids among the aggregates particles and to behave like a powder in the concrete ($V_{vfs\text{-}fill}$) which was derived from the analysis of test results in section 7.4.2 in chapter 7 as the following equation.

$$V_{vfs\text{-}fill} = \Omega . V_{vfs} \tag{4.31}$$

where

$V_{vfs\text{-}fill}$ is volume of the filling particles of very fine sand in the voids among compacted aggregates, m^3 of the mix.

V_{vfs} is volume of very fine sand, m^3 of the mix.

Ω is filling factor due to the use of very fine sand.

The filling factor due to the use of very fine sand (Ω) was found to be 0.32 for 10 % very fine sand replacement of the total fine aggregates. The proper function for Ω should be determined by conducting more tests in the future.

4.5 Model for Predicting Deformation Capacity of SCC

Slump flow value is generally used as the measuring value for deformation capacity of self-compacting concrete. Test results from the previous study by Ozawa, et al. (1992)

confirmed that free water content in mixture has a relationship with the slump flow of SCC. Therefore, the model for predicting slump flow was formulated based on the concepts of free water content in the mixture as mentioned before in section 4.2.

4.5.1 Relationship between Slump Flow and Free Water Content

It was found that the relationship between free water content and slump flow of SCC existed as seen in Fig. 4.40. The figure also shows that the greater slump flow was obtained from mixture with the larger paste content at constant volume of free water content, in other words, the secant slopes of slump flow vs. free water content curve increased with the increase of ratio between paste volume and void content of compacted aggregate phase (γ). In addition, by introducing superplasticizers, the dispersion of powder materials caused the secant slopes of slump flow vs. free water content curves to even increase, due to the increase of mobility of powder particles.

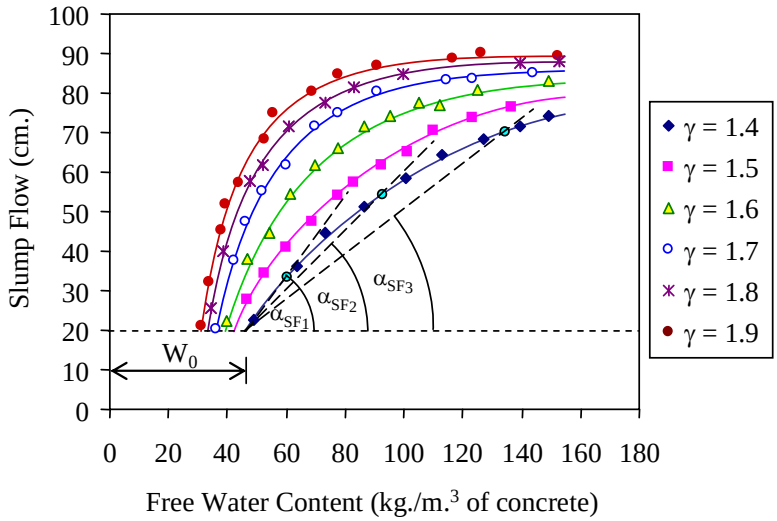

Fig. 4.40 Relationship between slump flow and free water content in the mixtures

Consequently, a linear equation was modified from Eq.(4.1) to relate the slump flow measurement with free water content and other parameters i.e. the secant slope of the slump flow vs. free water content curve, the minimum free water content required for initiating slump flow, and the dispersion factor due to the use of superplasticizers, as:

$$SF = \phi_{dps}.\alpha_{SF}.(W_{fr} - W_o) + 20 \quad (4.32)$$

where

SF	is slump flow value, cm.
ϕ_{dps}	is dispersion factor due to the application of superplasticizer.
α_{SF}	is secant slope of slump flow vs. free water content curve, cm/kg/m^3 of concrete.
W_{fr}	is volume of free water in the mixture, kg/m^3 of concrete.
W_o	is the minimum free water content required for making slump flow over 20 cm, kg/m^3 of concrete.

It is noted here that the minimum slump flow value is 20 cm as it is the bottom diameter of the test cone and this is the reason why "b" in Eq. (4.1) is set as 20 cm in Eq. (4.44). This equation is limited for the slump flow values not over 80 cm.

4.5.2 Secant Slope of Slump flow vs. Free Water Content Curve

It can be seen from Fig.4.40 that the secant slope of slump flow vs. free water content curve varied with free water content and depended on the ratio of paste volume to void content of compacted aggregate phase (γ). Fig. 4.41 indicated that at the same ratio of paste volume to void content of compacted aggregate phase, when free water content increased, the secant slope of slump flow vs. free water content curve decreased. It is considered to be due to the nature of powder-typed SCC, in which the lower viscosity and the smaller deformation capacity are usually obtained from the mixture that has the larger free water content (Tangtermsirikul, et al, 2000). This is supported by the relationship between slump flow and T_{50} of the mixtures with different free water content as presented in Fig. 4.42 that the mixtures with higher free water content have smaller T_{50} (lower viscosity).

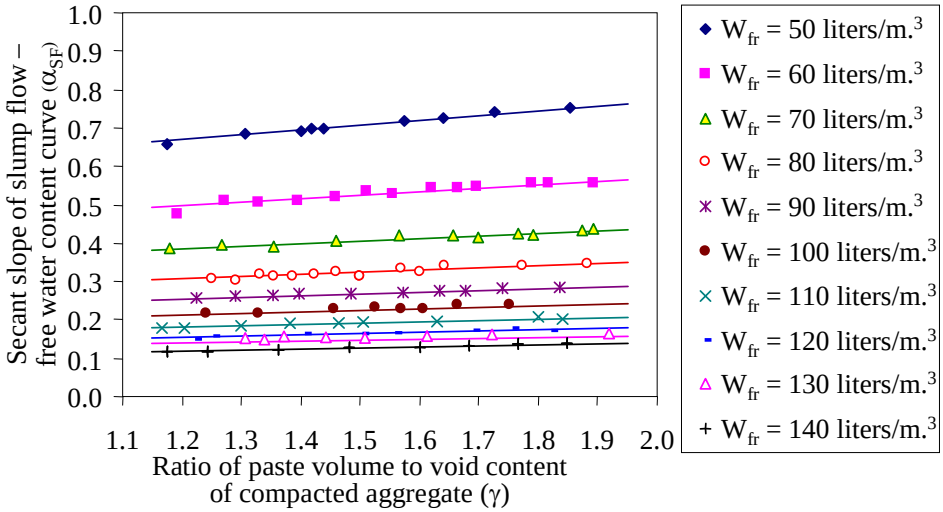

Fig. 4.41 Relationship between the secant slope of slump flow vs. free water content curve and the ratio of paste volume to void content of compacted aggregate (γ)

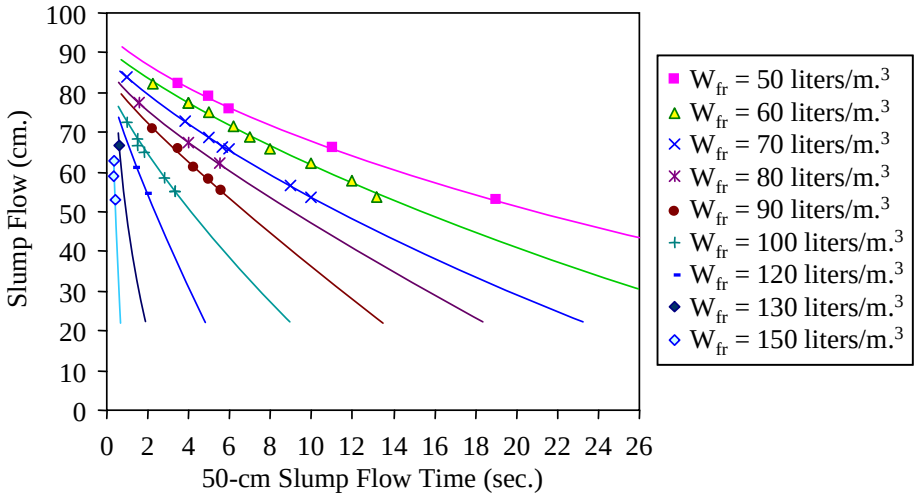

Fig. 4.42 Relationship between slump flow and 50-cm slump flow time for different free water contents

It is also seen from Fig. 4.41 that, at similar free water content, the secant slope of the slump flow vs. free water content curves slightly increased with the increase of ratio of paste volume to void content of compacted aggregate phase. It is considered to be due to the lubrication effect provided to aggregate particles by paste. In other words, in mixtures containing larger paste content, aggregates are well dispersed in paste and have larger distance between them, so the resistance against relative movement among aggregate particles is reduced.

As a result, the secant slope of slump flow vs. free water content curve (α_{SF}) was formed as a non-linear function of free water content and ratio of paste volume to void content of compacted aggregate phase as in the following equation.

$$\alpha_{SF} = \frac{459 \cdot \gamma^{0.10}}{W_{fr}^{1.66}} \tag{4.33}$$

where

α_{SF} is secant slope of slump flow vs. free water content curve, cm/kg/m^3 of concrete.
γ is ratio of volume of paste to volume of voids in the compacted aggregate phase.
W_{fr} is volume of free water in the mixture, kg/m^3 of concrete.

4.6 Model for Predicting Velocity of Deformation of SCC

Velocity of deformation, measured by 50-cm slump flow time (T_{50}), can be used to evaluate relatively the viscosity of the mixtures (Tangtermsirikul, et al., 2000). It was indicated in this study that T_{50} was mainly affected by free water content and effective surface area of solid particles in the mixtures. The prediction model for velocity of deformation was mainly formulated based on the concepts of free water, water retainability of solid particles, and inter-particle forces among the solid particles in the concrete, similar to that for deformation capacity.

4.6.1 Relationship between Velocity of Deformation and Free Water Content

It can be seen in Fig. 4.42 in section 4.5.2 that, at similar slump flow value, T_{50} reduced with increasing free water content in mixtures. It confirmed the previous report by Tangtermsirikul and Khayat (2000) that free water mainly influences the viscosity of fresh concrete. It is mainly because free water reduces the inter-particle forces among solid particles. Additionally, the amount of free water of the mixture must be enough to overcome the inter-particle surface forces which include friction and cohesion among solid particles to produce deformation, so the minimum free water content required for initiating deformation (W_o) or to make slump flow of SCC over 20 cm is inevitably required in formulation of the model for predicting velocity of deformation.

4.6.2 Effect of Effective Surface Area of Solid Particles on Velocity of Deformation

The inter-particle surface force, resisting flow due to friction and cohesion, is another main factor affecting the viscosity of fresh concrete (Tangtermsirikul, et al., 2000). According to the inter-particle surface force, considered in this study to vary with surface

area of the solids, it is seen from Figs. 4.43 that the relationship between T_{50} and free water content changes when the effective surface area of solid particles in the mixtures changes in such a manner that the higher effective surface area results in lower T_{50}.

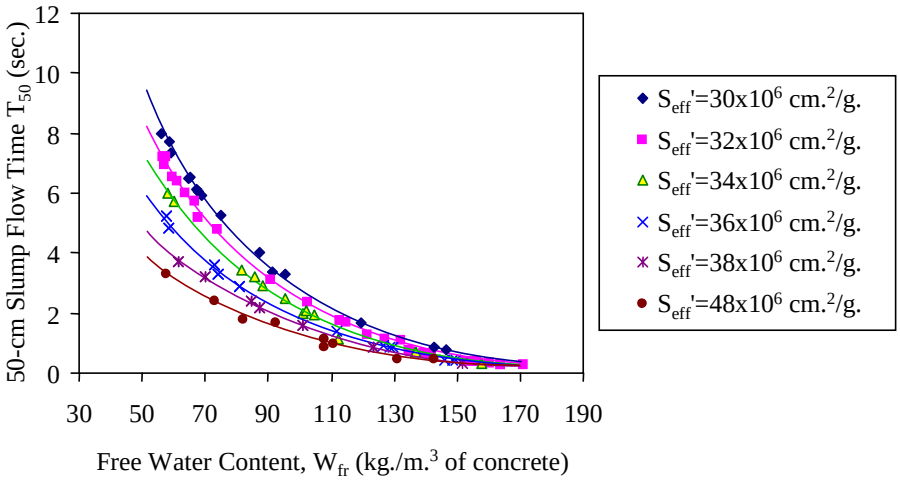

Fig. 4.43 Relationship between 50-cm slump flow time and free water content for different total effective surface areas of solid particles , S_{eff}'

By considering the effects of effective surface area of aggregates on this relationship as shown in Fig. 4.44, it reveals that at similar free water content, increasing effective surface area of aggregate increases slump flow time. It is considered to be due to the increase of inter-particle frictions by increasing possible aggregate contact.

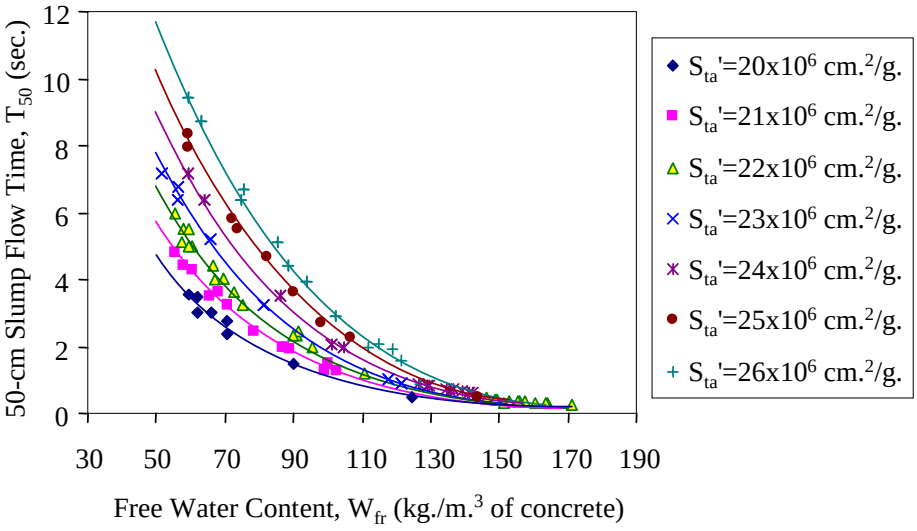

Fig. 4.44 Relationship between 50-cm slump flow time and free water content for different effective surface areas of total aggregates, S_{ta}'

Conversely, test results in Fig. 4.45 indicate that increasing effective surface area of powder materials reduces slump flow time. This could be explained that at the same free water content, increasing effective surface area of powder materials means increasing paste content and reducing possible aggregate contact, so the aggregate-to-aggregate friction is reduced.

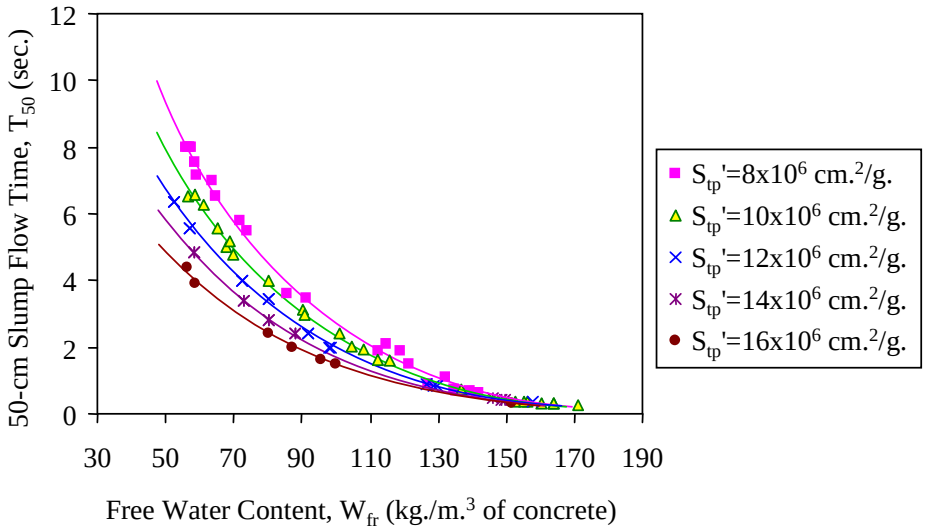

Fig. 4.45 Relationship between 50-cm slump flow time and free water for different effective surface areas of powder materials, S_{tp}'

Then, the effective surface area of aggregates and effective surface area of powder materials were taken into account, in addition to those primary parameters (free water and the minimum free water content required for initiating slump flow) to formulate the equation for predicting 50-cm slump flow time. In addition, the dispersion effect of powders due to the action of superplasticizers, defined by dispersion factor (ϕ_{dps}), was also incorporated in formulating the model as shown in Eq. (4.34).

$$T_{50} = \frac{S_{ta}'^{1.33}}{\phi_{dps}.(W_{fr} - W_o)^{1.28}.S_{tp}'^{0.97}} \qquad (4.34)$$

where

T_{50} is 50-cm slump flow time, sec.
ϕ_{dps} is dispersion factor due to the effect of superplasticizer.
W_{fr} is free water content of fresh concrete, kg/m^3 of concrete
W_o is the minimum free water content to initiate the deformation, kg/m^3 of concrete
$S_{ta'}$ is effective surface area of aggregates, cm^2/m^3 of the mix.
$S_{tp'}$ is effective surface area of powders, cm^2/m^3 of the mix.

4.7 Verifications

The proposed models were verified with test results obtained from the author and other researchers i.e. Nehdi, et al. (2001), Ghezal, et al. (2002), Bui, et al. (2002), and Patel, et al. (2004). The varied parameters were types of powders, replacement percentage of fly ash and limestone powder in total powder content, water to powder ratio, ratio of paste volume to void volume of compacted aggregate phase, type of aggregate, and type and dosage of superplasticizer. The details of materials and mix proportions used for verifications of slump flow and 50-cm slump flow time are shown in Table A-1 and B-7, respectively. It was assumed that the materials used by the author and other researchers have the same

properties, so the coefficients of the materials used in other references were determined based on the properties measured from the materials tested by the author. The coefficients of materials used are shown in Table A-3. However, the SCC mixtures with ultra-fine particles were not included in this verification test. The accuracies of both deformability models were verified by comparing the predicted results from the model with the test results.

It was observed by visual inspection that the mixtures with T_{50} less than 5 sec seemed to have slight segregation but the segregation was not severe during the short measurement period. Also, short T_{50} was due to the relatively higher paste and lower aggregate contents of those mixtures. Since the test for T_{50} took only a few minutes after mixing, the segregation and bleeding were still not severe at the time of measurement (the tests were conducted right after the mixing). As a result, it was found that the developed models could be used to predict the slump flow and 50 cm-slump flow time with satisfactory accuracies as the results in Table B-7 in Appendix B and in Figs. 4.46 and 4.47.

It is noted from the figures that the verified ranges of slump flow and 50-cm slump flow time were between 20-85 cm and 1-25 sec, respectively. The verified ranges are considered to be boarder than the practical ranges of the powder-typed SCC i.e. slump flow about 50-80 cm and T_{50} about 5-15 sec. However, the model is not applicable to predict deformability of SCC with severe segregation since the process of segregation has not been taken into account in the deformability model formulation.

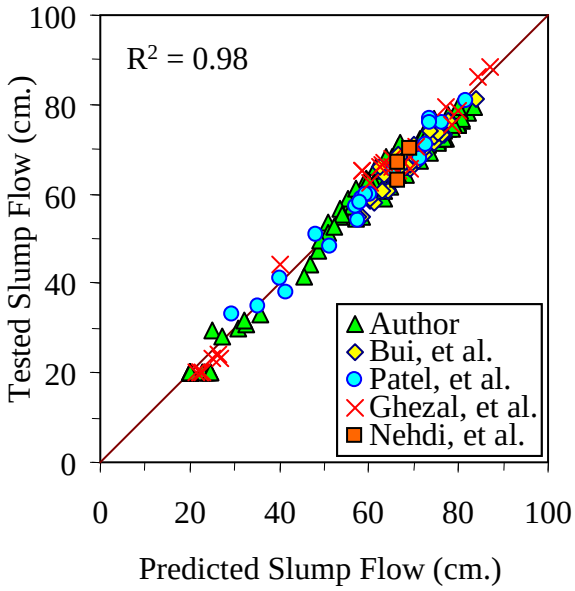

Fig. 4.46 Verification of slump flow model

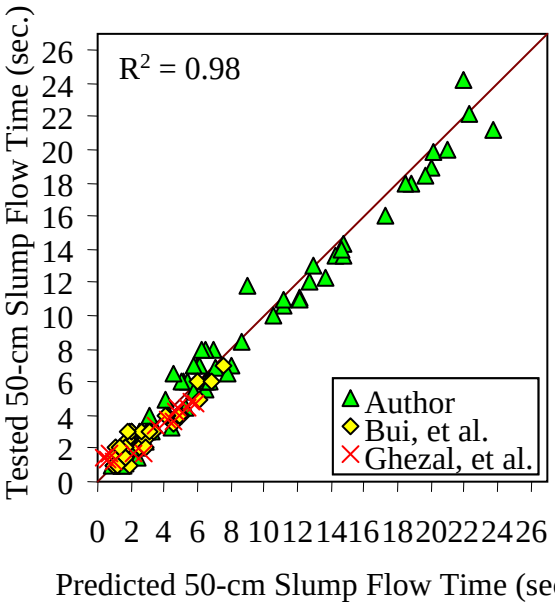

Fig. 4.47 Verification of 50-cm slump flow time model

4.8 Conclusions

Based on the proposed models and verification tests for predicting deformability of SCC, it was confirmed that slump flow and slump flow time varies mainly with free water content of the mixture. Free water content could be obtained when knowing unit water content, water retainability of powder materials and surface water retainability of aggregates and extra free water from filling powder. The amount of minimum free water required to initiate deformation is also another parameter influencing deformability and is considered to be resulted from inter-particle surface force among solid particles in the mixture.

It was found that at similar free water content, greater slump flow was obtained from the mixture with larger paste content due to the reduction of aggregate-to-aggregate frictions from the larger distance between aggregate particles. The dispersion effect from superplasticizers was considered to reduce water retainability of powders as well as friction and cohesion among solid particles. The dispersion effect also causes the increase of the secant slopes of slump flow vs. free water content curve and results in the increase of slump flow and decrease of slump flow time.

It was found from the analysis that the inter-particle force, which was a function of effective surface area of solid particles, influenced the velocity of deformation. Slump flow time increases with the increase of effective surface area of aggregates, due to the larger inter-particle surface friction of aggregate particles. On the other hand, it reduces when increasing effective surface area of powder materials, due to the reduction of aggregate contact and the lubrication effect provided to the aggregate particles from larger paste content.

The verification tests confirmed that the proposed models can be used to predict the deformation capacity (slump flow) and velocity of deformation (50-cm slump flow time, T_{50}) of the powder-type SCC with satisfactory accuracies.

Chapter 5

Model for Predicting Bleeding

5.1 General

Self-compacting concrete is recognized as a concrete that can flow into place and completely fill formwork with little or no vibration. This concept brings to mind an image of a concrete mixture that not only flows like water but also exhibits no segregation. Segregation of fresh concrete is critical both during placing concrete (dynamic state) as well as after finishing the placement (static state). The requirement of segregation resistance has significant impact on both filling ability and final hardened properties of the SCC mixture. A conventional concrete may not show the tendency of segregation during certain conditions of movement but segregates during other conditions such as when flowing through heavily reinforced sections (Skarendahl, 2000). Hence, SCC should not have any types of segregation in neither static nor dynamic states, such as bleeding of water, paste and aggregate segregation, coarse aggregate segregation leading to blocking (Tangtermsirikul, et al., 2000). It was also reported that among these four types of segregation, the segregation of coarse aggregate is considered as the decisive factor for the self-compactability when filling heavily reinforced area (Tangtermsirikul, et al., 2000). The relationship between bleeding and static segregation as well as blocking of coarse aggregate of SCC was focused in this study.

It is a fact that bleeding has close relationship with static segregation. It was also experienced from practice that SCC mixtures without bleeding had little segregation problem during flowing (Tangtermsirikul, 1989, 2000). Bleeding of fresh concrete is reasonably used as the primary indication of the static segregation, so the model for predicting bleeding was adopted and formulated in this study. In addition, a practical criteria of bleeding to avoid static segregation of SCC was proposed based on the relationship between bleeding capacity and static segregation.

Bleeding is a form of segregation resulted from rising of some water in the mixture to the surface of freshly placed concrete. Bleeding water is the water, called “movable water”, which is free from the restriction of the solid particles and can move independently from the solid in the mixture and is then gathered on the top surface of concrete. The mechanism of bleeding can be simply explained that weight of concrete is supported by the contacts among solid particles (effective stress) and the pore water pressure inside the concrete, consequently self-weight of the concrete will cause variation of effective stress and pore pressure along the vertical direction. Most of the concrete also has boundary of casting such as formwork which causes friction in the upward direction. These will cause differences of pore pressure along the vertical direction. Water will rise to the top surface of concrete because of this pore pressure difference (Tangtermsirikul, 1989). Basically, the initial bleeding proceeds at a constant rate, but subsequently the rate of bleeding decreases steadily (Tangtermsirikul, 1989). Two quantities concerning bleeding namely bleeding rate and bleeding capacity, or total bleeding volume, are generally used to describe the behavior of bleeding of concrete. (Tangtermsirikul, 1989, 2003).

In this study, the experimental program explained in section 3.8.2 in chapter 3 was conducted to clarify the behaviors of bleeding and static segregation of the SCC mixtures. Subsequently, the model for predicting bleeding capacity was extended from the original

model of Thumasujarit (2006), which was based on the concept of free water, water retainability of solid particles, effective surface area of solid particles, and average degree of reaction to also be able to predict bleeding capacity of the tested SCC mixtures. Furthermore, the effect of bleeding capacity on static segregation of the tested SCC mixture was studied. The influencing factors on bleeding and segregation including ratio of paste volume to void volume of aggregate phase (γ), water to binder ratio (w/b), dosage and type of superplasticizer, and concrete temperature were considered in the model formulation.

5.2 Model Formulation

It is known that rate of bleeding depends on the amount of free water in concrete, permeability of the fresh concrete and the hydraulic pressure in the free water phase (Tangtermsirikul, 1989, 2003). The amount of free water varies with water content and water retainability of the solid particles in the concrete (Tangtermsirikul, 1989, 2001). Permeability of the fresh concrete depends on the structures of voids among the solid particles and the air content. Air reduces the permeability of the fresh concrete since it blocks the flow of free water. Voids among solid particles are filled with water and air, therefore permeability of fresh concrete can be considered to vary with free water content of the concrete (Tangtermsirikul, 1989). By considering a constant void content of the solid phase, the use of solid particles with high fineness reduces free water content and permeability of the fresh concrete (Powers, 1986, Tangtermsirikul, 1989, and Neville, 1995). Hydraulic pressure in the free water phase depends on the unit weight of the concrete, height of the placing lift and contact stress or effective stress among the solid particles. The hydraulic pressure in free water will be higher when unit weight of concrete is higher, placing lift is larger, and contact stress among the solid particles is smaller. Smaller contact stress may be understood as larger inter-particle distances among the solids (Tangtermsirikul, 1989, 2003).

Bleeding capacity or total bleeding volume depends on the height of the placing lift, free water content in the concrete mixtures and contact stress. Smaller bleeding capacity is obtained for smaller placing lift, smaller free water content but higher contact stress. Mixture with large amount of free water is not always necessary to have large total bleeding volume if the contact stress among the solid particles is high so that the hydraulic pressure in the free water cannot be produced (Tangtermsirikul, 1989, 2003). Basically, bleeding of concrete continues until free water is too little and contact stress among the solid particles is large (pore pressure is too small) (Tangtermsirikul, 1989), due to the effects from the reactions of binders and settlement of the solid particles.

Therefore, it is assumed in this study that the main factors influencing bleeding capacity are free water, effective surface area of solid particles, and degree of reaction of binders. This was confirmed by a previous study of Thumasujarit and Tangtermsirikul (2005, 2006) that there existed the relationship between bleeding behaviors and the above mentioned factors. As a result, the model for predicting bleeding of fly ash concrete was proposed. In this study, the developed model was adopted and modified to also predict bleeding capacity of the SCC mixture. The prediction of bleeding capacity of SCC in this study is briefly explained by the flow chart in Fig. 5.1. Since the bleeding capacity is used as the primary indication of the static segregation, the limiting amount of total bleeding volume to ensure the avoidance of static segregation of SCC was also proposed based on the relationship between bleeding capacity and static segregation of the tested mixtures.

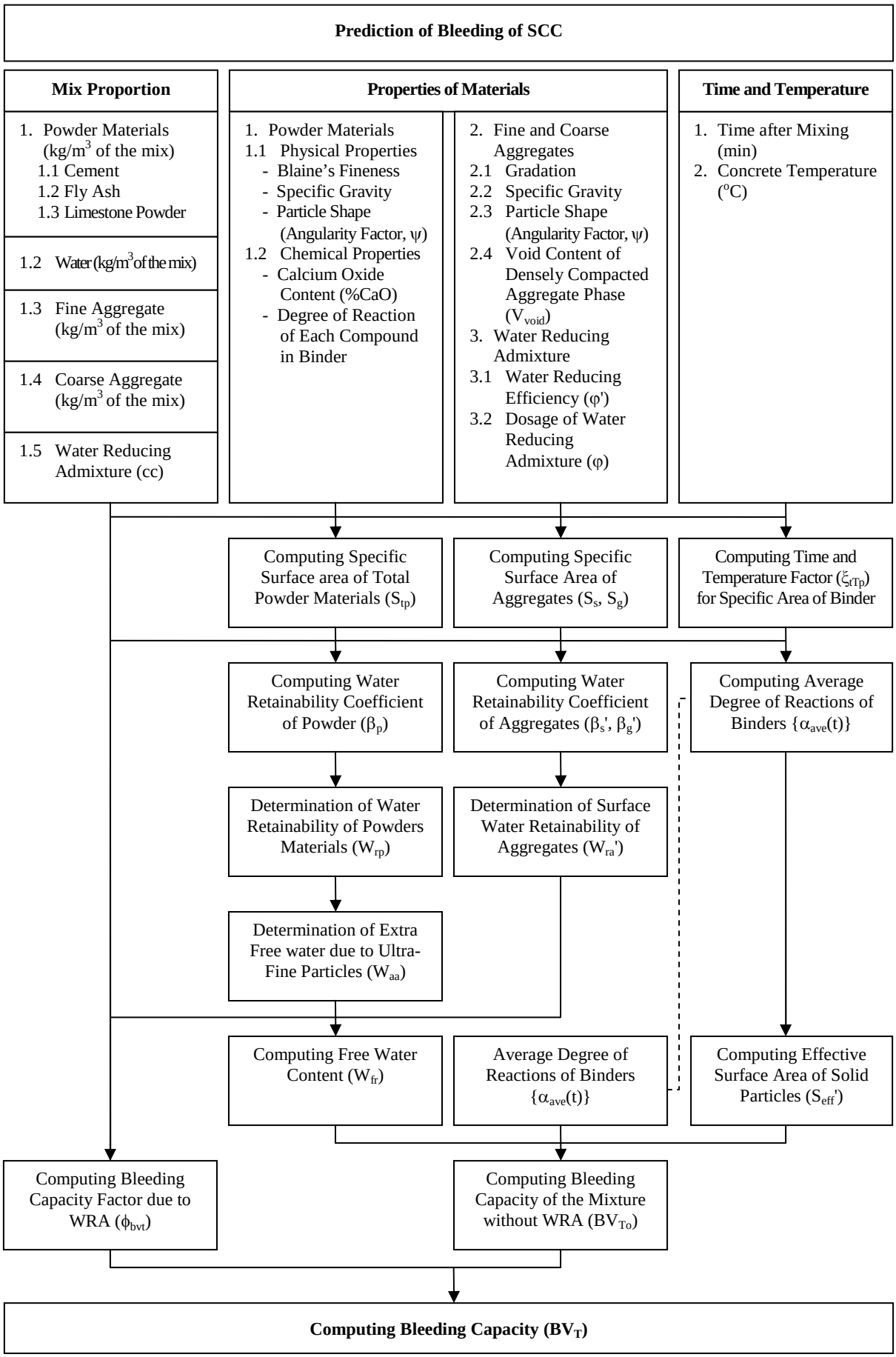

Fig. 5.1 Flow chart for predicting bleeding capacity of SCC

5.3 Parameters Used in Model Formulation

Parameters considered in the model for predicting bleeding capacity include free water, effective surface area of solid particles, and average degree of reactions. In order to understand fundamental characteristics of bleeding, two bleeding features i.e. bleeding rate and bleeding capacity will be explained in sections 5.3.1 and 5.3.2 which will be followed by the explanation on the model formulation parameters.

5.3.1 Bleeding Rate

Bleeding rate means the amount of bleeding per a unit period of time. Bleeding behavior of fresh concrete can be basically separated into two states, early age bleeding and later age bleeding, which have much difference in bleeding rate (Tangtermsirikul, 2003).

For the bleeding test in this study, the amount of bleeding water was collected on the concrete surface at 10 minutes intervals during the first 40 minutes and at 30 minutes intervals thereafter until cessation of bleeding. In order to simulate the time-dependent bleeding volume of fresh concrete mixture, the parameter called “Bleeding Rate” or “BR” was employed. Bleeding rate at a certain time can be obtained by differentiating the relationship between bleeding volume versus time.

$$BR(t) = \frac{d}{dt}(BV(t)) \tag{5.1}$$

where

BR(t) is bleeding rate at a certain time, cc/min.
BV(t) is bleeding volume at that time measured from the standard test (ASTM C232 Method A: Sample consolidated by tamping), cc.

Fig. 5.2 shows an example of determination of bleeding rate from a plot of bleeding volume versus time after mixing. Bleeding rate at certain time of this test can be obtained by differentiating the function of bleeding volume versus time (see Fig. 5.3).

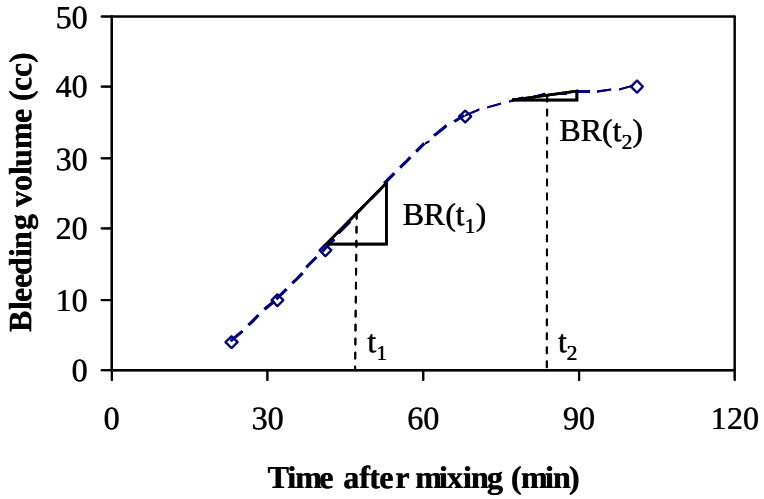

Fig. 5.2 Characteristic of bleeding volume versus time after mixing (Thumasujarit, 2006)

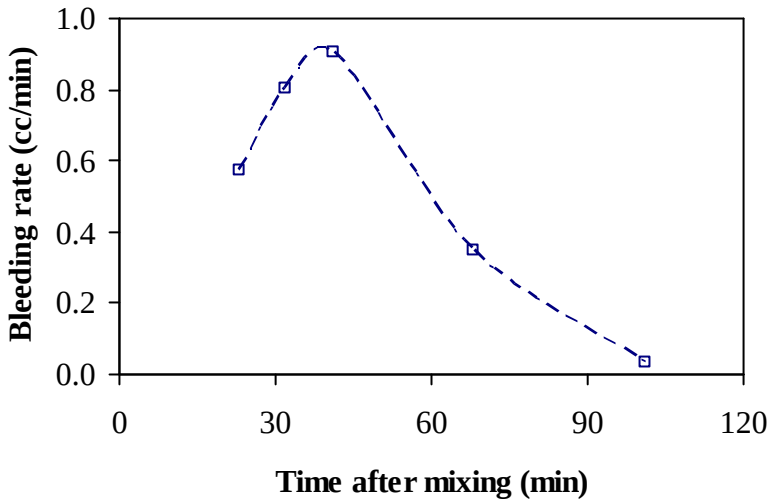

Fig. 5.3 Relationship between bleeding rate versus time obtained by differentiating the function of bleeding volume versus time (Thumasujarit, 2006)

5.3.2 Bleeding Capacity

Bleeding capacity or total bleeding volume means the sum of bleeding volume from the start of bleeding until the bleeding stops (Tangtermsirikul, 2003). It was assumed in this study that bleeding capacity has close relationship with static segregation, so limiting bleeding capacity to avoid static segregation was thus useful for mix proportioning of SCC.

The bleeding volume at any time can be derived from the following equation.

$$BV(t) = BV(t_o) + \int_{t_o}^{t} BR(t)dt \qquad (5.2)$$

where

BV(t)	is bleeding volume of the concrete at the considered time, cc.
$BV(t_o)$	is initial bleeding volume of concrete, cc.
BR(t)	is bleeding rate of concrete at the considered time, cc/min.
t_o	is starting time of bleeding.
t	is the considered time, min.

5.3.3 Free Water Content, Water Retainability and Effective Surface Area of Solid Particles

Free water content, water retainability and effective surface area of solid particles in the concrete are identical to those used in model formulation for predicting deformability, which can be obtained from Eqs. (4.5), (4.6), and (4.22) explained in Chapter 4, respectively.

5.3.4 Average Degree of Reactions of Cement and Fly Ash

When cement particles are in contact with water, there is an initial period of very rapid hydration reaction followed by a dormant period (typically of the order of three hours) during which little reaction takes place. During the hydration, surface of the cement particles becomes more irregular and their surface area increases (Neville, 1995), hence increasing their capacity to retain water on the surface. Furthermore, as the hydration reaction progresses with time, the pozzolanic reaction also occurs and the surfaces of the fly ash particles are also reacted, causing the increase of the surface areas leading to higher water retainability of fly ash particles (Wangchuk, et al., 2003). As a result, amount of free water causing bleeding in fresh concrete reduces with the increase of water retainability of the binder particles. Simultaneously, the hydraulic pressure gradient of fresh concrete reduces with the increase of the surface area of binder particles causing the increase of the contact stress among solid particles. Clearly, the degree of reactions of cement and fly ash (i.e. hydration and pozzolanic reaction, respectively) plays a significant role in bleeding behavior, so it was considered as the main parameter in the model formulation.

The average degree of hydration of cement at any time is defined by Saengsoy (2002) as the weight fraction of hydrated cement per total cement in the paste and can be determined by the following equation:

$$\alpha_{hy}(t) = \frac{\sum_{k=1}^{4} m_k \cdot \alpha_k(t)}{\sum_{k=1}^{4} m_k} \tag{5.3}$$

where

$\alpha_{hy}(t)$ is average degree of hydration reaction of paste at the considered age, %.
k is oxide compound of cement (C_3A, C_4AF, C_3S, C_2S).
m_k is mass of each oxide compound per cubic meter of cement paste at any water to binder ratio, kg/m^3.
$\alpha_k(t)$ is degree of hydration of each oxide compound in cement at the considered age, %.

The degree of pozzolanic reaction of fly ash was defined as the weight fraction of already reacted fly ash per total fly ash in the paste mixture and can be expressed by the following equation which was also proposed by Saengsoy (2002).

$$\alpha_{poz}(t) = \frac{\tan^{-1}[(0.049 \cdot T_c^{0.496} - 0.186 \cdot \frac{w}{b} - 0.135) \cdot t]}{\tan^{-1}[(0.049 \cdot T_c^{0.496} - 0.186 \cdot \frac{w}{b} - 0.135) \cdot 365]} \cdot \alpha_{poz}(365) \tag{5.4}$$

where

$\alpha_{poz}(t)$ is degree of pozzolanic reaction of fly ash at the considered age, %.
T_c is concrete temperature, ^oC.
w/b is water to binder ratio.
t is the considered age of concrete, days.
$\alpha_{poz}(365)$ is degree of pozzolanic reaction of fly ash at 365 days, %.

where

$$\alpha_{poz}(365) = \left\{100 - \left\{(102 - 0.1\cdot T_c)\cdot(0.416 + 0.0088\cdot(w/b)^{-1.822}\right.\right.$$
$$\left.\left.\cdot\tan^{-1}\left\{(7.927\cdot(w/b)^{-1.546} - 15.699)\cdot\left[(SiO_2/CaO_{eff}) - (\%SiO_{2c}/\%CaO_c)\right]\right\}\right\}\right\}$$
$$\cdot(1 - \%LOI/100)\cdot\left[0.948\cdot\tan^{-1}\left(7.227\cdot10^{-4}\cdot F_f\right)\right] \quad (5.5a)$$

$$SiO_2 = [(W_c\cdot\%SiO_{2c}) + (W_f\cdot\%SiO_{2f})] / 100 \quad (5.5b)$$

$$CaO_{eff} = [(W_c\cdot\%CaO_c) + (\varepsilon_f.(W_f\cdot\%CaO_f)] / 100 \quad (5.5c)$$

$$\varepsilon_f = \{1\text{-}\exp[-a\cdot(\%CaO_f)]\} / \{1+\exp[-a\cdot(\%CaO_f)]\} \quad (5.5d)$$

$$a = 0.0048\cdot(F_f / 3000)^{3.0734} + 0.0245 \quad (5.5e)$$

where

α_{poz} (365)	is degree of pozzolanic reaction of fly ash at 365 days, %.
t	is the considered time, days.
T_c	is concrete temperature, ^oC.
w/b	is water to binder ratio.
$\%CaO_c$	is calcium oxide content in cement, % by weight.
$\%CaO_f$	is calcium oxide content in fly ash, % by weight.
SiO_{2c}	is silicon dioxide content in cement, % by weight.
SiO_{2f}	is silicon dioxide content in fly ash, % by weight.
CaO_{eff}	is effective unit calcium oxide content in paste, kg/m^3.
SiO_2	is silicon dioxide content in paste, kg/m^3.
ε_f	is effectiveness of calcium oxide in fly ash.
W_c	is cement content in paste, kg/m^3.
W_f	is fly ash content in paste, kg/m$^{3.}$
F_f	is fineness of fly ash, cm^2/g.

As a result, the average degree of reactions (including hydration and pozzolanic reaction) can be obtained by Eq. 5.6 (Saengsoy, 2002, Wangchuk et al., 2003).

$$\alpha_{react}(t) = (1 - \%rFA/100)\cdot\alpha_{hy}(t) + (\%rFA/100)\cdot\alpha_{poz}(t) \quad (5.6)$$

where

α_{react} (t)	is average degree of reactions (including hydration and pozzolanic reaction), %.
%rFA	is replacement percentage of fly ash in total binders, % by weight.

5.3.5 Effects of Time and Temperature on Specific Surface Area of Binders

With the elapse of time after mixing, the surfaces of the binder particles deform along with the reactions. The surfaces become rougher and this increases the specific surface area of the binder particles. The increase of the specific surface area depends on the elapsed time and ambient temperature and therefore, a time and temperature factor for the specific surface was introduced as shown in Eq. (5.7) (Wangchuk, 2003).

$$Sp' = \zeta tTp.Sp \quad (5.7)$$

where

S_p' is specific surface area of binders with the effect of elapsed time and temperature, cm^2/g.
ζ_{tTp} is time and temperature factors for the specific surface of binders.
S_p is initial specific surface area of binders, cm^2/g.

Since surface area of the cement particles increases during hydration, it was considered that the specific surface area of cement increased with the average degree of hydration. The relationship between the time and temperature factor and the average degree of hydration was derived from the analysis of the test results of various mix proportions of the concrete as shown in the following equation (Wangchuk, 2003).

$$\zeta_{tTc} = 1 + \left(\frac{0.98 \cdot \alpha_{hy}(t)^{0.76}}{\exp\left(0.05 \cdot \alpha_{hy}(t)\right)} \right) \quad (5.8)$$

where

ζ_{tTc} is time and temperature factors for the specific surface area of cement, which is applicable for both mixtures with and without water reducing admixtures.
$\alpha_{hy}(t)$ is average degree of hydration, %.

During the progress of hydration reaction with time, pozzolanic reaction of fly ash also occurs, also resulting in the increase of the surface area of fly ash particles. It was assumed in this study that the specific surface area of fly ash increased with the degree of pozzolanic reaction. The relationship between the time and temperature factor versus the degree of pozzolanic reaction was also proposed by Wangchuk (2003) as shown in Eq. (5.9).

$$\zeta_{tTf} = 1 + 4.2 \cdot \alpha_{poz}(t)^{1.38} \cdot \left\{1 + \exp(2.71 - 9.94 \cdot \alpha_{poz}(t))\right\} \quad (5.9)$$

where

ζ_{tTf} is time and temperature factors for the specific surface area of fly ash, which is applicable for both mixtures with and without water reducing admixtures.
$\alpha_{poz}(t)$ is degree of pozzolanic reaction, %.

5.4 Effects of Influencing Factors on Bleeding Behaviors

Effects of the influencing factors on bleeding behaviors, i.e. water to powder ratio, ratio of paste volume to void volume of aggregate phase, type and dosage of superplasticizers, and concrete temperature, were investigated and discussed in this section.

5.4.1 Effect of Water to Powder Ratio on Bleeding Behavior

It was confirmed from Figs. 5.4 to 5.7 that the higher water to binder ratio caused the increase of bleeding rate and bleeding capacity due to larger amount of free water content in the mixtures.

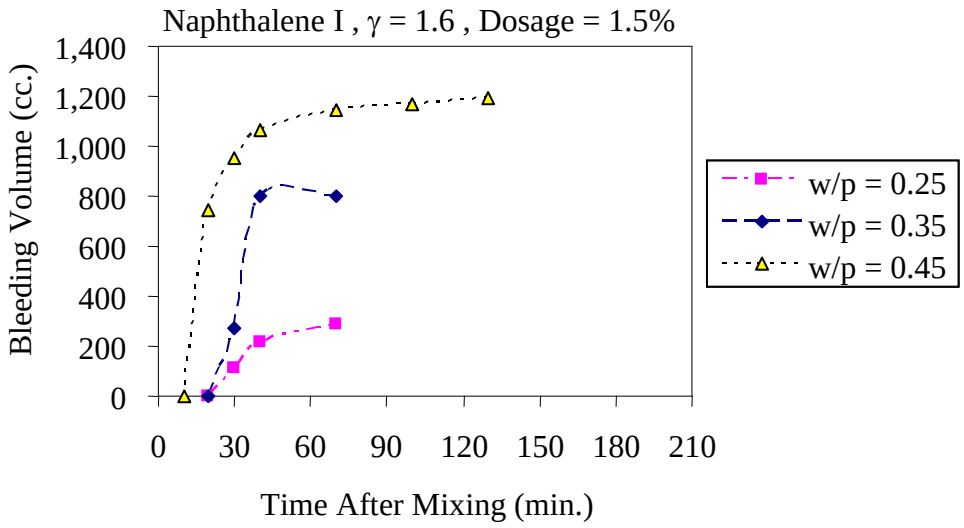

Fig. 5.4 Bleeding behaviors of the mixtures with different w/p ratios (dosage of naphthalene based superplasticizer I = 1.5 %, and γ = 1.6)

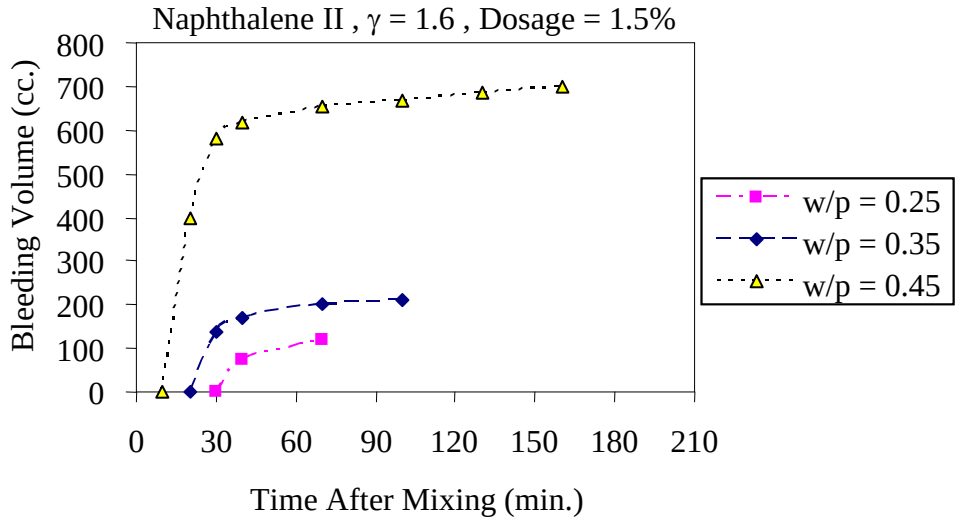

Fig. 5.5 Bleeding behaviors of the mixtures with different w/p ratios (dosage of naphthalene based superplasticizer II = 1.5 %, and γ = 1.6)

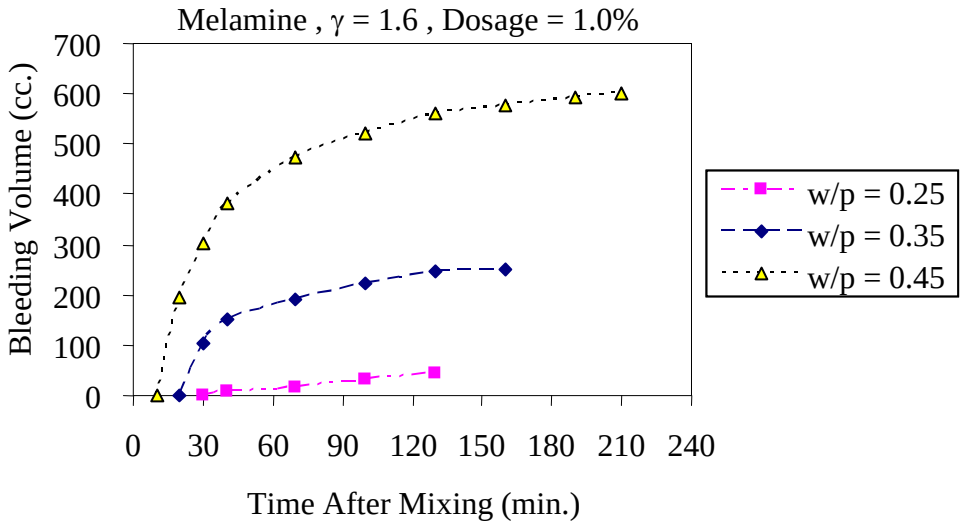

Fig. 5.6 Bleeding behaviors of the mixtures with different w/p ratios (dosage of melamine based superplasticizer = 1.0 %, and γ = 1.6)

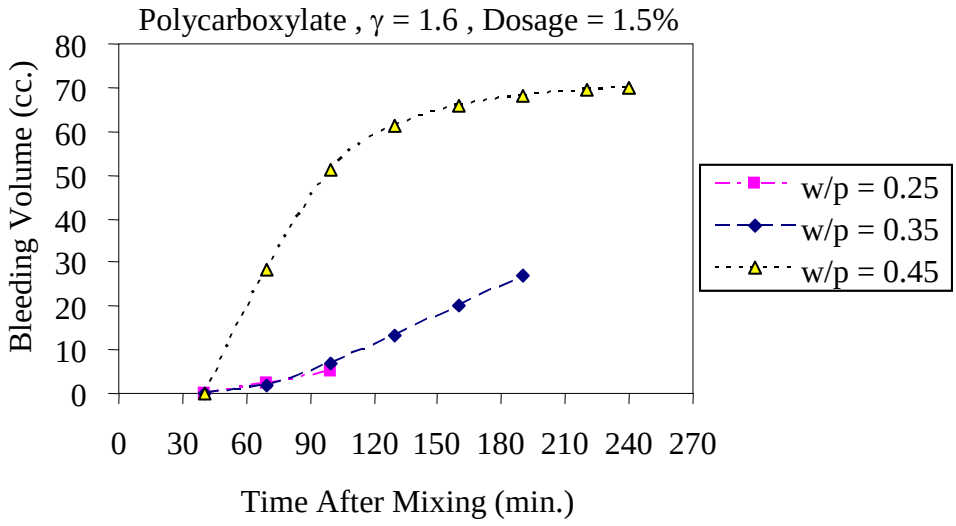

Fig. 5.7 Bleeding behaviors of the mixtures with different w/p ratios (dosage of polycarboxylate based superplasticizer = 1.5 %, and γ = 1.6)

5.4.2 Effect of Ratio of Paste Volume to Void Volume of Aggregate Phase on Bleeding Behavior

Figs. 5.8 to 5.11 indicate that, at similar water to powder ratio, bleeding rate and capacity of the tested mixtures increased with the increase of the ratio of paste volume to void volume of aggregate phase (γ). It was because the mixtures with higher paste content had the higher unit water content per concrete volume, resulting in the higher free water for bleeding.

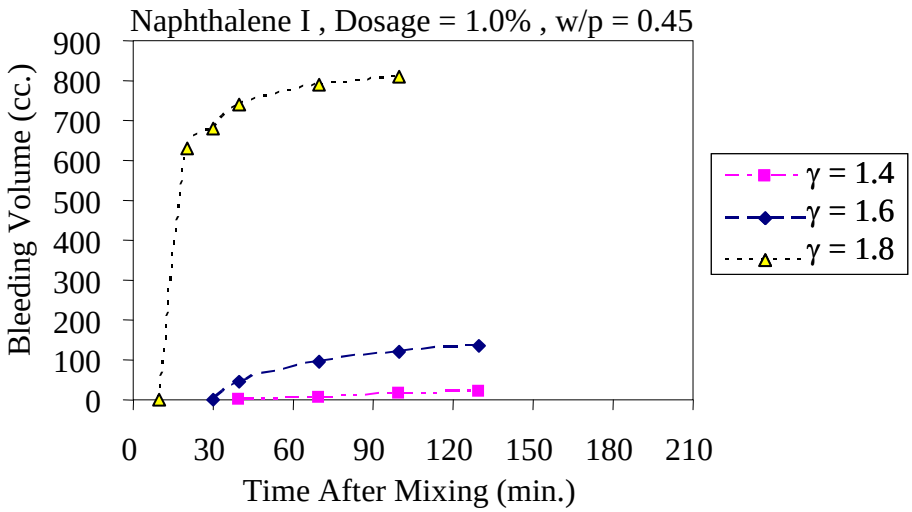

Fig. 5.8 Bleeding behaviors of the mixtures with different γ values (dosage of naphthalene based superplasticizer I = 1.0 %, and w/p = 0.45)

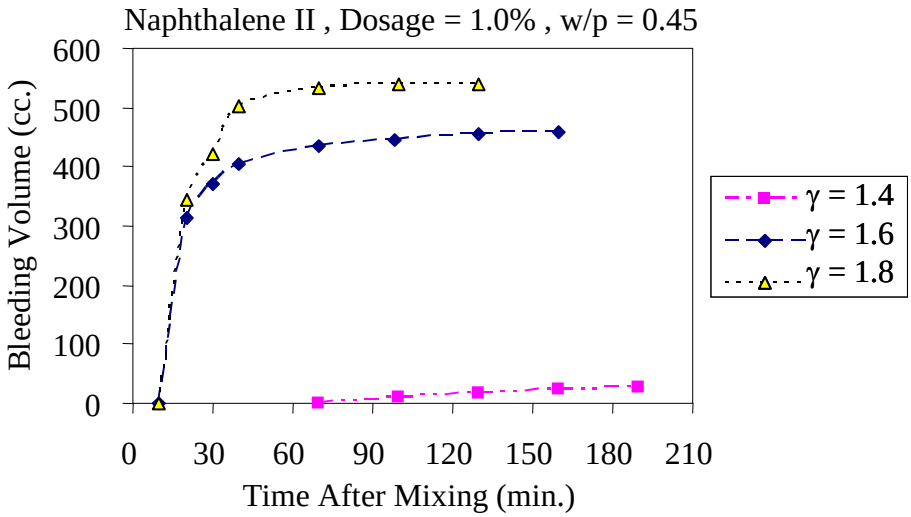

Fig. 5.9 Bleeding behaviors of the mixtures with different γ values (dosage of naphthalene based superplasticizer II = 1.0 %, and w/p = 0.45)

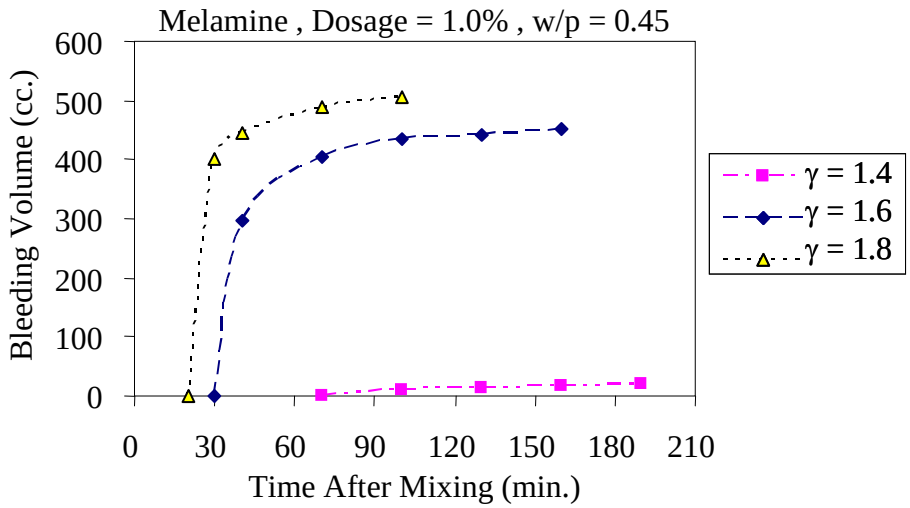

Fig. 5.10 Bleeding behaviors of the mixtures with different γ values (dosage of melamine based superplasticizer = 1.0 %, and w/p = 0.45)

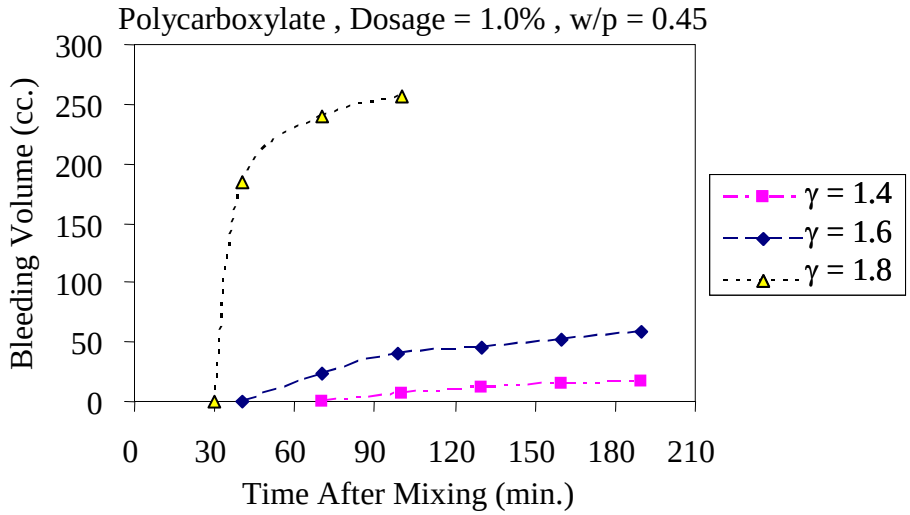

Fig. 5.11 Bleeding behaviors of the mixtures with different γ values (dosage of polycarboxylate based superplasticizer = 1.0 %, and w/p = 0.45)

5.4.3 Effect of Type of Superplasticizer on Bleeding Behavior

Four types of superplasticizer were introduced into the mixtures to investigate the effect of superplasticizers on bleeding behavior of SCC and the results were shown in Figs. 5.12 to 5.15. The figures show that at similar dosage of superplasticizer, the mixtures with naphthalene-I superplasticizer produced the highest rate of bleeding, followed by the mixtures with naphthalene-II, melamine, and polycarboxylate based superplasticizers. The higher bleeding rates of the mixtures with naphthalene and melamine based superplasticizers are considered to be due to the higher ability of particles dispersion. This effect resulted in the increase of free water content of the mixture. In other words, bleeding of the mixtures with naphthalene and melamine based superplasticizers increases with the increase of the water reducing efficiency. On the other hand, the polycarboxylate based superplasticizer had the highest water reducing efficiency but caused the lowest bleeding due to the difference of dispersion mechanisms of superplasticizers i.e. electrostatic repulsion and steric hindrance.

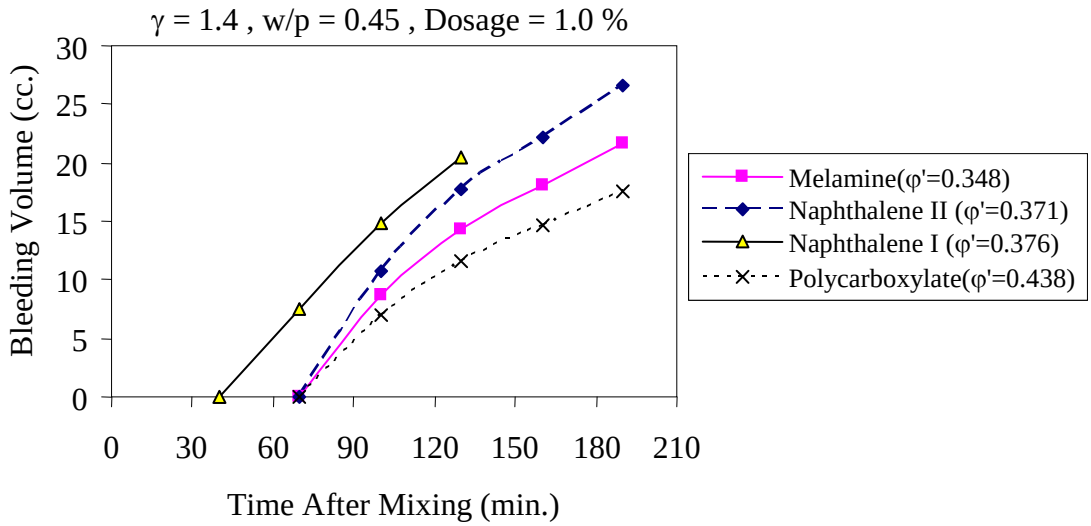

Fig. 5.12 Bleeding behaviors of the mixtures with different types of superplasticizer at dosage of 1.0 % by weight of powder (γ = 1.4 and w/p = 0.45)

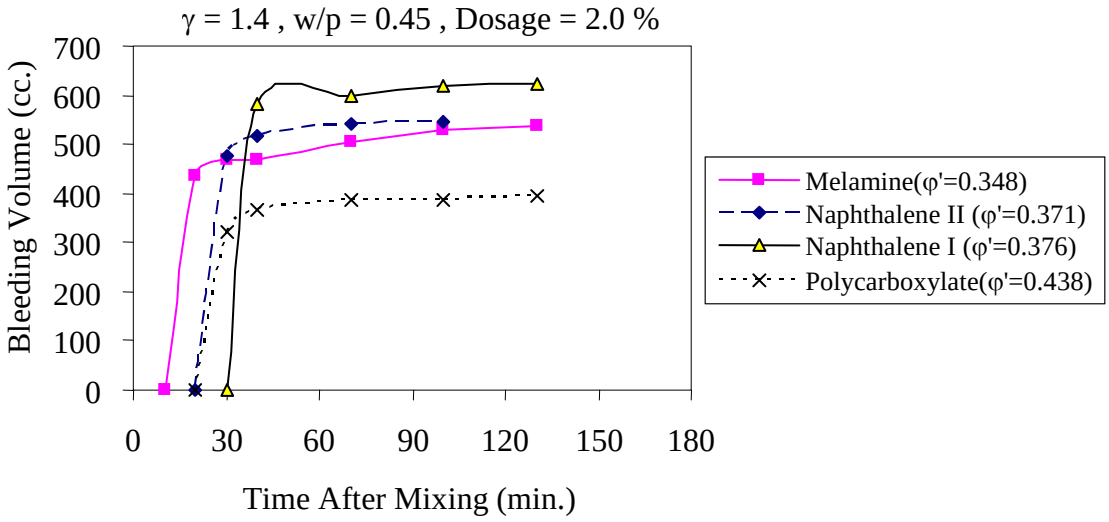

Fig. 5.13 Bleeding behaviors of the mixtures with different types of superplasticizer at dosage of 2.0 % by weight of powder (γ = 1.4 and w/p = 0.45)

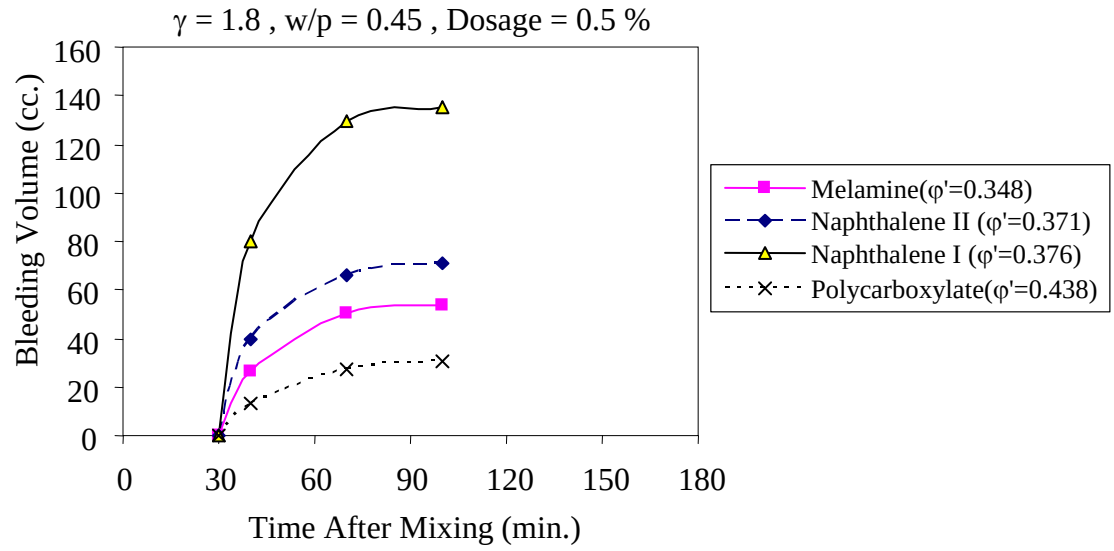

Fig. 5.14 Bleeding behaviors of the mixtures with different types of superplasticizer at dosage of 0.5 % by weight of powder (γ = 1.8 and w/p = 0.45)

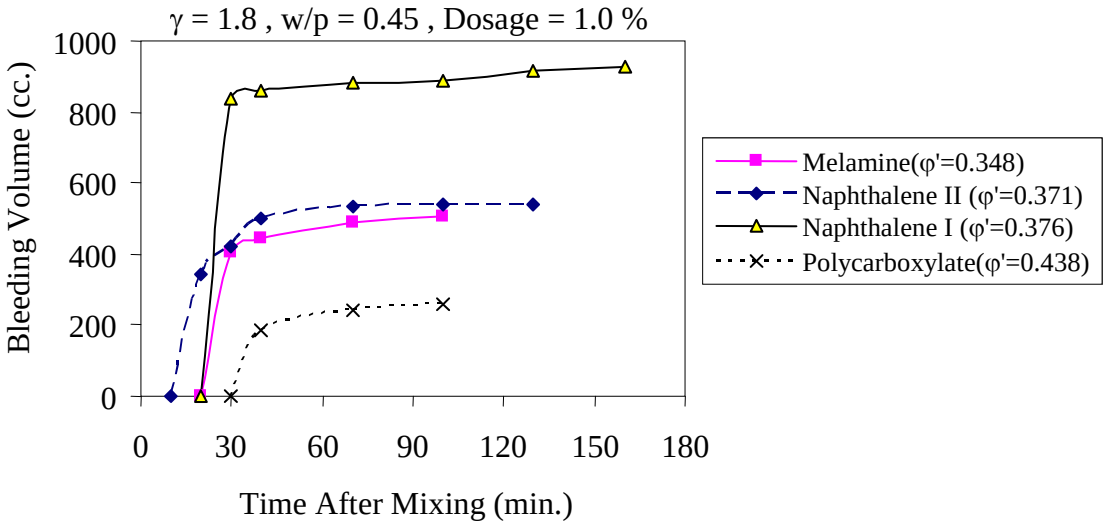

Fig. 5.15 Bleeding behaviors of the mixtures with different types of superplasticizer at dosage of 1.0 % by weight of powder (γ = 1.8 and w/p = 0.45)

5.4.4 Effect of Dosage of Superplasticizer on Bleeding Behavior

It was confirmed from Figs. 5.16 to 5.19 that bleeding of all tested mixtures increased with the increase of dosage of superplasticizers. It was due to the higher dispersion effect on mobility of powder materials resulting in the increase of free water content of the mixtures. It was also found from the test results of the mixtures with 2 % dosage of superplasticizers that bleeding increases tremendously when the mixtures were much overdosed with the superplasticizers. It should be noted that the unit water content is generally adjusted to control bleeding when using superplasticizer in actual practice.

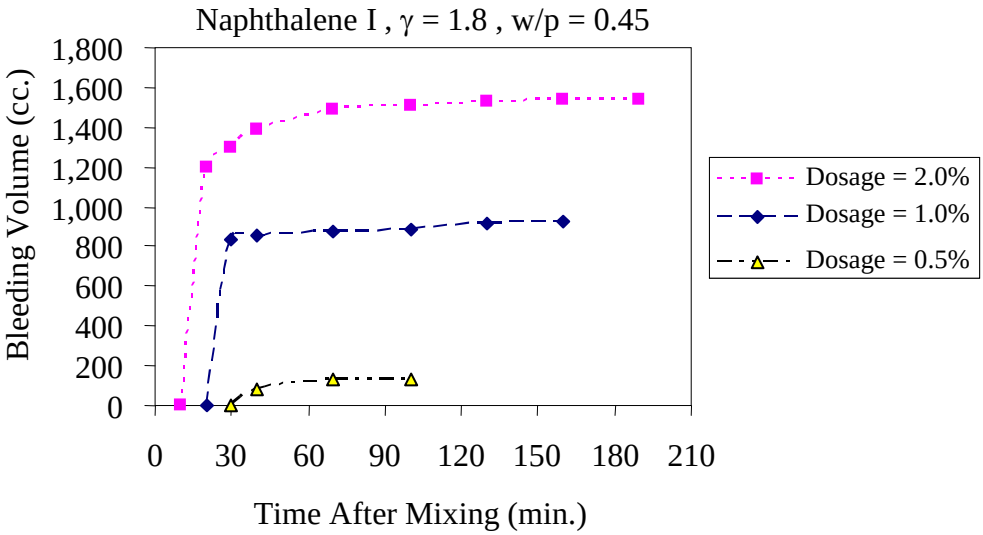

Fig. 5.16 Bleeding behaviors of the mixtures with different dosages of naphthalene based superplasticizer I (γ = 1.8 and w/p = 0.45)

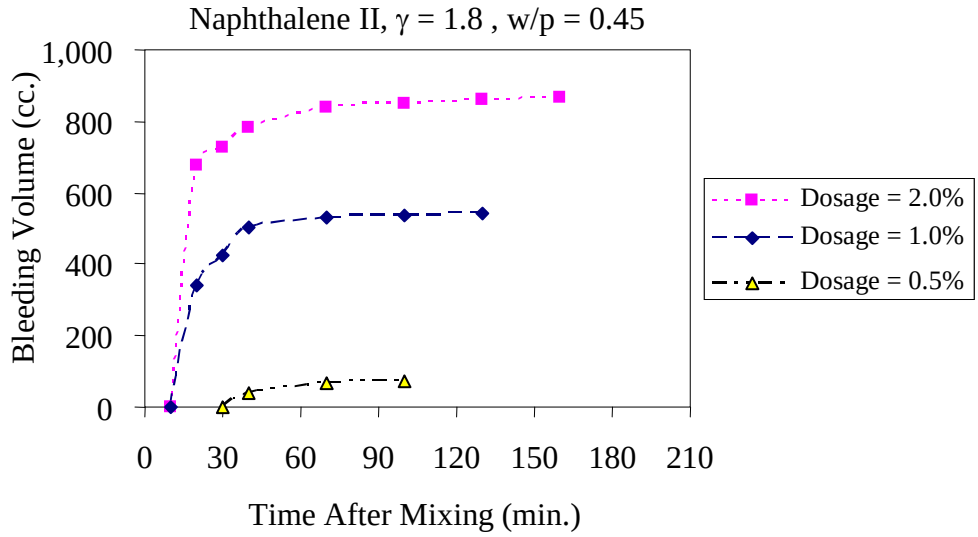

Fig. 5.17 Bleeding behaviors of the mixtures with different dosages of naphthalene based superplasticizer II (γ = 1.8 and w/p = 0.45)

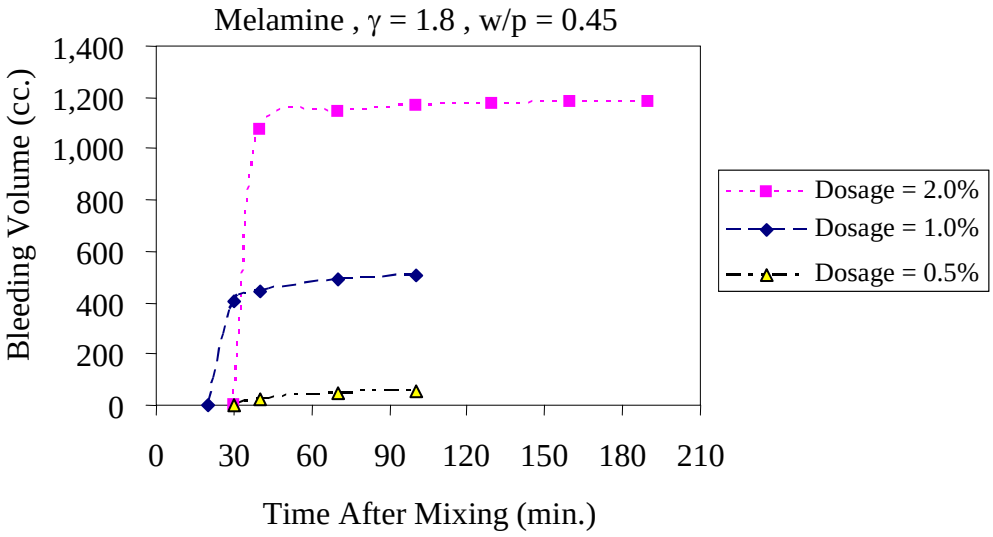

Fig. 5.18 Bleeding behaviors of the mixtures with different dosages of melamine based superplasticizer (γ = 1.8 and w/p = 0.45)

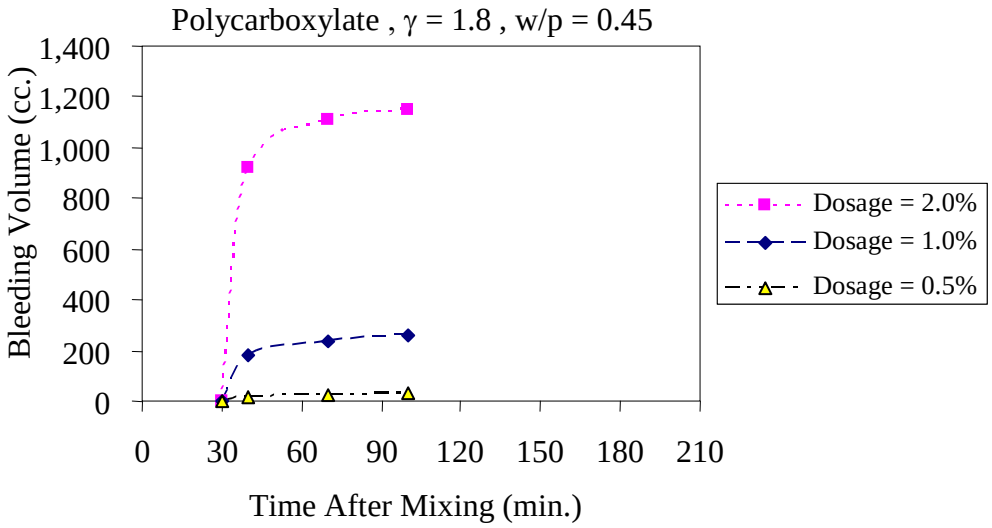

Fig. 5.19 Bleeding behaviors of the mixtures with different dosages of polycarboxylate based superplasticizer (γ = 1.8 and w/p = 0.45)

5.4.5 Effect of Concrete Temperature on Bleeding Behavior

It is a fact that a higher temperature of fresh concrete results in more rapid reactions of binders and so directly affects bleeding behaviors. To investigate bleeding behaviors at various temperatures, concrete temperatures at 25, 35, and 45 ºC were selected. It can be seen from the Figs. 5.20 to 5.23 that when increasing the concrete temperature, the earlier initiation and termination of bleeding, a bit higher bleeding rate and lower bleeding capacity of the tested mixtures were observed. It is considered to be due to the acceleration of the reactions of binders in the concrete.

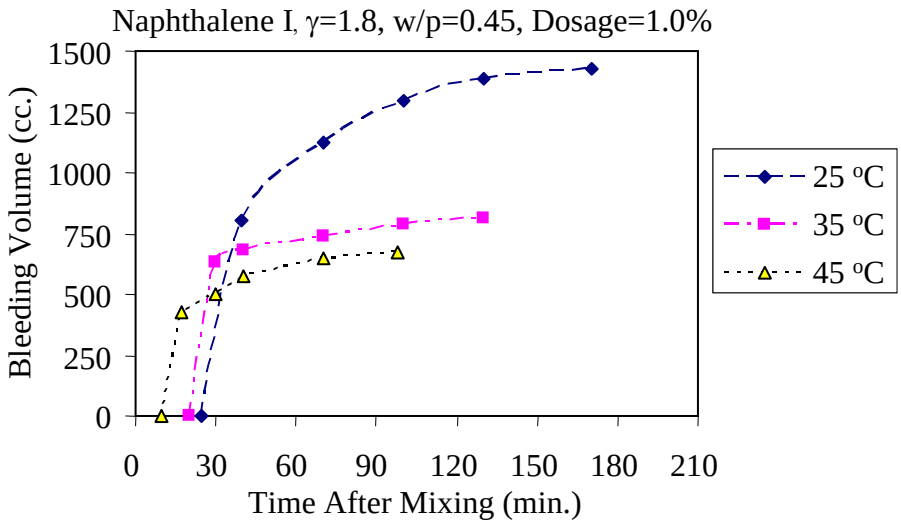

Fig. 5.20 Bleeding behaviors of the mixtures with dosage of naphthalene-I based superplasticizer of 1.0 %, γ = 1.8, and w/p = 0.45 at different concrete temperatures

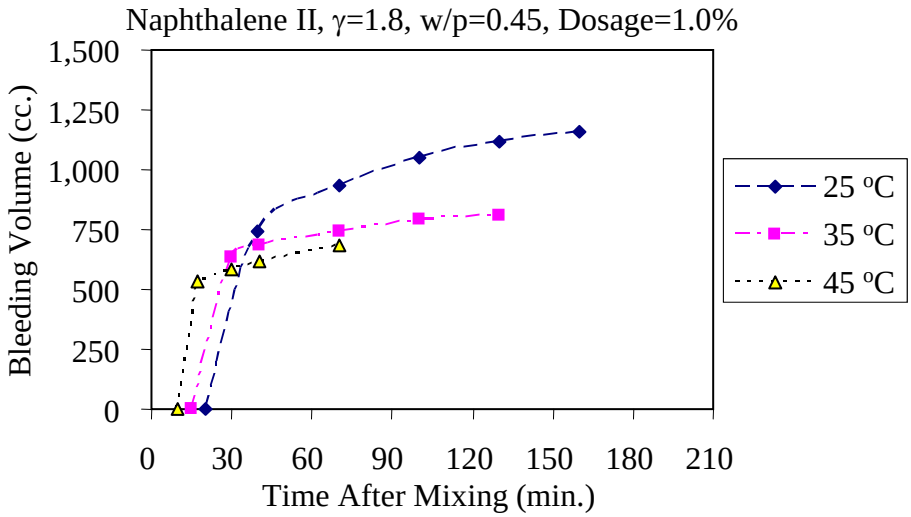

Fig. 5.21 Bleeding behaviors of the mixtures with dosage of naphthalene-II based superplasticizer of 1.0 %, γ = 1.8, and w/p = 0.45 at different concrete temperatures

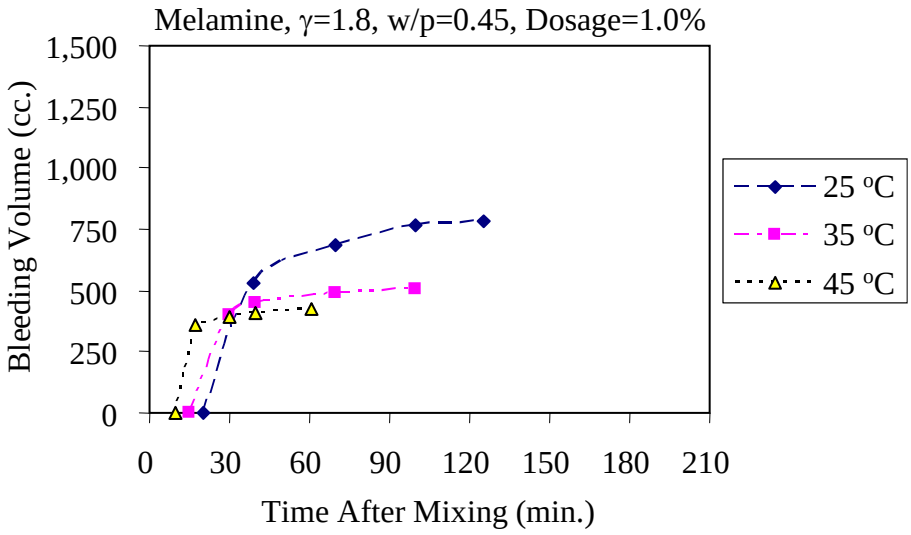

Fig. 5.22 Bleeding behaviors of the mixtures with dosage of melamine based superplasticizer of 1.0 %, γ = 1.8, and w/p = 0.45 at different concrete temperatures

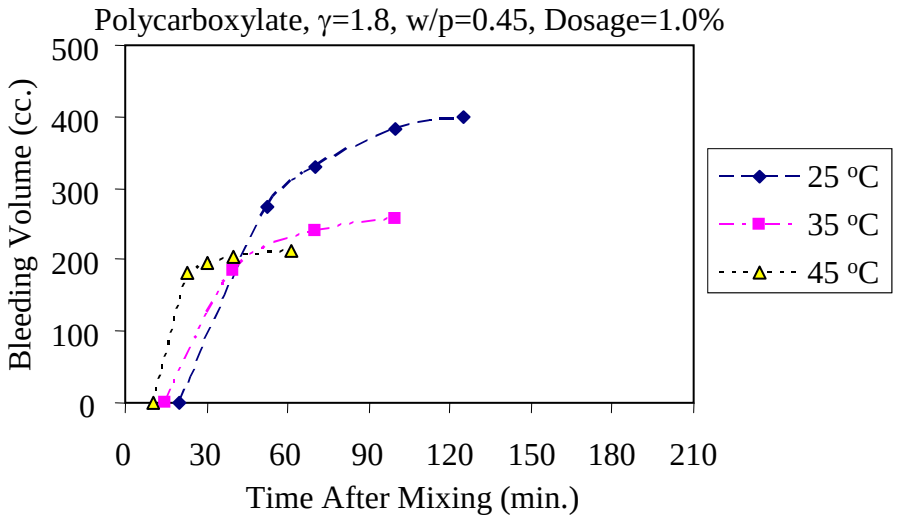

Fig. 5.23 Bleeding behaviors of the mixtures with dosage of polycarbxylic based superplasticizer of 1.0 %, γ = 1.8, and w/p = 0.45 at different concrete temperatures

5.5 Relationships between Analytical Parameters and Bleeding Capacity of SCC

Free water, effective surface area of solid particles, and average degree of reactions were considered as parameters affecting the amount of bleeding water due to their effects on bleeding capacity. They are employed in the model formulation for predicting total bleeding volume.

5.5.1 Relationship between Free Water and Bleeding Capacity

Fig. 5.24 confirmed the previous study by Thummasujatit, et al. (2006) that the increase of free water content increased bleeding capacity of the tested mixtures with the application of naphthalene and melamine based superplasticizers. On the other hand, there

was no strong relationship between bleeding capacity and free water content of the tested mixtures with polycarboxylate based superplasticizer. It is noted here that a higher free water amount due to the higher water reducing efficiency by steric hindrance mechanism results in the larger deformation of the concrete as discussed in section 4.4 in chapter 4, however the increased free water does not cause the increase of bleeding of the mixtures. This may be because the chains of polycarboxylate based superplasticizer prevent the settlement of powder particles.

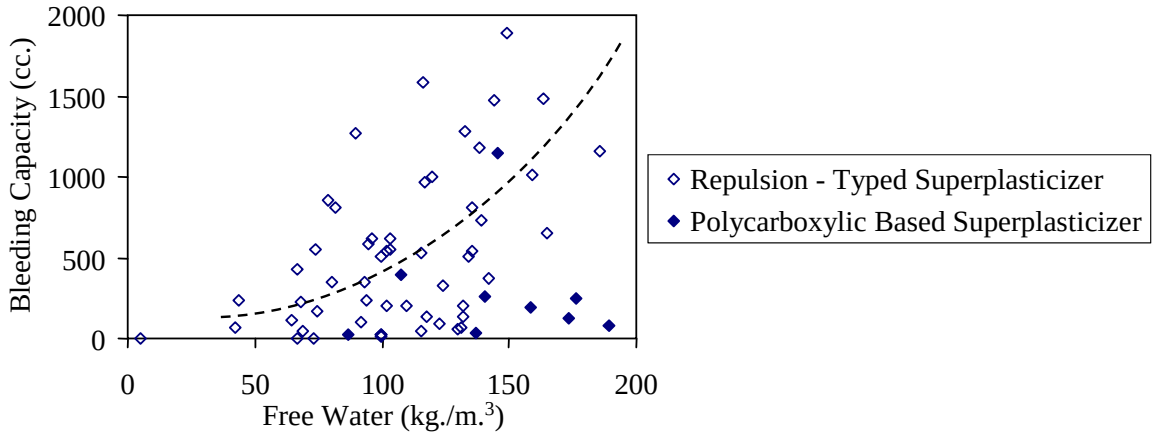

Fig. 5.24 Relationship between free water and bleeding capacity of the tested mixtures

5.5.2 Relationship between Effective Surface Area of Solid Particles and Bleeding Capacity

Effective surface area of solid particles indicates the possible contacts among fine aggregate, coarse aggregate and powder particles. Fig. 5.25 indicates that the increase of effective surface area of solid particles decreases the bleeding capacity. It can be explained that the larger surface area of solid particles causes the increase of solid stress, so the hydraulic pressure gradient of fresh concrete is reduced. Permeability is also lower when surface area is larger (comparing mixtures with the same free water content).

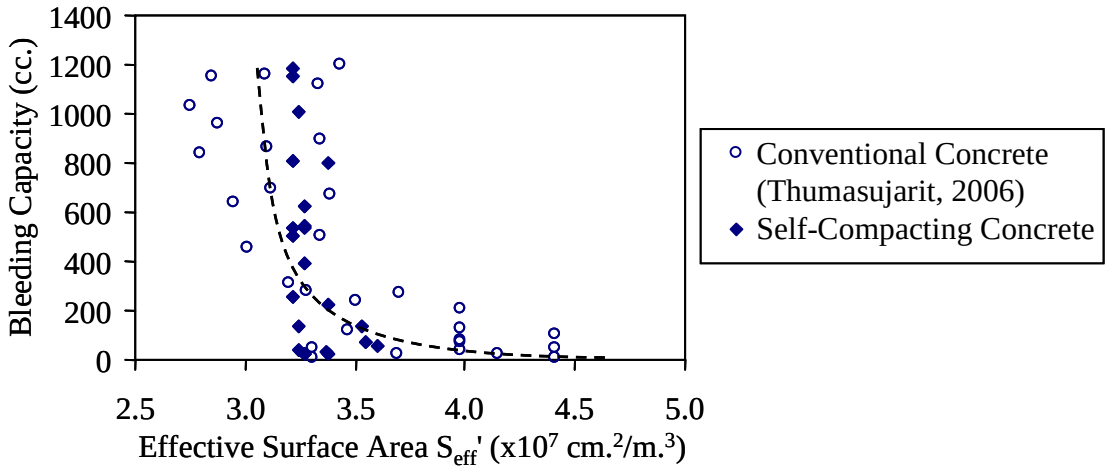

Fig. 5.25 Relationship between effective surface area of solid particles and bleeding capacity of the tested mixtures

5.5.3 Relationship between Average Degree of Reactions and Bleeding Capacity

The relationship between bleeding capacity of SCC and average degree of reactions is shown in Fig. 5.26. It can be seen that the increase of average degree of reaction decreases the bleeding capacity. These get along with the test results conducted by Thumasujarit (2006). This is because free water in the mixtures is utilized in the hydration and pozzolanic reactions, resulting in reduction of free water. More developed reactions also cause higher solid-to-solid friction which reduces hydraulic pressure.

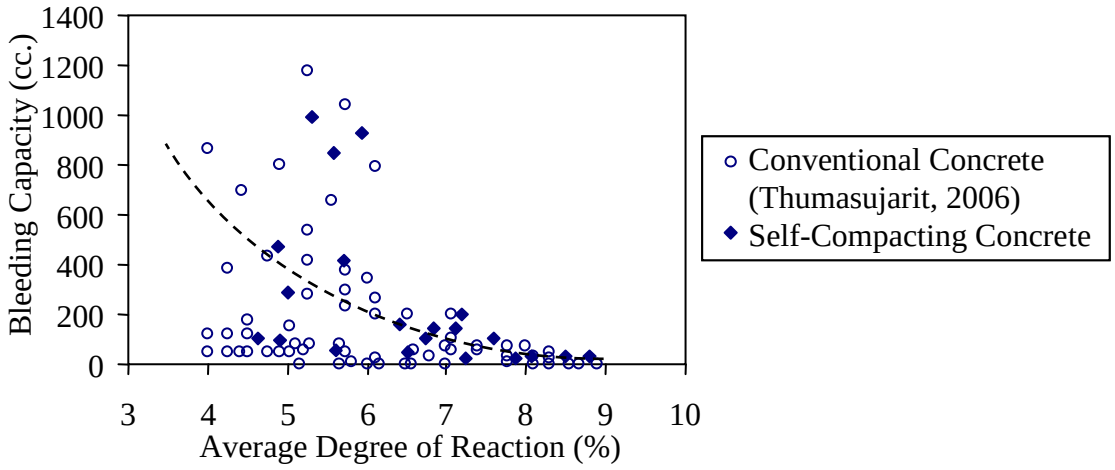

Fig. 5.26 Relationship between bleeding capacity and average degree of reactions of the tested mixtures

5.5.4 Relationship between Bleeding Capacity vs. Free Water Volume and Effective Surface Area of Solid Particles

Bleeding capacity, free water volume, and effective surface area of solid particles can be determined at a certain time when bleeding has been measured. It can be seen from Fig. 5.27 that at the same free water content, the bleeding capacity reduced with the increase of effective surface area of solid particles.

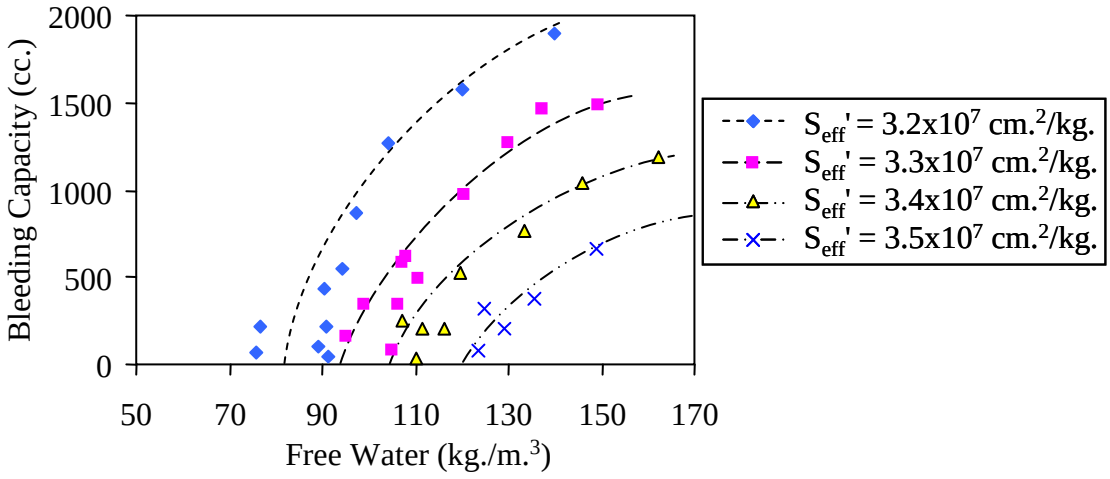

Fig. 5.27 Relationship between bleeding capacity and free water classified by different effective surface area of solid particles

5.6 Model for Predicting Bleeding Capacity of SCC

Since the relationship between free water content versus bleeding capacity of the tested mixtures with polycarboxylate based superplastizer had not yet been formulated, the model for predicting bleeding capacity of SCC was formulated by using only the results of the tested mixtures with the repulsion-typed superplasticizers, based on the modification of the proposed model of conventional concrete by Thumasujarit (2006). However, further studies are required to include the effect of steric hindrance mechanism by polycaboxylate based superplasticizer into the model.

Time at 30 minutes after mixing was selected to be the starting time because a period of time is needed for free water to rise to the top surface of freshly placed concrete and becomes obviously detectable from the concrete surface. The bleeding volume measured at 30 minutes was thus considered as the initial bleeding volume.

The model for predicting bleeding capacity of the mixtures was formulated based on test results presented in sections 5.4 and 5.5 and is shown in Eqs. (5.10) to (5.12).

$$BV_T = \phi_{bvt} \cdot BV_{To} \tag{5.10}$$

where

$$\begin{aligned} BV_{To} = {} & \alpha_{ave}(t_o)^{-8.22} \cdot \exp((-0.17) \cdot W_{fr}(t_o)) \cdot (-0.22 \cdot \alpha_{ave}(t_o)^{0.02} \\ & + S_{eff}'(t_o)^{-2.8} + 0.03 \cdot S_{eff}'(t_o) + 6.87 \times 10^{-4} \cdot W_{fr}(t_o) \\ & + (-0.04) \cdot \alpha_{ave}(t_o)) \cdot \exp(-41.46 \cdot \alpha_{ave}(t_o)^{-0.15} \\ & + W_{fr}(t_o)^{0.56} + 1.84 \cdot S_{eff}'(t_o)) \cdot W_{fr}(t_o)^{10.04} \\ & + 37.52 \cdot \alpha_{ave}(t_o) + 223.37 \\ & \geq 0 \end{aligned} \tag{5.11}$$

$$\begin{aligned} \phi_{bvt} = {} & 1 + \varphi \cdot (\varphi^{-10.47} \cdot \exp(0.58 \cdot \beta_c(t_o)^{-0.17} \\ & + 635.83 \cdot \beta_c(t_o) \cdot \varphi) \cdot (0.65 \cdot \varphi^{6.87} + 1.14 \cdot \beta_c(t_o) \\ & + (-0.65) \cdot \varphi') \cdot \exp(-5.16 \cdot \varphi'^{-0.68} \\ & + (-109.23) \cdot \varphi + (-13.71) \cdot \beta_f(t_o)) \\ & + (-70.58) \cdot \beta_c(t_o) + 14.86) \\ & \geq 0 \end{aligned} \tag{5.12}$$

where

BV_T is bleeding capacity of the concrete with water reducing admixture, cc.

BV_{To} is bleeding capacity of the mixture without water reducing admixtures, cc.

ϕ_{bvt} is bleeding capacity factor due to the application of water reducing admixtures (excluding polycarboxylate based superplasticizer)

t_o is starting time of bleeding (defined at 30 min).

$W_{fr}(t_o)$ is free water content at 30 min after mixing, kg/ m^3 of concrete.

$S_{eff}'(t_o)$ is effective surface area of solid particles at 30 min after mixing, cm^2/m^3 of concrete.

$\alpha_{ave}(t_o)$ is average degree of reaction at 30 min after mixing, %

φ	is dosage of water reducing admixture, % by weight of powder materials.
φ'	is water reducing efficiency of water reducing admixture.
$\beta_c(t_o)$	is water retainability coefficient of cement at 30 min after mixing.
$\beta_f(t_o)$	is water retainability coefficient of fly ash at 30 min after mixing.

It is noted here that the cessation of bleeding will be valid only when bleeding rate is zero. Hence, bleeding capacity at any time can not be less than zero in all cases. The proposed model is applicable for the powder-typed SCC mixture with the ratio of paste volume to void volume of the compacted aggregate phase between 1.4 to 1.8 and the use of repulsion-typed superplasticizer.

5.7 Verification of Bleeding Model

The bleeding capacity of the tested mixtures prepared by the author and Thumasujarit (2006) was calculated from the proposed model and was compared with that obtained from the tests. The details of materials and mix proportions used for verification tests can be seen in Table A-1 and B-2 in the Appendixes A and B, respectively. Fig. 5.28 shows the verification tests of bleeding capacity (total bleeding volume) of the tested mixtures with both repulsion-typed and polycarboxylate based superplasticizers. It is shown that the developed models can be used to predict the bleeding capacity of the mixtures with repulsion-typed superplasticizers with satisfactory accuracy (with coefficients of correlation 0.96); however it is not applicable for the mixtures with polycarboxylate based superplasticizer.

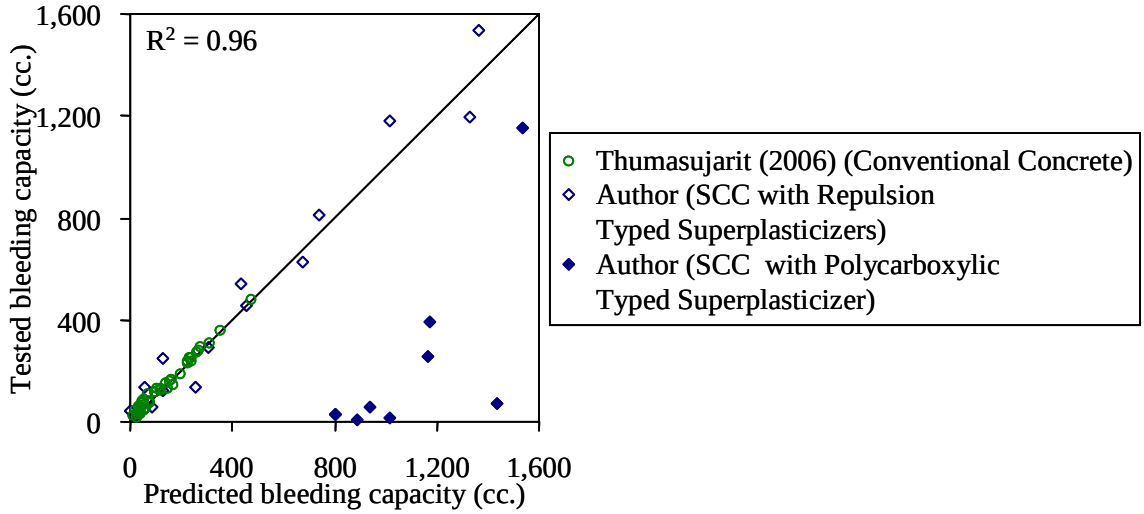

Fig. 5.28 Comparison between tested and predicted bleeding capacity (total bleeding volume)

5.8 Relationship between Bleeding Capacity and Static Segregation

It is assumed that effective resistance to static segregation can be achieved by limiting bleeding capacity of fresh concrete below a specified value. The relationship between bleeding capacity and static segregation was analyzed to determine the limit of bleeding capacity as the minimum requirement to avoid static segregation of SCC.

Test results in Fig. 5.29 show that L-box passing ability of the tested mixtures reduces with the increase of the differences of coarse aggregate weight ratios to total concrete between the top and the bottom concrete portions (S_G). As the L-box passing ability of 60 % was recommended as the passing condition for the test, the condition of good passing ability through narrow spaces was recognized for the mixtures with S_G less than 10 %. As a result, the SCC mixtures with the S_G smaller than 10 % were judged to be the mixtures that could avoid the aggregate blocking at clear spacing between steel bars due to static segregation.

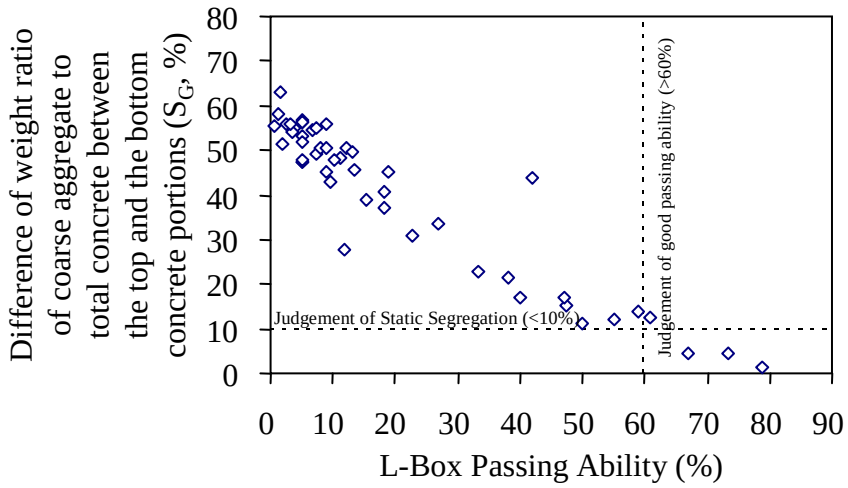

Fig. 5.29 Relationship between L-box passing ability and differences of weight ratio of coarse aggregate to total concrete between the top and the bottom concrete portions (S_G)

Fig. 5.30 indicates that S_G of the tested mixtures increases with the increase of bleeding capacity. Test results indicate that even though the bleeding capacity of the tested mixtures was either very low or none, the blocking due to dynamic segregation of the tested mixtures (L-box passing ability below 60 %, which was indicated by S_G larger than 10 %) could sometimes be observed. This led to the recommendation to avoid static segregation that SCC should have no bleeding. Hence, the tested bleeding capacity of 0 % was specified as the minimum requirement for mix proportioning of SCC, though passing ability may not be always satisfied when the mixture has zero bleeding especially when the condition of the opening is severe. It should be noted that this conclusion is only true for the condition of L-box used in the test. In actual construction, the condition of reinforcement is usually less severe and passing ability is usually satisfied in such case even though the SCC has a little bleeding.

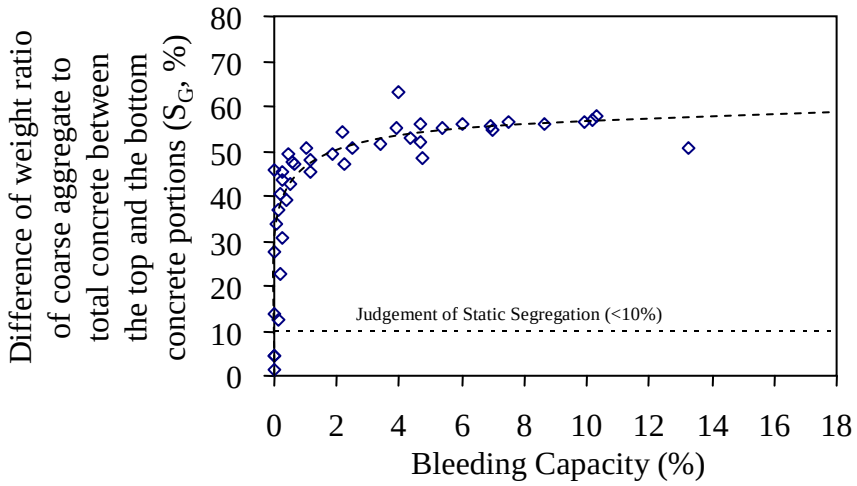

Fig. 5.30 Relationship between bleeding capacity and differences of weight ratio of coarse aggregate to total concrete between the top and the bottom concrete portions (S_G)

5.9 Conclusions

Based on the test results and the proposed prediction model for bleeding and static segregation of SCC, it was found that the increase of water to binder ratio increased the bleeding rate and bleeding capacity due to the larger amount of free water for bleeding in the mixtures. Moreover, bleeding capacity increased with the increase of ratio of paste volume to void volume of aggregate phase (γ) due to the increase of free water content directly caused by the higher unit water content of the tested mixtures. It was also found that bleeding capacity of the mixtures with naphthalene and melamine based superplasticizers increased with the increase of the water reducing efficiency. However, polycarboxylate based superplasticizer showed lower bleeding though having higher water reducing efficiency than the others due to the difference of dispersion mechanisms of superplasticizers i.e. electrostatic repulsion and steric hindrance. It was found that the higher concrete temperature caused the earlier initiation and termination of bleeding, a bit higher bleeding rate, and lower bleeding capacity of the tested mixtures due to the acceleration of the reactions of binder particles in the concrete.

It was confirmed that the main factors influencing bleeding of the SCC mixtures included free water content, effective surface area of solid particles, and average degree of reaction of binders. However, the relationship between bleeding capacity and free water content of the tested mixtures with polycarboxylate based superplasticizer was not existed. As a result, prediction model for bleeding capacity or total bleeding volume of the SCC mixtures only with the repulsion-typed superplasticizers was developed based on the modification of the previously proposed model of conventional concrete.

The verification tests confirmed that the proposed model can be used to predict bleeding capacity of the tested SCC mixtures with appropriate accuracy. However, further development of the proposed model requires inclusion of the effect of steric hindrance mechanism.

To avoid static segregation, it was suggested that zero bleeding capacity should be specified as the minimum requirement for mix proportioning of the powder-typed SCC.

Chapter 6

Model for Predicting Passing Ability

6.1 General

In cases of narrow spaces in formwork or congested reinforcement, filling ability of SCC has to be fulfilled by the functional requirement namely passing ability through narrow openings in addition to good deformability and enough resistance to segregation. Passing ability is defined as the ability to flow through narrow spaces such as closely spaced reinforcement without segregating or blocking of aggregate particles (Skarendahl, 2000). In practice, there has to be compatibility between the size and amount of large solid particles in the self-compacting concrete and the clear spacing between reinforcing bars and formwork openings that the concrete must flow through (Tangtermsirikul, et al., 2000).

To briefly describe mechanism of blocking, when concrete flows through an opening, the aggregate particles around the opening have to change their flowing path to be able to flow through the opening. As a result, collision among the aggregate particles arises, creating many instantaneous contacts among the aggregate particles at the vicinity of the opening. By these aggregate contacts, there is a possibility that some aggregate particles form a stable arch, which blocks the rest of the flow of the concrete (Tangtermsirikul, et al., 2000). Fig. 6.1 illustrates the above mentioned explanation of the mechanism of aggregate blocking.

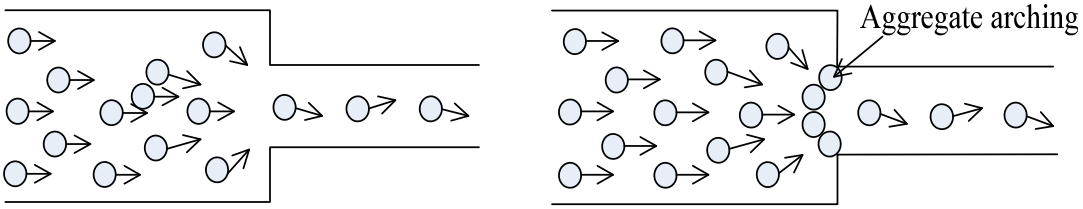

Fig. 6.1 Mechanism of aggregate blocking at narrow openings (Tangtermsirikul, et al., 2000)

In actual, filling ability of SCC depends not only on the internal factors i.e. deformability and segregation resistance of the concrete but also the external factors such as the congestion of the reinforcement. The effects of fresh concrete properties and reinforcement configurations on blocking mechanism were therefore considered as analytical parameters in the model formulation, which includes size distribution, volumetric ratio, shape and maximum size of aggregates, clear spacing and size of the reinforcement, as well as viscosity of the concrete. However, it is noted here that the proposed models are limited for self-compacting concrete without visual segregation and containing no viscosity agents. The diagram of influencing factors on passing ability through narrow openings of SCC is illustrated as in Fig. 6.2

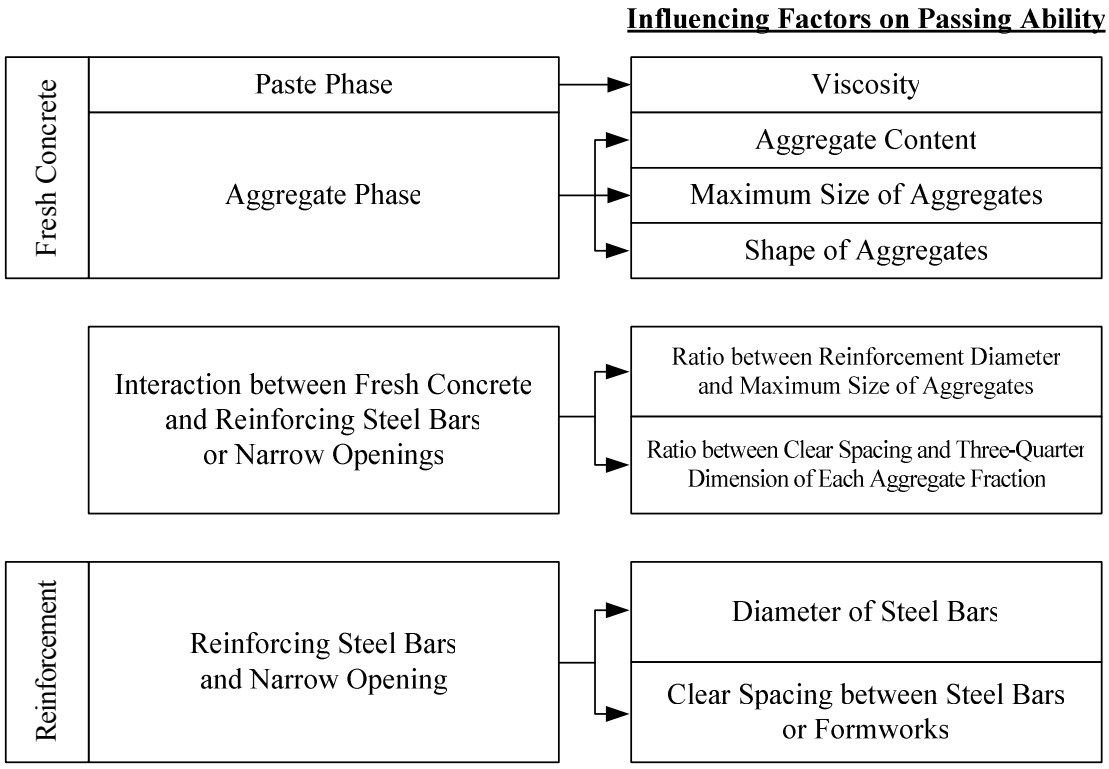

Fig. 6.2 Diagrammatic illustration of influencing factors on passing ability through narrow openings of SCC

6.2 Model Formulation

Based on mechanism of blocking of mortar flowing through round openings investigated by Ozawa, Tangtermsirikul, and Maekawa (1992), it was reported that the volume of sand which caused blocking depended on the amount of larger size of the sand and ratio of opening size to the sand particle size. It was found that the larger amount of large particles led to higher risk of blocking and the blocking volume of sand increased linearly with the ratio of the opening diameter to the mean size of sand

With regards to the blocking mechanism of SCC studied by Tangtermsirikul and Bui (1995, 2002), it was investigated that the larger aggregate volume and larger maximum size of aggregate resulted in higher risk of blocking. In addition, the aggregate blocking volume ratio is not only affected by the ratio of reinforcement clear spacing to aggregate particle size but also by the ratio between reinforcement diameter and maximum aggregate particle size, and by the inter-particle friction and properties of liquid phase of the mixture such as viscosity. They also proposed the analytical diagram for predicting the blocking aggregate volume formulated based on the blocking criteria with respect to the effects from type, size and volume of aggregates, and clear spacing and diameter of the reinforcements by assuming that the blocking volume ratios are independent on paste properties as long as the mixture has no static segregation (see Fig. 6.3).

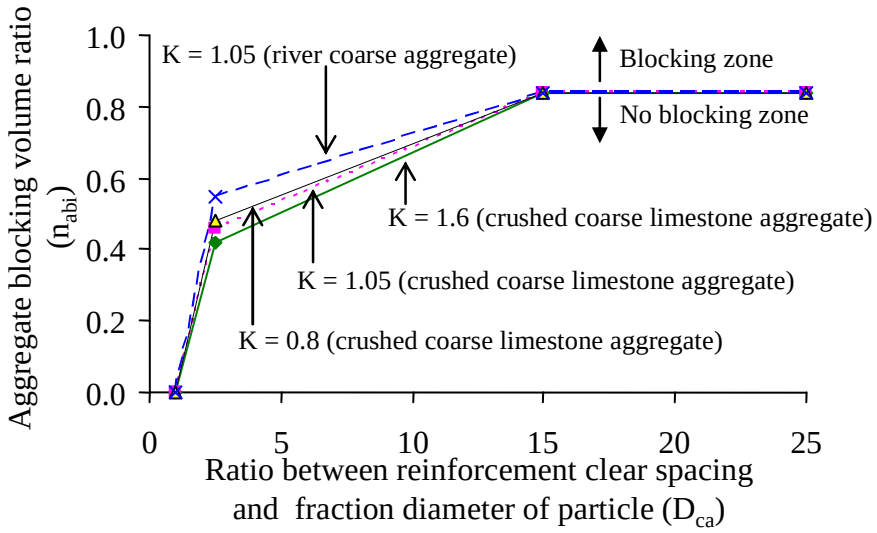

Fig. 6.3 Analytical diagram for predicting aggregate blocking volume proposed by Tangtermsirikul, et al. (2002)

As seen in the analytical aggregate blocking diagram (Fig. 6.3), the blocking and no blocking zones are divided by the calculated lines regarded as the criteria of blocking. The blocking criteria for aggregate phase relate the volume ratio of aggregate blocking to the ratio between reinforcement diameter and maximum aggregate size as well as the ratio between reinforcement clear spacing and three-quarter of each aggregate fraction. The proposed blocking criteria can be reasonably used to predict maximum aggregate volume which causes blocking called “aggregate blocking volume”. The proposed diagram is intentionally used for controlling particle size and content of aggregates in the concrete by considering reinforcement condition in order to avoid aggregate blocking. However, it is recommended that the blocking criteria should be implemented together with the concept of maximum average distance between aggregate particle surfaces to ensure the avoidance of blocking of the aggregate with the minimum paste content (Tangtermsirikul, et al., 2000, 2002).

In this study, the original blocking criteria concept of Tangtermsirikul, et al. (1995, 2002) was adopted and extended to include the effects of particle shape of coarse aggregate and viscosity of the concrete, in addition to the originally proposed parameters i.e. distribution, volumetric ratio and maximum size of the aggregates, and clear spacing and diameter of the reinforcements. However, it is noted here that the proposed model is limited for powder-typed self-compacting concrete without visual segregation and containing no viscosity agents. Prediction of passing ability through narrow opening in this study is illustrated by the flow chart shown in Fig. 6.4.

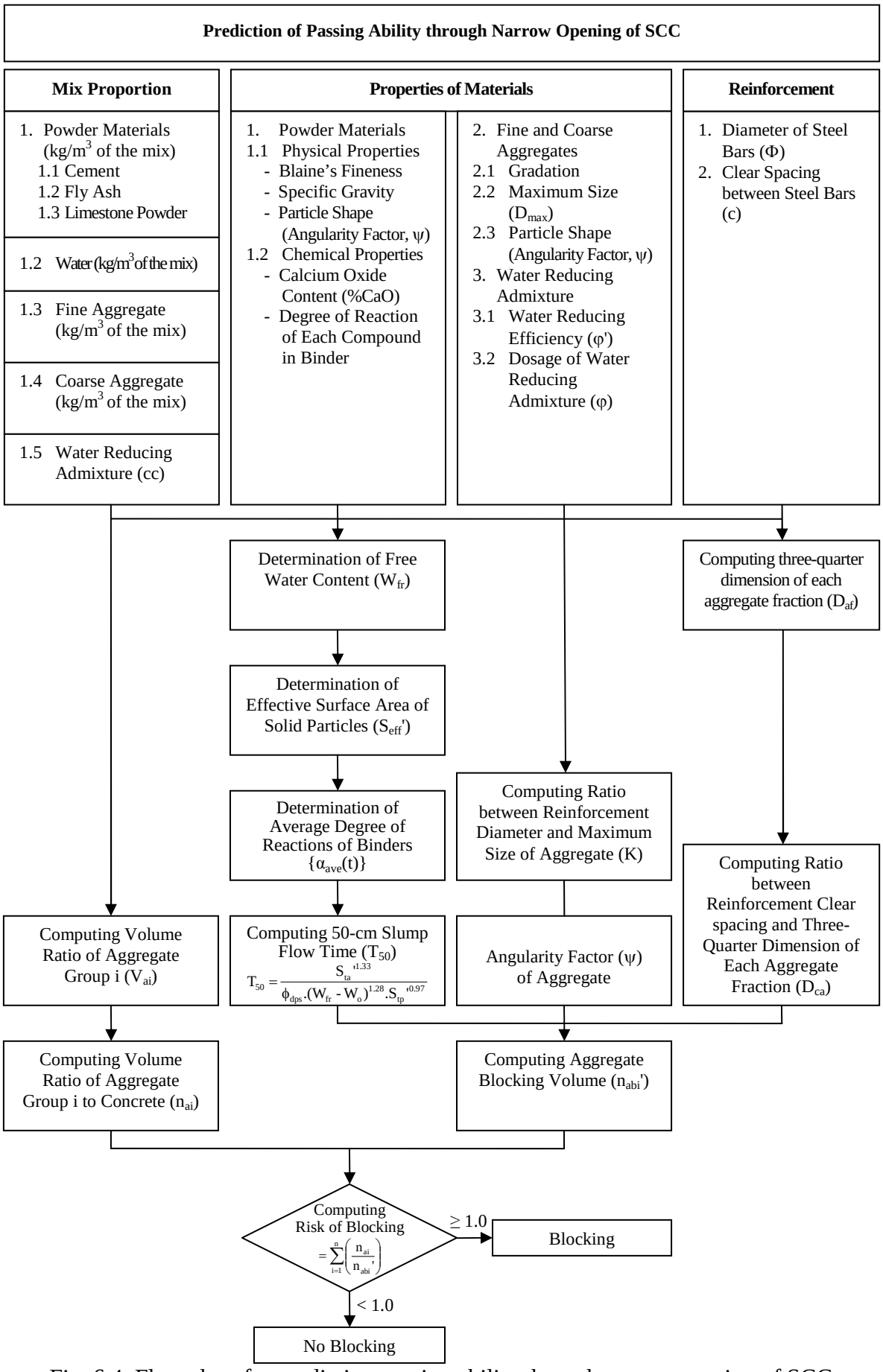

Fig. 6.4 Flow chart for predicting passing ability through narrow opening of SCC

6.3 Parameters Used in Model Formulation

The below mentioned concepts and parameters were used in this study to formulate the model for predicting the blocking volume ratio which means the maximum aggregate to concrete volume ratio that does not cause blocking through aggregate bridging at narrow openings.

6.3.1 Risk of Blocking

Properties and volume of aggregates in the concrete play a significant role on passing ability through narrow openings since concrete with excessively large aggregate or too much large aggregate content usually can not fill the heavily reinforced area due to blocking of the aggregate. In addition, the tendency of blocking increases with tendency of segregation of coarse aggregate particles. It is known that even though larger volume and larger maximum size of aggregate require lower paste content, this can cause a higher risk of blocking (Tangtermsirikul, et al. 2000, 2002).

An equation for computing the blocking risk of SCC as shown in Eq. (6.1) was proposed by Tangtermsirikul, et al. (2002) based on the mechanism of blocking of SCC flowing through narrow openings and the roles of fine and coarse aggregates on blocking.

$$\text{Risk of blocking} = \sum_{i=1}^{n}\left(\frac{n_{ai}}{n_{abi}}\right) \tag{6.1}$$

$$= \sum_{i=1}^{n}\left(\frac{V_{ai}/V_t}{V_{abi}/V_t}\right) \tag{6.1a}$$

$$= \sum_{i=1}^{n}\left(\frac{V_{ai}}{V_{abi}}\right) \tag{6.1b}$$

where

n_{ai}	is volume ratio of aggregate group i to total concrete.
n_{abi}	is blocking volume ratio of aggregate group i to total concrete.
V_{ai}	is volume of aggregate group i, m^3 of the mix.
V_{abi}	is the blocking volume of aggregate group i, m^3 of the mix.
V_t	is total volume of the concrete mixture, m^3.
n	is number of aggregate size groups.

The maximum total aggregates volume which does not cause blocking can be derived at the value of blocking risk equal to 1.0, as in Eqs. (6.2) and (6.3) (Tangtermsirikul, et al., 2002).

$$\sum_{i=1}^{n}\left(\frac{V_{ai}}{V_{abi}}\right) = 1.0 \tag{6.2}$$

$$V_{atmax} = \sum_{i=1}^{n} V_{ai} = V_a \tag{6.3}$$

where

V_{atmax} is the maximum total aggregate volume, m^3 of the mix.
V_{ai} is volume of aggregate group i.
V_{abi} is blocking volume of aggregate group i.
V_a is volume of total aggregates, m^3 of the mix

6.3.2 Aggregate Blocking Volume Ratio

Considered as the main parameter used for the blocking criteria concept, the aggregate blocking volume ratio means the maximum volume ratio of aggregates to total concrete, which does not cause blocking during concrete flowing through narrow opening. It can be derived from Eq. (6.4) (Tangtermsirikul, et al., 2002)

$$n_{abi} = \frac{V_{abi}}{V_t} \tag{6.4}$$

where

n_{abi} is blocking volume ratio of aggregate group i.
V_{abi} is blocking volume of aggregate group i, m^3 of the mix.
V_t is total volume of the concrete mixture, m^3 of the mix.

The analytical blocking volume of single-sized aggregate can be computed from Eq. (6.5) which was formulated based on the diagram in Fig. 6.2 (Tangtermsirikul, et al., 2002).

$$n_{abi} \begin{cases} = (-0.05K+0.36)D_{ca} + (0.05K-0.36) & ; \text{when } 1.0 \le D_{ca} < 2.5 \\ = (0.01K+0.02)D_{ca} + (-0.09K+0.48) & ; \text{when } 2.5 \le D_{ca} < 15 \\ = 0.84 & ; \text{when } D_{ca} \ge 15 \end{cases} \tag{6.5}$$

where

n_{abi} is blocking volume ratio of aggregate group i.
D_{ca} is ratio between reinforcement clear spacing and three-quarter dimension of each aggregate fraction, which will be discussed in section 6.3.4.
K is ratio between reinforcement diameter and maximum size of aggregate. It will be explained in section 6.3.5.

Also as another parameter to obtain risk of blocking as appeared in Eq. (6.1), the volume ratio between total aggregates and total volume of the concrete is defined as in Eq. (6.6) (Tangtermsirikul, et al., 2002).

$$n_a = \frac{V_a}{V_t} \tag{6.6}$$

where

n_a is volume ratio of total aggregates to total concrete.
V_a is volume of total aggregates, m^3 of the mix.
V_t is total volume of the concrete mixture, m^3.

6.3.3 Volume Ratio of Coarse Aggregate to Total Aggregates

Coarse to fine aggregates ratio affects the void content and total surface area of the aggregate phase. The optimum coarse to fine aggregates ratio must lead to a less required paste volume, and simultaneously satisfying the requirement of fresh concrete and hardened concrete properties (Tangtermsirikul, et al., 2002). However, when the ratio of coarse aggregate to fine aggregate is too high, fresh concrete can face the blocking problem. Therefore, the volume ratio of coarse aggregate to total aggregate was used in this study as one of the significant parameters for mix proportioning of the SCC mixture to avoid the blocking of aggregate. The volume ratio of coarse aggregate to total aggregate is defined in the following equation (Tangtermsirikul, et al., 2002).

$$N_{ga} = \frac{V_g}{V_g + V_s} \tag{6.7}$$

or $$N_{ga} = 1- s/a \tag{6.8}$$

where

N_{ga} is volume ratio of coarse aggregate to total aggregates in the concrete, m^3 of the mix.
V_g is volume of coarse aggregate in the concrete, m^3 of the mix.
V_s is volume of fine aggregate in the concrete, m^3 of the mix.
s/a is sand to total aggregate ratio.

6.3.4 Ratio between Clear Spacing of Reinforcement and Three-Quarter Dimension of Each Aggregate Fraction

The arching of aggregate particles is developed easier when the size of aggregate is large and also the content of aggregate is high. For smaller aggregate size, arching occurs at the higher content of aggregate, however arching can not occur if the solid particles are too small when compared to dimension of the opening (Tangtermsirikul, et al. 1995). It is suggested that the blocking of the SCC with excellent deformability and resistance to segregation will occur in the conditions of either too large maximum size of the aggregate or excessively high content of large-sized aggregate (Tangtermsirikul, et al. 2000, 2002). Therefore, ratio between clear spacing of reinforcement and three-quarter dimension of each aggregate fraction was proposed by Tangtermsirikul, et al., 2002 to account for the effect of clear spacing between the steel bars as well as the volume and size of coarse aggregate on blocking through aggregate bridging. It can be expressed in the following equations (Tangtermsirikul, et al., 2002).

$$D_{ca} = \frac{c}{D_{af}} \tag{6.9}$$

where

$$D_{af} = M_{i-1} + 3/4\ (M_i - M_{i-1}) \quad (6.10)$$

where

D_{ca} is ratio between reinforcement clear spacing and three-quarter dimension of each aggregate fraction
c is clear spacing of the reinforcements, mm.
D_{af} is three-quarter dimension of each aggregate fraction, mm.
M_i,M_{i-1} are upper and lower sieve dimensions of aggregate group i, respectively, mm.

6.3.5 Ratio between Reinforcement Diameter and Maximum Size of Aggregate

Maximum size and volume of large particles of aggregate in the concrete mainly influence passing ability through narrow openings and they are the decisive factors to result in the ability to flow through the reinforcement area (Tangtermsirikul, et al. 2000, 2002). When using SCC with a specific maximum size of aggregate and content of large-sized aggregate, the use of reinforcement with large diameter is more subjective to blocking even though the clear spacing between bars is the same, because large reinforcement provides a more stable support for the aggregate arch (Tangtermsirikul, et al. 2000).

Ratio between reinforcement diameter and maximum size of aggregate was proposed to incorporate the effects of the size of steel bars and maximum size of coarse aggregate on the aggregate blocking of the SCC mixture. The ratio can be obtained from Eq. (6.11) (Tangtermsirikul, et al. 2002).

$$K = \frac{\Phi}{D_{max}} \quad (6.11)$$

where

K is ratio between reinforcement diameter and maximum size of aggregate.
Φ is reinforcement diameter, mm.
D_{max} is maximum size of aggregate, mm.

6.4 Effects of Influencing Factors on Passing Ability through Narrow Openings

The effects of influencing factors on the aggregate blocking of SCC, which includes particle shape and maximum size of coarse aggregate, diameter of steel bars, and viscosity of the concrete, was discussed and analyzed to formulate the analytical diagram for aggregate blocking volume as the model for predicting passing ability through narrow spaces of SCC. It is noted here that the tested mixtures was prepared to have slump flow in the range between 65 to 70 cm by varying dosage of superplasticizer.

6.4.1 Effect of Particle Shape of Coarse Aggregate on Passing Ability through Narrow Openings

It can be seen from Figs. 6.5 to 6.7 that L-box passing ability reduced with the increase of irregularity of coarse aggregate particles due to the higher inter-particle frictions and interlocking of the aggregate particles. In other words, the coarse aggregate with rounded shape has higher aggregate blocking volume ratio, allowing higher content of coarse aggregate in the concrete than that of coarse aggregate with more irregular shape.

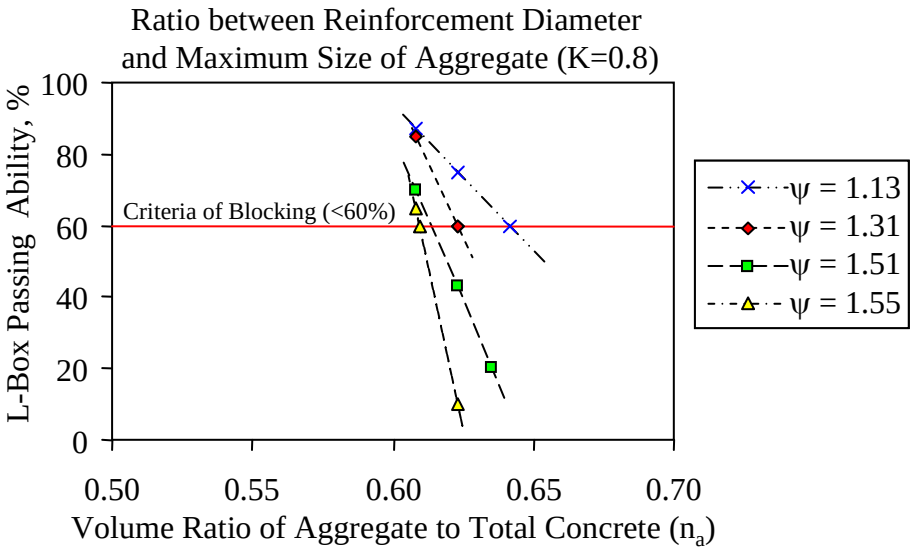

Fig. 6.5 Relationship between volume ratio of aggregate to total concrete and L-box passing ability of the mixtures with various shapes of coarse aggregate for the ratio between reinforcement diameter and maximum size of aggregate (K) of 0.80

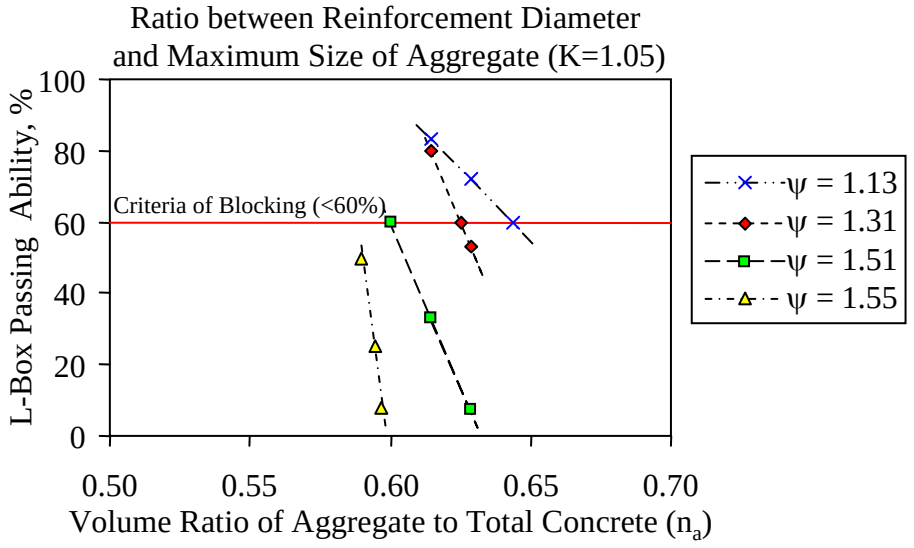

Fig. 6.6 Relationship between volume ratio of aggregate to total concrete and L-box passing ability of the mixtures with various shapes of coarse aggregate for the ratio between reinforcement diameter and maximum size of aggregate (K) of 1.05

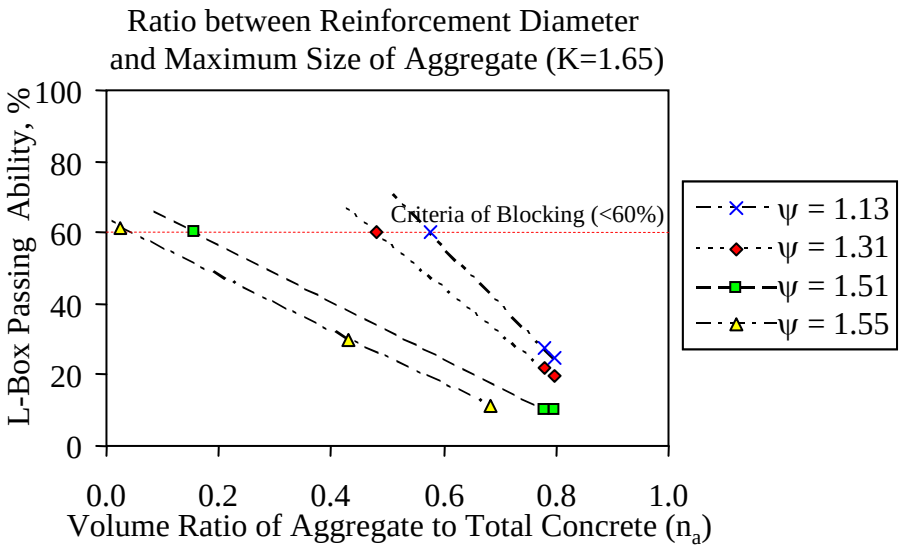

Fig. 6.7 Relationship between volume ratio of aggregate to total concrete and L-box passing ability of the mixtures with various shapes of coarse aggregate for the ratio between reinforcement diameter and maximum size of aggregate (K) of 1.65

6.4.2 Effect of Maximum Size of Coarse Aggregate on Passing Ability through Narrow Openings

Fig. 6.8 shows the effects of maximum size of aggregate on L-box passing ability. It can be seen that at similar aggregates content, the larger maximum size of coarse aggregate resulted in the lower L-box passing ability. It confirms that when using the larger maximum size of aggregate, the aggregate blocking volume ratio is reduced.

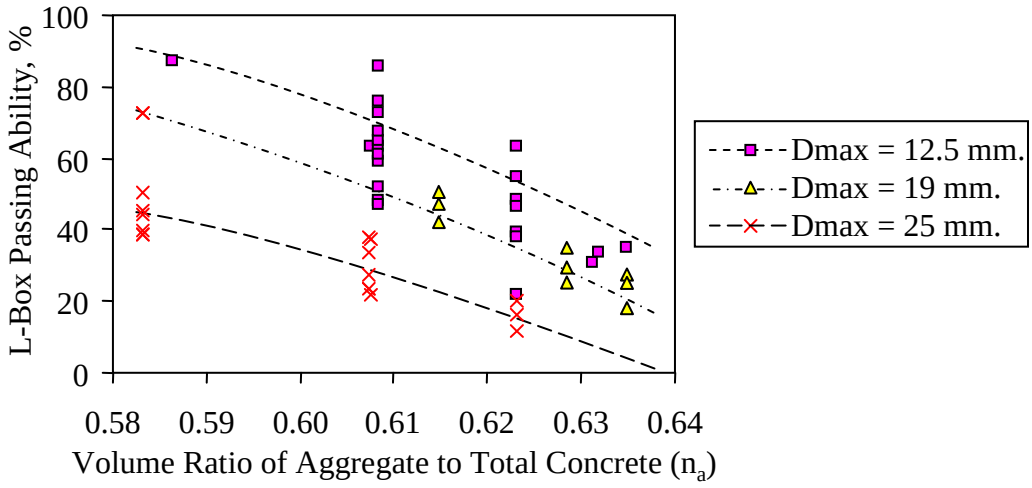

Fig. 6.8 Relationship between volume ratio of aggregate to total concrete and L-box passing ability of the tested mixtures with various maximum size of coarse aggregate

6.4.3 Effect of Diameter of Reinforcements on Passing Ability through Narrow Openings

It was confirmed from Fig. 6.9 that at similar aggregate content and clear spacing between steel bars, the larger reinforcement diameter caused the lower L-box passing ability. It is because the larger rebars provide better supports for the aggregate bridging at the opening.

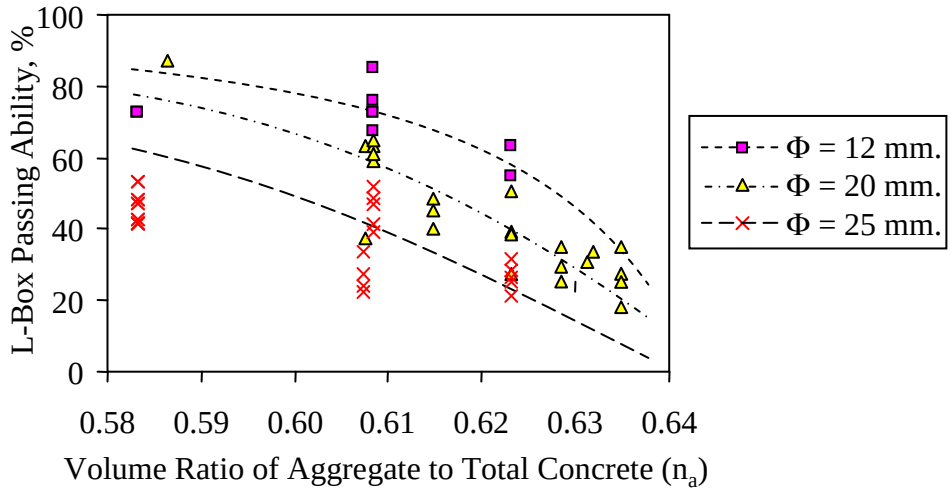

Fig. 6.9 Relationship between volume ratio of aggregate to total concrete and L-box passing ability of the tested mixtures by the L-box passing ability installed with different sizes of steel bars

6.4.4 Effect of Velocity of Deformation of the Mixtures on Passing Ability through Narrow Openings

In this study, the tested mixtures were prepared to have similar slump flow in order to investigate the effect of viscosity of the mixture (measured by T_{50}) on passing ability through narrow openings. It can be seen from Fig. 6.10 that for similar particle shape of the coarse aggregate, the highest L-box passing ability of the mixtures was achieved when T_{50} was within the optimum ranges. It was clear that the optimum ranges of the T_{50} were narrower when the particle shape of coarse aggregate was more irregular. This indicates that the range of the optimum T_{50} to satisfy L-box passing ability of the SCC mixed with more irregular coarse aggregate is smaller, leading to more difficulty in quality control of fresh concrete. It was also found that the L-box passing ability varied parabolically with T_{50}. It can be explained that the lower L-box passing ability of the tested mixtures was caused by the increase of resisting forces between the concrete mixtures and the wall sides and the reinforcement of the test apparatus, when the mixtures had too high viscosity (too high T_{50}), as well as by the blocking of the mixtures due to segregation and bleeding, if the viscosity of mixtures was too low (too low T_{50}). In addition, it was observed that at similar viscosity of the mixtures, the aggregate with higher irregularity resulted in the lower L-shape passing ability, which was due to the higher inter-particle frictions and interlocking among the aggregate particles.

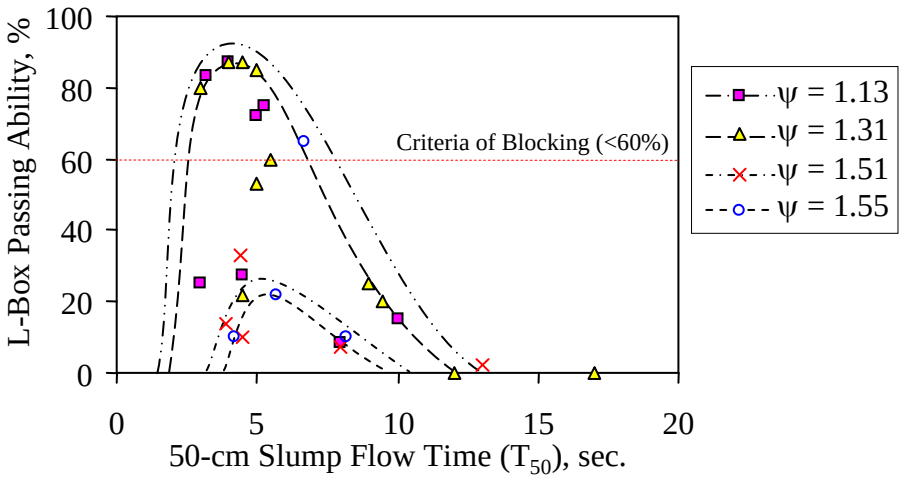

Fig. 6.10 Relationship between 50-cm slump flow time (T_{50}) and L-box passing ability of the mixtures with various shapes of coarse aggregate (ψ)

Similarly, Fig. 6.11 shows that the optimum range of T_{50} giving the highest L-box passing ability is larger when the volume of coarse aggregate is smaller. Test results indicate that to achieve the higher L-box passing ability, the variation of viscosity can be larger when the mixtures had a smaller aggregates volume. Also, it can be seen that at similar T_{50}, the smaller aggregate content gave the higher L-box passing ability due to smaller inter-particle frictions and lower possibility of interlocking of the aggregate particles resulted from the larger inter-particle distance or better dispersion of aggregate particles in the paste.

The results from Figs. 6.10 and 6.11 imply that practice on SCC is more difficult when the SCC incorporates aggregate with higher irregularity and/or higher coarse aggregate content because the SCC will be more sensitive to viscosity of the mixture.

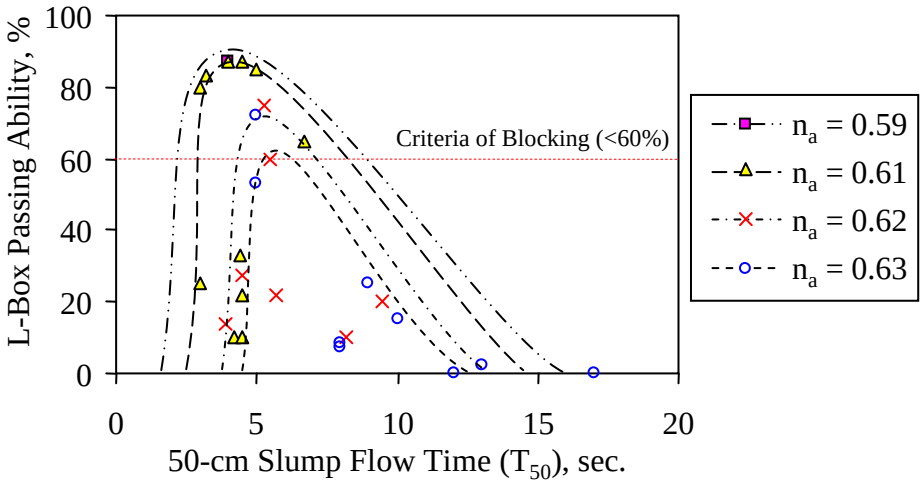

Fig. 6.11 Relationship between 50-cm slump flow time (T_{50}) and L-box passing ability of the mixtures with various volume ratios of total aggregates to total concrete (n_a)

6.5 Model for Predicting Passing Ability through Narrow Openings

Considered as the prediction model for passing ability in this study, the analytical diagram and equation to determine the blocking aggregate volume were established based on the analysis of test results in section 6.4. The proposed analytical diagram and equation for aggregate blocking volume are used for controlling volume of the aggregates in SCC mixtures to achieve the satisfactory passing ability through narrow openings.

6.5.1 Model for Predicting Aggregate Blocking Volume Ratio with the Effects of Particle Shape of Coarse Aggregate and 50-cm Slump Flow Time

6.5.1.1 Equation and Analytical Diagrams for Determining Aggregate Blocking Volume Ratio with the Effect of Particle Shape of Coarse Aggregate

From test results in this study, it is confirmed that the blocking volume of aggregate reduces with the increase of volume ratio of coarse aggregate to total aggregates (reduction of s/a ratio) and also with the increase of maximum size of coarse aggregate. Moreover, the larger ratio between reinforcement diameter and maximum size of aggregate gives the smaller aggregate blocking volume ratio. The coarse aggregate with higher irregularity gives the smaller aggregate blocking volume ratios for all ratios between reinforcement diameter and maximum size of aggregate. As a result, the equations and analytical diagrams for determining the blocking volume ratio of single-sized aggregate to total concrete were established and are shown in Eq. (6.12) and Figs. 6.12 to 6.14.

$$n_{abi} \begin{cases} = [(-0.0189\exp^{(2.431K)} \times \psi + 0.468\exp^{(0.855K)} - 0.15) \times (D_{ca}-1) / 1.5] \\ \quad \times \exp^{(-0.39K)} / (-0.63K^2 + 1.15K + 0.42) & ; \text{when } 1.0 \le D_{ca} < 2.5 \\ = [(0.84-(-0.0189\exp^{(2.431K)} \times \psi + 0.468\exp^{(0.855K)} - 0.15)) / 12.5 \\ \quad \times (D_{ca}-15) + 0.84] \times \exp^{(-0.39K)} / (-0.63K^2 + 1.15K + 0.42) & ; \text{when } 2.5 \le D_{ca} < 15 \\ = 0.84 & ; \text{when } D_{ca} \ge 15 \end{cases} \quad (6.12)$$

where

n_{abi} is blocking volume ratio of aggregate with size group i.
T_{50} is 50-cm slump flow time, sec.
ψ is angularity factor, which can be obtained from Eq. (4.7) in Chapter 4.
K is ratio between reinforcement diameter and maximum size of aggregate.
D_{ca} is ratio between reinforcement clear spacing and three-quarter dimension of each aggregate fraction.

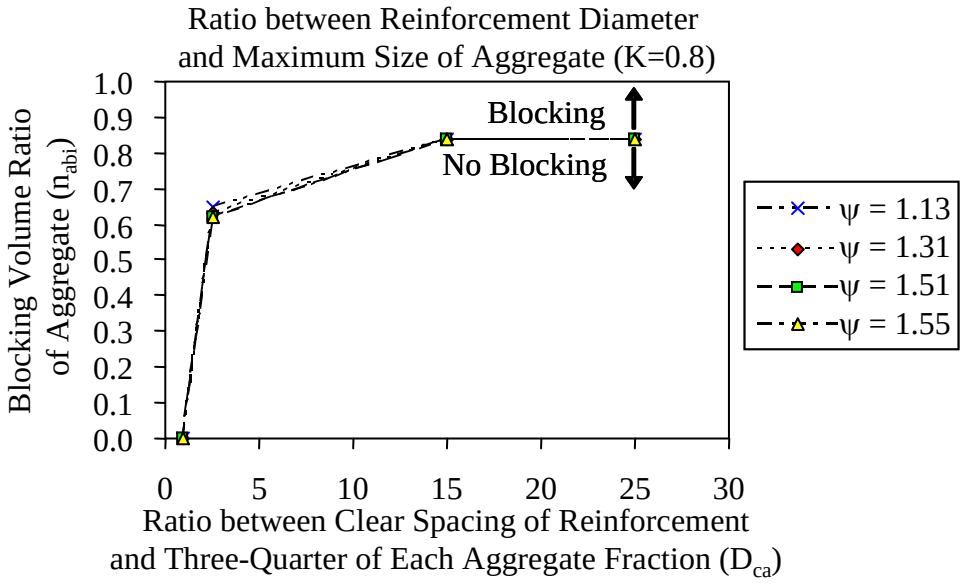

Fig. 6.12 Analytical diagram for determining the blocking volume ratio between single-size aggregate to total concrete of the tested mixtures with various shapes of coarse aggregate for the ratio between reinforcement diameter and maximum size of aggregate (K) of 0.80

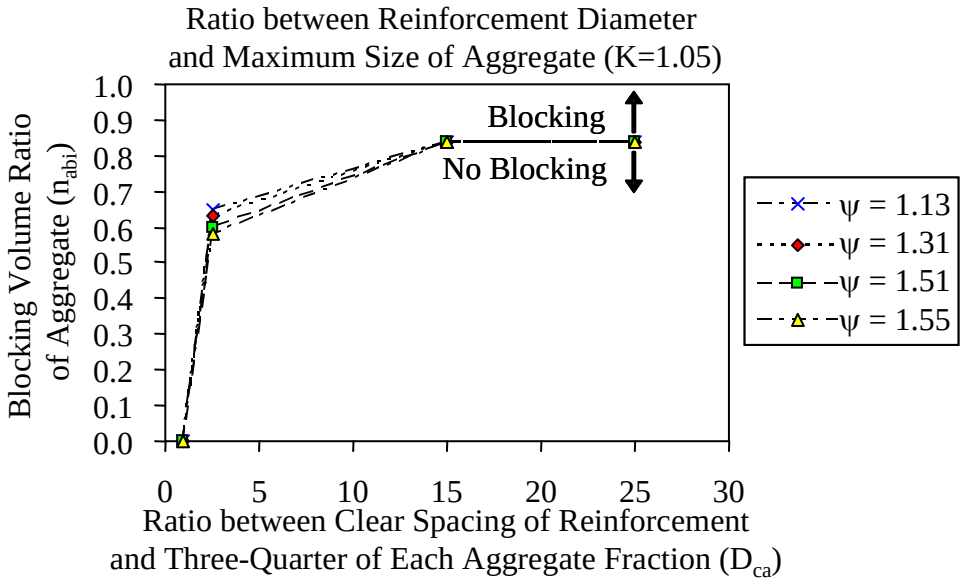

Fig. 6.13 Analytical diagram for determining the blocking volume ratio between single-size aggregate to total concrete of the tested mixtures with various shapes of coarse aggregate for the ratio between reinforcement diameter and maximum size of aggregate (K) of 1.05

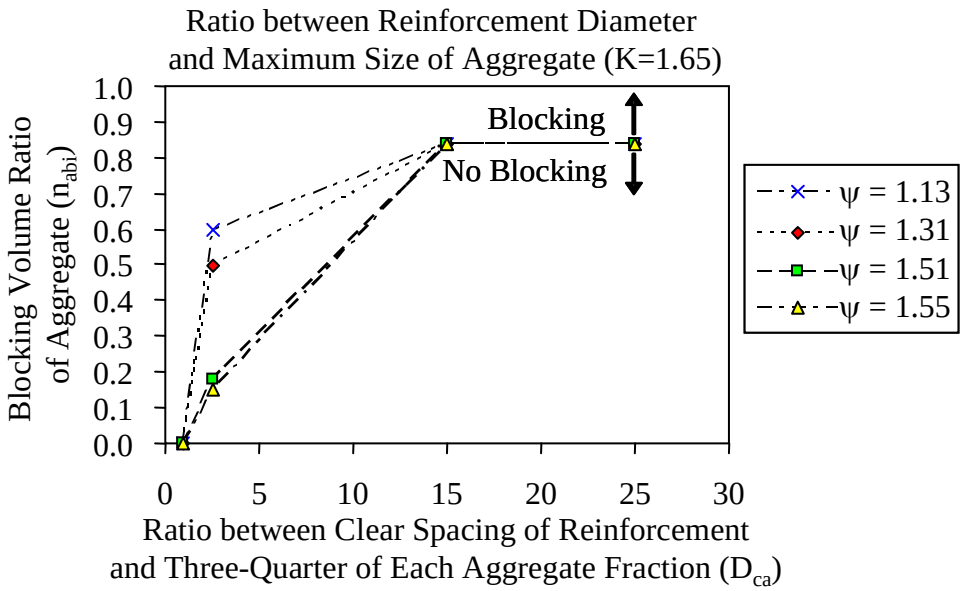

Fig. 6.14 Analytical diagram for determining the blocking volume ratio between single-size aggregate to total concrete of the tested mixtures with various shapes of coarse aggregate for the ratio between reinforcement diameter and maximum size of aggregate (K) of 1.65

6.5.1.2 Viscosity Factor for Aggregate Blocking Volume Ratio due to the Effect of Viscosity of the Mixture

Test results indicate that at similar slump flow and particle shape of coarse aggregate, the largest blocking volume of the aggregate can be achieved when T_{50} is within the optimum ranges (not neither too low nor too high). Moreover, at similar T_{50}, the coarse aggregate with lower irregularity gives the larger volume of aggregate blocking. In model formulation, the effect of viscosity of the mixtures on the blocking volume of single-sized aggregate was considered by introducing a factor called "viscosity factor" to modify the blocking aggregate volume ratios obtained from Eq. (6.5). The viscosity factor was assumed to have linear relationship with L-box passing ability by which the L-box passing ability of 60 % was determined by the viscosity factor of 1.0, which is considered as the judgment of blocking condition of the mixture (see Fig. 6.15).

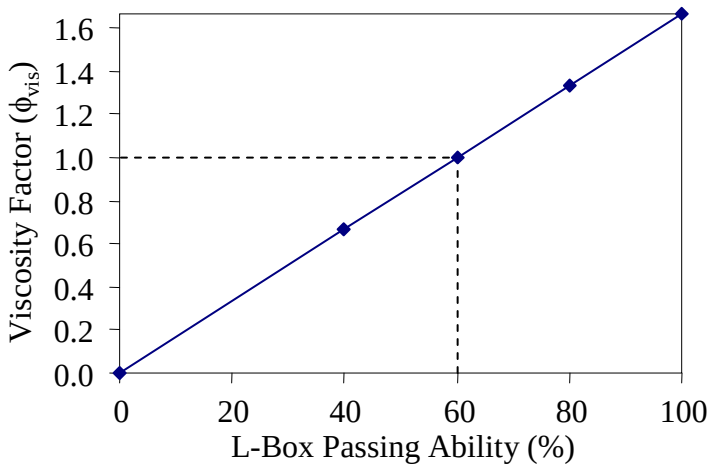

Fig. 6.15 Relationship between viscosity factor (ϕ_{vis}) and L-box passing ability

The viscosity factor was formulated from the analysis of the experimental data in Table B-3 in Appendix B as a function of 50-cm slump flow time, volume ratio of total aggregate to total concrete and angularity factor as expressed in Eq. (6.13).

$$\phi_{vis} = [(-7.3n_a + 3.2)T_{50}^{0.5} + (-316.2n_a + 175.7) / T_{50}^2 + 24n_a - 9.7] \times (1.08+0.002T_{50}^{1.5}+0.3/T_{50}) \times \exp^{((-0.29 - 0.003T_{50}^{1.5} - 0.33 / T_{50}) \times \psi)} \quad (6.13)$$

where

ϕ_{vis} is viscosity factor for the aggregate blocking volume.
T_{50} is 50-cm slump flow time, sec.
n_a is volume ratio of total aggregate to total concrete.
ψ is angularity factor of coarse aggregate.

The relationship between viscosity factor and 50-cm slump flow time is shown in Fig. 6.16.

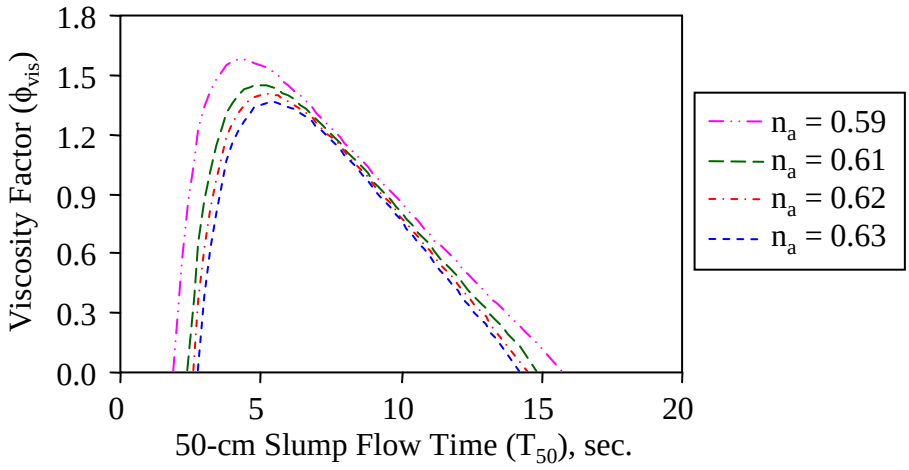

Fig. 6.16 Relationship between viscosity factor (ϕ_{vis}) and 50-cm slump flow time

6.5.1.3 Equation and Analytical Diagrams for Determining Aggregate Blocking Volume Ratio with the Effects of Particle Shape of Coarse Aggregate and 50-cm Slump Flow Time

Based on the concepts discussed in section 6.5.1.1 and 6.5.1.2, the equation for determining the blocking volume ratio of single-sized aggregate to total concrete could be finally formulated to include the effects of angularity factor, 50-slump flow time, volume ratio of total aggregate to total concrete, ratio between reinforcement diameter and maximum size of aggregate, and ratio between reinforcement clear spacing and three-quarter dimension of each aggregate fraction, as given in Eq. (6.14) and examples of analytical diagrams are shown in Figs. 6.17 to 6.22.

$$n_{abi}' = \phi_{vis}. n_{abi} \quad (6.14)$$

where

n_{abi}' is blocking volume ratio of aggregate group i, with the effects of particle shape of the coarse aggregate and viscosity of the mixtures.

n_{abi} is blocking volume ratio of aggregate group i, which can be obtained from Eq. (6.5).

ϕ_{vis} is viscosity factor for the aggregate blocking volume.

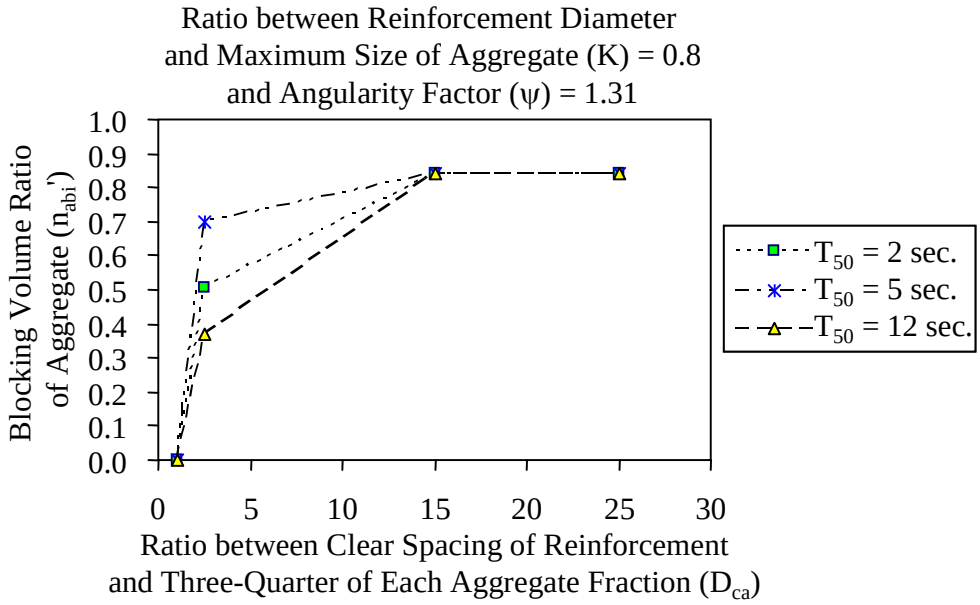

Fig. 6.17 Analytical diagram for determining the blocking volume ratio of single-sized aggregate of the tested mixtures with various 50-cm slump flow times {for the ratio between reinforcement diameter and maximum size of aggregate (K) = 0.80 and angularity factor of coarse aggregate (ψ) = 1.31}

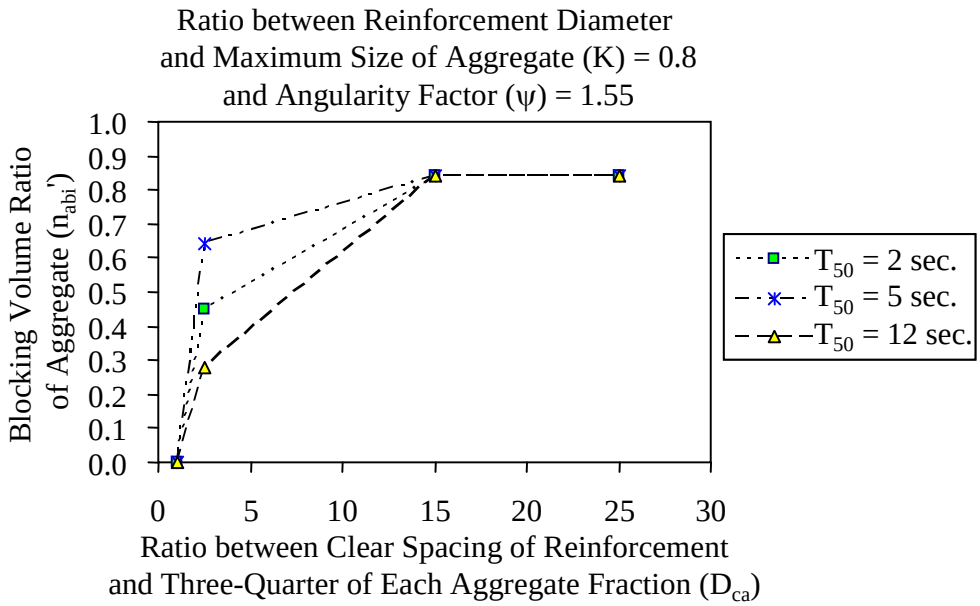

Fig. 6.18 Analytical diagram for determining the blocking volume ratio of single-sized aggregate of the tested mixtures with various 50-cm slump flow times {for the ratio between reinforcement diameter and maximum size of aggregate (K) = 0.80 and angularity factor of coarse aggregate (ψ) = 1.55}

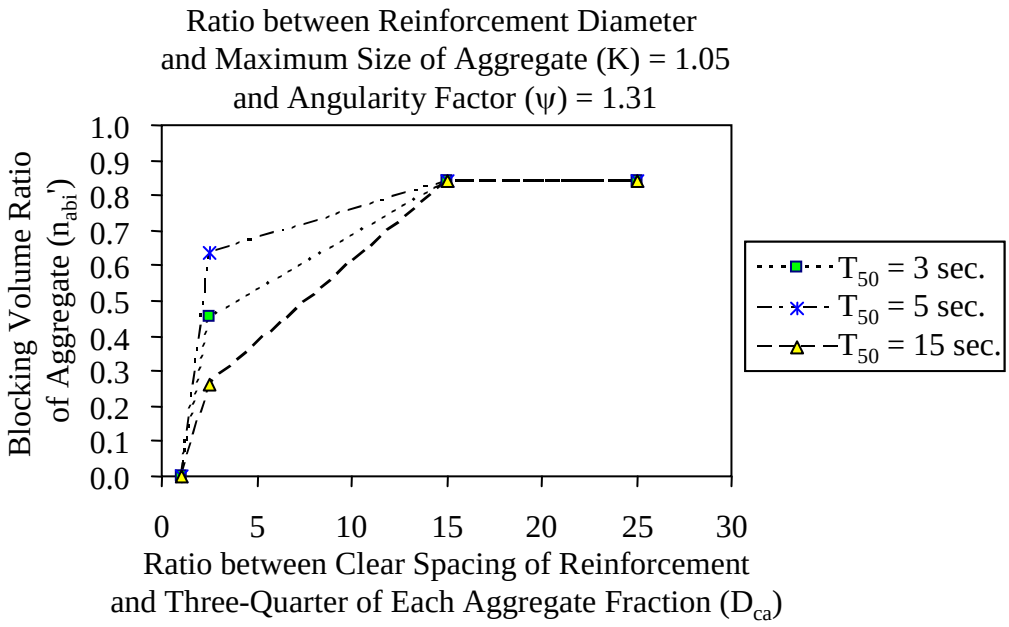

Fig. 6.19 Analytical diagram for determining the blocking volume ratio of single-sized aggregate of the tested mixtures with various 50-cm slump flow times {for the ratio between reinforcement diameter and maximum size of aggregate (K) = 1.05 and angularity factor of coarse aggregate (ψ) = 1.31}

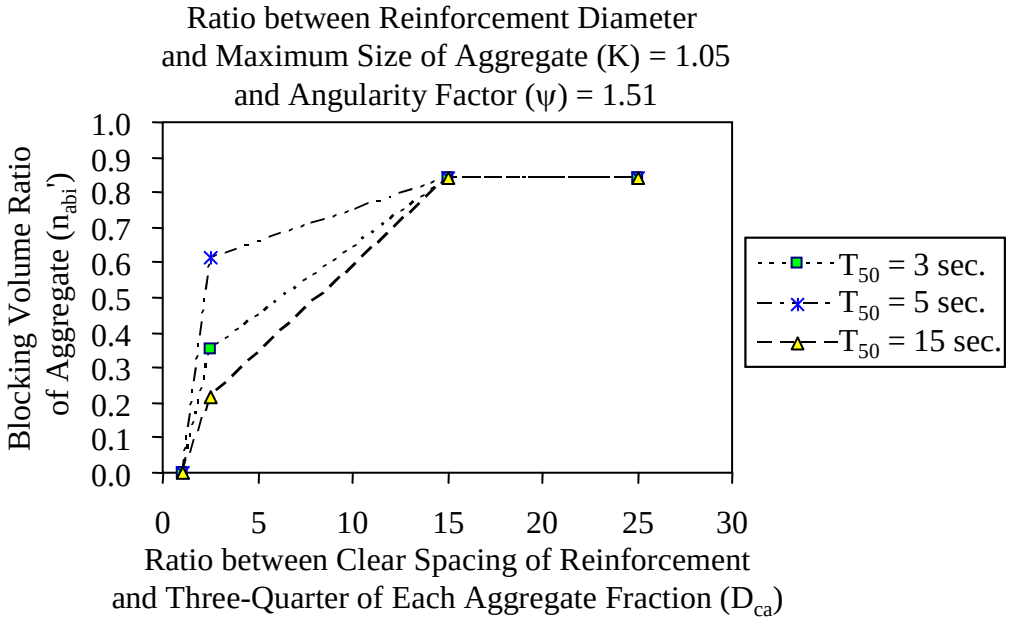

Fig. 6.20 Analytical diagram for determining the blocking volume ratio of single-sized aggregate of the tested mixtures with various 50-cm slump flow times {for the ratio between reinforcement diameter and maximum size of aggregate (K) = 1.05 and angularity factor of coarse aggregate (ψ) = 1.51}

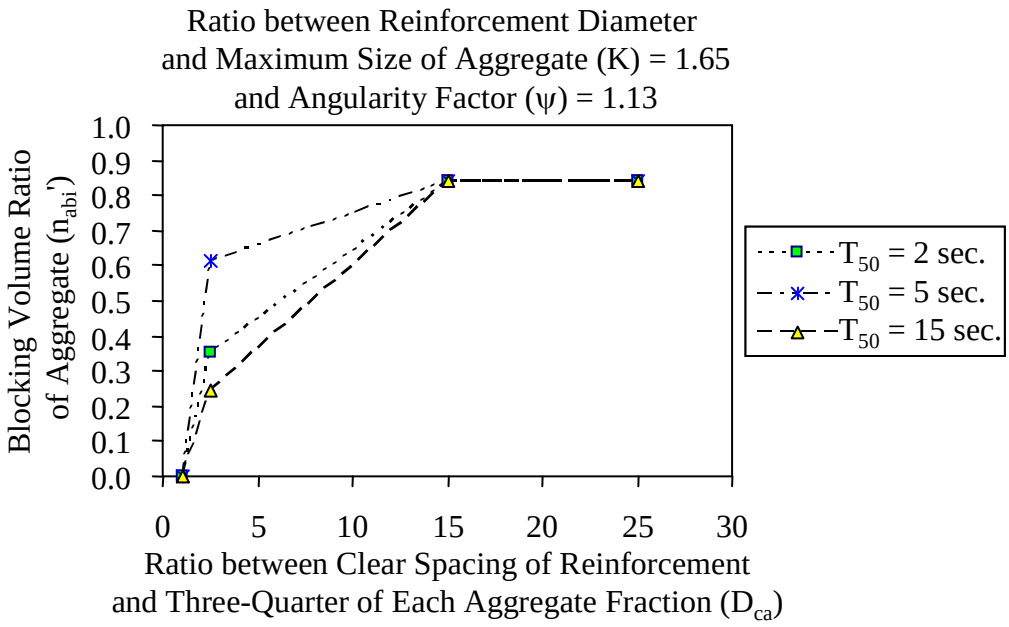

Fig. 6.21 Analytical diagram for determining the blocking volume ratio of single-sized aggregate of the tested mixtures with various 50-cm slump flow times {for the ratio between reinforcement diameter and maximum size of aggregate (K) = 1.65 and angularity factor of coarse aggregate (ψ) = 1.13}

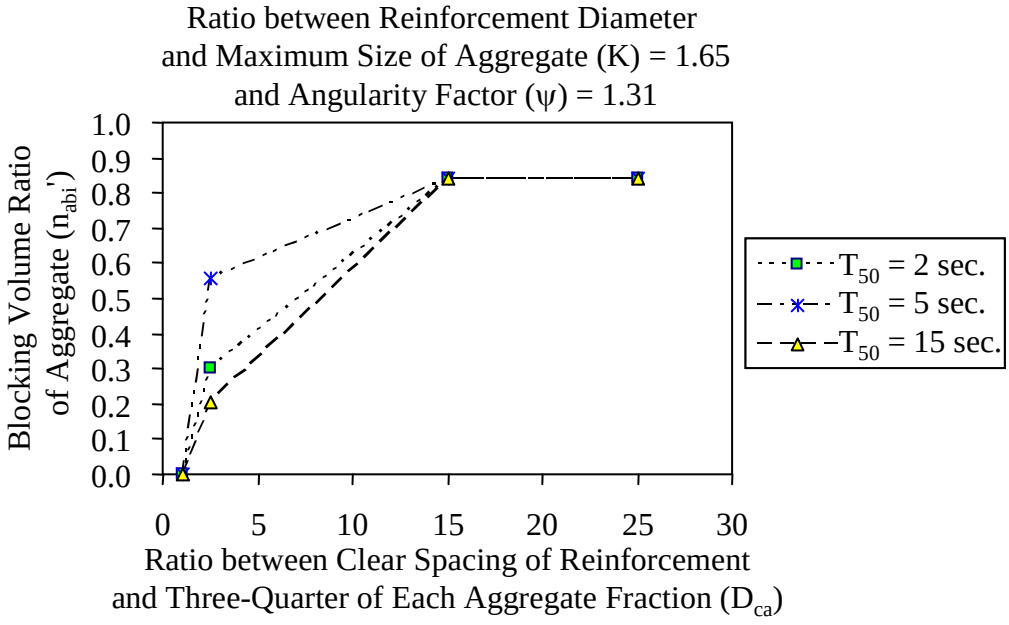

Fig. 6.22 Analytical diagram for determining the blocking volume ratio of single-sized aggregate of the tested mixtures with various 50-cm slump flow times {for the ratio between reinforcement diameter and maximum size of aggregate (K) = 1.65 and angularity factor of coarse aggregate (ψ) = 1.31}

6.5.2 Relationship between Aggregate Blocking Volume Ratio and Coarse Aggregate to Total Aggregates Ratio

Eqs. (6.12) to (6.14) for determining blocking volume ratio of single-sized aggregates to total concrete (n_{abi}') were used to compute the blocking aggregate volume ratio of total aggregates (n_{ab}') with regarding gradations of the tested aggregates. The gradations of fine and coarse aggregates used in this study were shown in Table A-4 in Appendix A.

The computed blocking volume ratios of total aggregates to total concrete was plotted against volume ratios of the coarse aggregate to total aggregates of the tested mixtures as analytical blocking criteria indicating boundary between blocking and no blocking conditions of the tested mixtures (see Figs. 6.23 to 6.28). The figures indicate that for similar ratio between diameter of reinforcement and maximum size of aggregates, similar particle shape of coarse aggregate and similar volume ratio of total aggregates to total concrete, when T_{50} were out of the optimum ranges, the volume of total aggregates has to be reduced to avoid the aggregate blocking. It is also indicated that at similar volume ratio of coarse aggregates to total aggregates and T_{50}, the coarse aggregate with high irregularity gives the smaller aggregate blocking volume.

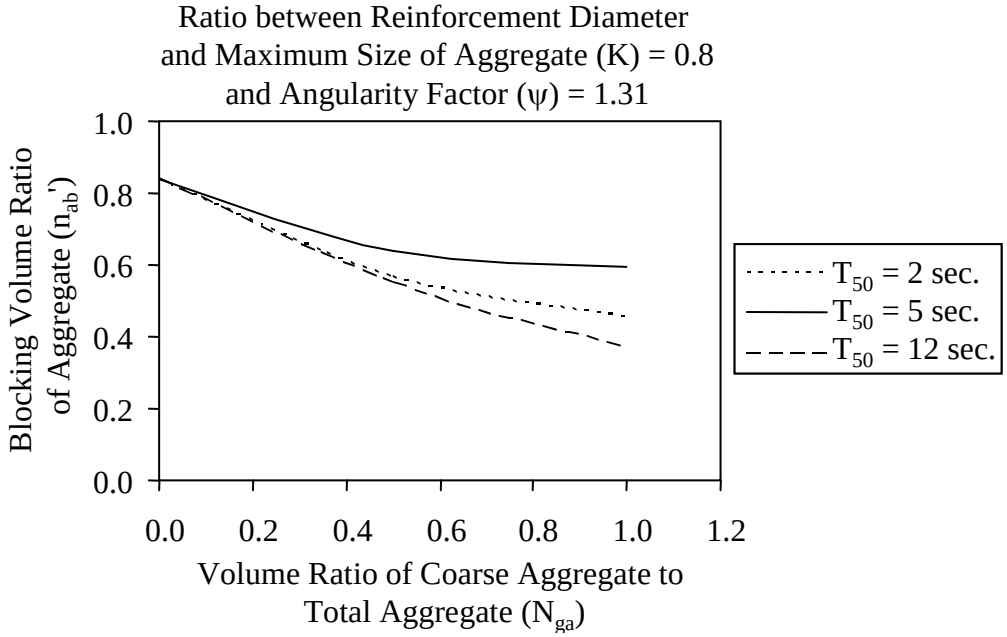

Fig. 6.23 Relationship between blocking volume ratio of aggregates (n_{ab}') vs. volume ratio of coarse aggregate to total aggregates (N_{ga}) of mixtures with various 50-cm slump flow times {for the ratio between reinforcement diameter and maximum size of aggregate (K) = 0.80 and angularity factor of coarse aggregate (ψ) = 1.31}

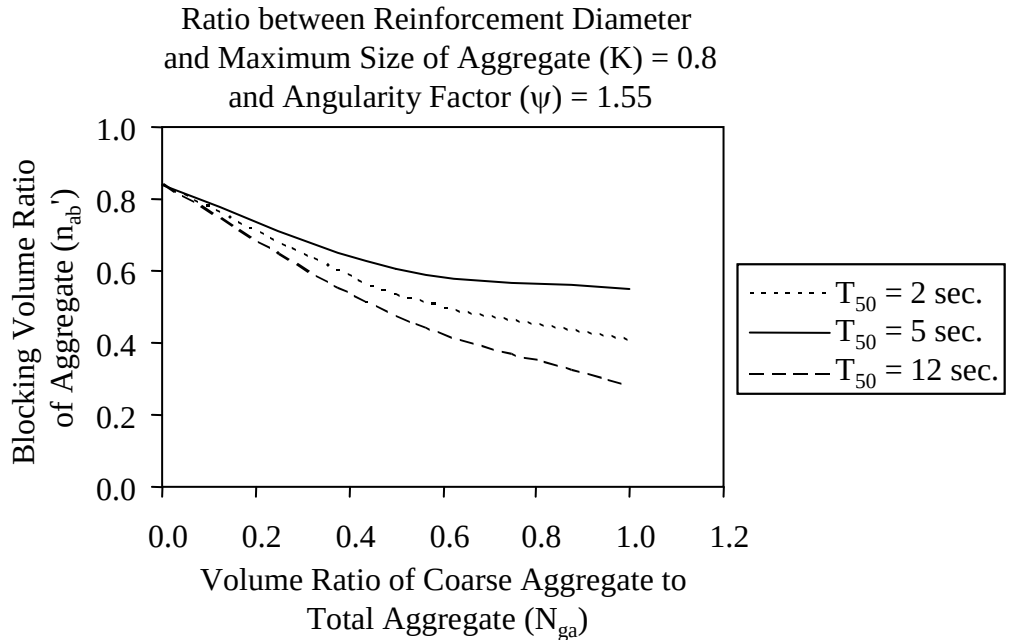

Fig. 6.24 Relationship between blocking volume ratio of aggregates (n_{ab}') vs. volume ratio of coarse aggregate to total aggregates (N_{ga}) of mixtures with various 50-cm slump flow times {for the ratio between reinforcement diameter and maximum size of aggregate (K) = 0.80 and angularity factor of coarse aggregate (ψ) = 1.55}

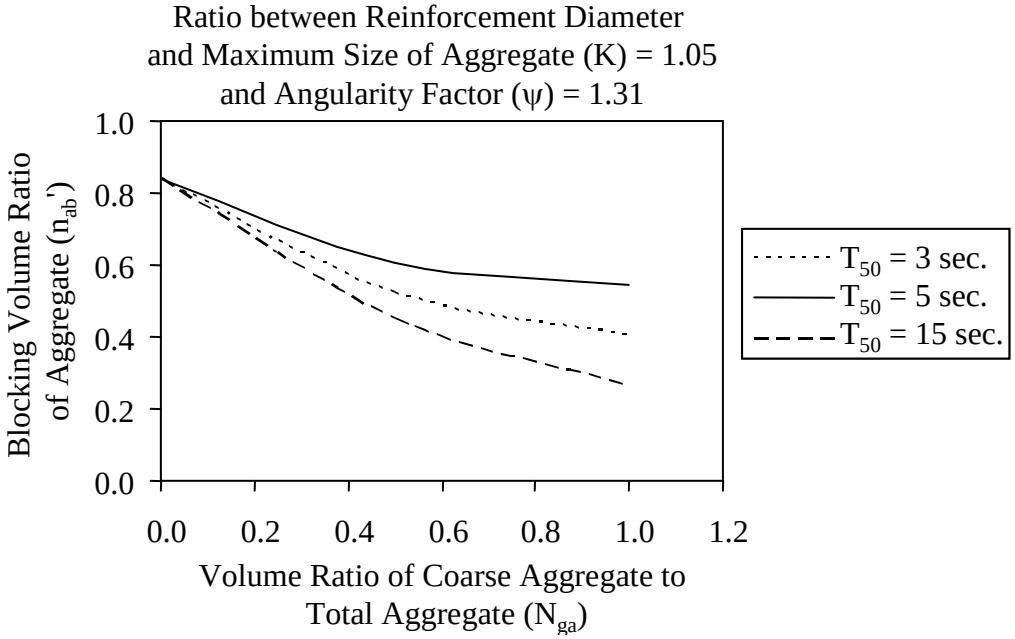

Fig. 6.25 Relationship between blocking volume ratio of aggregates (n_{ab}') vs. volume ratio of coarse aggregate to total aggregates (N_{ga}) of mixtures with various 50-cm slump flow times {for the ratio between reinforcement diameter and maximum size of aggregate (K) = 1.05 and angularity factor of coarse aggregate (ψ) = 1.31}

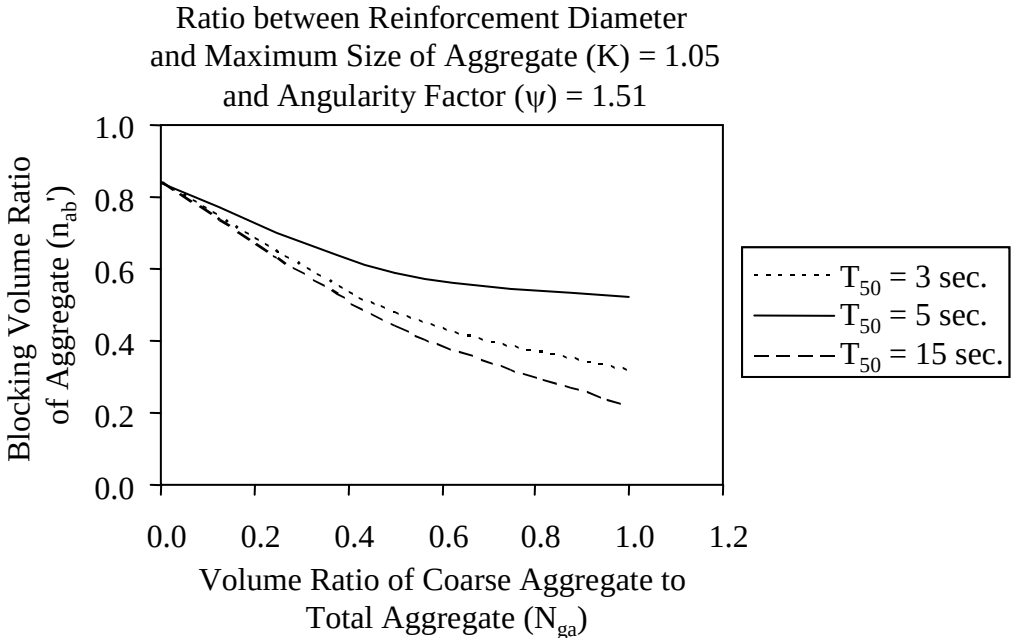

Fig. 6.26 Relationship between blocking volume ratio of aggregates (n_{ab}') vs. volume ratio of coarse aggregate to total aggregates (N_{ga}) of mixtures with various 50-cm slump flow times {for the ratio between reinforcement diameter and maximum size of aggregate (K) = 1.05 and angularity factor of coarse aggregate (ψ) = 1.51}

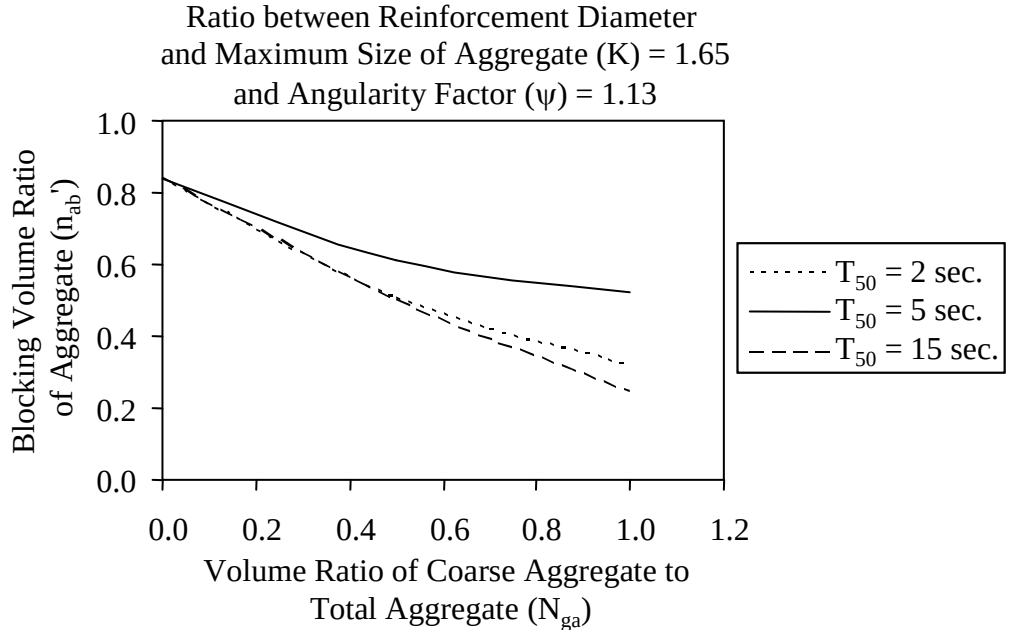

Fig. 6.27 Relationship between blocking volume ratio of aggregates (n_{ab}') vs. volume ratio of coarse aggregate to total aggregates (N_{ga}) of mixtures with various 50-cm slump flow times {for the ratio between reinforcement diameter and maximum size of aggregate (K) = 1.65 and angularity factor of coarse aggregate (ψ) = 1.13}

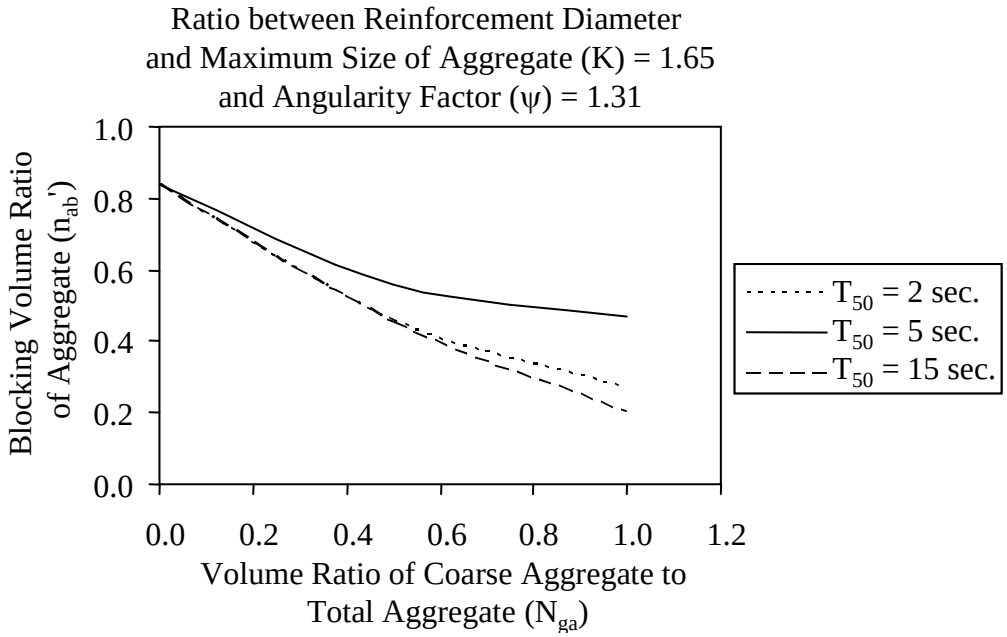

Fig. 6.28 Relationship between blocking volume ratio of aggregates (n_{ab}') vs. volume ratio of coarse aggregate to total aggregates (N_{ga}) of mixtures with various 50-cm slump flow times {for the ratio between reinforcement diameter and maximum size of aggregate (K) = 1.65 and angularity factor of coarse aggregate (ψ) = 1.31}

6.5.3 Relationship between Aggregate Blocking Volume Ratio and Ratio of Reinforcement Diameter to Maximum Size of Aggregate (K)

The relationships between the computed total aggregates blocking volume ratio vs. ratio of reinforcement diameter to maximum size of aggregate (K) are shown in Figs. 6.29 to 6.32. It is confirmed that for similar ratio between reinforcement clear spacing and three-quarter dimension of each aggregate fraction (D_{ca}) and similar shape of coarse aggregate, the aggregate blocking volume reduces with the increase of ratio of reinforcement diameter to maximum size of aggregate (K). It also indicates that at similar ratio of reinforcement diameter to maximum size of aggregate, the highest blocking volume ratio can be achieved at the optimum T_{50}.

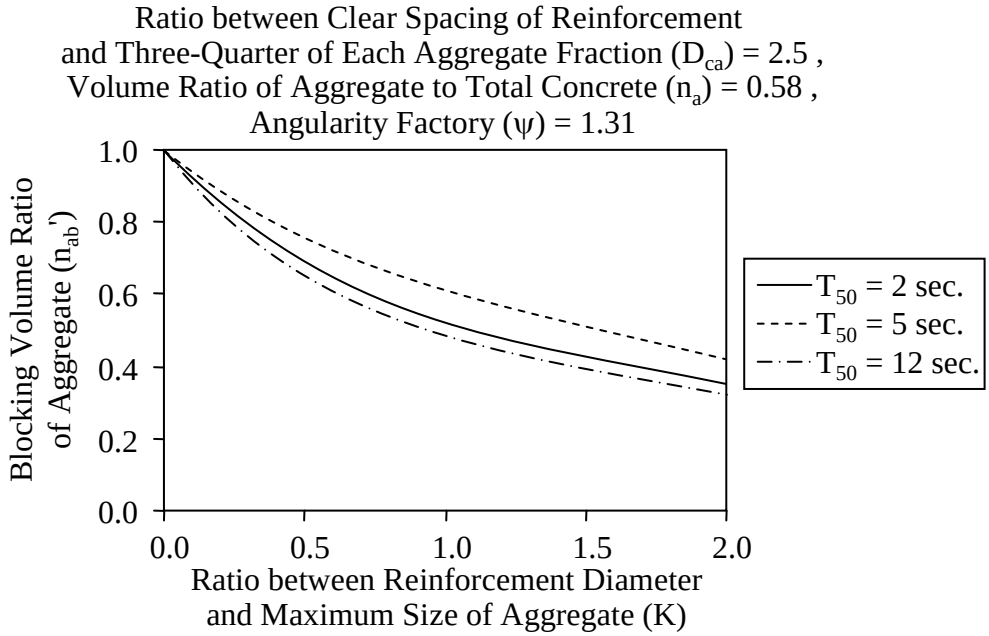

Fig. 6.29 Relationship between blocking volume ratio of aggregates (n_{ab}') vs. ratio of reinforcement diameter to maximum size of aggregate (K) of mixtures with various 50-cm slump flow times {for the ratio between clear spacing of reinforcement and three-quarter dimension of each aggregate fraction (D_{ca}) = 2.5, volume ratio of aggregate to total concrete (n_a) = 0.58 and angularity factor of coarse aggregate (ψ) = 1.31}

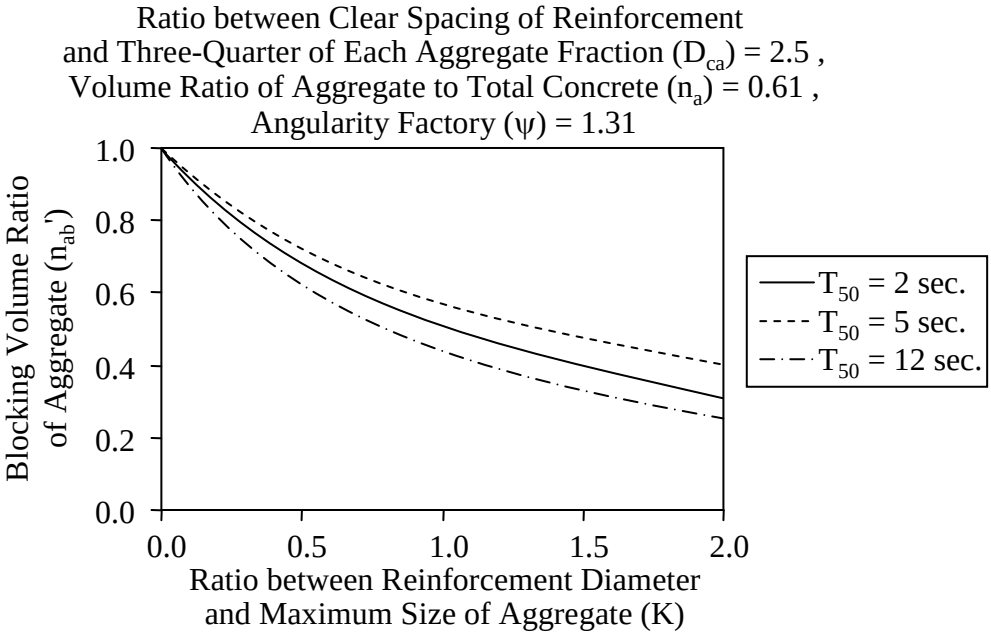

Fig. 6.30 Relationship between blocking volume ratio of aggregates (n_{ab}') vs. ratio of reinforcement diameter to maximum size of aggregate (K) of mixtures with various 50-cm slump flow times {for the ratio between clear spacing of reinforcement and three-quarter dimension of each aggregate fraction (D_{ca}) = 2.5, volume ratio of aggregate to total concrete (n_a) = 0.61 and angularity factor of coarse aggregate (ψ) = 1.31}

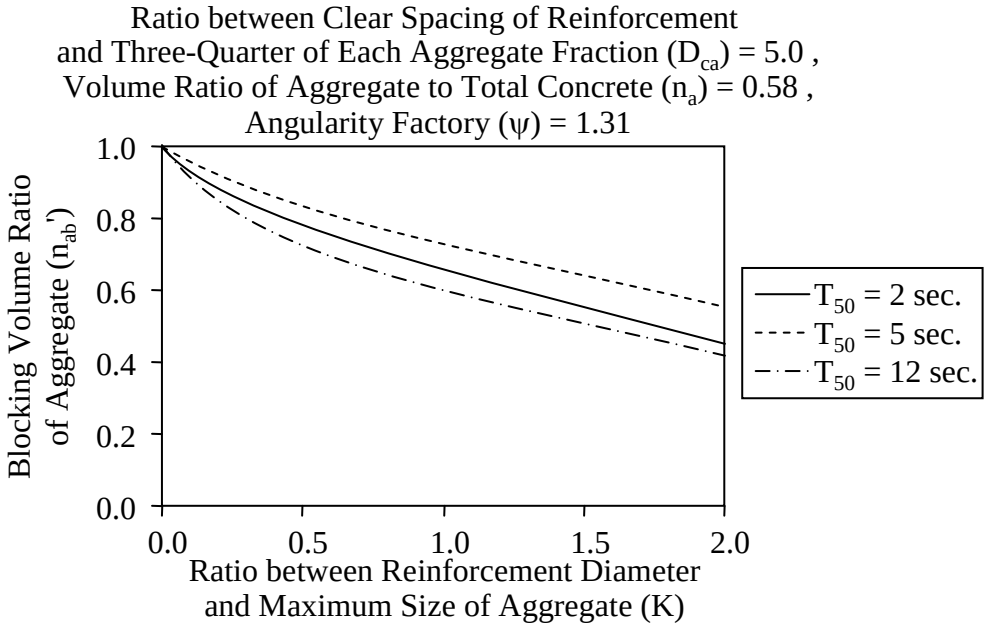

Fig. 6.31 Relationship between blocking volume ratio of aggregates (n_{ab}') vs. ratio of reinforcement diameter to maximum size of aggregate (K) of mixtures with various 50-cm slump flow times {for the ratio between clear spacing of reinforcement and three-quarter dimension of each aggregate fraction (D_{ca}) = 5.0, volume ratio of aggregate to total concrete (n_a) = 0.58 and angularity factor of coarse aggregate (ψ) = 1.31}

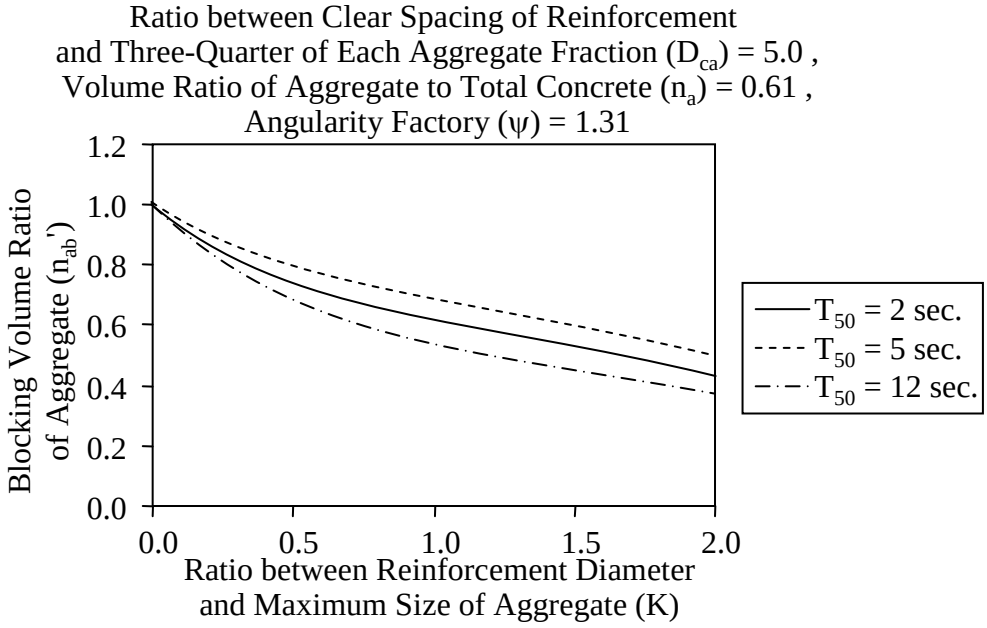

Fig. 6.32 Relationship between blocking volume ratio of aggregates (n_{ab}') vs. ratio of reinforcement diameter to maximum size of aggregate (K) of mixtures with various 50-cm slump flow times {for the ratio between clear spacing of reinforcement and three-quarter dimension of each aggregate fraction (D_{ca}) = 5.0, volume ratio of aggregate to total concrete (n_a) = 0.61 and angularity factor of coarse aggregate (ψ) = 1.31}

6.5.4 Relationship between Aggregate Blocking Volume Ratio and Angularity Factor of Coarse Aggregate (ψ)

Figs. 6.33 to 6.36 show the relationships between the computed total aggregates blocking volume ratio vs. angularity factor of coarse aggregate. Figures indicate that for similar ratio between reinforcement clear spacing and three-quarter dimension of each aggregate fraction (D_{ca}) and ratio of reinforcement diameter to maximum size of aggregate (K), the volume of total aggregates should be reduced to avoid the aggregate blocking when the particle shape of coarse aggregate is more irregular.

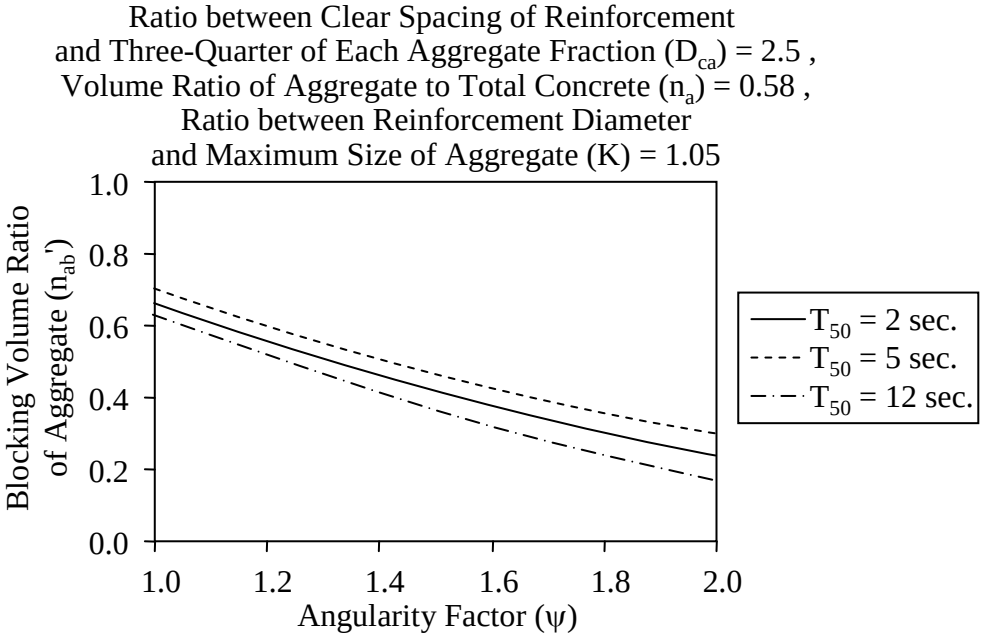

Fig. 6.33 Relationship between blocking volume ratio of aggregates (n_{ab}') vs. angularity factor of coarse aggregate (ψ) of mixtures with various 50-cm slump flow times {for the ratio between reinforcement clear spacing and three-quarter dimension of each aggregate fraction (D_{ca}) = 2.5, volume ratio of aggregate to total concrete (n_a) = 0.58 and ratio of reinforcement diameter to maximum size of aggregate (K) = 1.05}

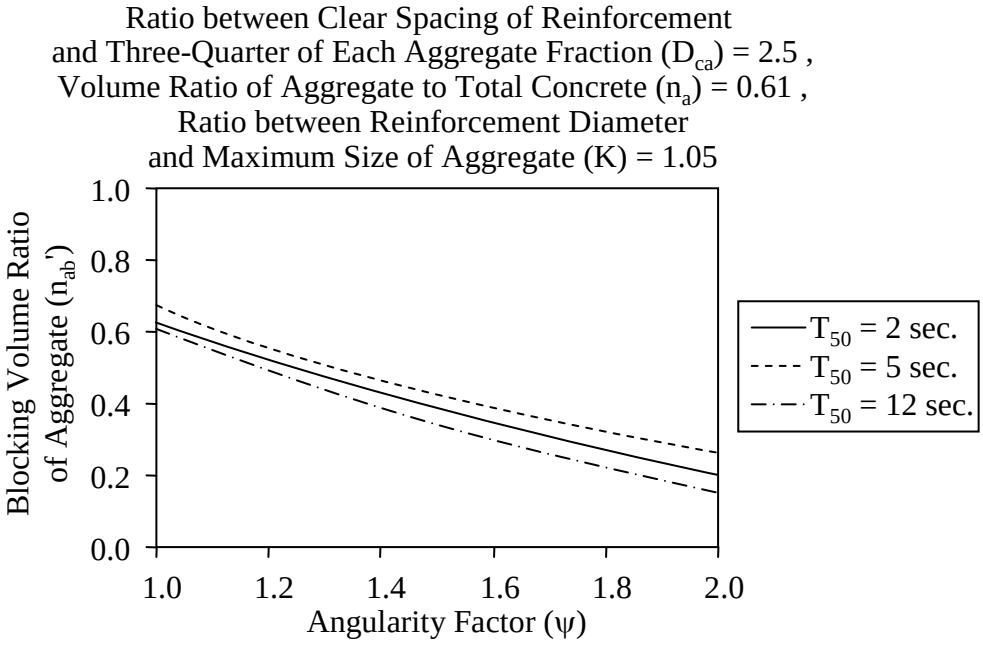

Fig. 6.34 Relationship between blocking volume ratio of aggregates (n_{ab}') vs. angularity factor of coarse aggregate (ψ) of mixtures with various 50-cm slump flow times {for the ratio between reinforcement clear spacing and three-quarter dimension of each aggregate fraction (D_{ca}) = 2.5, volume ratio of aggregate to total concrete (n_a) = 0.61 and ratio of reinforcement diameter to maximum size of aggregate (K) = 1.05}

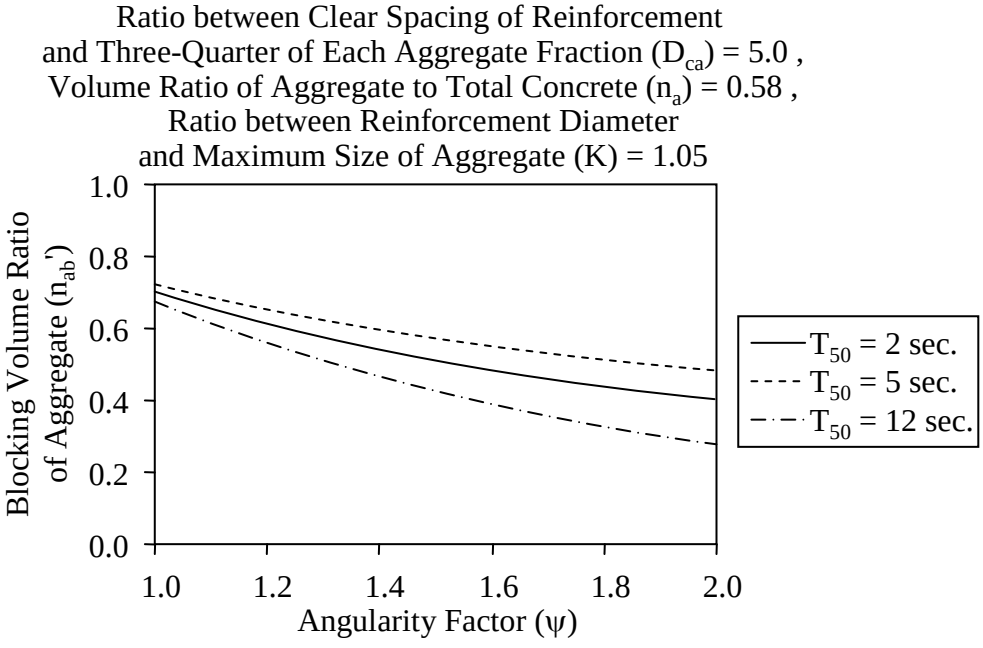

Fig. 6.35 Relationship between blocking volume ratio of aggregates (n_{ab}') vs. angularity factor of coarse aggregate (ψ) of mixtures with various 50-cm slump flow times {for the ratio between reinforcement clear spacing and three-quarter dimension of each aggregate fraction (D_{ca}) = 5.0, volume ratio of aggregate to total concrete (n_a) = 0.58 and ratio of reinforcement diameter to maximum size of aggregate (K) = 1.05}

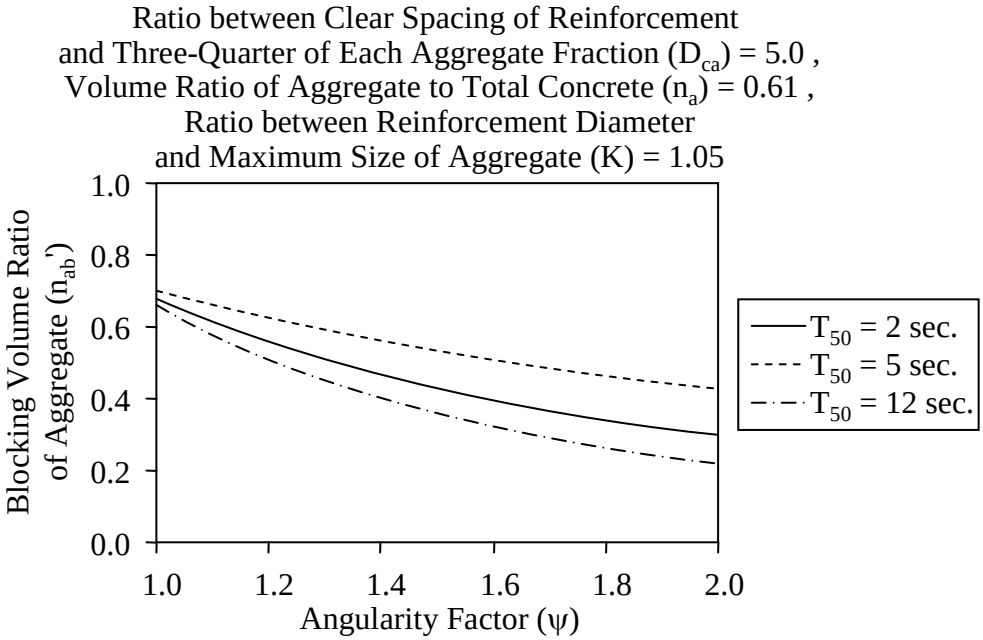

Fig. 6.36 Relationship between blocking volume ratio of aggregates (n_{ab}') vs. angularity factor of coarse aggregate (ψ) of mixtures with various 50-cm slump flow times {for the ratio between reinforcement clear spacing and three-quarter dimension of each aggregate fraction (D_{ca}) = 5.0, volume ratio of aggregate to total concrete (n_a) = 0.61 and ratio of reinforcement diameter to maximum size of aggregate (K) = 1.05}

6.6 Verifications

The accuracies of the proposed models were verified by comparing the predicted blocking conditions computed from the prediction model with L-box passing ability of the tested mixtures. The test results for verification were carried out by the author and Tangtermsirikul et al. (2002). Properties of materials and mix proportions of the tested mixtures together with the test results are shown in Table A-1 and B-3, respectively. In the verification tests, the linear combination rules using the proposed diagrams and Eqs. (6.12) to (6.14) were applied to determine the aggregate blocking volume of the tested mixtures. Then, relationships between the aggregate blocking volume obtained from the proposed diagrams versus volume ratio of coarse aggregate to total aggregates and 50-cm slump flow time were plotted to classify the tested mixtures in zones of “blocking” or “no blocking” in the diagrams. Figs. 6.37 to 6.48 show the blocking conditions of the tested mixtures. The figures and test results indicate that the developed models can be used to predict the blocking conditions of the tested mixtures. However, the accuracies of the model should be further verified by carrying out more verification tests in the future especially when the arrangement of the rebars is not one way as in the tested condition.

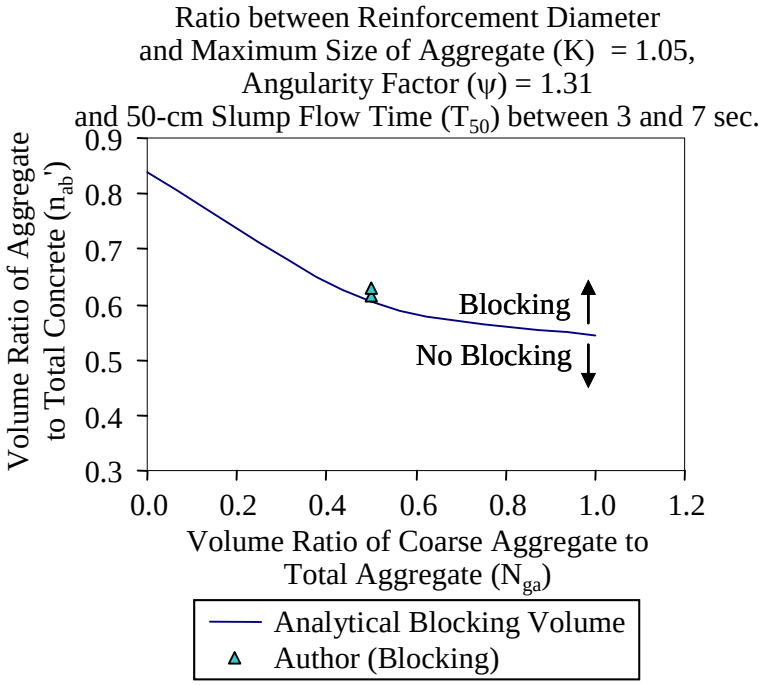

Fig. 6.37 Relationship between blocking volume ratio of aggregates (n_{ab}') vs. volume ratio of coarse aggregate to total aggregates (N_{ga}) of the coarse aggregate with angularity factor (ψ) = 1.31 and 50-cm slump flow times between 3 and 7 sec for ratio between reinforcement diameter and maximum size of aggregate (K) = 1.05

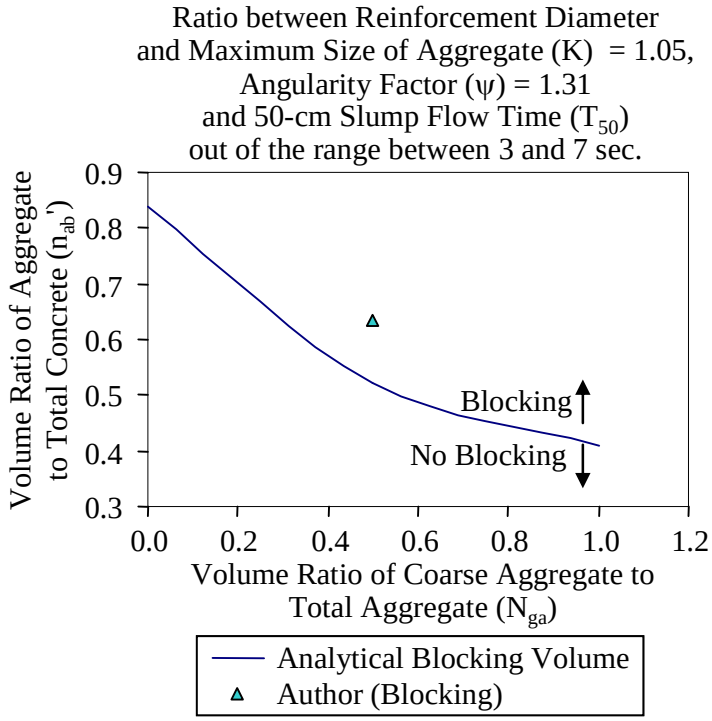

Fig. 6.38 Relationship between blocking volume ratio of aggregates (n_{ab}') vs. volume ratio of coarse aggregate to total aggregates (N_{ga}) of the coarse aggregate with angularity factor (ψ) = 1.31 and 50-cm slump flow times out of the range between 3 and 7 sec for ratio between reinforcement diameter and maximum size of aggregate (K) = 1.05

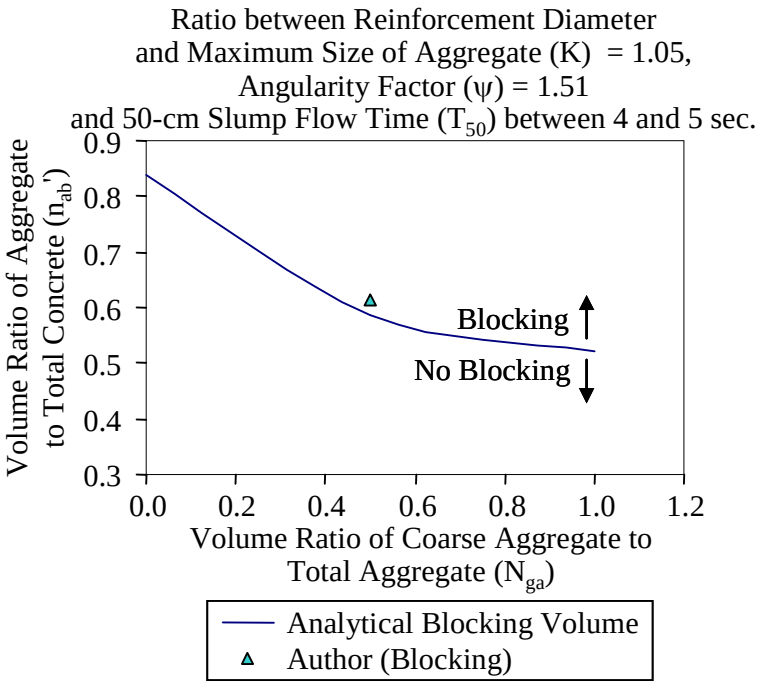

Fig. 6.39 Relationship between blocking volume ratio of aggregates (n_{ab}') vs. volume ratio of coarse aggregate to total aggregates (N_{ga}) of the coarse aggregate with angularity factor (ψ) = 1.51 and 50-cm slump flow times between 4 and 5 sec for ratio between reinforcement diameter and maximum size of aggregate (K) = 1.05

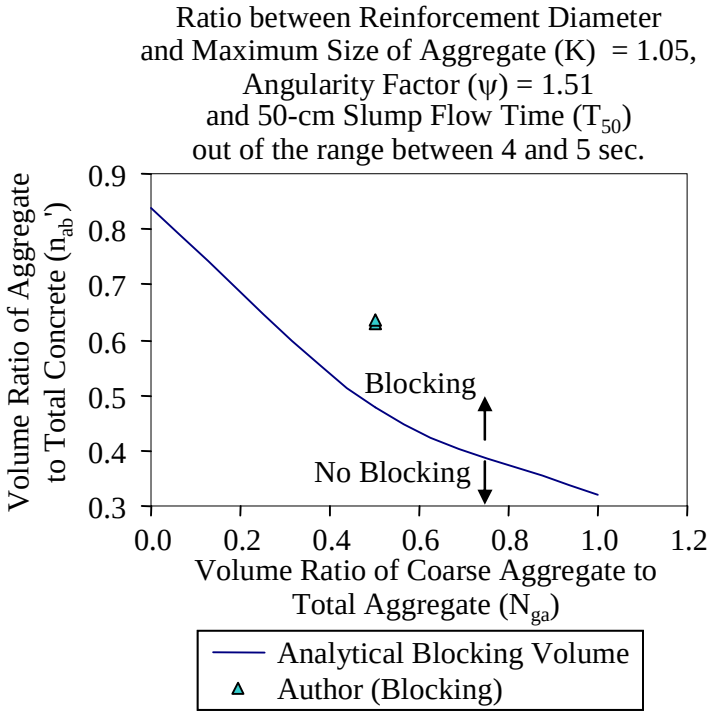

Fig. 6.40 Relationship between blocking volume ratio of aggregates (n_{ab}') vs. volume ratio of coarse aggregate to total aggregates (N_{ga}) of the coarse aggregate with angularity factor (ψ) = 1.51 and 50-cm slump flow times out of the range between 4 and 5 sec for ratio between reinforcement diameter and maximum size of aggregate (K) = 1.05

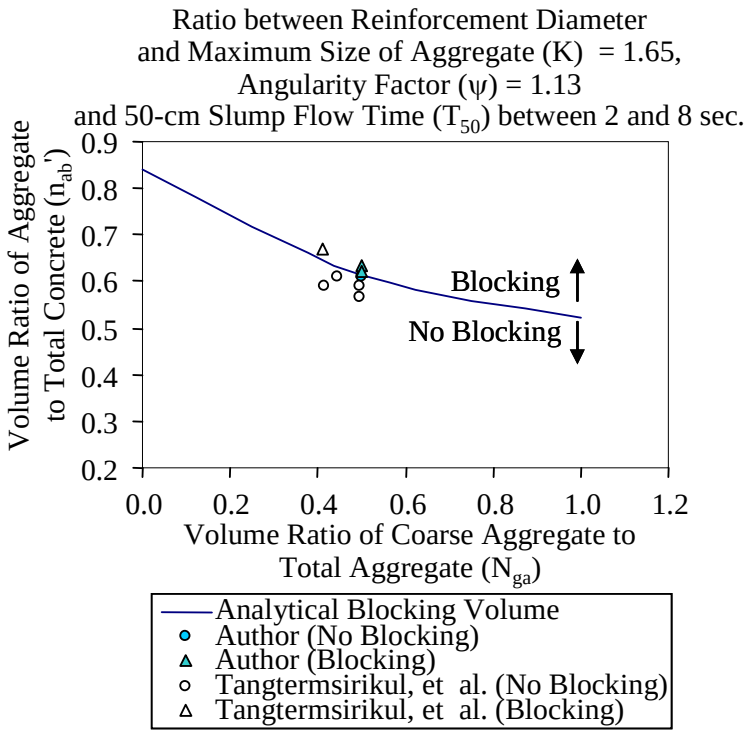

Fig. 6.41 Relationship between blocking volume ratio of aggregates (n_{ab}') vs. volume ratio of coarse aggregate to total aggregates (N_{ga}) of the coarse aggregate with angularity factor (ψ) = 1.13 and 50-cm slump flow times between 2 and 8 sec for ratio between reinforcement diameter and maximum size of aggregate (K) = 1.65

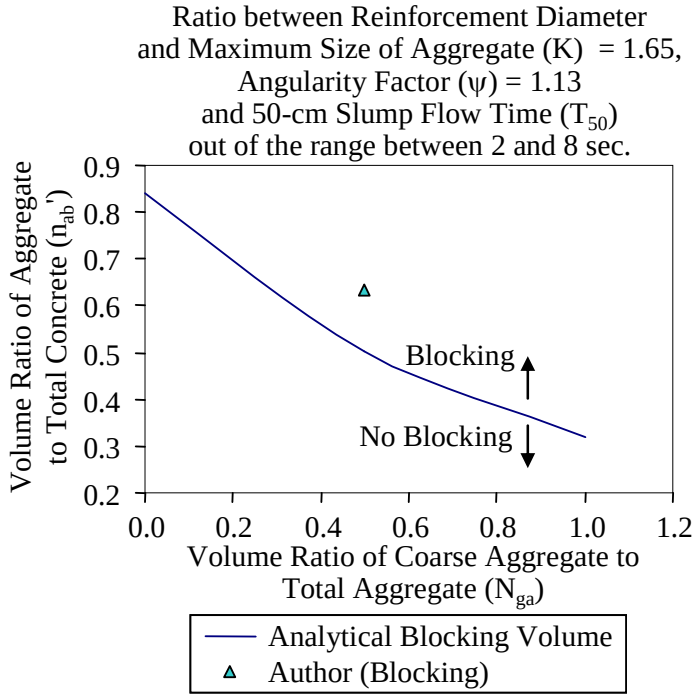

Fig. 6.42 Relationship between blocking volume ratio of aggregates (n_{ab}') vs. volume ratio of coarse aggregate to total aggregates (N_{ga}) of the coarse aggregate with angularity factor (ψ) = 1.13 and 50-cm slump flow times out of the range between 2 and 8 sec for ratio between reinforcement diameter and maximum size of aggregate (K) = 1.65

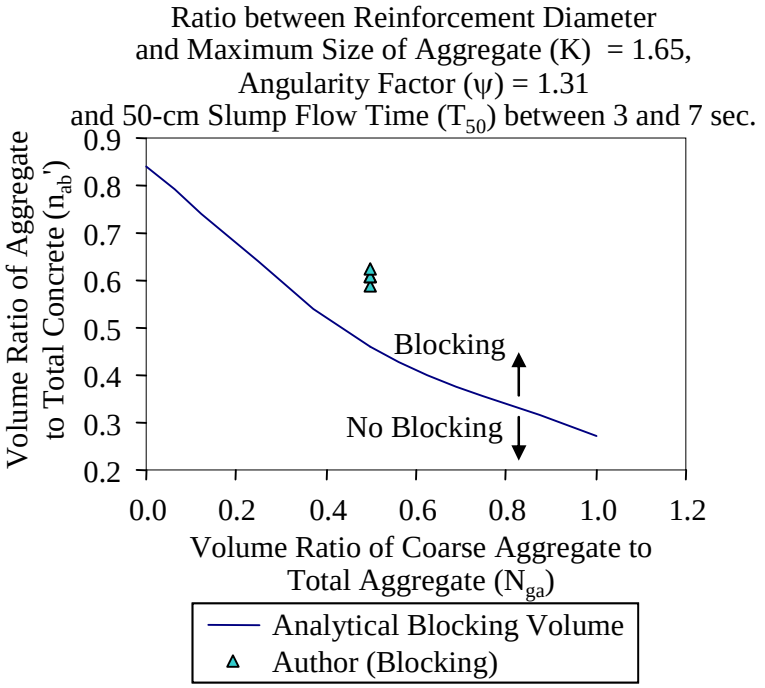

Fig. 6.43 Relationship between blocking volume ratio of aggregates (n_{ab}') vs. volume ratio of coarse aggregate to total aggregates (N_{ga}) of the coarse aggregate with angularity factor (ψ) = 1.31 and 50-cm slump flow times between 3 and 7 sec for ratio between reinforcement diameter and maximum size of aggregate (K) = 1.65

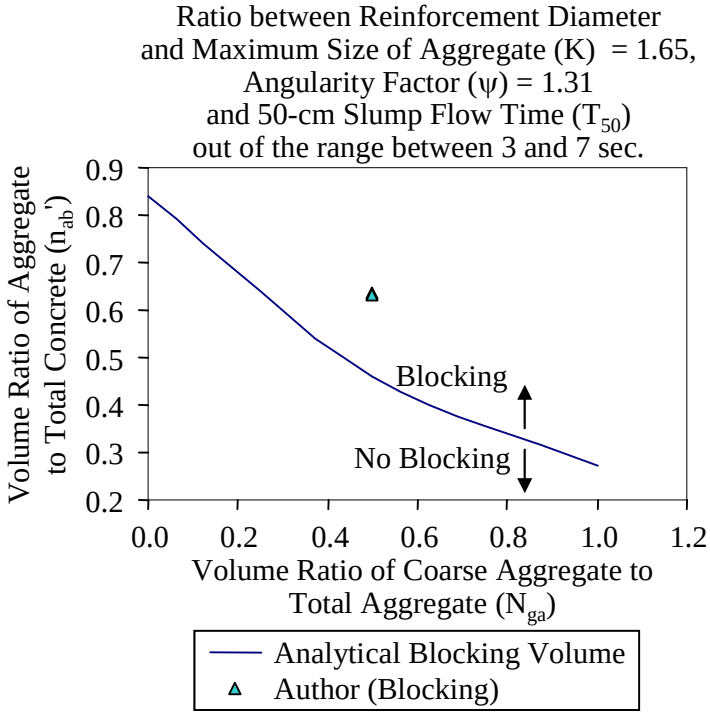

Fig. 6.44 Relationship between blocking volume ratio of aggregates (n_{ab}') vs. volume ratio of coarse aggregate to total aggregates (N_{ga}) of the coarse aggregate with angularity factor (ψ) = 1.31 and 50-cm slump flow times out of the range between 3 and 7 sec for ratio between reinforcement diameter and maximum size of aggregate (K) = 1.65

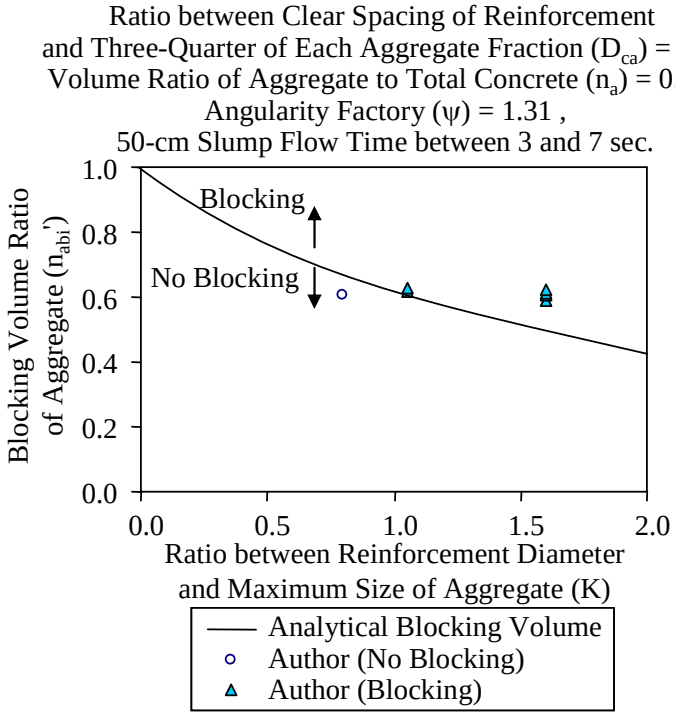

Fig. 6.45 Relationship between blocking volume ratio of aggregates (n_{ab}') vs. ratio of reinforcement diameter to maximum size of aggregate (K) for the ratio between clear spacing of reinforcement and three-quarter of each aggregate fraction (D_{ca}) = 2.5, volume ratio of aggregate to total concrete (n_a) = 0.58, coarse aggregate with angularity factor (ψ) = 1.31 and 50-cm slump flow times between 3 and 7 sec

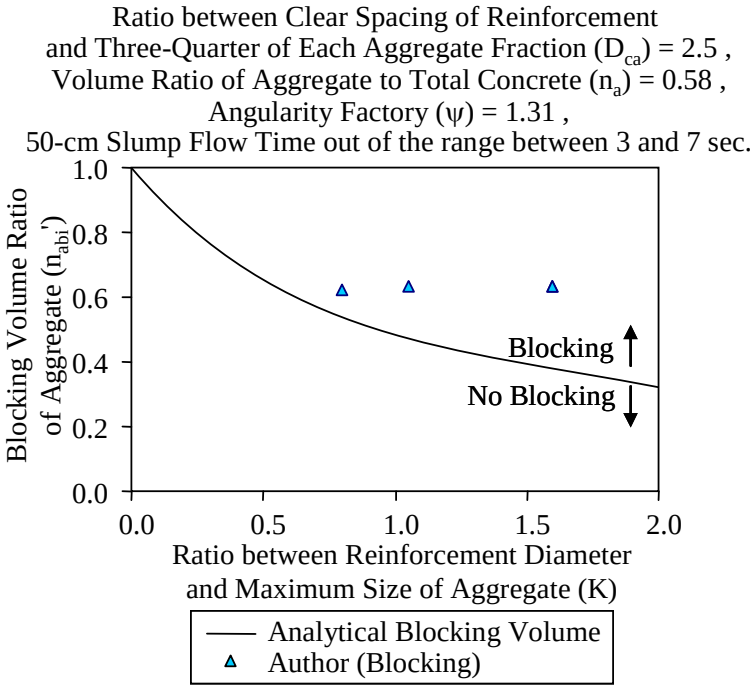

Fig. 6.46 Relationship between blocking volume ratio of aggregates (n_{ab}') vs. ratio of reinforcement diameter to maximum size of aggregate (K) for the ratio between clear spacing of reinforcement and three-quarter of each aggregate fraction (D_{ca}) = 2.5, volume ratio of aggregate to total concrete (n_a) = 0.58, coarse aggregate with angularity factor (ψ) = 1.31 and 50-cm slump flow times out of the range between 3 and 7 sec

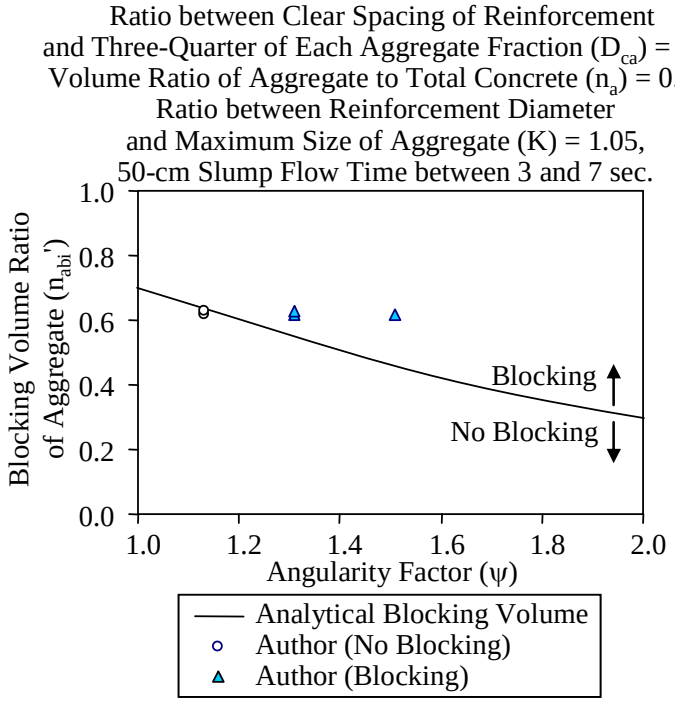

Fig. 6.47 Relationship between blocking volume ratio of aggregates (n_{ab}') vs. angularity factor of coarse aggregate (ψ) for the ratio between clear spacing of reinforcement and three-quarter of each aggregate fraction (D_{ca}) = 2.5, volume ratio of aggregate to total concrete (n_a) = 0.58, ratio of reinforcement diameter to maximum size of aggregate (K) = 1.05 and 50-cm slump flow times between 3 and 7 sec

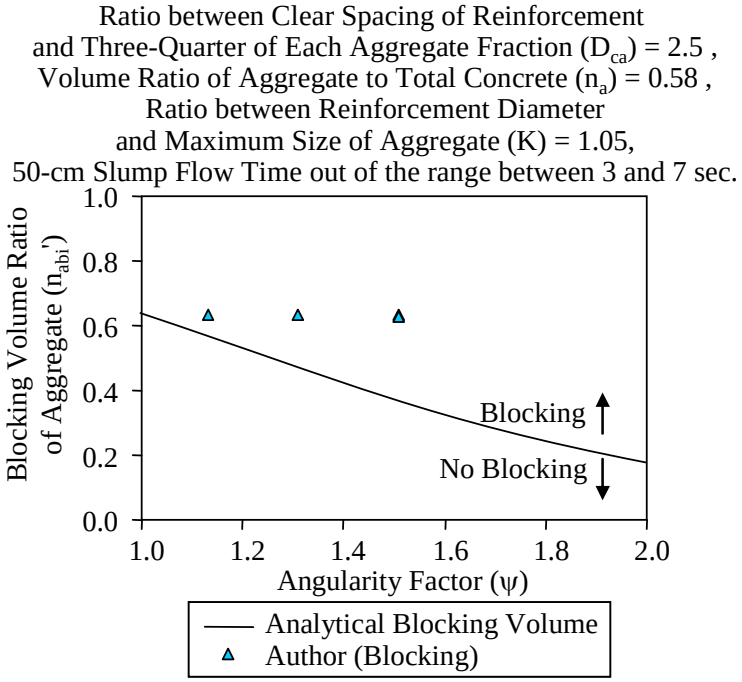

Fig. 6.48 Relationship between blocking volume ratio of aggregates (n_{ab}') vs. angularity factor of coarse aggregate (ψ) for the ratio between clear spacing of reinforcement and three-quarter of each aggregate fraction (D_{ca}) = 2.5, volume ratio of aggregate to total concrete (n_a) = 0.58, ratio of reinforcement diameter to maximum size of aggregate (K) = 1.05 and 50-cm slump flow times out of the range between 3 and 7 sec

6.7 Conclusions

It was found from the test results that L-box passing ability reduced with the increase of irregularity of aggregate particles due to the higher inter-particle frictions and interlocking among aggregate particles. Test results showed that at similar particle shape and volume of the aggregates, the highest L-box passing ability of the mixtures was achieved when 50-cm slump flow time (T_{50}) was within the optimum ranges. The maximum L-box passing ability and width of optimum range of T_{50} were smaller when the irregularity and volume of the aggregates were increased. This indicates that variation of T_{50} should be controlled within the smaller optimum range when the concrete contains the larger aggregate volume or when using the aggregate with higher irregularity. It was also found that the curves of relationship between L-box passing ability and T_{50} were expressed in parabolic shape due to the increase of resisting forces between the mixtures having too high viscosity and the wall sides of the test apparatus, as well as the blocking caused by segregation and bleeding of the mixtures with too low viscosity.

Based on the proposed models and verification tests for predicting the aggregate blocking volume ratio, it is confirmed that the blocking volume of aggregate reduces when maximum size of coarse aggregate or volume ratio of coarse aggregate to total aggregates are larger (lower s/a). Moreover, the larger ratio between reinforcement diameter and maximum size of aggregate gives the smaller aggregate blocking volume ratio due to the larger supports of rebar to create the aggregate bridging at the narrow spacing. Coarse aggregate with higher irregularity gives the smaller aggregate blocking volume ratios for all ratios between reinforcement diameter and maximum size of aggregate due to the higher inter-particle frictions and interlocking among aggregate particles. Also, at similar viscosity of the mixtures, the aggregate blocking volume can be increased if the particle shape of coarse aggregate is more rounded.

In verification tests, the blocking conditions obtained from test results of the SCC mixtures with at lest 60 cm slump flow and without visual segregation were compared with the blocking boundary derived from the proposed model. It was confirmed that the proposed models can be used to predict the blocking or no blocking conditions of the tested mixtures. However, the accuracies of the model should be further verified by carrying out more verification tests in the future.

Chapter 7

Use of Industrial Wastes in Self-Compacting Concrete

7.1 General

Popularity of using self-compacting concrete (SCC) in concrete construction has increased in many countries, since SCC is effectively applied for improving durability and increasing reliability of structures while reducing the need of skilled workers at the construction site. However, its use is still limited in Thailand due its high cost as the main reason. In general, the cost of SCC is 20-40 % higher than that of conventional concrete. Use of industrial wastes and by-products in concrete is the general solution to reduce the cost of concrete with the achievements of natural resources and environment conservations. The industrial waste materials are generally used as constituents of concrete by two main approaches i.e. as pozzolanic materials to replace cement and as materials for partially or totally replacing aggregates. Examples of the industrial wastes regarded as the pozzolanic materials are such as fly ash, rice husk ash, and ground granulated blast furnace slag (GGBS) etc. The use of these materials is considered as an effective solution to reduce cost of concrete and at the same time to improve concrete properties. The use of low-cost wastes to replace natural aggregates is another alternative solution to achieve a reasonable concrete cost, since about 60 to 80 % of concrete volume is occupied by aggregates. It is noted here that if river sand, mainly used as fine aggregate with the average cost of 250 Baht/m^3 of concrete, can be partially replaced by bottom ash at the minimum content of 10 % of total fine aggregate, the cost of SCC can be reduced by at least 25 Baht/m^3 of concrete (about 2% of the unit cost of concrete on average), which is still significant for cost saving in concrete industry.

Bottom ash is the companion to fly ash in process of coal-burning with an approximate amount of 20 % by volume of the total ash, depending on the type of boiler, dust collection system, burning temperature and the type of coal. Its particle is porous, irregular, and coarser than that of fly ash but its chemical composition is not much different (Cheriaf, et al., 1999). Some studies on the usage of bottom ash in concrete had been focused on its potential to replace or partially replace fine aggregate due to its similar particle size to that of normal sand (Bai, et al., 2003, Ghafoori and Bucholc, 1996, 1997, Churchill, et al., 1999). Various attempts to apply bottom ash as a pozzolanic material had also been reported (Jaturapitakkul, et al., 2003, Targan, et al., 2004). Bottom ash produced annually in Thailand, with an estimated amount of 750,000 tons, has been mostly dumped in landfill sites. As an example, the bottom ash produced from Maemoh power plant, the largest coal-power plant in Thailand, has been completely dumped at the plant as class I waste (non-toxic waste). If this bottom ash is value-added by being used to partially replace river sand of SCC, the concrete cost can be reduced. Though, fly ash had been proved to enhance various properties of SCC, there has been no studies on the effects of bottom ash on SCC's properties. Therefore, this study focused mainly on the essential properties of powder-typed SCC incorporating bottom ash as partial fine aggregate replacement. These properties include filling ability (i.e. slump flow, 50-cm slump flow time, segregation and L-box passing ability), physical and mechanical properties of hardened concrete (i.e. porosity, pore size distribution compressive and splitting tensile strengths, and modulus of rupture), and durability (i.e. chloride penetration, carbonation depth, shrinkage in drying environment, and expansion in sodium sulfate solution).

Very fine sand is a by product from the production process of normal sand used in concrete industry. At present, major amount of the produced very fine sand is also dumped in landfill due to the limitation on its application. It is only used in masonry works, particularly decoration purpose such as plastering mortar and decorative sculpture, due to its very fine particle size. Its amount used by this application is relatively small compared to the total production. In this study, it was introduced as partial content of fine aggregate with the aim to improve filling ability of SCC, particularly resistance to segregation and passing ability, due to its higher specific surface area. Deformability, resistance to segregation, and passing ability through narrow openings of the SCC incorporating very fine sand as partial replacement of fine aggregate was therefore investigated

As the main objective, the basic information on using bottom ash and very fine sand in SCC mixtures was provided in this study in order to reduce cost and promote the application of SCC in Thailand's construction.

7.2 A Proposed Method to Determine Water Retainability of Porous Fine Aggregate

Porous materials such as lightweight aggregate and bottom ash are used as concrete aggregate for the purposes of waste management and concrete properties improvement. One of the main problems for the use of porous aggregates is their moisture property which is usually higher than that of normal aggregate. Previous studies by Lemmer, et al. (1995), Ghafoori and Bucholc (1996, 1997) reported that concrete mixed with bottom ash and recycled concrete-crush was very stiff and non-workable due to a significant water demand from their porous properties. In addition, workability reduced due to the immobility of the porous aggregate caused by its higher surface frictions from irregular shape and rough texture. The difficulty to measure the true moisture property of bottom ash was also reported by Landgren (1994), Lemmer, et al. (1995), Ghafoori and Bucholc (1996, 1997). Water retainability has been introduced by Ozawa, et al. (1991, 1992), Tangtermsirikul, et al. (1999), and Khunthongkaew, et al. (2003) for analysis and design of fresh concrete properties. It is defined as the water required to completely fill in pores and dependently restricted on surface of aggregate particles under gravitational condition as illustrated in Fig. 7.1.

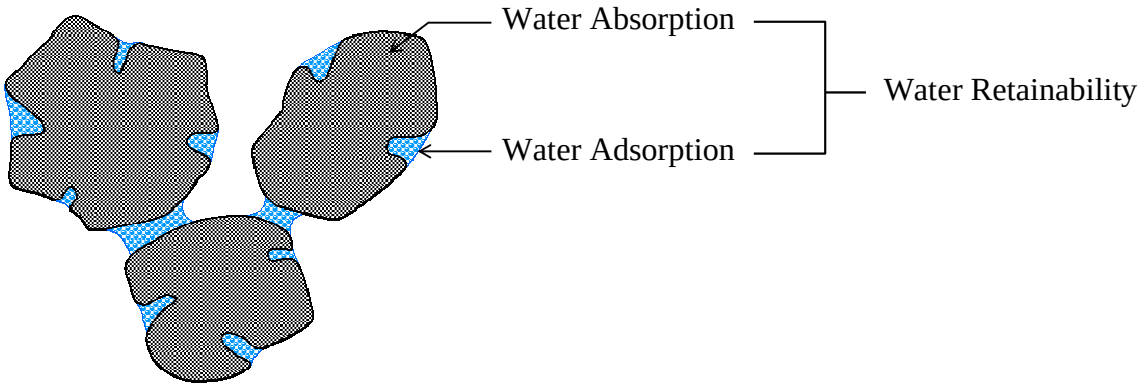

Fig. 7.1 Composition of water retainability of porous aggregate

Moisture property of concrete consists of water absorption and water adsorption and affects the free water amount in fresh concrete (Ozawa, et al., 1991, Tangtermsirikul, et al., 1999, Khunthongkaew, et al., 2003). For concrete incorporating porous aggregate, it is

reasonable to apply water retainability in stead of water absorption to design mixture proportion and to control fresh concrete properties, especially workability. According to the test method of ASTM C 128 applied to measure absorption of fine aggregate, the moisture condition of “saturated surface dry” (SSD) is achieved by air drying on sample until inter-particle cohesion produced by surface moisture is lost. Many efforts have been carried out to determine surface-dryness of aggregate. One method is based on the process of water displacement by dry aggregate, in which the absorption can be calculated by measuring the original bulk volume of dry aggregate and the decreased bulk volume due to absorption of water inside the aggregate pores (Saxer, et al., 1956, Black, et al., 1986). Another method is to force moisture-saturated air through compaction of aggregate particles and surface dryness is defined as a specific break in the curve relating time of drying and aggregate weight (Hughes, et al., 1971). For lightweight aggregate, the surface-dried from initially wet aggregate can be obtained by centrifuging the aggregate for a fixed period of time (Landgren, 1994). The centrifugal test method is theoretically recommended for determining water retainability of lightweight aggregate. However, it is rather sophisticated for practical implementation. Therefore, the aim of this study is to develop a test method to determine the water retainability of the porous fine aggregate in place of centrifugal test, which can provide a reliable result by a simple approach.

7.2.1 Design of Apparatus and Test Procedure

7.2.1.1 Theoretical Concept

According to the concept of centrifugal test, the amount of water retained by solid particles can be obtained from the relationship between water retainability coefficient (β) and the centrifugal acceleration level (G) (Tangtermsirikul, 1989) (see Fig. 7.2).

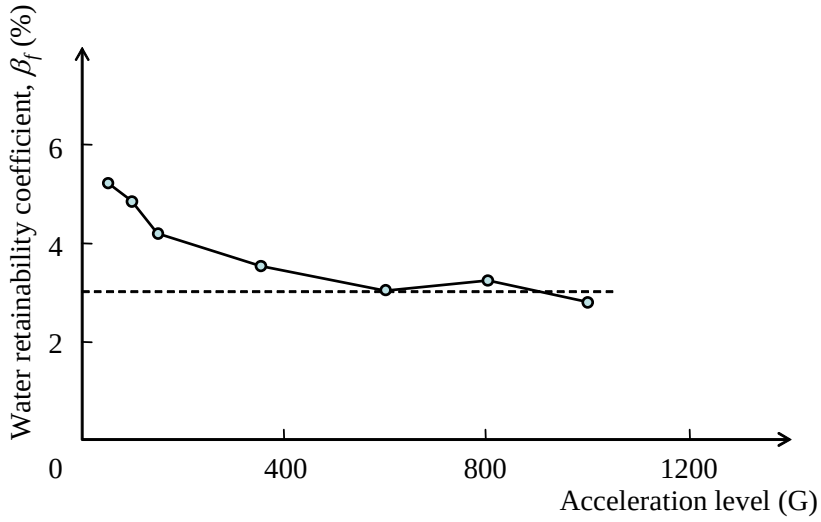

Fig. 7.2 Water retainability of river sand (Tangtermsirikul, 1989)

The coefficient of water retainability (β) is the ratio of the weight of water retained in solid particles to the dry weight of the solid particles. The acceleration level (G) represents the applied centrifugal force level to expel the water from the solid particles. This concept of testing is implemented by applying a centrifugal force with a gradual increase, so the water retainability coefficient is decreased until nearly constant at very

high acceleration (Ozawa, et al., 1991). The water retainability was theorically determined from the coefficient at the acceleration of 1g in the centrifugal test.

However, for a centrifuge machine, it is not possible to apply the acceleration level of 1 g. An alternative application was simulated by allowing the non-restricted water (free water) to be removed gravitationally from the compacted aggregate sample. According to this concept, the absorbed and adsorbed water shall be restricted by the aggregate while the excess water shall drop down. From a set of trial water content, the maximum water content which provides all portions of tested sample with the uniform moisture content is regarded as the water retainability of the aggregate. The diagrammatic explanation of the test concept is illustrated in Fig. 7.3.

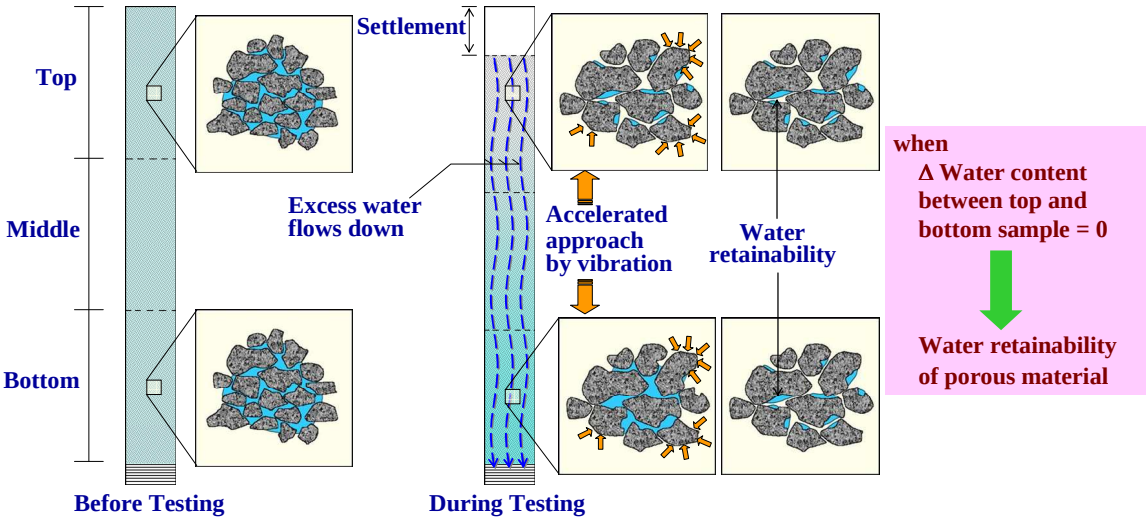

Fig. 7.3 Diagrammatic illustration for concept of the proposed test method

7.2.1.2 Apparatus

The apparatus comprised a hollow cylinder pipe and a bottom plug. The cylinder pipe having inner diameter of 75 mm and 750 mm in length was adopted in order to have a minimum sample volume of 3.0 liters. By placing the cylinder vertically, if the trial water content is more than the true water retainability, the excess water shall flow down and then accumulated at the bottom under gravitational effect. At the bottom of the cylinder, a capping container is assembled to collect the excess water. This water shall be considered as a part of the water content of the bottom portion of the test sample. A sieve no. 100 was inserted between the cylinder and the plug to screen the aggregate particles from the excess water. Furthermore, to prevent water loss in the process, plastic sheet and a sealant material were applied at the top end and the connection. The detail of the apparatus and its facilities is illustrated in Fig. 7.4.

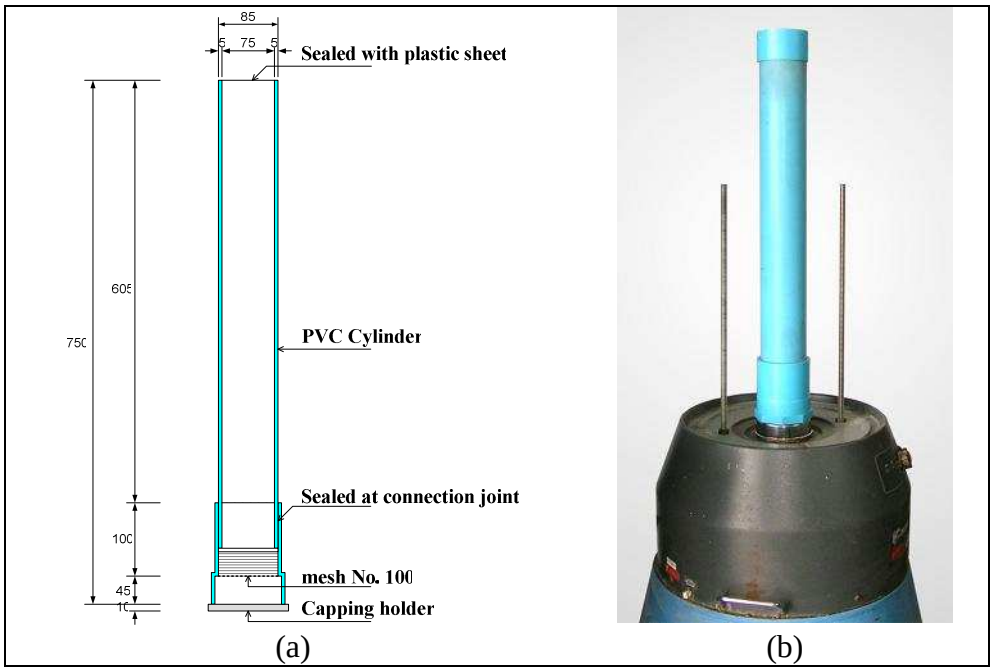

Fig. 7.4 The proposed test method (a) Dimensions of the designed apparatus (b) A vibration machine for the accelerated method

Two methods to expel excess water i.e. the static method and accelerated method were proposed in this study. The static method was conducted by remaining the apparatus undisturbed for a fixed period, while the mechanical vibration was applied to the apparatus for the accelerated method.

7.2.1.3 Test Procedure

(1) Test sample preparation

1.1 Obtain the sample with the size of approximately 125 to 200 % of the quantity required to fill the cylinder (3 to 5 kg.) and dry it to a constant mass, preferably in an oven at 110 ± 5 °C and allow it to cool to comfortable handling temperature.

1.2 Mix dry aggregates with a specified amount of water throughout the mixture in a container, and wrap the container with a plastic sheet to prevent water evaporation. For an aggregate, a range of trial moisture content shall be performed.

1.3 Keep the moist specimen in a covered tray at the room temperature for 24 ± 4 hours.

(2) Testing

With a completely assembled apparatus, fill the cylinder up to one-third of its volume with the prepared aggregate; then compact the layer with 30 external hits of one-pound rubber hammer for 15 times alternatively on each side, evenly along the height of the filled sample. The aggregate particles will arrange themselves in a compacted condition.

2.1 Fill the container up to two-third of its volume and compact again as above. Finally fill the container until overflowing and externally hit again in the same manner.

Level the surface of aggregate with a straightedge. Seal the top end and connection joint of cylinder with plastic or sealant materials for moisture loss prevention. Allow the test sample contained in the apparatus in static condition for hours (for static method) or with vibration for minutes (for accelerated method)

2.2 Remove two separate portions of the test samples from the top and bottom ends of the cylinder with each minimum weight of 500 ± 10 g. Weigh both separate portions of the aggregate (B), and then dry it to a constant weight (A) to obtain the moisture content of each portion (top and bottom), by the expression as:

$$m_i = \frac{(B - A)100}{A} \tag{7.1}$$

where

m_i is moisture content of aggregate, %

A, B are weight of oven-dry aggregate sample and weight of the sample after test, respectively, g.

2.3 Obtain the difference of moisture content of tested aggregate between the top and bottom portions as follows;

$$\Delta_m = m_b - m_t \tag{7.2}$$

where

Δ_m is difference of moisture content of the tested aggregate, %.

m_t,m_b are moisture contents of the top and bottom portions, respectively, %

(3) Water retainability

The water retainability of aggregate is specified by the largest mass ratio of water to dry aggregate that creates the zero difference of moisture content between the top and bottom portions ($\Delta_m = 0$). A relationship between the moisture difference of the top and bottom tested aggregate samples and the corresponding trial moisture is plotted, and the water retainability is the moisture value at the interception between the curve and the axis of the trial moisture content (see Fig. 7.5)

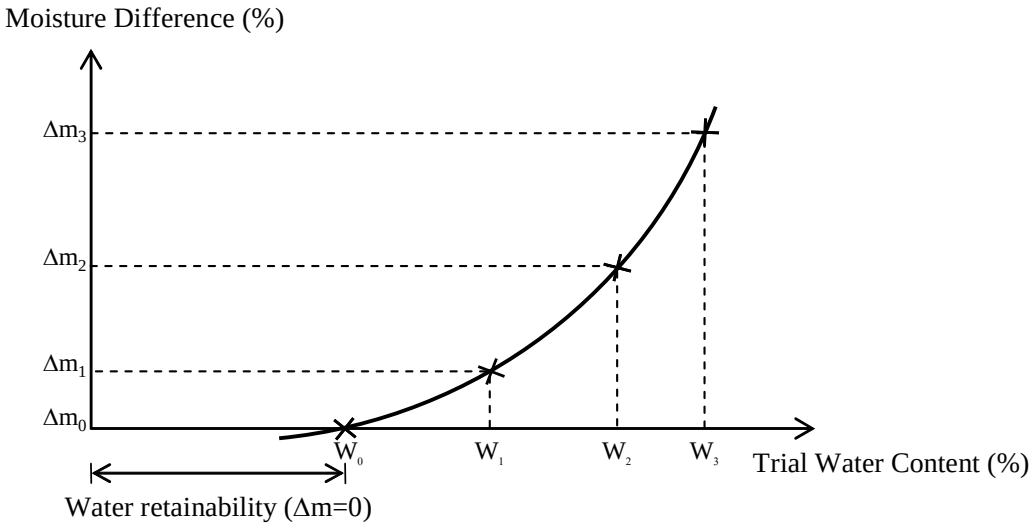

Fig. 7.5 Relationship between the moisture difference after testing and the specified water content in sample preparation to determine the water retainability

7.2.2 Experimental Results and Discussions

7.2.2.1 ASTM C 128 Test Method for Water Absorption

For river sand sample, it was observed that after removing surface moisture by air drying, the saturated surface-dry (SSD) condition was monitored by the cone test with a sign of slightly slump. The water absorption of 0.7 % was then obtained. However, the identical procedure was difficult for all porous fine aggregates. The test samples still maintained the molded shape after removing the cone. By continuing drying, the collapsed slump of the test samples was suddenly found in stead of the slight slump and the samples were so dry, thus leading to the difficulty to judge their SSD conditions (see Fig.7.6).

BA I (Saraburi) Water absorption = 14.3 %

BA II (Mae Moh) Water absorption = 3.5 %

Expanded Clay Water absorption = 24 %

Fig. 7.6 Appearance of porous fine aggregates having moisture content equal to the ASTM C 128 water absorption

This is due to the fact that porous aggregates had high porosity and irregular shape, leading to high surface friction. As a result, the average measured values of absorption became fairly low, which were 14.3 %, 3.5 %, and 24 % for the bottom ash type I (BA-I), bottom ash type II (BA-II) and expanded clay (EC), respectively. For each porous fine aggregate, the water absorptions were tested by different persons. Results of the standard deviations were obtained as 4.2 %, 1.3 %, and 4.8 % for the bottom ash type I, bottom ash type II and expanded clay, respectively (see Table 7.1).

Table 7.1 Water retainability by the proposed method and absorption by the ASTM C 128

Test Method	Aggregate Types	Water Retainability and Absorption Test Results (%)					
		Test No.1	Test No.2	Test No.3	Test No.4	Average	SD
Proposed Method	Bottom Ash I	30	31	31	28	30	1.4
	Bottom Ash II	9	10	11	10	10	0.8
	Expanded Clay	37	40	38	37	38	1.4
ASTM C 128	Bottom Ash I	14.3	12.8	9.9	20.0	14.3	4.2
	Bottom Ash II	1.9	4.4	4.7	2.9	3.5	1.3
	Expanded Clay	21.6	18.5	27.4	28.6	24.0	4.8

7.2.2.2 Proposed Method for Water Retainabilty

From visual observation, the trial moisture amounts from 20 to 60 % and 10 to 30 % by weight of the sample were varied in the sample preparation for bottom ashes I and II, respectively. The appearance of the test samples during testing is shown in Fig. 7.7.

BA I (Saraburi) Water retainability = 30 %

BA II (Mae Moh) Water retainability = 10 %

Expanded Clay Water retainability = 38 %

Fig. 7.7 Appearance of porous fine aggregates having moisture content equal to the water retainability tested by the proposed method

From the relationships between the moisture difference and the trial water amount shown in Figs. 7.8 to 7.10, it revealed that the longer testing period gave the larger moisture difference (Δ Moisture Content in Figs. 7.8 to 7.10).

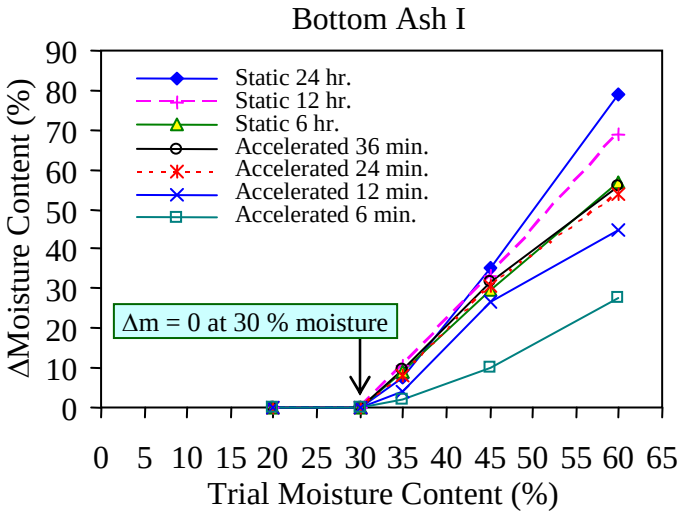

Fig. 7.8 Relationship between the moisture difference (Δ_{mi}) and the specified water content of bottom ash type I

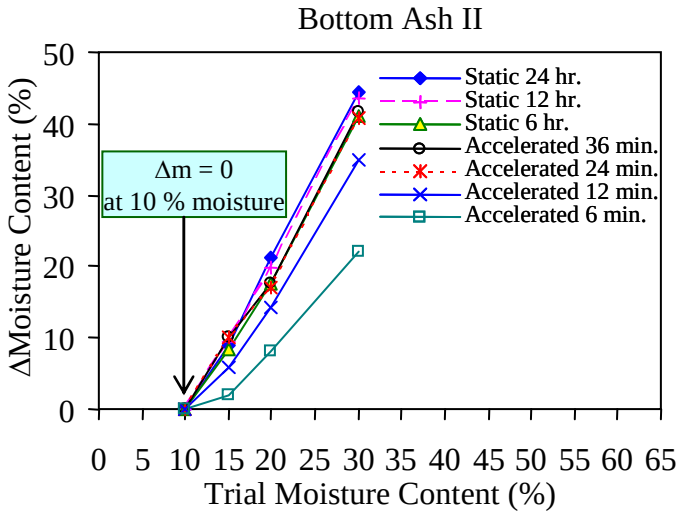

Fig. 7.9 Relationship between the moisture difference (Δ_{mi}) and the specified water content of bottom ash type II

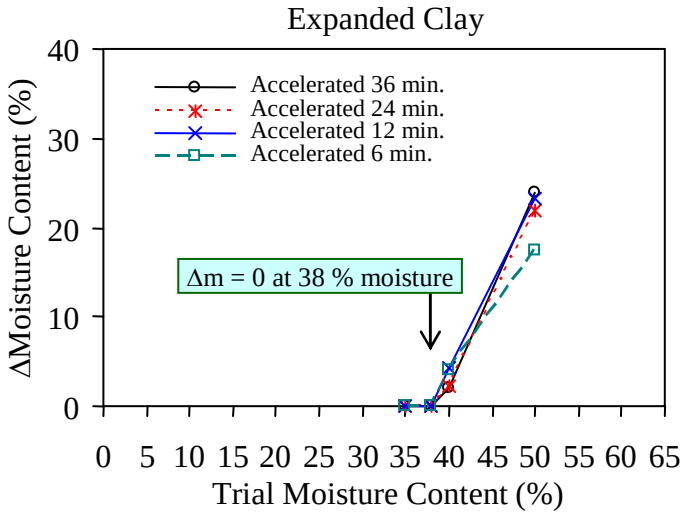

Fig. 7.10 Relationship between the moisture difference (Δ_{mi}) and the specified water content of fine expanded clay

Also, the larger moisture differences were obtained with increasing in the trial water content. For the same trial moisture content, the moisture difference of the static test method was higher than that of the accelerated method because of longer test period in static method. It is clear from the figures that the static method with 6-hour testing period is applicable to estimate water retainability of high porosity materials. The curves for the same types of tested porous material were stretched to zero moisture difference at the same trial moisture content. For bottom ashes I and II, the curves stretched to the zero moisture difference at the moisture content of 30 % and 10 %, respectively (see Figs. 7.8 and 7.9). These values are specified as the water retainability of the two bottom ashes. The moisture content of 38 % was determined as the water retainability of the expanded clay from the trial moistures of 35 %, 38 %, 40 %, and 50 % as seen in Fig. 7.10. The variation of test results subject to different testing skills was represented by the standard deviation values of 1.4 %, 0.8 %, and 1.4 %, conducted by four different persons, for the bottom ash type I, bottom ash type II and expanded clay, respectively.

It was observed that the curves of the accelerated method showed the same tendency as those of the static method but the tested curves of 6 and 12 minutes expressed small moisture differences for all trial moisture values and for all aggregate samples. It is, therefore, suggested that the minimum testing period for the accelerated method should be 24 minutes. Relationships between the moisture contents of the tested samples and the trial water content are shown in Figs. 7.11 and 7.12 after 6 hours of the static test and 24 minutes of the accelerated test, respectively. The moisture content of the top portion of each aggregate initially increased with increasing of the trial water content but became constant after the trial moistures reached its water retainability value. In contrast, the moisture content of the bottom portion increased linearly with the increase of trial moisture content due to the accumulated excess water at the bottom portion.

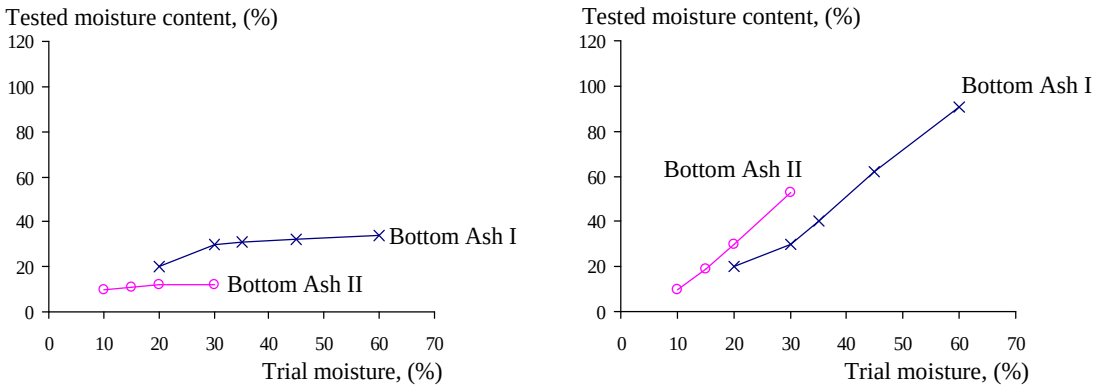

a) Top Portion b) Bottom Portion

Fig. 7.11 Relationship between moisture content after tests and trial moisture by static method with 6-hour testing period

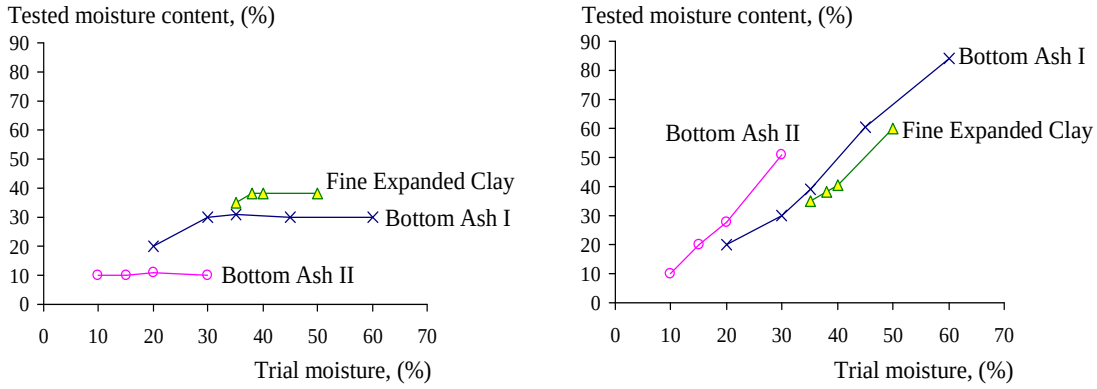

a) Top Portion b) Bottom Portion

Fig. 7.12 Relationship between moisture content after tests and trial moisture by accelerated method with 24-min testing period

Figs. 7.13 shows the comparison between the values of water retainability from intercepting point at zero moisture difference versus the moisture contents obtained from the top portion after tests. It can be seen that the tested moisture contents of the top portions were almost the same as the obtained water retainability from intercepting point at zero moisture difference of all porous aggregates. The results indicated that by performing this test method with the high trial water content in sample preparation, the water retainability value could be simply obtained from the value of the top portion moisture. This could much simplify the proposed method.

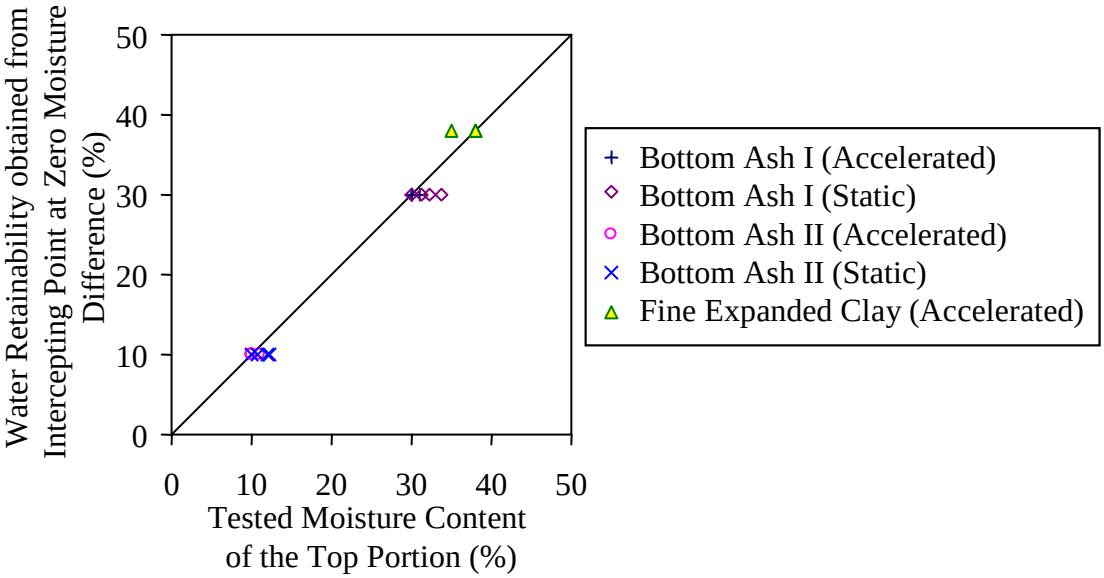

Fig. 7.13 Relationship between water retainability from intercepting point at zero moisture difference and moisture contents obtained from the top portions after tests

7.2.2.3 Comparisons between the ASTM C 128 Test Method and the Proposed Test Method

The comparison of test results is summarized in Table 7.1 in section 7.2.2.1 and shown in Fig. 7.14. Water absorptions measured from the ASTM C 128 were much lower than those of water retainability obtained from the proposed method for all porous aggregates.

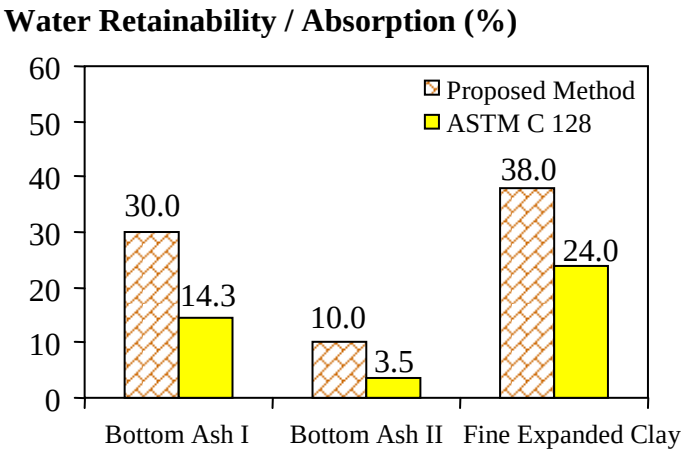

Fig. 7.14 Comparison of results obtained by the proposed test method and the ASTM C 128

During testing, the appearances of the test samples are shown in Figs. 7.6 and 7.7 in sections 7.2.2.1 and 7.2.2.2. It was confirmed that the moisture conditions of the samples at the point of cone collapsing in the ASTM C 128 test looked very dry and their moisture contents were believed to be below the actual point of SSD because some portions became white color due to excessive drying. In comparison, the samples in the proposed test method, at the moisture state of their water retainability, appeared reasonably moist and exhibited in molded shape from the cone test. By comparing the standard deviation values of the test results from both test methods, the variation of the proposed method was smaller than that of the ASTM C128 test method for the same porous fine aggregate. It indicated

that the collapsed-cone criterion specified in the ASTM C 128 test to find the SSD state was not appropriate for the porous fine aggregates with high inter-particle frictions as the cone shape could still be maintained even with excessively dry condition. In addition, the proposed test method could reduce the test result's variation subject to the tester's skills. So, this implied that the proposed test method for water retainability gave better precision and consistency than the ASTM C 128 test method for porous fine aggregates.

7.2.3 Application of the Proposed Test Method

The proposed test method and the ASTM C 128 test method were applied to obtain the water retainability and the water absorption, respectively, of the porous aggregates for being used in mix proportioning of conventional concrete (CVC) and self-compacting concrete (SCC). Due to its high sensitivity in consistency with the variation of aggregate moisture, SCC was also adopted. Properties of CVC and SCC proportioned by using the ASTM C 128 test method and the authors' proposed test method were compared to verify the effectiveness of the proposed method. It is noted here that the control concretes were prepared by using river sand with the identical gradations to those of the combined river sand and each porous aggregate at 10 % and 20 % replacement levels in order to eliminate effects of the aggregate gradation on fresh concrete properties.

7.2.3.1 Conventional Concrete

Test results of conventional concrete (CVC) are shown in Fig. 7.15. The concrete mixed with bottom ashes gave the lower slump than the control concrete. This was due to low particle mobility or high inter-particle friction of the bottom ash. However, the slump of mixtures with BA-I and BA-II, proportioned by using the water retainability from the proposed method, was closer to those of the control concrete than the slump values of the bottom ash concrete proportioned by using the ASTM C 128 water absorption for both 10 % and 20 % bottom ash contents.

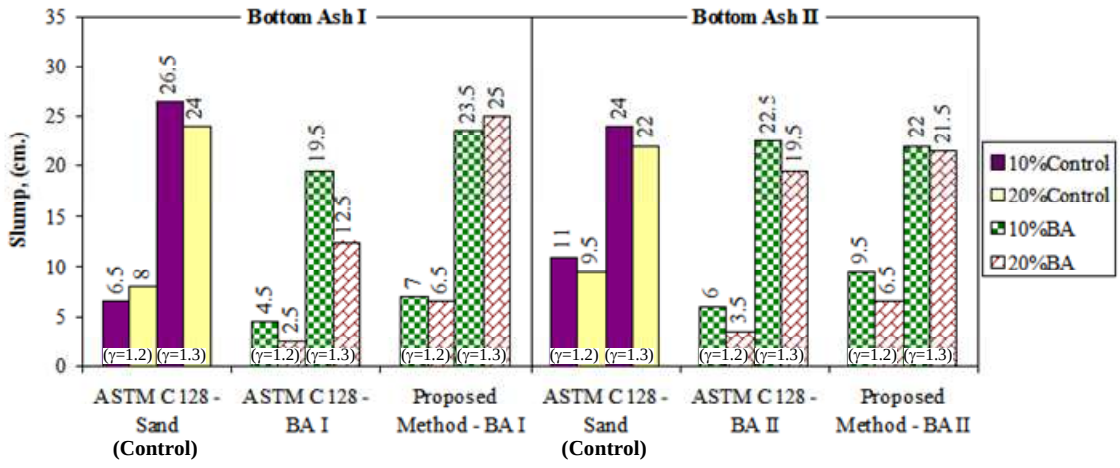

Fig. 7.15 Comparison of slump of CVC proportioned by using water absorption from ASTM C 128 and water retainability from the proposed method

Fig. 7.16 shows that 28-day compressive strengths of the CVC mixtures with BA-I and BA-II proportioned by using the water retainability from the proposed method were similar to the compressive strength of the control concrete. On the other hand, the bottom ash concrete proportioned by using the water absorption from the ASTM C 128 exhibited

much higher compressive strength than the control concrete. Though, there might be some contribution from pozzolanic reaction of the bottom ashes, it is not likely for the tested bottom ash mixtures to have higher strengths than the control mixtures. The reason of the higher strength was due to the underestimation of retained water, especially inside the particles, of the bottom ash when the absorption values tested by ASTM C 128 were used for mixture proportioning.

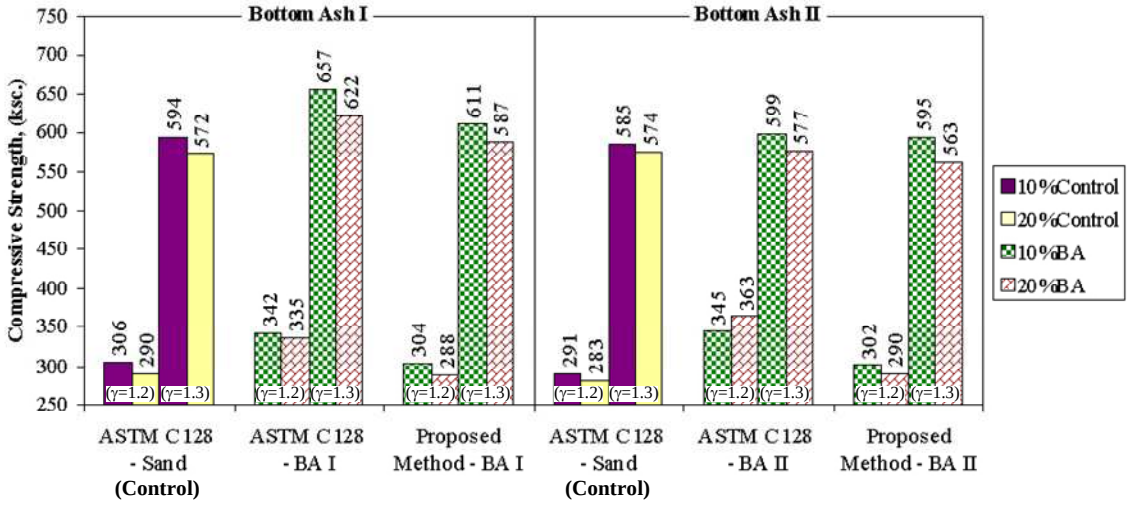

Fig. 7.16 Comparison of 28-day compressive strength of CVC proportioned by using water absorption from ASTM C 128 and water retainability from the proposed method

7.2.3.2 Self-Compacting Concrete

For self-compacting concrete (SCC), the slump flow given in Figs. 7.17 to 7.19 revealed that the SCC incorporating three types of porous fine aggregate showed lower slump flow values than those of the control concrete. It was due to the same reason of high inter-particle friction of the porous aggregates. Similar to the case of CVC, it was found that the mixtures proportioned by using water retainability from the proposed method gave the closer slump flow to those of the corresponding control SCC mixtures, while those designed by using the water absorptions obtained by the ASTM C 128 test method were apparently much less workable.

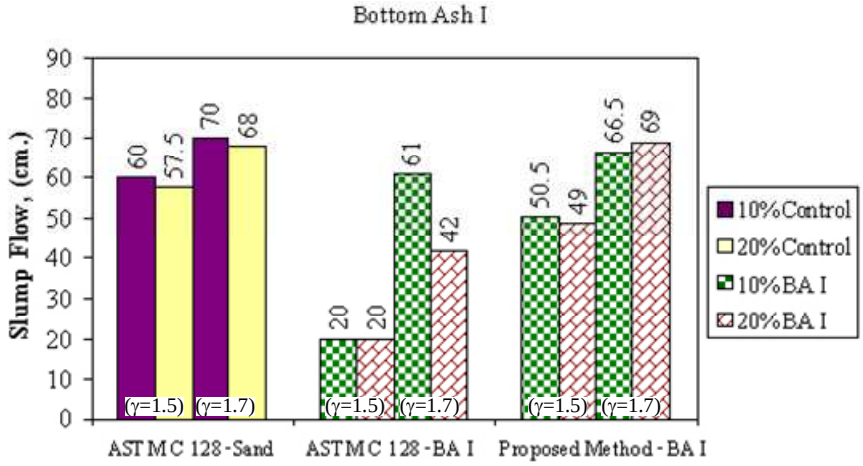

Fig. 7.17 Comparison of slump flow of SCC mixed with bottom ash type I and proportioned by using water absorption from ASTM C 128 and water retainability from the proposed method

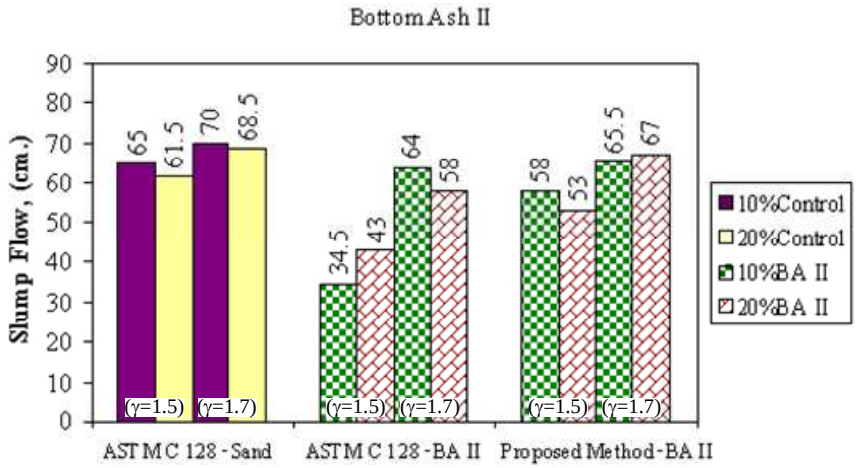

Fig. 7.18 Comparison of slump flow of SCC mixed with bottom ash type II and proportioned by using water absorption from ASTM C 128 and water retainability from the proposed method

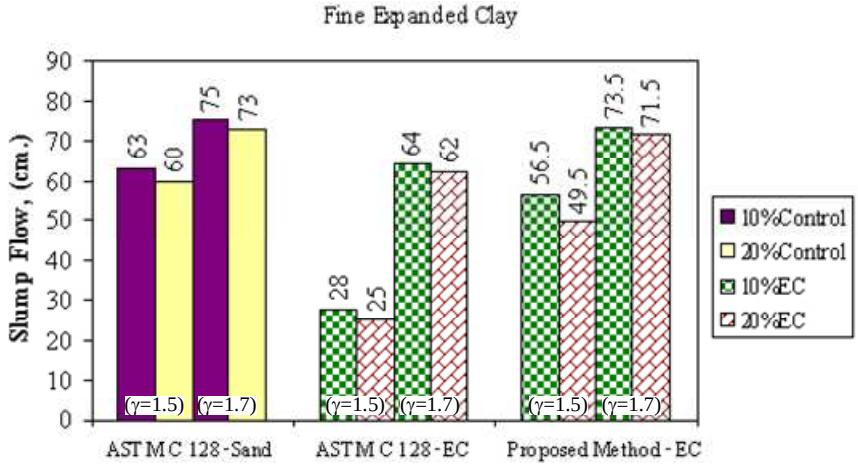

Fig. 7.19 Comparison of slump flow of SCC mixed with fine expanded clay and proportioned by using water absorption from ASTM C 128 and water retainability from the proposed method

Fig. 7.20 shows that the 28-day compressive strength of the SCC mixed with bottom ashes and proportioned by the ASTM C 128 water absorption were higher than those of the control concrete, while those proportioned by using the water retainability from the proposed method gave the lower compressive strength than the control concrete. The strength decreases with increasing bottom ash contents, which was the same tendency as the strength behavior of the SCC containing the fine expanded clay. However, it was noted that the SCC mixed with bottom ashes gave the higher strength than those mixed with the fine expanded clay probably due to the strength improvement from the pozzolanic reaction of fly ash partially mixed in the bottom ashes. It is well understood that the compressive strength of concrete decreases when incorporating the expanded clay because of its high porosity and non-reactivity, but when designed by using the obtained water absorptions from the ASTM C 128, the higher strength was observed. This is again due to the underestimation of the ability to keep water of the porous fine aggregate.

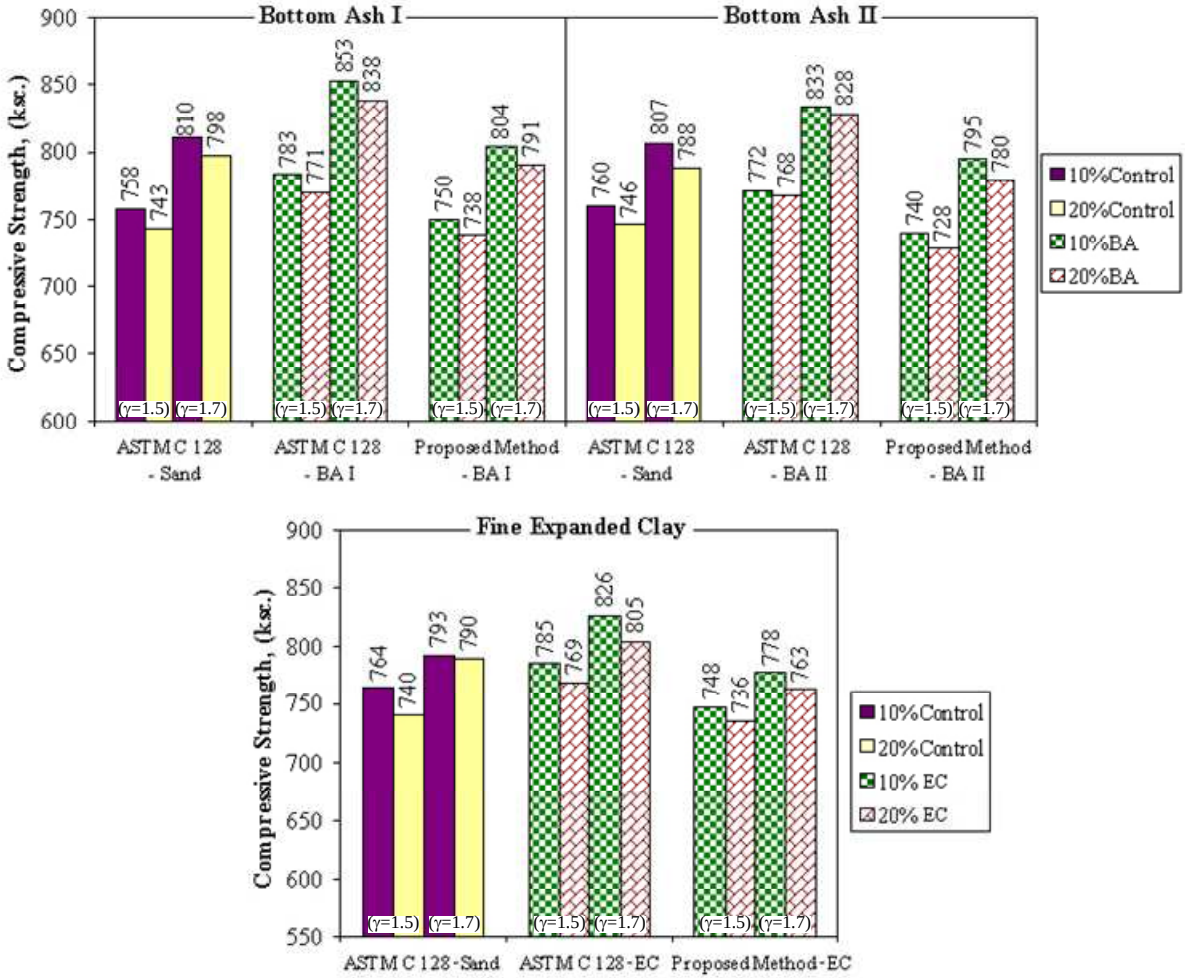

Fig. 7.20 Comparison of 28-day compressive strength of SCC proportioned by using water absorption from ASTM C 128 and water retainability from the proposed method

As a result, it is recommended that the water retainability is reasonably adopted instead of the absorption in the mixture preparation of concrete incorporating porous fine aggregates.

7.2.4 Conclusions

Water absorption of aggregate was necessary for design and proportioning of concrete mixtures containing the conventional aggregate. However, when using porous fine aggregates, the water retainability of the aggregate was more practical. A test method for water retainability was developed based on the concept of flow of free water under gravity condition. From a relationship between the moisture difference between two portions (top and bottom) of the tested sample and the trial water contents, water retainability is defined as the highest trial water content that results in zero moisture difference between the top and bottom portions.

A simplified method was proposed by performing this test method with the high trial water content (very wet sample) and water retainability could be determined from the moisture content of the top portion of the sample after the test. Test results conducted by different persons showed that the proposed test method for water retainability gave better

consistency of the results when compared to the water absorption by ASTM C 128. Appearance also indicated very dry condition of the samples at the point of cone collapsing in ASTM C 128 test method when compared to the condition of the samples at the point of water retainability by the proposed method. It was due to the high surface friction of porous fine aggregates. This friction reduced the workability of both conventional concrete (CVC) and the self-compacting concrete (SCC) mixed with various types of porous fine aggregates. Workability of the CVC and SCC mixtures with porous fine aggregates proportioned by the proposed water retainability test were closer to those of the control CVC and SCC concrete (with river sand only) than the CVC and SCC mixtures proportioned by the water absorption from the ASTM C 128 test method. The higher compressive strength of both CVC and SCC mixtures with porous fine aggregates proportioned by using the ASTM C 128 water absorption also indicated that ability to retain water of porous aggregates was underestimated if the value of absorption by ASTM C 128 was used to proportion the mixtures. It is recommended that the proposed water retainability test method is more practical for mix proportioning and quality control of the concrete with porous fine aggregates.

7.3 Use of Bottom Ash as Partial Replacement of Fine Aggregate for SCC

The essential properties of powder-typed SCC incorporating bottom ash as partial fine aggregate replacement of normal sand at 0 %, 10 %, 20 % and 30 % by weight were investigated in this study. These properties include deformability and filling ability (i.e. slump flow, 50-cm slump flow time, and L-box passing ability), hardened concrete properties (i.e. porosity, pore size distribution and compressive strength) and durability (i.e. chloride penetration, carbonation depth, shrinkage in drying environment, and expansion in sodium sulfate solution). As the reasons explained in section 7.2, the proposed test method in section 7.2 was adopted to determine the water retainability of bottom ash for mix proportioning of the tested mixtures with bottom ash.

7.3.1 Effects of Bottom Ash on Deformation Capacity

Slump flow value is typically used as the measuring value for deformation capacity of self-compacting concrete. The effect of bottom ash on slump flow of SCC at different levels of bottom ash replacement is shown in Fig. 7.21.

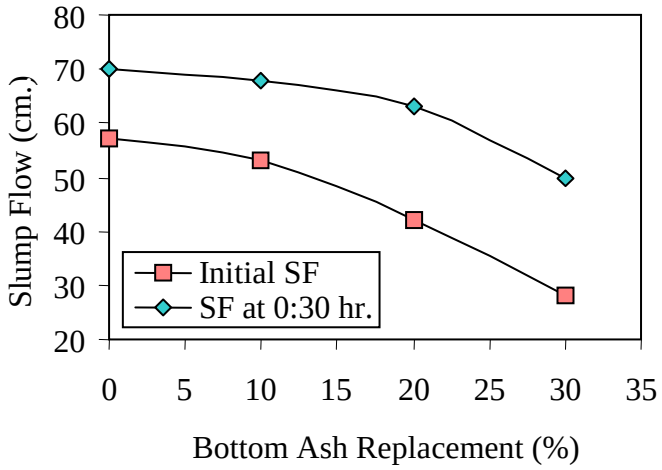

Fig. 7.21 Slump flow of the mixtures with bottom ash 0 %, 10 %, 20 % and 30 % of total fine aggregates

It can be seen that the slump flow of SCC mixed with 10 % bottom ash was slightly lower than that of the control mixture. However, when the bottom ash content was more than 10 %, the slump flow of the bottom ash SCC decreased significantly with the increase of bottom ash content. It is considered to be due to the increase of aggregate-to-aggregate friction from the highly irregular shape and rough texture of bottom ash particles. However, the slump flow of SCC mixtures with bottom ash could be increased by adding an extra superplasticizer dosage with the increase of bottom ash content as shown in Table 7.2.

Table 7.2 Mix proportions of the SCC mixtures with water to powder ratio of 0.31 the ratio of paste volume to void volume of compacted aggregate phase ($\gamma = 1.5$)

Mix		SCC-BA0% (Control)	SCC-BA10%	SCC-BA20%	SCC-BA30%
Cementitious Materials					
Cement-Type I	kg./m.^{3}	385	385	385	385
PFA	kg./m.^{3}	165	165	165	165
Water	l./m.^{3}	170	170	170	170
Fine Aggregates					
River Sand	kg./m.^{3}	850	765	680	595
Bottom Ash	kg./m.^{3}	-	85	170	255
Coarse Aggregates					
Limestone (3/4"-#4)	kg./m.^{3}	850	850	850	850
Admixtures					
Water reducer-Type D	cc./m.^{3}	1,200	1,200	1,200	1,200
Superplasticizer-Naphthalene based	cc./m.^{3}	5,800	5,800	5,800	5,800
Extra dosage of superplasticizer to obtain slump flow 70 cm.	cc./m.^{3}	0	300	1,400	2,200
w/p ratio		0.31	0.31	0.31	0.31
s/a ratio		0.5	0.5	0.5	0.5

This finding corresponds to the studies of effects of bottom ash on slump of conventional concrete by Ghafoori and Bucholc (1996, 1997) and workability of asphaltic concrete by Churchill, et al. (1999). It was also found that the mixtures with 20 % and 30 % bottom ash lost their slump flow significantly at 30 minutes after mixing when compared with either the control mixture or the mixture with 10 % bottom ash content. It indicated that the loss of slump flow must be paid attention for SCC incorporating bottom ash as partial replacement of river sand especially if the replacement percentage is over 10 %. Proper use of retarding admixture can be a solution to the slump flow loss problem.

7.3.2 Effects of Bottom Ash on Velocity of Deformation

The measurement of 50-cm slump flow time (T_{50}) was conducted to evaluate the velocity of deformation of the tested SCC mixtures (Tangtermsirikul, et al., 2000). Fig. 7.22 shows the effect of bottom ash on T_{50}. The figure shows that T_{50} increases as the bottom ash content increases. The larger T_{50} of the bottom ash SCC is considered to be due to the increase of inter-particle frictions among aggregate particles produced from bottom ash particles. It is also seen that when increasing bottom ash content, the trend of slump flow time at 30 min after mixing was similar to that of the initial time just after mixing.

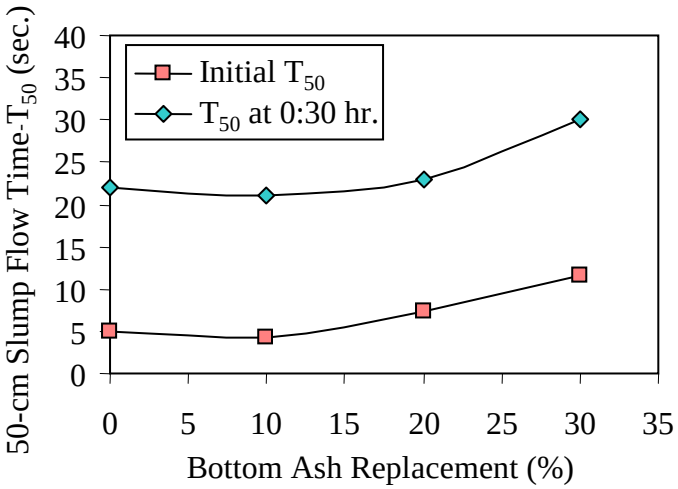

Fig. 7.22 50-cm slump flow time of the mixtures with bottom ash 0 %, 10 %, 20 % and 30 % of total fine aggregates

7.3.3 Effects of Bottom Ash on Segregation

By visual inspection during the slump flow test, segregation was not found in all tested SCC mixtures with bottom ash as seen in Fig. 7.23. The mixtures were stiffer when increasing bottom ash content.

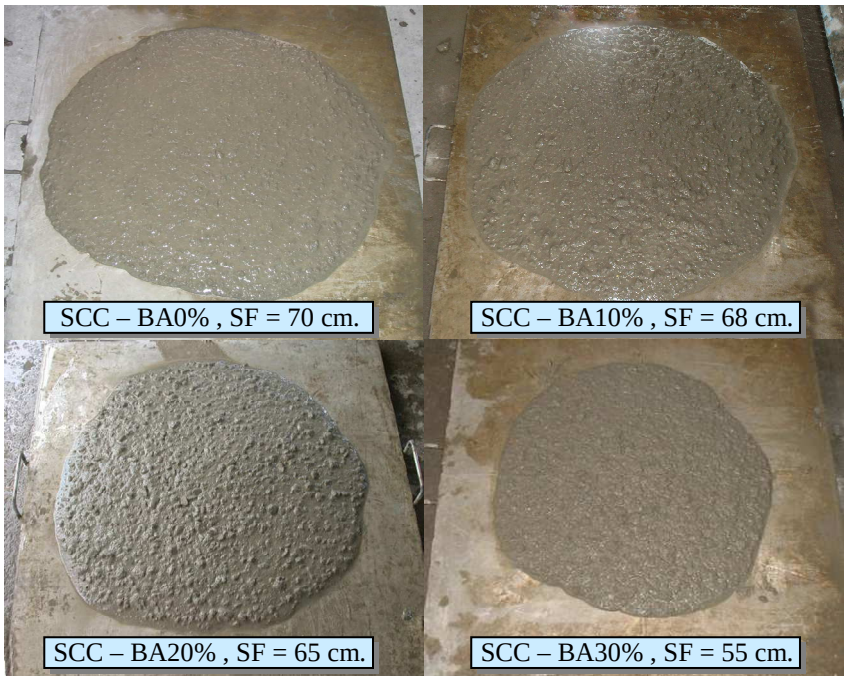

Fig. 7.23 Appearances after slump flow test of the mixtures with bottom ash 0 %, 10 %, 20 % and 30 % of total fine aggregates

7.3.4 Effects of Bottom Ash on Segregation and Passing Ability

Fig. 7.24 shows the test results of passing ability through narrow openings evaluated by using L-box apparatus. The values of passing ability of SCC-BA 0 %, SCC-BA 10 %, SCC-BA 20 % and SCC-BA 30 % are 83.0 %, 80.0 % 60.0 % and 5.0 %, respectively. It

reveals that L-box passing ability of SCC-BA 10 % was slightly lower than that of the control SCC but with the continuing increase of the replacement levels of bottom ash (20 % and 30 %), passing ability decreased significantly. Aggregate blocking was observed in mixture SCC-BA 30 % due to the higher inter-particle friction caused by the bottom ash particles, promoting the aggregate bridging at the vicinity of clear spacing between steel bars. As the L-box passing ability of at least 60 % was recommended as the passing condition for the test, the good L-box passing ability was recognized for the control mixture and the mixture containing 10 % and 20 % bottom ash. It should be noted here that the condition of the bar spacing in the L-box test is more critical than many of the real construction condition.

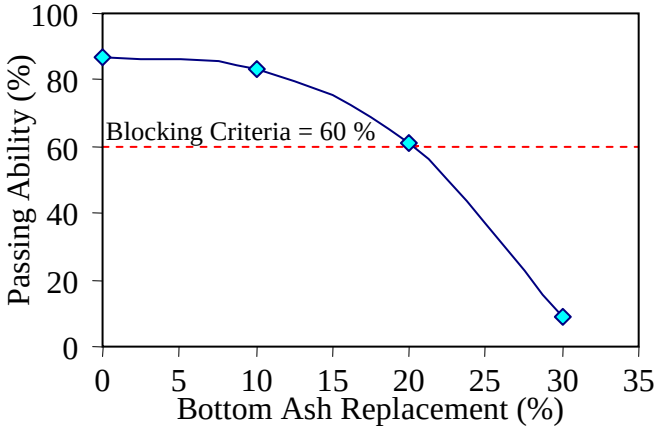

Fig. 7.24 L-shape passing ability of the mixtures with bottom ash 0 %, 10 %, 20 % and 30 % of total fine aggregates

7.3.5 Effects of Bottom ash on Physical Properties of Hardened SCC

From the test results presented in Fig. 7.25, it was observed that SCC-BA 30 % had the highest porosity at the concrete age of 28 days, followed by SCC-BA 20 %, SCC-BA 10 % and the control SCC, respectively. This is because the highly porous property of bottom ash particles increases total porosity of concrete. At the age of 56 days, total porosity of all SCC mixtures reduced, however total porosity of bottom ash SCC mixtures were still higher than that of the control concrete.

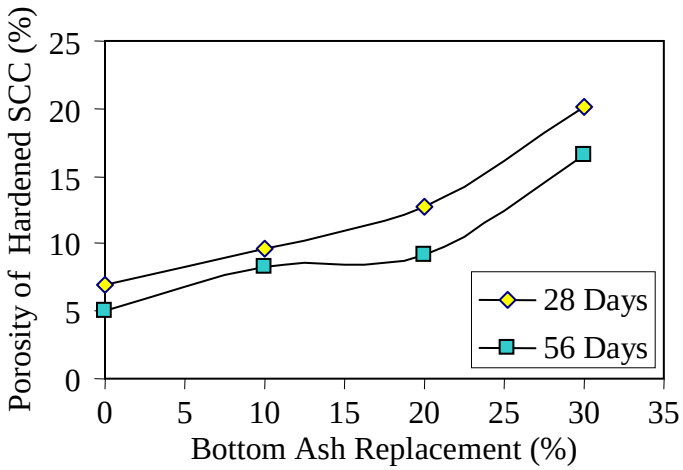

Fig. 7.25 Porosity of hardened the mixtures with bottom ash 0 %, 10 %, 20 % and 30 % of total fine aggregates at the ages of 28 and 56 days

Fig. 7.26 shows that at the age of 28 days, all tested SCC mixtures had equivalent average pore size. The figure also reveals that comparing to the results at 28 days, the average pore size of all bottom ash SCC mixtures at 56 days of age became smaller while that of the control mixture was almost unchanged. It is considered to be due to the pore refinery effect by pozzolanic reaction especially from fine ash particles.

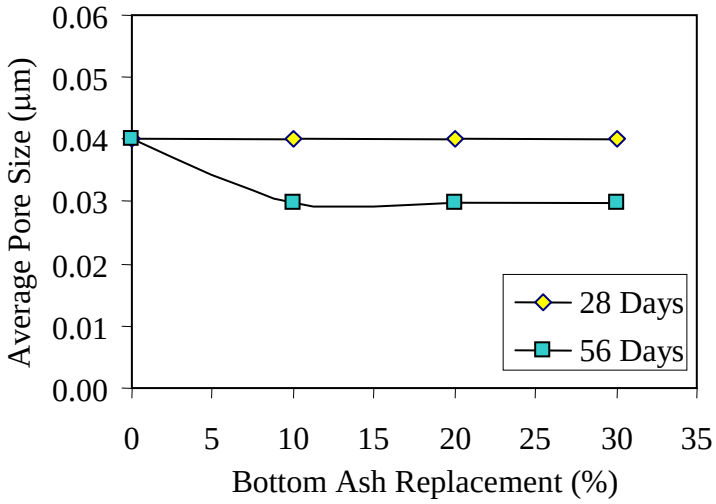

Fig. 7.26 Average pore size of hardened the mixtures with bottom ash 0 %, 10 %, 20 % and 30 % of total fine aggregates

Figs. 7.27 to 7.30 present the relationships between porosity of hardened SCC mixtures and their mechanical properties (i.e. compressive strength, splitting tensile strength) and durability (i.e. chloride permeability and carbonation depth). The figures show that there are relations between porosity and properties of hardened SCC incorporating bottom ash, which will be discussed in the sections of the related properties.

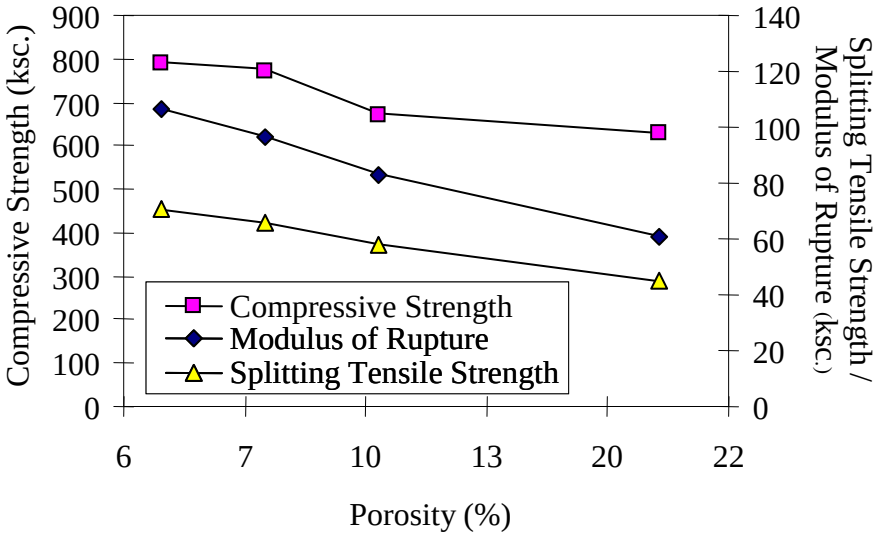

Fig. 7.27 Relationship between porosity versus compressive strength, splitting tensile strength, and modulus of rupture of the mixtures tested at the age of 28 days

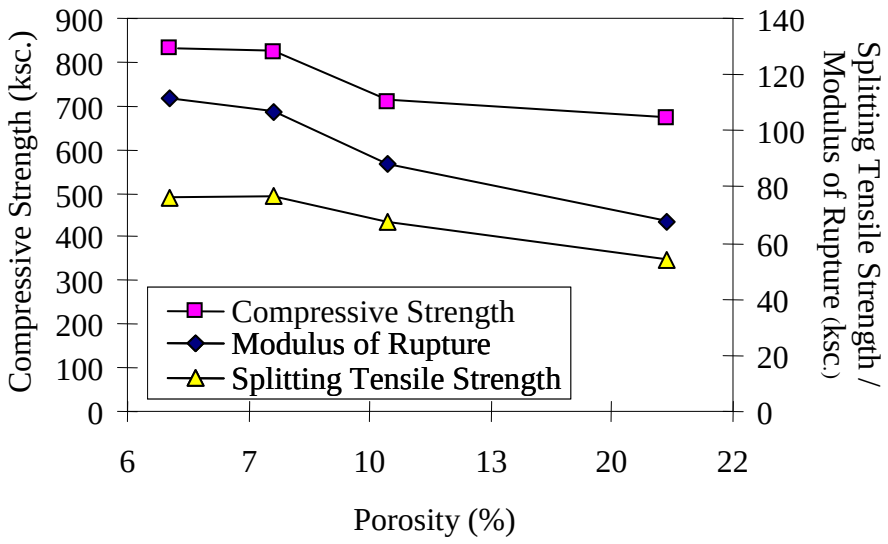

Fig. 7.28 Relationship between porosity versus compressive strength, splitting tensile strength, and modulus of rupture of the mixtures tested at the age of 56 days

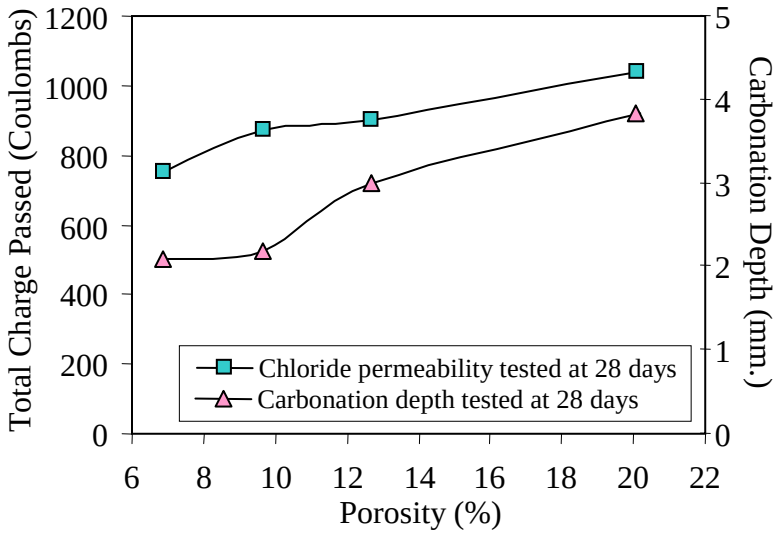

Fig. 7.29 Relationship between porosity versus rapid chloride permeability and carbonation depth of the mixtures tested at the age of 28 days

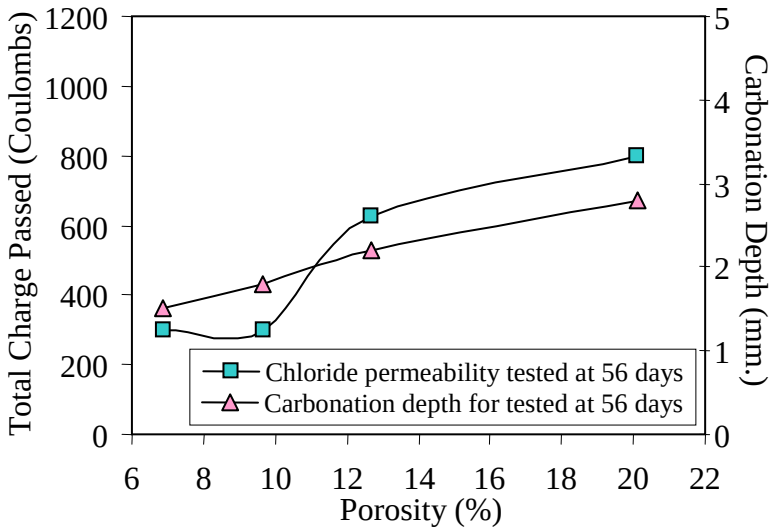

Fig. 7.30 Relationship between porosity versus rapid chloride permeability and carbonation depth of the mixtures tested at the age of 56 days

7.3.6 Effect of Bottom Ash on Mechanical Properties

7.3.6.1 Compressive Strength

Fig. 7.31 presents the effect of bottom ash on compressive strength of SCC when it was used to replace river sand at different percentages. It was found that almost all of the bottom ash mixtures except for SCC-BA 10 % had lower compressive strength than the control SCC at all concrete ages. At the replacement levels higher than 10 %, the compressive strength of bottom ash SCC decreased with increasing bottom ash content. It can be explained by considering Figs. 7.27 that the increase of porosity in hardened concrete due to the use of bottom ash results in the reduction of compressive strength. At the age of 28 days, the compressive strength of the SCC mixture with 10 % bottom ash was equivalent to that of the control SCC and became higher than that of the control SCC at the age of 56 days, while those of the mixtures containing 20 % and 30 % bottom ash were still lower. This may be due to the pore refinery effect especially at long term, by pozzolanic reaction of bottom ash, which dominates over the effect of increase of porosity at the replacement level of 10 %. At the levels of 20 % and 30 % bottom ash content, the pore refinery effect by pozzolanic reaction is not dominant when compared to the increase of porosity (average pore size did not reduce on the other hand increased slightly when bottom ash replacement was increased from 10 % to 20 % and 30 % while the porosity greatly increased). So, this indicates that the long term compressive strength of SCC can be enhanced by replacing 10 % of total fine aggregate with the bottom ash.

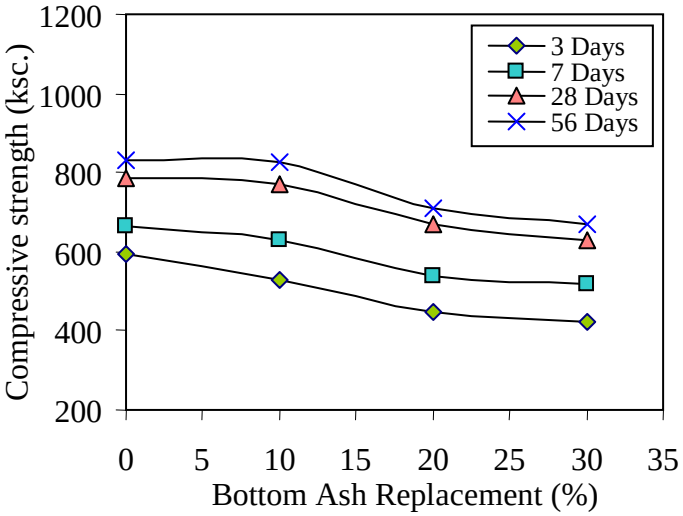

Fig. 7.31 Compressive strength of the mixtures with bottom ash 0 %, 10 %, 20 % and 30 % of total fine aggregates

7.3.6.2 Splitting Tensile Strength

The test results of splitting tensile strength are expressed in Fig. 7.32. Similar tendency to compressive strength, the increase of bottom ash content reduced the splitting tensile strength. In long term, the 56-day splitting tensile strength slightly increased at the 10 % bottom ash replacement level but decreased when bottom ash contents were beyond this replacement level. The reason is the same as that explained for compressive strength in the previous section.

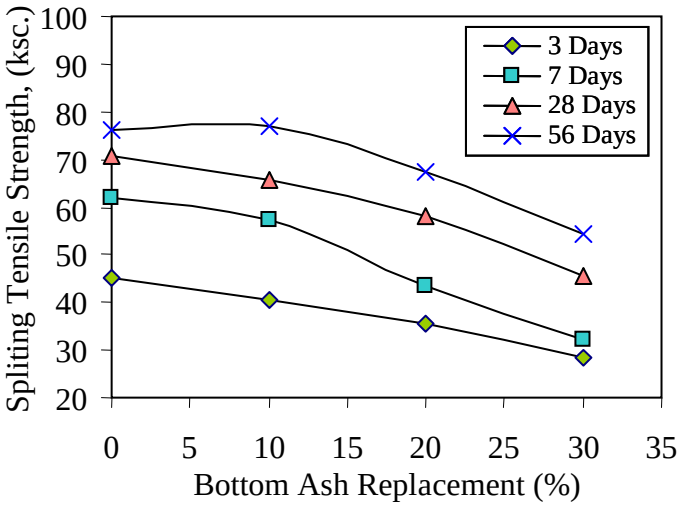

Fig. 7.32 Splitting tensile strength of the mixtures with bottom ash 0 %, 10 %, 20 % and 30 % of total fine aggregates

7.3.6.3 Modulus of Rupture

Fig. 7.33 shows that the increase of bottom ash replacement level resulted in the reduction of modulus of rupture, exhibiting the similar tendency as those of the compressive strength and splitting tensile strength for all concrete ages. It was due to the higher porosity in hardened concrete as indicated in Fig. 7.27.

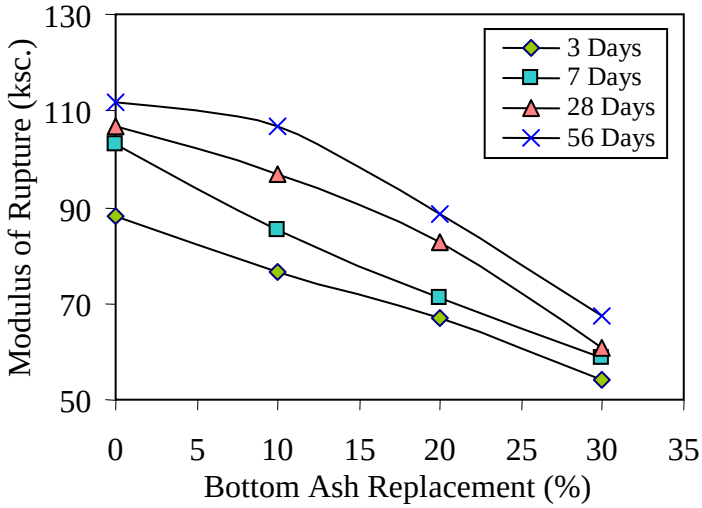

Fig. 7.33 Modulus of rupture of the mixtures with bottom ash 0 %, 10 %, 20 % and 30 % of total fine aggregates

7.3.7 Effects of Bottom Ash on Durability

7.3.7.1 Chloride Permeability

The chloride permeability of the tested SCC mixtures is shown in Fig. 7.34. It was found that the higher the bottom ash content the higher the chloride permeability at the concrete age of 7 days. It was also revealed that the chloride charge passed of all SCC-BA mixtures reduced with the age of concrete. At the age of 28 days, all tested SCC mixtures had not much different Cl^- permeability. The same tendency was also found for 56 days of age. It was mainly influenced by the tightness of the long-age mixtures due to low water to powder ratio. At the concrete age of 56 days, the Cl^- permeability of SCC-BA10 % was about the same as, in fact a little lower than, that of the control concrete, while those of SCC-BA 20 % and SCC-BA 30 % were higher. This reduction of chloride diffusion is considered to be due to the improved pore structure (reduced pore size) by pozzolanic reaction at the optimum bottom ash content (10 %) and long term water-curing.

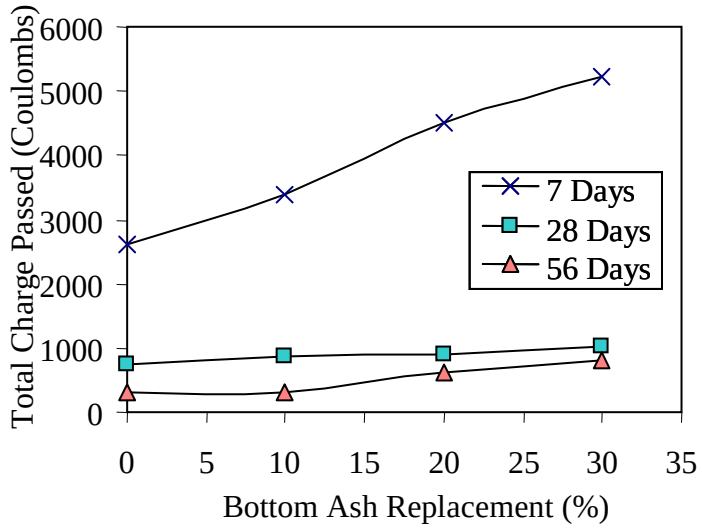

Fig. 7.34 Rapid chloride permeability of the mixtures with bottom ash 0 %, 10 %, 20 % and 30 % of total fine aggregates

7.3.7.2 Carbonation Depth

According to the test results of carbonation depth, shown in Figs. 7.35 and 7.36, tested for one month in an acceleration chamber, the carbonation depth, tested at concrete ages of 28 and 56 days, increased with the increase of bottom ash content. The carbonation depths of SCC containing 10 % bottom ash were a little larger than those of the control concrete. On the other hand, carbonation depths of SCC-BA 20 % and SCC-BA 30 % were much larger than those of the control mixtures. Figs. 7.29 and 7.30 show the strong relations between the tested carbonation depth and porosity implying that higher CO_2 diffusion was attributed to higher porosity of concrete due to the increase of bottom ash content. The carbonation depth of bottom ash SCC mixtures was smaller when tested at the longer concrete age due to the effect of pore densification by pozzolanic reaction of bottom ash.

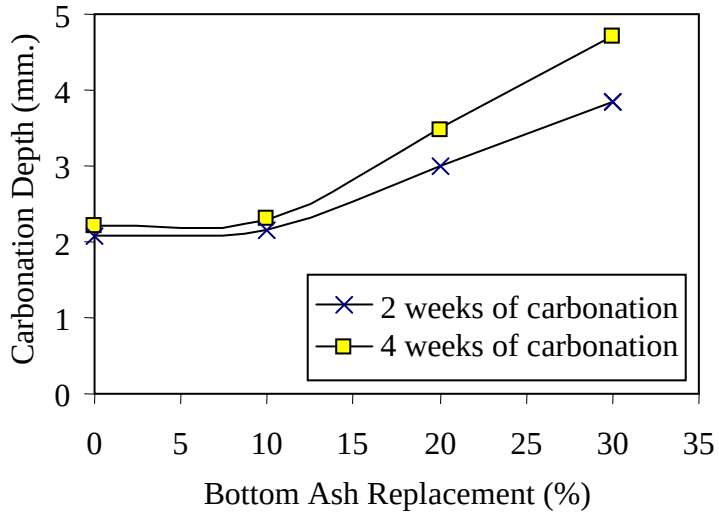

Fig. 7.35 Carbonation depth of the mixtures with bottom ash 0 %, 10 %, 20 % and 30 % of total fine aggregates tested after 28 days of curing

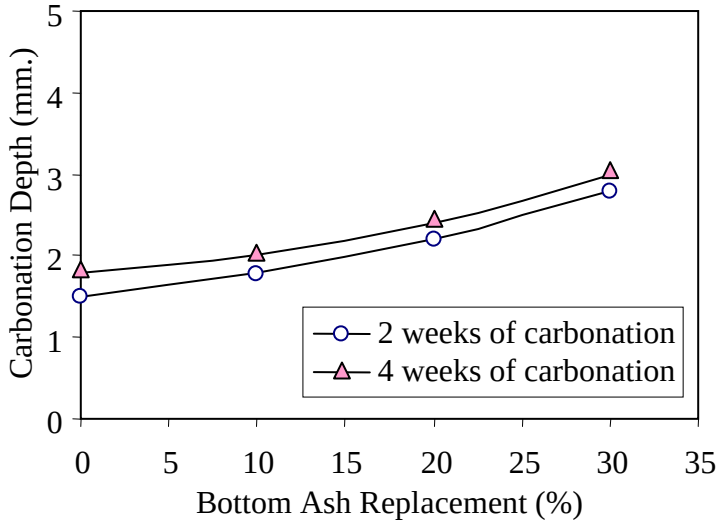

Fig. 7.36 Carbonation depth of the mixtures with bottom ash 0 %, 10 %, 20 % and 30 % of total fine aggregates tested after 56 days of curing

7.3.7.3 Shrinkage in Drying Environment

Since the tested mixtures had very low water to powder ratio, the shrinkage measured in drying environment includes both autogeneous and drying shrinkages. Fig.7.37 indicates that the trend of shrinkage of the test samples increased with drying period and gradually stabilized after about 91 days of drying. It was also found that the mixture with higher bottom ash content displayed larger shrinkage, whereas the control concrete exhibited the smallest shrinkage. Basically, the rate of water evaporation from concrete depends on the pore structures of concrete i.e. pores size and pore volume, and the condition of environment (Lea, 1970). Test results of porosity indicate that the higher rate of concrete drying is attributed to the increase of porosity due to the increase of bottom ash content.

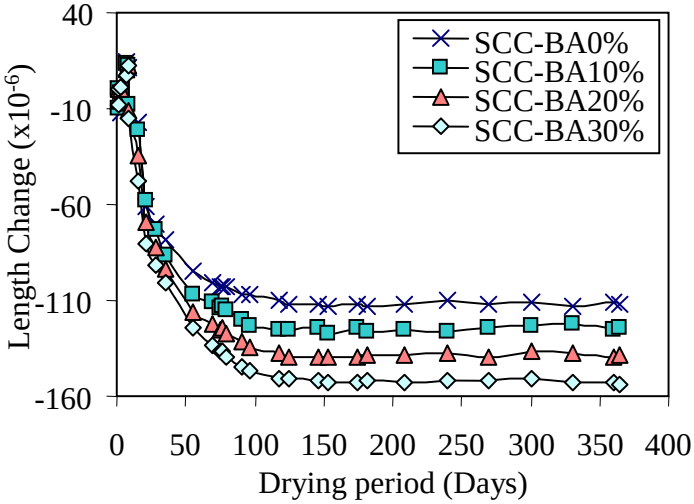

Fig. 7.37 Shrinkage in drying environment of the mixtures with bottom ash 0 %, 10 %, 20 % and 30 % of total fine aggregates

7.3.7.4 Expansion Induced by Sodium Sulfate

The results of length change of specimens due to external sodium sulfate attack at various immersion times are shown in Fig. 7.38. The expansion of all concrete specimens increased prominently with the submerging period during the first 196 days. After that, the expansion of each mixture was nearly stabilized until the end of the test period (12 months). It revealed that the expansion of the control SCC was the largest, followed by SCC-BA 10 %, SCC-BA 20 % and SCC-BA 30 %, respectively. Specimen break-down was not found in this study possibly because of the dense matrix of SCC due to low water to powder ratio. The dense matrix significantly reduced permeability and then diffusion of SO_4^{2-} ions into the concrete. Test results indicate that the increase of bottom ash content results in better resistance to sodium sulfate. This is because the calcium hydroxide which produces gypsum by reacting with sodium sulfate, resulting in secondary ettringite to cause expansion in concrete (Khatri, 1997), is reduced by the pozzolanic reaction of bottom ash. In spite of the higher porosity, the expansion of SCC mixtures with bottom ash decreases with the increase of bottom ash content. This indicates that the sodium sulfate resistance can be achieved by pozzolanic reaction of bottom ash, which dominates over the increase of porosity. The improvement on sulfate resistance is beneficial for SCC application in sulfate exposing structures such as underground structures, bored piles, and undersea structures etc.

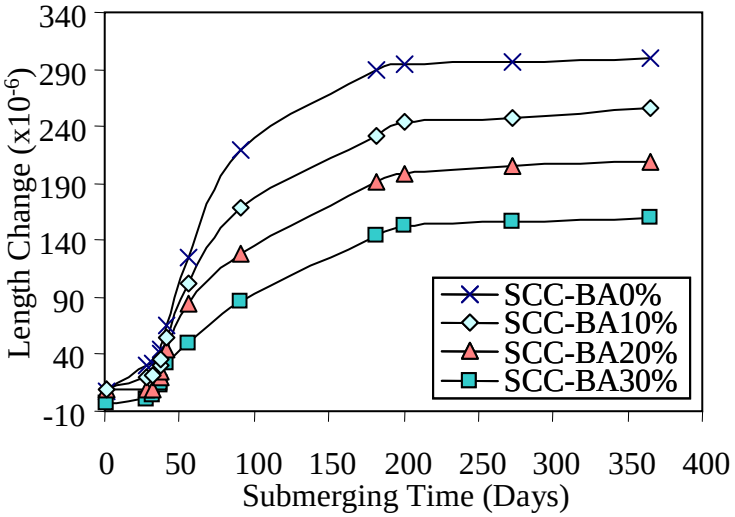

Fig. 7.38 Expansion in sodium sulfate of the mixtures with bottom ash 0 %, 10 %, 20 % and 30 % of total fine aggregates

7.3.8 Conclusions

Experimental results revealed that slump flow and L-box passing ability of the SCC mixtures with bottom ash reduced, while the slump flow loss and 50-cm slump flow time (T_{50}) increased with the increase of bottom ash replacement level. However, the required slump flow could be maintained by adding an extra dosage of superplasticizer.

The increase of bottom ash content resulted in the reduction of compressive strength, splitting tensile strength and modulus of rupture and caused the increase of porosity of hardened concrete. However, at 10 % bottom ash replacement of fine aggregate, the compressive strength and splitting tensile strength at 56 days of age were improved by pore refinement effect due to pozzolanic reaction which dominated over the increase of porosity.

In terms of durability, chloride ion permeability, carbonation depth and shrinkage in drying environment of most of the tested bottom ash SCC mixtures except for the mixture with 10 % bottom ash were larger than those of the control SCC, mainly due to higher porosity. On the other hand, the resistance against sodium sulfate was enhanced with the increase of bottom ash content. The durability of SCC mixtures with bottom ash could be improved in long term by pore refinement due to pozzolanic reaction when water-curing was conducted.

As a result, it is reasonable to conclude that if mechanical properties and some durability performances are concerned, the optimum replacement for the tested bottom ash is about 10 % by weight of total fine aggregate. However, the bottom ash replacement level higher than 10 % may be applied for particular works depending on total concrete cost and construction condition.

7.4 Use of Very Fine Sand as Partial Replacement of Fine Aggregate for SCC

This study focused on the effects of the use of very fine sand as partial replacement of normal river sand on filling ability of the SCC mixtures. Mix proportions of the tested SCC mixtures were determined by using the ratio of fine aggregate to total aggregate that

gives the minimum void content of aggregate phase and fixing powder content at 520 and 540 kg/m^3 and water to powder ratio (w/b) of 0.28. Slump flow of 65 cm without bleeding was controlled by adjusting dosage of superplasticizer of the mixtures.

7.4.1 Effects of Very Fine Sand on Void Content of Aggregate Phase

The minimum void contents were obtained from the tests of the combined aggregates mixtures between coarse aggregate versus normal sand mixed with very fine sand at various percentages. It is known that the larger specific surface area of aggregates results in the higher minimum water content required to initiate deformation of fresh concrete. Therefore, the compatibility between void content and specific surface area of the aggregates were considered in this study to achieve the effective mix proportion of SCC.

7.4.1.1 Effects of Very Fine Sand on Void Content of the Combined Normal and Very Fine Sands Mixture

It was found from Fig. 7.39 that void content of the compacted normal sand mixed with very fine sand was the lowest at the very fine sand amounts of 5 % and 10 % of the total fine aggregate mixture. Beyond these amounts, the void content increased with the increase of very fine sand content.

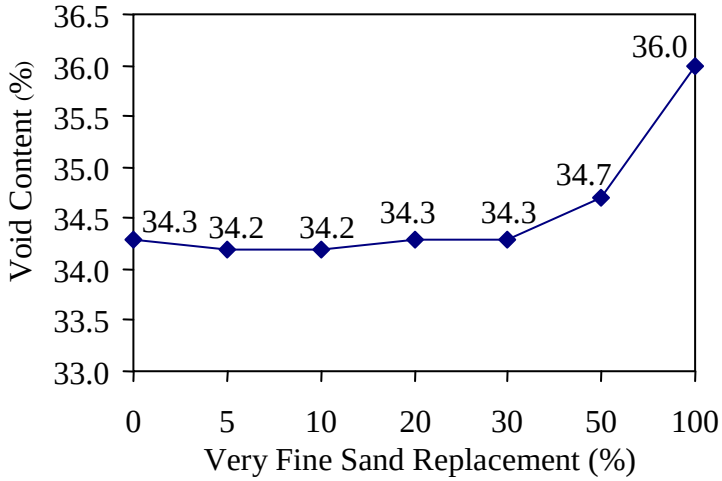

Fig. 7.39 Void content of normal sand mixed with very fine sand at 0 %, 5 %, 10 %, 20 %, 30 %, 50 %, and 100 %

Similarly, it was confirmed that the calculated specific surface area of the tested combined sand mixtures increased with the increase of percentage of very fine sand as shown in Fig.7.40.

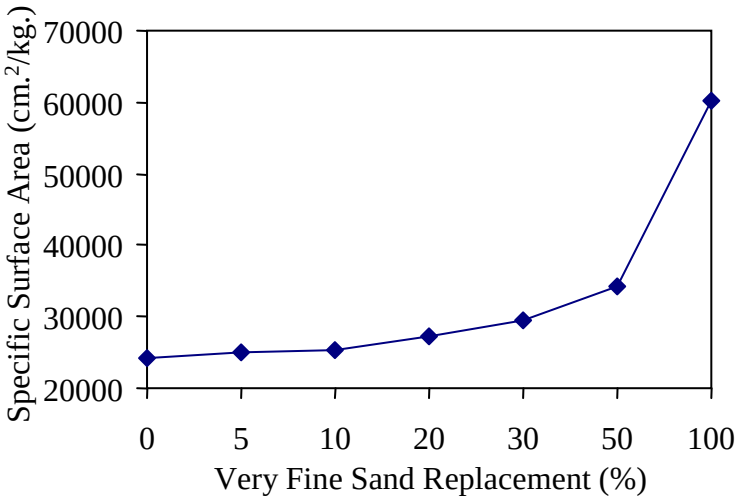

Fig. 7.40 Specific surface area of normal sand mixed with very fine sand at 0 %, 5 %, 10 %, 20 %, 30 %, 50 %, and 100 %

7.4.1.2 Effects of Very Fine Sand on Void Content of the Combined Normal-Very Fine Sands and Coarse Aggregate Mixture

Test results of void content in Fig. 7.41 show that by varying the weight ratio of fine aggregate to total aggregates (s/a) from 0.35 to 0.50, the minimum void contents of the combined aggregates between coarse aggregate and normal sand mixed with different contents of very fine sand were obtained at different ratios of fine aggregate to total aggregates. The mixture between coarse aggregate and normal sand with 50 % very fine sand had the lowest void content i.e. 21.8 % at the ratio of sand to total aggregates of 0.42. However, it can be seen that almost all of combined normal-very fine sands coarse aggregate mixtures gave the minimum void contents at the similar sand to total aggregates ratio of 0.45. Consequently, the s/a value of 0.45 was used to determine the mix proportion of the tested SCC mixtures for this study.

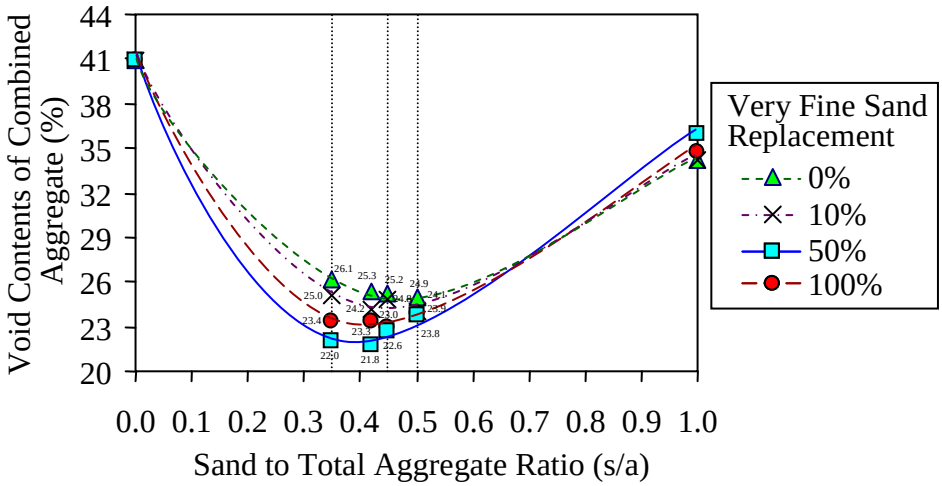

Fig. 7.41 Relationship between weight ratio of sand to total aggregate (s/a) and void of the combined normal-very fine sands and coarse aggregates mixtures

It can be seen from Fig. 7.42 that at the s/a ratio of 0.45, the increase of very fine sand content reduces the void content of the combined normal-very fine sands and coarse

aggregates mixtures. It is considered to be due to the higher ability of smaller particles of sand to fill voids among the compacted aggregate particles. However, the specific surface area increased with the increase of very fine sand content. Therefore, to achieve the effective mix proportion of SCC, the optimum replacement of very fine sand of total fine aggregate should be determined by considering the compatibility of these two physical properties in company with the test results of the properties of SCC.

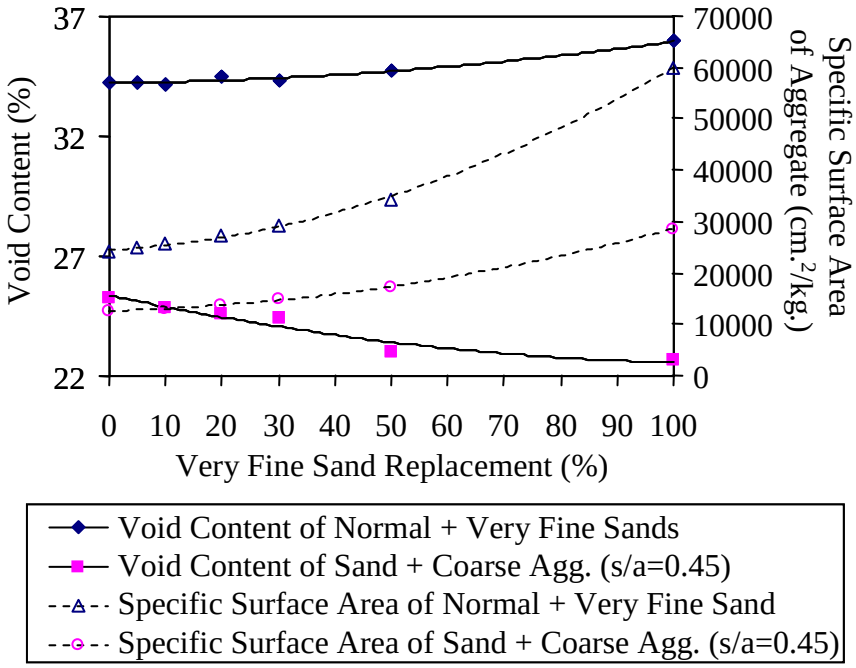

Fig. 7.42 Relationship between specific surface area and void content of the tested aggregates

7.4.2 Effect of Very Fine Sand on Deformation Capacity of SCC

From the test results shown in Fig. 7.43, it was found that at the same powder contents, slump flows of the mixtures with 10 % very fine sand content were similar to (in case of powder content = 520 kg/m^3) and slightly higher (in case of powder content = 540 kg/m^3) than that of the control concrete. It is considered due to the effective compatibility between void content and specific surface area of the tested aggregates. However, when the very fine sand contents were over 10 %, slump flow of the tested SCC reduced with the increase of very fine sand content. It was because when increasing very fine sand content, the larger specific surface area of the aggregates causing the higher required water content to initiate deformation is dominant over the lower void content of the compacted aggregates.

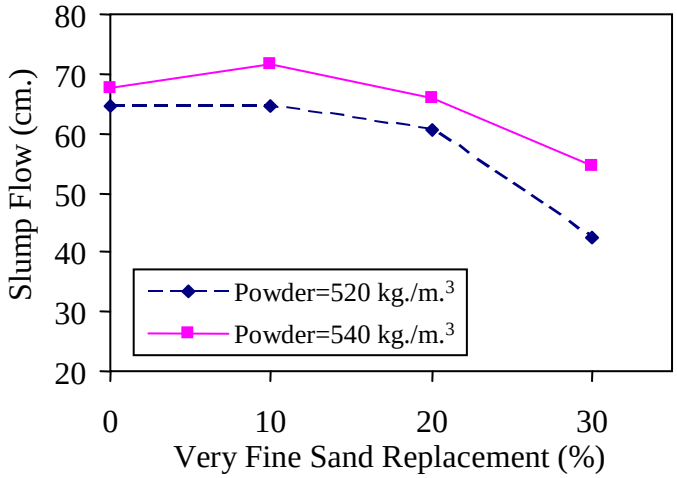

Fig. 7.43 Slump flow of the SCC mixtures with very fine sands at 0 %, 10 %, 20 %, and 30 %.

7.4.3 Effect of Very Fine Sand on Velocity of Deformation of SCC

Fig. 7.44 shows that the increase of very fine sand content increased T_{50} except for the mixtures with 10 % very fine sand. It is considered due to the higher effective surface area of total aggregates, which is confirmed by the relationship between free water content vs. T_{50} at different effective surface area of aggregates as shown in Fig. 4.41 in chapter 4.

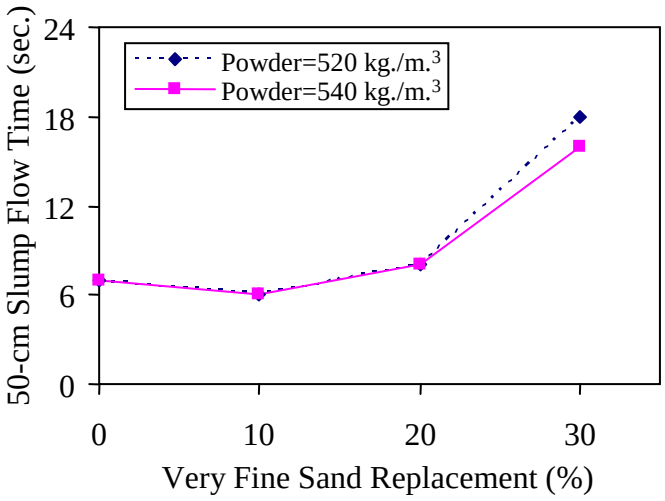

Fig. 7.44 50-cm slump flow of the SCC mixtures with very fine sands of 0 %, 10 %, 20 %, and 30 %.

7.4.4 Effects of Very Fine Sand on Segregation and Passing Ability through Narrow Openings of SCC

Segregation was not found in all tested SCC mixtures with very fine sand. On the other hand, it could be observed during testing that the mixtures were more viscous when increasing the percentage of very fine sand. It was due to the increase of effective surface area of aggregates causing the reduction of free water of the mixtures, which is beneficial to improve the resistance to segregation of SCC.

It can be seen from Fig. 7.45 that, L-box passing ability of the mixtures with powder content of 520 kg/m^3 increased with the increase of very fine sand content. This

indicates that the increase of very fine content benefits the mixtures with smaller powder content. On the other hand, L-box passing ability of the mixtures with powder content of 540 kg/m^3 was highest at 10 % very fine sand content but the passing ability reduced when very fine sand contents were increased to 20 % and 30 %.

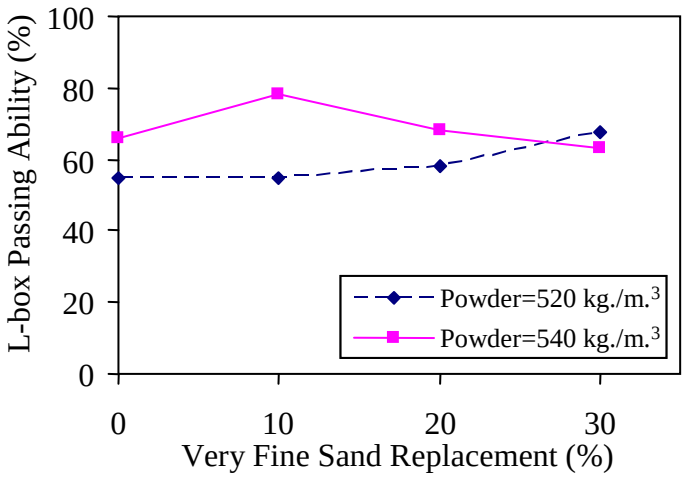

Fig. 7.45 L-box passing ability of the mixtures with 0 %, 10 %, 20 %, and 30 % very fine sand contents

7.4.5 Conclusions

Very fine sand contains a significant content of very fine particles; therefore it improves segregation resistance and passing ability through narrow openings of SCC. It was found in this study that the minimum void content of the compacted normal sand mixed with very fine sand was obtained at 5 % and 10 % very fine sand contents and the specific surface area increased with the increase of very fine sand content. It was also found that the minimum void contents of the aggregate mixtures between coarse aggregate and normal sand mixed with different contents of very fine sand were obtained at different ratios of sand to total aggregates. Also, almost all of combined normal-very fine sands and coarse aggregate mixtures gave the minimum void contents at the similar sand to total aggregates ratio of 0.45 which was used to determine the mix proportion of the tested SCC mixtures. It was also indicated that void content of combined normal-very fine sands and coarse aggregates mixtures was reduced with the increase of very fine sand contents.

It was found from test results of the tested SCC mixtures that at the same powder contents, slump flows of the mixtures with 10 % very fine sand content were similar to (in case of powder content = 520 kg/m^3) and slightly higher (in case of powder content = 540 kg/m^3) than that of the control concrete due to the effective compatibility between void content and specific surface area of the tested aggregates. However, when the very fine sand contents were over 10 %, slump flow of the tested SCC reduces with the increase of very fine sand content because the larger specific surface area of the aggregates due to the increase of very fine sand results in the higher required water content to initiate deformation. Test results also indicate that the increase of very fine sand content increases T_{50} due to the higher effective surface area of total aggregates.

Segregation was not found in all tested SCC mixtures with very fine sand because very fine sand improved the resistance to segregation of SCC. It was also found that L-box

passing ability of the mixtures with powder content of 520 kg/m^3 increased with the increase of very fine sand content, while those of the mixtures with powder content of 540 kg/m^3 was highest at 10 % very fine sand content but reduced with the increase of very fine sand content when very fine sand contents were over 10 %.

As a result, it is reasonable to conclude that deformability, resistance to segregation, and passing ability of the SCC mixtures could be improved by using the tested very fine sand at the optimum replacement of about 10 % by weight of total fine aggregate.

Chapter 8

Conclusions and Recommendations

8.1 Conclusions

Based on the proposed models, test results and verification tests, the following conclusions can be drawn.

As the measuring values of deformability of SCC, slump flow and 50-cm slump flow time (T_{50}) vary mainly with free water content of the mixture. Free water content is obtained when knowing unit water content, water retainability of powder materials and surface water retainability of aggregates and extra free water from fillable powder. The amount of minimum free water required to initiate deformation is also another parameter influencing deformability and is considered to be resulted from inter-particle surface force among solid particles in the mixture. At similar free water content, greater slump flow is obtained from the mixture with larger paste content due to the reduction of aggregate-to-aggregate frictions owing to the larger distance between aggregate particles. The dispersion effect from superplasticizers is considered to reduce not only water retainability of powders but also friction and cohesion among solid particles. The dispersion effect also causes the increase of the secant slopes of slump flow vs. free water content curve and results in the increase of slump flow and decrease of T_{50}. The inter-particle force in the concrete is considered to vary with the effective surface area of solid particles. T_{50} increases with the increase of effective surface area of aggregates due to the larger inter-particle surface friction of aggregate particles. On the other hand, it reduces when increasing effective surface area of powder materials, due to the reduction of aggregate contact and the lubrication effect provided to the aggregate particles from larger paste content. The verification tests proved that the proposed models can be used to predict the deformation capacity (slump flow) and velocity of deformation (T_{50}) of the powder-typed SCC with satisfactory accuracies.

Bleeding in the mixture is considered as the primary indication of static segregation of SCC. The increase of water to binder ratio increases bleeding rate and bleeding capacity due to the larger amount of free water for bleeding in the mixtures. Moreover, bleeding capacity increases with the increase of ratio of paste volume to void volume of aggregate phase (γ) due to the increase of free water content directly caused by the higher unit water content of the tested mixtures. When unit water content is kept constant, bleeding capacity of the mixtures with naphthalene and melamine based superplasticizers increases with the increase of the water reducing efficiency. However, polycarboxylate based superplasticizer shows lower bleeding though having higher water reducing efficiency than the others. This contradicting result of the polycarboxylate based superplasticizer from those of the naphthalene and melamine based superplasticizers is considered due to the difference of dispersion mechanisms between electrostatic repulsion in naphthalene and melamine based superplasticizers and steric hindrance in polycarboxylate based superplasticizer. The higher concrete temperature causes the earlier initiation and termination of bleeding, a little higher bleeding rate, and lower bleeding capacity of the tested mixtures due to the acceleration of

the reactions of binder particles in the concrete. Prediction model for bleeding capacity of the SCC mixtures was developed based on the effects from main factors influencing bleeding i.e. free water content, effective surface area of solid particles, and average degree of reaction of binders. However, the model for predicting bleeding capacity of the mixtures with polycarboxylate based superplasticizer has still not derived. To avoid static segregation, the bleeding capacity of 0 % is specified as the minimum requirement for mix proportioning of SCC, though passing ability may not be always satisfied when the mixture has zero bleeding especially when the condition of the opening is severe. The verification tests confirmed that the proposed model can be used to predict bleeding capacity of the tested SCC mixtures with appropriate accuracy. However, further development of the proposed model requires inclusion of the effect of steric hindrance mechanism.

The maximum volume ratio of aggregate to concrete that does not cause blocking by aggregate bridging at narrow openings can be determined to achieve the satisfactory L-box passing ability. The L-box passing ability reduces with the increase of irregularity of aggregate particle shape due to the higher inter-particle frictions and interlocking among aggregate particles. At similar particle shape and volume of the aggregates, the highest L-box passing ability of the mixtures is achieved when T_{50} is within the optimum ranges. The maximum L-box passing ability and width of the optimum range of T_{50} are smaller in cases of higher irregularity and larger volume of aggregates. This indicates that the variation of the T_{50} should be controlled within the smaller optimum range when the concrete contains the larger aggregate volume and/or the aggregate with higher irregular particle shape. The blocking volume of aggregate reduces when maximum size of coarse aggregate or volume ratio of coarse aggregate to total aggregates is larger (lower s/a). Moreover, the larger ratio between reinforcement diameter and maximum size of aggregate gives the smaller aggregate blocking volume ratio due to the larger supports of rebar for the aggregate bridging at the narrow spaces. Coarse aggregate with higher irregularity gives the smaller aggregate blocking volume ratios due to the higher inter-particle frictions and interlocking among aggregate particles. Also, at similar viscosity of the mixtures, the larger aggregates blocking volume can be determined if the particle shape of coarse aggregate is more rounded. In verification tests, it was confirmed that the proposed models can be used to predict the blocking or no blocking conditions of the tested mixtures with satisfactory accuracies.

For the concrete with porous fine aggregates, the water retainability is more practical for being used in mix proportioning and quality control than the water absorption of the aggregate. A test method for water retainability was developed based on the concept of flow of free water under gravity condition. From the proposed method, water retainability of fine porous aggregates is derived from the highest trial water content that results in zero moisture difference between the top and bottom portions of aggregate sample from a relationship between the moisture difference between two portions (top and bottom) of the tested sample and the trial water contents. A simplified method is also proposed by performing the same testing procedure but with the high trial water content (very wet sample) and water retainability can be determined from the moisture content of the top portion of the sample after the test. By comparing the standard deviation within the group of test results conducted by different persons, the proposed test method for water retainability gives better consistency of the results when compared to the water absorption by ASTM C 128. The high surface friction of porous fine aggregates results in very dry condition of samples at the point of cone collapsing in ASTM C 128 test method and it reduces the workability of both conventional concrete (CVC) and the self-compacting

concrete (SCC) mixed with the porous fine aggregates. By applying the proposed method in process of mix proportioning, workability and compressive strength of the CVC and SCC mixtures with porous fine aggregates proportioned by the proposed water retainability test are more qualitatively consistent and closer to those of the control CVC and SCC mixtures with river sand only than the CVC and SCC concrete proportioned by the water absorption from the ASTM C128 test method.

By using bottom ash to partially replace sand at 0 %, 10 %, 20 % and 30 % by weight, slump flow and L-box passing ability of the SCC mixtures with bottom ash reduce, while the slump flow loss and T_{50} increases with the increase of bottom ash replacement level. However, the required slump flow can be maintained by adding an extra dosage of superplasticizer. Compressive strength reduces with the increase of bottom ash content while porosity of hardened concrete increases. However, at 10 % bottom ash replacement of fine aggregate, the compressive strength at 56 days of age is improved by pore refinement effect due to pozzolanic reaction which dominated over the increase of porosity. In terms of durability, chloride ion permeability, carbonation depth and shrinkage in drying environment (autogeneous shrinkage and drying shrinkage) of most of the tested bottom ash SCC mixtures except for the mixture with 10 % bottom ash are larger than those of the control SCC, mainly due to higher porosity. At the bottom ash replacement level of 10 %, tested at concrete age of 56 days, the Cl^- permeability of mixtures with 10 % bottom ash is reduced to be about the same as that of the control concrete and the carbonation depth and shrinkage in drying environment are a little larger than those of the control concrete. These long term improvements are due to the effect of pore densification by pozzolanic reaction. In addition, the expansion induced by sodium sulfate of SCC mixtures with bottom ash decreases with the increase of bottom ash content. If mechanical properties and some durability performance are concerned, the optimum replacement for the tested bottom ash is about 10 % by weight of total fine aggregate. However, the bottom ash replacement level higher than 10 % may be applied for particular works depending on total concrete cost, construction condition and required performances.

Very fine sand is a by-product to be used to replace some part of normal fine aggregate in SCC. The minimum void content of the compacted normal sand mixed with very fine sand can be achieved at 5 % and 10 % very fine sand replacement of total fine aggregates and the specific surface area increases with the increase of very fine sand content. Almost all of the combined normal-very fine sands and coarse aggregate mixtures give the minimum void contents at the similar sand to total aggregates ratio of 0.45. Void content of combined normal-very fine sands and coarse aggregates mixtures is reduced with the increase of very fine sand contents. Deformability and passing ability of the SCC mixtures can be improved by using very fine sand at the optimum replacement of about 10 % by weight of total fine aggregate. At the same powder contents, slump flow of the mixtures with 10 % very fine sand content is similar to (in case of powder content = 520 kg/m^3) and slightly higher (in case of powder content = 540 kg/m^3) than that of the control concrete due to the effective compatibility between void content and specific surface area of the tested aggregates. However, slump flow of the mixture with very fine sand over 10 % reduces with the increase of very fine sand content due to the higher required water content to initiate deformation resulted from the larger specific surface area of the aggregates. Also, the increase of very fine sand content increases T_{50} due to the higher effective surface area of total aggregates which results the reduction of free water in the concrete and the larger inter-particle surface friction of aggregate particles. The use of higher very fine sand reduces the bleeding of fresh concrete due to the increase of specific

surface area of solid particles causing the reduction of free water content. The L-box passing ability of the mixtures with powder content of 520 kg/m^3 increases with the increase of very fine sand contents up to 30 %, while those of the mixtures with powder content of 540 kg/m^3 are the highest at 10 % very fine sand content but reduces with the increase of very fine sand contents over 10 %.

8.2 Recommendations for future studies

The future studies are recommended as follows:

Models for predicting deformability, segregation and passing ability through narrow openings should be extended for the SCC mixture with viscosity modified agents.

Model for predicting the loss of deformability in SCC should be proposed.

Model for predicting dynamic segregation of SCC should be proposed.

The model for predicting passing ability should be extended to include different kinds of narrow openings such as different clear spacing of steel bars and cross-reinforcement installation.

The use of powders with wider range in their properties may be verified for more reliability of the proposed model for predicting deformation capacity and velocity of deformation.

The effect of steric hindrance mechanism of polycaboxylate based superplasticizer on bleeding and segregation should be clarified.

The mixtures with wider range in paste contents may be verified for more reliability of the proposed model for predicting bleeding capacity.

The use of other types of powder may be verified for more reliability of the model for predicting bleeding capacity.

More verification of the model for predicting passing ability may be carried out for the general use, especially the aggregate blocking volume of the mixtures with wider ranges of slump flow and 50-cm slump flow time.

References

Assaad, J., Khayat, K. H., and Daczko, J., (2004), "Evaluation of Static Stability of Self-Consolidating Concrete", ACI Materials Journal, Vol. 101, No. 3, May-June, pp. 207-215.

Baguant, B. K., (1995) "Properties of Concrete with Bagasse Ash as Fine Aggregate", ACI Special Publication - SP 153-26, Vol. 153, June, pp. 459-478.

Bai, Y., and Basheer, P. A. M., (2003), "Influence of furnace bottom ash as fine aggregate on properties of concrete", Structures and Buildings, Vol. 156 No. 1, February, pp. 85-92.

Bai, Y., Darcy, F., and Basheer, P. A. M., (2005), "Strength and Drying Shrinkage Properties of Concrete Containing Furnace Bottom Ash as Fine Aggregate", Construction and Building Materials, Vol. 19, No. 9, November, pp. 691-697.

Bakoshi, T., Kohno, K., Kawasaki, S. and Yamaji, N., (1995) "Strength and Durability of Concrete Using Bottom Ash as Replacement for Fine Aggregate", ACI Special Publication- SP 179-10, Vol. 179, June, pp. 159-172.

Black, R. W., (1986), "The Determination of Specific Gravity Using Siphon-Can Method" Cement, Concrete, and Aggregates, American Society for Testing and Materials, summer 1986, p. 46-54.

Bucholc, J., and Ghafoori, N., (1996), "Investigation of Lignite-Based Bottom Ash for Structural Concrete, " Journal of Materials in Civil Engineering, American Society of Civil Engineer, Vol. 8, No. 3, August, pp. 128-137.

Bui, V. K., Shah, S. P., and Akkaya, Y., (2002) "A New Approach in Mix Design of Self-Consolidating Concrete", Proceeding of First North American Conference on the Design and Use of Self-Consolidating Concrete (SCC), November, 2002, Illinois, U.S.A.

Bui, V. K., Akkaya, Y., and Shah, S. P., (2002) "Rheological Model for Self-Consolidating Concrete", ACI Material Journal, Vol. 99, No. 6, November-December, pp. 549-559.

Chan, Y. W., Li, V. C., and Kong, H. J., (1998), "Development of Self-Compacting Engineered Cementitious Composites", Proceeding of International Workshop on Self-Compacting Concrete, August, 1998, Kochi University of Technology, Japan, pp. 46-59.

Cheriaf, M., Cavalcante, J., Pera, J., (1999), "Pozzolanic Properties of Pulverized Coal Combustion Bottom Ash", Cement and Concrete Research, Vol. 29, pp. 1387-1391.

Churchill, E. V., and Amiirkhanian, S. N., (1999), "Coal Ash Utilization in Asphalt Concrete Mixtures", Journal of Materials in Civil Engineering, Vol. 11, No. 4, February, pp. 48-53.

Domone, P., (2000), “Mix design”, Self-Compacting Concrete, State-of-the-Art report of RILEM Technical Committee 174-SCC, 2000, pp. 49-65.

Domone, P., and Jin, J., (1999), “Properties of Mortar for Self-Compacting Concrete”, Self-Compacting Concrete, Proceedings of First International RILEM Symposium on Self-Compacting Concrete, Stockholm, Sweden, September, 1999, pp. 109-120.

Domone, P., Chai, H., and Jin, J., (1999), “Optimum Mix Proportioning of Self-Compacting Concrete”, Proceedings of International Conference on Innovation in Concrete Structures: Design and Construction, Dundee, September 1999, Thomas Telford, London, pp. 227-285.

Edamatsu, Y., Nishida, N., and Ouchi, M., (1999), “A Rational Mix-Design Method for Self-Compacting Concrete Considering Interaction between Coarse Aggregate and Mortar Particles”, Self-Compacting Concrete, Proceedings of First International RILEM Symposium on Self-Compacting Concrete, Stockholm, Sweden, September, 1999, pp. 309-320.

El-Chabib, H., and Nehdi, M., (2006), “Effect of Mixture Design Parameters on Segregation of Self-Consolidating Concrete”, ACI Materials Journal, Vol. 103, No. 5, September-October, pp. 374-383.

Felekoglu, B., Tosun, K., Baradan, B., Altun, A., and Uyulgan, B., (2006), “The Effect of Fly ash and Limestone Fillers on the Viscosity and Compressive Strength of Self-Compacting Repair Mortars”, Cement and Concrete Research, Vol. 36, No. 9, September, pp. 1719-1726.

Fumoto, T., and Yamada, M. (2004) “Influence of Quality of Powder on Rheology of High-Fluidity Concrete”, ACI Special Publication- SP 221-21, Vol. 221, May, pp. 367-380.

Ghafoori N., and Bucholc, J., (1997), “Properties of High-Calcium Dry Bottom Ash for Structural Concrete”, ACI Materials Journal, Vol. 94, No. 2, March- April, pp. 90-101.

Ghafoori N., and Cai, Y., (1998), “Laboratory-Made Roller Compacted Concretes Containing Dry Bottom Ash: Part I - Mechanical Properties”, ACI Materials Journal, Vol. 95, No. 3, March- April, pp. 121-130.

Ghafoori N., and Cai, Y., (1998), “Laboratory-Made Roller Compacted Concretes Containing Dry Bottom Ash: Part II - Long-Term Durability”, ACI Materials Journal, Vol. 95, No. 3, May- June, pp. 244-251.

Ghezal, A., and Khayat, K. H., (2002), “Optimizing Self-Consolidating Concrete with Limestone Filler by using Statistical Factorial Design Methods”, ACI Material Journal, Vol. 99, No. 3, May-June, pp. 264-272.

Hoshino, M., (1989), “Relationship between Bleeding, Coarse Aggregate, and Specimen Height of Concrete”, ACI Materials Journal, Vol. 86, No. 2, pp. 185-190.

Hughes, B.P. and Famili, H., (1971), “Absorptions of Concrete Aggregates, Part 1-Absorption of Concrete Aggregates, Part 2-Saturated Air Techniques for Determining the absorption of Aggregates,” RR/C8, Birmingham University, Great Britain.

Jaturapitakkul, C., and Cheerarot, R., (2003), "Development of Bottom Ash as Pozzolanic Material", Journal of Materials in Civil Engineering, Vol. 15, No. 1, February, 48-53.

Jianxiong, C., Xincheng, P., and Yubin, H. (1999), "A study of self-compacting HPC with superfine sand and pozzolanic additives", Self-Compacting Concrete, Proceedings of First International RILEM Symposium on Self-Compacting Concrete, Stockholm, Sweden, September, 1999, pp. 549-560.

Kampmann, R., and Ping, W. V., (2006), "Self-Consolidating Concrete: Case Study of a Mix Design Methodology Based on Raw Material Properties", Self-Compacting Concrete, Proceedings of 2006 Airfield and Highway Pavements Specialty Conference, Atlanta, Georgia, USA, April-May, 1999.

Kasemchaisiri, R., and Tangtermsirikul, S., (2005), "A Test Method for Water Retainability of Porous Fine Aggregate", Proceedings of the First Annual Concrete Conference, Thai Concrete Association, October, 2005, Rayong, Thailand, pp. CON 88-CON 94.

Kasemchaisiri, R., and Tangtermsirikul, S., (2005), "Modelling of Filling Ability and Mix Design of Self-Compacting Concrete", Proceedings of the First Annual Concrete Conference, Thai Concrete Association, October, 2005, Rayong, Thailand, pp. CON 95-CON 100.

Kasemchaisiri, R., and Tangtermsirikul, S., (2007), "A Method to Determine Water Retainability of Fine Porous Aggregate for Design and Quality Control of Fresh Concrete", Journal of Construction and Building Materials, Vol. 21, pp. 1322-1334.

Kasemsamrarn, N., and Tangtermsirikul, S., (2005), "A Design Approach for Self-Compacting Concrete Based on Deformability, Segregation Resistance and Passing Ability Models", Proceedings of the First International Symposium on Design, Performance and Use of Self-Consolidating Concrete, RILEM Proceeding PRO 42, May 2005, Changsha, Hunan, China, pp. 47-54.

Khatri, R. P. and Sirivivatnanon, V., (1997), "Role of Permeability in Sulphate Attack", Cement and Concrete Research, Vol. 27, No. 8, pp. 1179-1189.

Khayat, K. H., (1999), Workability, "Testing, and Performance of Self-Consolidating Concrete", ACI Material Journal, Vol. 96, No. 3, May-June, pp. 346-353.

Khunthongkeaw J., and Tangtermsirikul, S., (2003), "Vibration Consistency Prediction Model for Roller Compacted Concrete", ACI Material Journal, Vol. 100, No. 1, January-February, 2003, pp. 149-157.

Khunthongkeaw, J., (2001), "Workability Prediction Model for Concrete and Mortar with and Without Mineral and Chemical Admixture", Master Thesis, School of Civil Engineering and Technology, Sirindhorn International Institute of Technology, Thammasat University, Pathumthani.

Kitticharoenkiat, P., (1998), "A Slump Prediction Model Based on Water Retainability and Free Water Concepts", Master Thesis, School of Civil Engineering and Technology, Sirindhorn International Institute of Technology, Thammasat University. Pathumthani.

Kourd, A. A. E., (1989), “Properties of Concrete Incorporating Natural and Crushed Stone Very Fine Sand”, ACI Materials Journal, Vol. 86, No. 4, July-August, pp. 417-424.

Landgren R., (1994), “Unit Weight, Specific Gravity, Absorption, and Surface Moisture,” Significance of Tests and Properties of Concrete-Making Materials, ASTM STP 169C, American Society for Testing and Materials, Philadelphia, p. 421-430.

Lane, R.O., (1983), “Effects of Fly Ash on Freshly Mixed Concrete”, Concrete International: Design and Construction, Vol. 5, No. 10, pp. 50-52.

Lea, F.M., (1970), “The Chemistry of Cement and Concrete”, 3rd Edition, Edward Arnold, London.

Lemmer, C., Ruhl, M., and Nealen, A., (1995) “Correction of Consistency of Concrete Made with Aggregate Derived from Concrete Rubble” www.b-i-t.de/public/tudmassiv/ dacon13lemmerruehl.htm

Malhotra, V.M., Zhang, M. H., Read, P. H., and Ryell, J., (2000) “Long-tern mechanical Properties and Durability Characteristics of High-Strength/High-Performance Concrete Incorporating Supplementary Cementing Materials Under Outdoor Exposure Conditions”, ACI Material Journal, Vol. 97, No. 5, January-February, pp. 518-525.

Malier, Y., (1992), “High Performance Concrete: From Material to Structure”, E and FN SPON, London.

McBride, J., and Mukai, D. J., (2006), “Coarse Aggregate and Self-Consolidating Concrete Passing Ability”, ACI Special Publication - SP 233-06, Vol. 233, March, pp. 77-96.

Mehta, P. K., and Monteiro, P. J. M., (1993), “Concrete Structure, Properties, and Materials”, A Simon & Schuster Company Engleweed Cliffs, New Jersey, 548 pp.

Meyer, L.M., and Perenchio, W.F., (1979), “Theory of Concrete Slump Loss as Related to the Use of Chemical Admixtures”, Concrete International, Vol. 1, No. 1, pp. 36-43.

Muroga, Y., Ohsuga, T., Date, S., and Hira-ta, A. (1999), “A Flow Analysis for Self-Compacting Concrete”, Self-Compacting Concrete, Proceedings of First International RILEM Symposium on Self-Compacting Concrete, Stockholm, Sweden, September, 1999, pp.71-82.

Nabil, B., (1999), “Blended Fly Ash Cements”, ACI Materials Journal Vol. 96, No.6, pp. 641-651.

Naik, T. R., Chun, Y.-M., Kraus, R. N., Ramme, B. W., and Siddique, R. (2004), “Precast Concrete Products Using Industrial By-Products”, ACI Materials Journal, Vol. 101, No. 3, May-June, pp. 199-206.

Naik, T. R., Singh, S. S., Tharaniyil, M. P., and Wendorf, R. B., (1996), “Application of Foundry By-Product Materials in Manufacture of Concrete and Masonry Products”, ACI Materials Journal, Vol. 93, No. 1, January-February, pp. 51-60.

Nehdi, M, Chabib, H. El, and Naggar, M. H. El, (2001), “Predicting Performance of Self-Compacting Concrete Mixtures Using Artificial Neural Networks”, ACI Material Journal, Vol. 98, No. 5, September-October, pp. 394-401.

Noguchi, T., Oh, S.G., and Tomosawa, F., (1999), “Rheological approach to passing ability between reinforcing bars of self-compacting concrete”, Self-Compacting Concrete, Proceedings of First International RILEM Symposium on Self-Compacting Concrete, Stockholm, Sweden, September, 1999, pp. 59-70.

Neville, A. M., (1995), “Properties of Concrete”, Longman Scientific & Technical, London, 779 pp.

Oh, S.G., Noguchi, T., and Tomosawa, F., (1999), “Toward mix design for rheology of self-compacting concrete”, Self-Compacting Concrete, Proceedings of First International RILEM Symposium on Self-Compacting Concrete, Stockholm, Sweden, September, 1999, pp. 361-372.

Okamura, H., and Ouchi, M., (1999), “Self-compacting concrete, Development, present use and future”, Proceedings of First International RILEM Symposium on Self-Compacting Concrete, Stockholm, Sweden, September, 1999, pp. 3-14.

Okamura, H., and Ozawa, K., (1995), “Mix Design for Self-Compacting Concrete” Concrete Library of JSCE 25, pp. 107-120.

Okamura, H., Maekawa, K., and Ozawa, K., (1993), “High Performance Concrete” (written in Japanese), Gihodo Shuppan, Tokyo, Japan.

Ouchi, M., and Edamatsu, Y., (1999), “A simple evaluation method for interaction between coarse aggregate and mortar particles in self-compacting concrete”, Self-Compacting Concrete, Proceedings of First International RILEM Symposium on Self-Compacting Concrete, Stockholm, Sweden, September, 1999, pp. 121-130.

Ouchi, M., Hibino, M., and Okamura H., (1996), “Effect of Superplasticizer on Self-Compactability of Fresh Concrete”, Advances in Concrete and Concrete Pavement, (Construction Transportation Research Record No. 1574), National Research Council, pp. 37-40.

Ouchi, M., Ozawa, K., and Okamura H., (1998), “A Rational Mix-Design Method for Mortar in Self-Compacting Concrete”, Proceedings of the Sixth South-East Asia Pacific Conference on Structural Engineering and Construction Taipei, Taiwan, 1998, pp. 1307-1312.

Ozawa, K., Maekawa, K, Kunishima, M., and Okamura H., (1989), “Development of high performance concrete based on the durability design of concrete structures”, Proceedings of the second East-Asia and Pacific Conference on Structural Engineering and Construction (EASEC-2), Vol. 1, January 1989, pp. 445-450.

Ozawa, K., Maekawa, K., and Nanayakkara, A., (1991), “Solid Stiffness Model for Analysis of Fresh Concrete Flow, Gravel, Sand, and Cement Slurry Mixture” ASME, 4th Symposium on Solid-Liquid Flows, p.39-49.

Ozawa, K., Maekawa, K., and Okamura, H., (1990), “The High Performance Concrete with High Filling Capacity”, Proceeding of RILEM Symposium on Admixtures for Concrete, pp. 51-62.

Ozawa, K., Maekawa, K., and Okamura, H., (1992), “Development of High Performance Concrete”, Journal of the Faculty of Engineering, The University of Tokyo, Vol. 41, No. 3, pp. 381-439.

Ozawa, K., Tangtermsirikul, S. and Maekawa, K., (1992), “Role of Powder Materials on the Filling Capacity of Fresh Concrete”, The Fourth CANMET/ACI International Conference on Fly Ash, Silica Fume, Slag and Natural Pozzolans in Concrete, Supplementary Papers, pp. 121-130.

Patel, R., Hossaain, M. A., Shehata, M., Bouzoubaa N., and Lachemi, M., (2004), “Development of Statistical Models for Mixture Design of High-Volume Fly Ash Self-Consolidating Concrete”, ACI Material Journal, Vol. 101, No. 4, July-August, pp. 294-302.

Petersson, O., and Billberg, P., (1999), “Investigation on Blocking of Self-Compacting Concrete with Different Maximum Aggregate Size and Use of Viscosity Agent Instead of Filler, Self-Compacting Concrete”, Proceedings of First International RILEM Symposium on Self-Compacting Concrete, Stockholm, Sweden, September, 1999, pp. 333-344.

Power, T. C., (1968), “Properties of Fresh Concrete”, Wiley, New York, 664 pp.

Ravina, D., (1995), “Slump Retention of Fly Ash Concrete With and Without Chemical Admixtures”, Concrete International: Design and Construction, Vol. 17, No. 4, pp. 25-29.

Roshavelov, T. T., (1999), “Concrete Mixture Proportioning with Optimal Dry Packing”, Self-Compacting Concrete, Proceedings of First International RILEM Symposium on Self-Compacting Concrete, Stockholm, Sweden, September, 1999, pp. 385-396.

Saak, A. W., Jennings, H. M., and Shah S. P., (1999), “Characterization of the Rheological Properties of Cement Paste for Use in Self-Compacting Concrete”, Self-Compacting Concrete, Proceedings of First International RILEM Symposium on Self-Compacting Concrete, Stockholm, Sweden, September, 1999, pp. 83-93.

Saak, A. W., Jennings, H. M., and Shah, S. P., (2001), “New Methodology for Designing Self-Compacting Concrete”, ACI Materials Journal, Vol. 98, No. 6, November-December, pp. 429-439.

Safawi, M. I., Iwaki, I., and Miura, T., (2004), “The Segregation Tendency in the Vibration of High Fluidity Concrete”, Cement and Concrete Research, Vol. 34, No. 2, February, pp. 219-226.

Sahmaran, M., Yaman, I. O., and Tokyay, M. (2006) “Fresh Properties of High-Volume Fly Ash Self Consolidating Concretes”, ACI Special Publication- SP 235-13, Vol. 235, March, pp. 189-202.

Saxer, E. L., (1956), “A direct Method of Determining Absorption and Specific Gravity of Aggregates”, Rock Products, May, pp. 78-84.

Skarendahl, A., (1998), “Self-Compacting Concrete in Sweden, Research and Application”, Proceeding of International Workshop on Self-Compacting Concrete, August, 1998, Kochi University of Technology, Japan, pp. 60-71.

Skarendahl, A., (2000), “Definition and Development Objectives”, Self-Compacting Concrete, State-of-the-Art report of RILEM Technical Committee 174-SCC, 2000, pp.3-13.

Sonebi, M., (2001), “Applications of Statistical Models in Proportioning Medium-Strength Self-Consolidating Concrete”, ACI Materials Journal, Vol. 101, No. 5, September-October, pp. 339-346.

Soshiroda, T., (1981), “Segregation Characteristics of Concrete Containing a High-Range Water-Reducing Admixture”, ACI Special Publication- SP 68-07, Vol. 68, January, pp. 121-138.

Su, N., Hsu, K.-C., and Chai, H.-W., (2001), “A Simple Mix Design Method for Self-Compacting Concrete”, Cement and Concrete Research, Vol. 31, No. 12, December, pp. 1799-1807.

Tangtermsirikul, S., (1989), “Modeling of the Quasi-Static Behavior of Fresh Concrete”, A Doctoral Thesis submitted to the University of Tokyo, Japan.

Tangtermsirikul, S., (1998), “Design and Construction of Self-Compacting Concrete in Thailand” , Proceeding of International Workshop on Self-Compacting Concrete, August, 1998, Kochi University of Technology, Japan, pp. 73-85.

Tangtermsirikul, S., (2003), “Durability and Mix Design of Concrete”, First Edition, Thammasat University Press, Bangkok, 200 pp.

Tangtermsirikul, S., Bui, V. K., and Aoyagi, Y. (1994), "Optimum Proportioning Method for the Aggregate Phase of Highly Durable Vibration-Free Concrete", Proceedings of the 1st National Convention on Civil Engineering, November 1994, Nakornrachasima, Thailand, pp.53-62.

Tangtermsirikul, S., and Bui, V. K., (1995), “Blocking Criteria for Aggregate Phase of Self-Compacting High Performance Concrete”, Proceedings of the Regional Symposium on InfraStructures Development in Civil Engineering, Bangkok, Thailand, pp.58-65.

Tangtermsirikul, S., and Bui, V. K. (2002), “Optimum Aggregate Phase Based on Deformability and Blocking Criteria of Self-Compacting Concrete”, Research and Development Journal, Volume 13 No.2, The Engineering Institute of Thailand”, pp. 18-28.

Tangtermsirikul, S., and Khayat, K. H., (2000), “Fresh Concrete Properties”, Self-Compacting Concrete, State-of-the-Art report of RILEM Technical Committee 174-SCC, 2000, pp. 17-21.

Tangtermsirikul, S., Khunthongkeaw J., and Kitticharoenkiat, P., (2001), “A Slump Model for Predicting Workability of Fresh Mortar and Concrete”, Journal of Materials, Concrete Structures and Pavements, JSCE, No. 676, pp. 149-157.

Tangtermsirikul, S., Matsuoka, Y., Shindo, T., and Sakamoto, J., (1992), "A Study on Velocity of Deformation of Super Workable Concrete", Proceeding of the JCI Annual Conference, Vol. 14, No. 1, pp. 1161-1166.

Targan, S., Olgun, A., Erdogan, Y., and Sevinc, V. (2004), "Mineralogy and Organic Matter Content of Bottom Ash Samples from Agios Demitrios Power Plant, Greece", Bulletin of the Geological Society of Greece, Vol. 36, Proceeding of the Tenth international Congress, Thessaloniki, pp.321-326.

Tattersall, G. H., (1991), "Workability and Quality Control of Concrete", E & FN Spon, London, 262 pp.

Thumasujarit, K. and Tangtermsirikul, S., (2004), "Experimental Investigations on Bleeding of Fly Ash Concrete", EIT Research and Development Journal, Vol. 15, No. 3, pp. 40-47.

Thumasujarit, K. and Tangtermsirikul, S., (2005), "Experimental Study on Bleeding of Fly Ash Concrete with Water Reducing Admixtures", EIT Research and Development Journal, Vol. 16, No. 3, pp. 1-7.

Uchikawa, H., Hanehara, S., and Hirao, H., (1996), "High Volume Wastes Concrete (HVWC)", ACI Special Publication - SP 179-02, Vol. 179, June, pp. 23-38.

Wallevik, J. E., (2006), "Relationship between the Bingham Parameters and Slump", Cement and Concrete Research, Vol. 36, No. 7 , July, pp. 1214-1221.

Walrawen, J. C., (1998), "The Development of Self-Compacting Concrete in the Netherlands", Proceeding of International Workshop on Self-Compacting Concrete, August, 1998, Kochi University of Technology, Japan, pp. 87-96.

Wangchuk, S, (2003), "Workability Prediction Model: Effect of Water Reducing Admixtures and Slump Loss", Master Thesis, School of Civil Engineering and Technology, Sirindhorn International Institute of Technology, Thammasat University, Pathumthani, Thailand.

Wangchuk, S., Khunthongkeaw, J. and Tangtermsirikul, S., (2003) "Effects of Water-Reducing Admixtures on Initial Slump of Fresh Concrete", EIT Research and Development Journal, Vol. 14, No. 1, pp. 19-26.

Wangchuk, S., Khunthongkeaw, J. and Tangtermsirikul, S., (2003), "A Slump Loss Prediction Model for Concrete", EIT Research and Development Journal, Vol. 14, No. 2, pp. 33-39.

Wangchuk, S., Khunthongkeaw, J., and Tangtermsirikul, S., (2002) "Workability Prediction Model: Effects of Water Reducing Admixtures and Slump Loss", Proceedings of the 8th National Convention on Civil Engineering, Vol. 3, October 2002, Kon Kaen, Thailand, pp. MAT-68 to MAT-73.

Whiting, D., and Dziedzic, W., (1992) “Effects of Conventional and High-Range Water Reducers on Concrete Properties”, Research and Development Bulletin RD107, Portland Cement Association.

Yahia, A., Tanimura, M., Shimabukuro, A., and Shimoyama, Y., (1999), “Effect of rheological parameters on self compactability of concrete containing various mineral admixtures”, Self-Compacting Concrete, Proceedings of First International RILEM Symposium on Self-Compacting Concrete, Stockholm, Sweden, September, 1999, pp. 523-535.

Yamamoto, Y., and Kobayashi, S., (1986), “Effect of Temperature on the Properties of Superplasticized Concrete”, ACI Material Journal, Vol. 83, No.1, January-February, pp. 80-88.

Appendix A
Properties of Materials

Table A-1 Properties of cement, fly ash, and lime stone powder used in model formulation and verification tests throughout this study.

Chemical Composition of Cement			**Used by Author**	**Used by Ghezal, et al.**	**Used by Patel, R., et al.**
Silicon dioxide	(SiO_2)	(%)	20.63	20.7	19.44
Aluminum oxide	(Al_2O_3)	(%)	5.26	4.0	5.33
Iron oxide	(Fe_2O_3)	(%)	3.07	2.6	2.34
Calcium oxide	(CaO)	(%)	64.97	62.9	61.77
Magnesium oxide	(MgO)	(%)	0.95	2.3	2.34
Sulfur Trioxide	(SO_3)	(%)	2.59	-	3.78
Loss on Ignition	(LOI)	(%)	1.20	3.0	2.06
Sodium oxide	(Na_2O)	(%)	0.12	0.76	0.23
Potassium oxide	(K_2O)	(%)	0.61	-	1.11
Free CaO		(%)	1.21	-	0.8
Insoluble Residue		(%)	0.14	-	-
Tricalcium Silicate	(C_3S)	(%)	61	59.6	53.8
Dicalcium Silicate	(C_2S)	(%)	13	14.5	15.15
Tricalcium Aluminate	(C_3A)	(%)	8.7	6.4	10.16
TetraCa-Al-Ferrite	(C_4AF)	(%)	9	7.9	7.12
Gypsum		(%)	5.6	-	-
Physical Properties of Cement					
Blaine Fineness : Air Permeability Test (ASTM C 204-00)		cm^2/g	3,330	3,450	3,740
Specific Gravity			3.15	3.14	3.14
Passing 45 μm		(%)	-	88.9	87.0
Air Content : (ASTM C185)		(%)	-	-	8.1
Soundness : Autoclave Expansion (ASTM C 151-98a)		(%)	-0.02	-	-
Time of Setting: Initial : Vicat Test (ASTM C 191-01a)		min.	113	-	121
Time of Setting: Final : Vicat Test (ASTM C 191-01a)		min.	225	-	-
Compressive Strength : (ASTM C 109/C109 M-99)					
Flow		(%)	117	-	-
Water used (W/C)		(%)	48	-	-
Compressive Strength : Mortar Cube 3 days		MPa	24.9	20.4	-
Compressive Strength : Mortar Cube 7 days		MPa	29.7	27.2	33.78
Compressive Strength : Mortar Cube 28 days		MPa	40.6	-	40.98
Chemical Composition of Fly ash					
Silicon dioxide	(SiO_2)	(%)	38.07	-	52.4
Aluminum oxide	(Al_2O_3)	(%)	22.89	-	23.4
Iron oxide	(Fe_2O_3)	(%)	12.12	-	4.7
Calcium oxide	(CaO)	(%)	18.40	-	13.4
Magnesium oxide	(MgO)	(%)	2.26	-	1.3
Sulfur Trioxide	(SO_3)	(%)	1.77	-	0.2
Loss on Ignition	(LOI)	(%)	0.03	-	0.3
Sodium oxide	(Na_2O)	(%)	1.09	-	3.6
Potassium oxide	(K_2O)	(%)	2.29	-	0.6
Free CaO		(%)	0.72	-	-
Moisture		(%)	0.03	-	-

Physical Properties of Fly ash			**Used by Author**	**Used by Ghezal, et al.**	**Used by Patel, R., et al.**
Blaine Fineness : Air Permeability Test (ASTM C 204-00)		cm^2/g	2,640	-	3,060
Passing 45 micron : (ASTM C430-96)		(%)	53.9	-	83.6
Specific Gravity : (ASTM C 188-95)		(%)	2.30	-	2.08
Soundness					
Normal Consistency : (ASTM C 187-98)		(%)	22.5	-	-
Autoclave Expansion : (ASTM C 151-98a)		(%)	-0.02	-	-
Strength Activity Index with Portland Cement : (ASTM C 311-98b)					
Water required in percent of control		(%)	98.3	-	99.2
Compressive Strength of control mix At 7 day		MPa	30.2	-	-
Compressive Strength of test mix At 7 day		MPa	24.3	-	-
Strength Activity Index At 7 days		(%)	80.5	-	94.5
Compressive Strength of control mix At 28 day		MPa	42.4	-	-
Compressive Strength of test mix At 28 day		MPa	32.9	-	-
Strength Activity Index At 28 days		(%)	77.6	-	106.9
Chemical Composition of Limestone Powder					
Silicon dioxide	(SiO_2)	(%)	< 0.01	-	7.2
Aluminum oxide	(Al_2O_3)	(%)	< 0.01	-	1.42
Iron oxide	(Fe_2O_3)	(%)	0.08	-	0.49
Calcium oxide	(CaO)	(%)	55.34	-	50.46
Magnesium oxide	(MgO)	(%)	0.53	-	0.53
Sulfur Trioxide	(SO_3)	(%)	-	-	-
Loss on Ignition	(LOI)	(%)	43.91	-	39.2
Sodium oxide	(Na_2O)	(%)	-	-	0.34
Potassium oxide	(K_2O)	(%)	-	-	-
Free CaO		(%)	-	-	-
Moisture		(%)	0.05	-	-
Physical Properties of Limestone Powder					
Blaine Fineness : Air Permeability Test (ASTM C 204-00)		cm^2/g	4,350	-	5,650
Passing 45 micron : (ASTM C430-96)		(%)	98.8	-	97.2
Specific Gravity : (ASTM C 188-95)		(%)	2.70	-	2.64
Normal Consistency : (ASTM C 187-98)		(%)	24.0	-	-
Water required in percent of control		(%)	97.50	-	-

Grading of coarse and fine aggregate prepared by Patel, R., et al.

Sieve size	Coarse aggregate (% passing)	Sieve size	Fine aggregate (% passing)
19 mm	0	4.75 mm	99.28
12.5 mm	94.6	2.36 mm	90.15
9.5 mm	74.5	1.18 mm	79.80
4.75 mm	4.3	600 micron	56.2
-	-	300 micron	20
-	-	150 micron	4.46

Table A-2 Chemical composition and physical properties of bottom ashes and expanded clay

Chemical compositions	Bottom Ash I	Bottom Ash II	Fine Expanded Clay
SiO_2 (%)	49.75	38.64	-
Al_2O_3 (%)	20.26	21.15	-
Fe_2O_3 (%)	6.26	11.96	-
CaO (%)	0.73	13.80	-
MgO (%)	0.84	2.75	-
SO_3 (%)	0.30	0.61	-
Na_2O (%)	<0.01	0.90	-
K_2O (%)	2.88	2.06	-
Free lime (%)	0.01	0.03	-
Loss on ignition (%)	17.83	7.24	-
Physical compositions			
Blaine fineness (cm^2/g)	-	-	-
Specific gravity (in ground form)	1.63	2.28	2.63

Table A-3 Coefficients of materials used

Materials	Water retainability coefficient of powder (β_p)	Reduction factor for water retainability coefficient of powder materials (ϕ_{rb})	Surface water retainability coefficients (β_s', β_g')	Angularity factor (ψ)	Lubrication Coefficient (L)	Filling Coefficient (F)	Water reducing efficiency (φ')	Effective contact area ratio of powder and aggregate (η_p, η_a)	Reduction factor (ϕ_{rn})
Powders									
- Cement	0.23	-	-	1.4	-	-	-	0.012	-
- Fly Ash	0.16	-	-	1.1	1.24	0.025	-	0.012	-
- Limestone Powder	0.21	-	-	1.4	1.05	0.003	-	0.012	-
Aggregates			-						
- Fine Aggregate	-	-	0.02982	1.2	-	-	-	1	-
- Coarse Aggregate	-	-	0.00391	1.4		-	-	1	-
Superplasticisers									
- Naphthalene-I	-	0.77	-	-	-	-	0.376	-	0.40
- Naphthalene-II	-	0.77	-	-	-	-	0.371	-	0.40
- Melamine	-	0.79	-	-	-	-	0.348	-	0.40
-Polycarboxylate	-	0.73	-	-	-	-	0.438	-	0.40

Table A-4 Gradations of normal sand and very-fine sand

Sieve No.	Sieve Size (mm.)	Normal Sand	Very-fine Sand
3/8”	9.5	100	100
#4	4.75	100	100
#8	2.36	93	100
#16	1.18	69	100
#30	0.6	47	85
#50	0.3	22	40
#100	0.15	0	10
Pan	0	0	0

Table A-5 Gradations of the combined mixtures of normal sand and very-fine sand at various replacement levels of very fine sand

Sieve No.	Sieve Size (mm.)	VFS-0 (Normal Sand)	VFS-100 (Very-fine Sand)	VFS-5	VFS-10	VFS-20	VFS-30	VFS-50
3/8”	9.5	100	100	100	100	100	100	100
#4	4.75	100	100	100	100	100	100	100
#8	2.36	93	100	93	93	94	95	96
#16	1.18	69	100	71	72	75	78	84
#30	0.6	47	85	48	50	54	58	66
#50	0.3	22	40	23	23	25	27	31
#100	0.15	0	10	1	1	2	3	5
Pan	0	0	0	0	0	0	0	0

Remark: VFS is very fine sand.

Table A-6 Gradation of coarse aggregates used in this study

Sieve Size (mm.)	12.5 – 4 mm (12/" - #4)	19.0 – 4.75 mm (3/4" - #4)	25 – 4 mm (1" - #4)
37.5	-	-	100
25.0	-	100	97
19.0	100	97	70
12.5	97	64	37
9.5	48	42	21
4.75	8	8	6
2.36	3	4	2
Pan	0	0	0

Table A-7 Properties of water reducing admixture and superplasticizers used in this study

Properties	Lignosulfonate (with Retarder)	Naphthalene–I	Naphthalene–II	Melamine	Polycarboxylate
ASTM C494 Type	D	F	F	F	F
Trade Name	Daratard 500	Mighty MX	Sikament FF	Sikament F6	ABVA 105
Specific Gravity	1.227	1.20	1.20	1.183	N/A
Solid content (%)	48.08	40.0	35.18	33.77	N/A
pH	7.20	9.0	9.57	9.27	N/A
Water Reducing Efficiency	0.247	0.376	0.371	0.348	0.438

Appendix B
Mix Proportions

Table B-1 Mix proportions to be used in model formulation and verification tests for predicting slump flow and 50-cm slump flow time.

Mix No.	Mix. Code	Cement (kg)	Fly Ash (kg.)	LSP (kg.)	Water (liter)	Gravel 3/4"-#4 (kg.)	Sand (kg.)	Type D (cc.)	Super-plasticizer (cc.)	Tested Slump Flow (cm)	Tested 50-cm Slump Flow Time (sec.)	Predicted Slump Flow (cm)	Predicted 50-cm Slump Flow Time (sec.)
Mix proportion prepared by the author													
1	γ1.4w/b0.25Dos0	594	-	-	149	890	890	-	0	20	-	20	-
2	γ1.4w/b0.25Dos0.5NI	594	-	-	149	890	890	-	2,970	20	-	20	-
3	γ1.4w/b0.25Dos0.5M	594	-	-	149	890	890	-	2,970	20	-	20	-
4	γ1.4w/b0.25Dos0.5NII	594	-	-	149	890	890	-	2,970	20	-	20	-
5	γ1.4w/b0.25Dos0.5P	594	-	-	149	890	890	-	2,970	20	-	20	-
6	γ1.4w/b0.25Dos1.0NI	594	-	-	149	890	890	-	5,940	20	-	20	-
7	γ1.4w/b0.25Dos1.0M	594	-	-	149	890	890	-	5,940	20	-	20	-
8	γ1.4w/b0.25Dos1.0NII	594	-	-	149	890	890	-	5,940	20	-	20	-
9	γ1.4w/b0.25Dos2.0M	594	-	-	149	890	890	-	11,880	29.5	-	25	-
10	γ1.4w/b0.25Dos2.0NII	594	-	-	149	890	890	-	11,880	28	-	27	-
11	γ1.8w/b0.25Dos0	764	-	-	191	760	760	-	0	20	-	20	-
12	γ1.8w/b0.25Dos0.5NI	764	-	-	191	760	760	-	3,820	20	-	24	-
13	γ1.8w/b0.25Dos0.5M	764	-	-	191	760	760	-	3,820	20	-	20	-
14	γ1.8w/b0.25Dos0.5NII	764	-	-	191	760	760	-	3,820	20	-	23	-
15	γ1.8w/b0.25Dos1.0NI	764	-	-	191	760	760	-	7,640	33	-	36	-
16	γ1.4w/b0.45Dos1.0NI	440	-	-	198	890	890	-	4,400	64	3	63	4
17	γ1.4w/b0.45Dos1.0NII	440	-	-	198	890	890	-	4,400	62.5	2	62	2
18	γ1.4w/b0.45Dos2.0NI	440	-	-	198	890	890	-	8,800	68.5	1	65	2
19	γ1.4w/b0.45Dos2.0M	440	-	-	198	890	890	-	8,800	64	2	62	2
20	γ1.4w/b0.45Dos2.0NII	440	-	-	198	890	890	-	8,800	70.5	1	67	2
21	γ1.4w/b0.45Dos2.0P	440	-	-	198	890	890	-	8,800	71.5	1	67	1
22	γ1.8w/b0.45Dos0	566	-	-	255	760	760	-	0	30	-	31	-
23	γ1.6w/b0.25Dos0	678	-	-	170	830	830	-	0	20	-	20	-
24	γ1.6w/b0.25Dos0.5NI	678	-	-	170	830	830	-	3,390	20	-	20	-
25	γ1.6w/b0.25Dos0.5M	678	-	-	170	830	830	-	3,390	20	-	20	-
26	γ1.6w/b0.25Dos0.5NII	678	-	-	170	830	830	-	3,390	20	-	20	-
27	γ1.6w/b0.25Dos1.0M	678	-	-	170	830	830	-	6,780	20	-	24	-
28	γ1.6w/b0.25Dos2.0M	678	-	-	170	830	830	-	13,560	31	-	33	-
29	γ1.6w/b0.45Dos0.5NI	502	-	-	226	830	830	-	2,510	44	-	47	-
30	γ1.6w/b0.45Dos1.0P	502	-	-	226	830	830	-	5,020	57	1	55	1
31	γ1.4w/b0.35Dos0	506	-	-	177	890	890	-	0	20	-	20	-
32	γ1.4w/b0.35Dos1.5M	506	-	-	177	890	890	-	7,590	68.5	4	64	3
33	γ1.4w/b0.35Dos1.5P	506	-	-	177	890	890	-	7,590	65	2	62	2.7
34	γ1.6w/b0.35Dos0	578	-	-	202	830	830	-	0	20	-	20	-
35	γ1.6w/b0.25Dos0.8NI	426	184	-	150	830	830	-	5,085	20	-	29	-
36	γ1.7w/b0.22Dos0.8NI	470	202	-	150	800	800	-	5,600	20	-	23	-
37	γ1.8w/b0.20Dos0.8NI	516	222	-	150	770	770	-	6,150	20	-	20	-
38	γ1.5w/b0.33Dos0.8NI	352	152	-	165	860	860	-	4,200	62	14	65	15
39	γ1.6w/b0.29Dos0.8NI	398	172	-	165	830	830	-	4,750	57	7	59	6
40	γ1.5w/b0.39Dos0.8NI	324	140	-	180	860	860	-	3,870	59	6	63	6
41	γ1.6w/b0.34Dos0.8NI	368	158	-	180	830	830	-	4,385	72.5	2	74	2
42	γ1.7w/b0.30Dos0.8NI	416	180	-	180	800	800	-	4,970	77	2	76	2
43	γ1.7w/b0.24Dos0.8NI	308	308	-	150	800	800	-	5,135	53.5	44	57	45
44	γ1.7w/b0.29Dos0.8NI	288	288	-	165	800	800	-	4,800	75.5	1	81	1
45	γ1.8w/b0.26Dos0.8NI	318	318	-	165	770	770	-	5,300	71	6	76	6
46	γ1.4w/b0.29Dos0.9NI	260	260	-	150	940	770	-	4,700	72	6	77	7
47	γ1.4w/b0.28Dos0.9NI	260	260	-	145	940	770	-	4,500	71.5	6	75	5
48	γ1.4w/b0.28Dos0.8NI	260	260	-	145	940	770	-	4,200	55	11	61	12
49	γ1.5w/b0.29Dos0.8NI	260	260	-	150	940	770	-	4,240	64.5	6	70	5
50	γ1.5w/b0.29Dos0.8NI	260	260	-	150	940	770	-	4,240	60.5	8	66	7
51	γ1.5w/b0.29Dos0.8NI	260	260	-	150	940	770	-	4,400	64.5	8	69	7
52	γ1.6w/b0.29Dos1.0NI	260	260	-	150	940	770	-	5,000	47.5	-	51	-
53	γ1.5w/b0.28Dos0.9NI	270	270	-	152	930	760	-	4,600	67.5	7	74	8
54	γ1.5w/b0.28Dos0.9NI	270	270	-	152	930	760	-	4,600	71.5	6	75	7
55	γ1.5w/b0.28Dos0.9NI	270	270	-	152	930	760	-	4,600	66	8	70	6
56	γ1.5w/b0.28Dos0.9NI	270	270	-	152	930	760	-	4,600	54.5	16	60	17
57	γ1.7w/b0.28Dos0.9NI	200	300	100	165	810	760	600	5,000	72.5	6	74	5
58	γ1.8w/b0.32Dos0	320	160	160	206	740	740	-	0	20	-	24	-
59	γ1.8w/b0.42Dos0	280	140	140	236	740	740	-	0	31.5	-	32	-
60	γ1.6w/b0.34Dos0	280	140	140	188	810	810	-	0	20	-	24	-
61	γ1.7w/b0.28Dos1.2NI	295	295	-	168	790	790	1,200	5,800	71.5	4	76	3
62	γ1.9w/b0.26Dos1.0NI	340	340	-	180	740	740	1,200	5,400	74	3	77	3
63	γ1.9w/b0.26Dos1.0NI	340	340	-	180	740	717	1,200	5,800	76	3	80	2
64	γ1.9w/b0.26Dos1.2NI	340	340	-	180	740	694	1,200	6,800	76.5	3	81	2
65	γ1.7w/b0.28Dos1.2NI	295	295	-	168	790	790	1,200	5,900	74.5	3	78	3
66	γ1.7w/b0.28Dos1.2NI	295	295	-	168	790	765	1,200	5,900	75.5	3	80	2
67	γ1.7w/b0.28Dos1.2NI	295	295	-	168	790	741	1,200	5,900	78	2	82	2

Mix No.	Mix. Code	Cement (kg)	Fly Ash (kg.)	LSP (kg.)	Water (liter)	Gravel 3/4"-#4 (kg.)	Sand (kg.)	Type D (cc.)	Super-plasticizer (cc.)	Tested Slump Flow (cm)	Tested 50-cm Slump Flow Time (sec.)	Predicted Slump Flow (cm)	Predicted 50-cm Slump Flow Time (sec.)
68	γ1.8w/b0.28Dos1.2NI	315	315	-	176	760	760	1,200	6,300	74.5	5	79	5
69	γ1.9w/b0.26Dos1.0NI	340	340	-	180	740	740	1,200	5,440	78.5	3	80	2
70	γ1.9w/b0.26Dos1.0NI	340	340	-	180	740	717	1,200	5,440	77	2	81	2
71	γ1.5w/b0.29Dos1.3NI	384	164	-	158	860	833	1,200	5,754	69.5	8	59	8
72	γ1.6w/b0.29Dos1.2NI	275	275	-	160	830	830	1,200	5,500	72.5	5	75	4
73	γ1.6w/b0.29Dos1.2NI	275	275	-	160	830	804	1,200	5,500	69	7	74	8
74	γ1.4w/b0.32Dos1.3NI	343	147	-	155	890	890	1,200	5,145	63.5	18	59	19
75	γ1.8w/b0.28Dos1.0NI	315	315	-	176	760	760	1,200	5,040	79.5	2	82	2
76	γ1.8w/b0.28Dos1.0NI	315	315	-	176	760	736	1,200	5,040	79.5	2	84	2
77	γ1.5w/b0.29Dos1.3NI	384	164	-	158	860	833	1,200	5,754	51.5	40	51	41
78	γ1.5w/b0.29Dos1.3NI	384	164	-	158	860	821	1,200	5,754	20	-	32	-
79	γ1.5w/b0.29Dos1.3NI	384	164	-	158	860	782	1,200	5,754	56.5	49	53	50
80	γ1.5w/b0.30Dos1.2NI	385	165	-	165	850	850	1,200	5,500	66	7	62	6
81	γ1.5w/b0.30Dos1.2NI	385	165	-	165	850	823	1,200	5,500	61.5	11	61	11
82	γ1.5w/b0.30Dos1.2NI	385	165	-	165	850	797	1,200	5,500	62.5	10	61	11
83	γ1.6w/b0.28Dos1.3NI	413	177	-	165	830	804	1,200	6,195	61	12	57	13
84	γ1.6w/b0.28Dos1.3NI	413	177	-	165	830	778	1,200	6,195	55.5	20	54	21
85	γ1.7w/b0.27Dos1.2NI	448	192	-	172	790	765	1,200	6,720	69	5	62	4
86	γ1.8w/b0.26Dos1.2NI	476	204	-	180	760	712	1,200	7,140	71	4	65	3
87	γ1.7w/b0.29Dos1.2NI	294	294	-	170	790	790	1,200	5,865	75.5	3	79	3
88	γ1.8w/b0.26Dos1.2NI	324	324	-	170	760	760	1,200	6,455	77.5	3	78	3
89	γ1.5w/b0.36Dos1.6NI	234	234	-	170	860	860	1,200	6,090	72.5	3	77	3
90	γ1.7w/b0.29Dos1.5NI	294	294	-	170	790	790	1,200	7,625	72.5	3	77	3
91	γ1.8w/b0.26Dos1.5NI	324	324	-	170	760	760	1,200	8,390	79.5	2	80	3
92	γ1.7w/b0.26Dos1.3NI	306	306	-	160	790	790	900	7,330	73.5	7	72	5
93	γ1.7w/b0.26Dos1.6NI	306	306	-	160	790	790	900	9,165	73.5	5	73	6

NI = Naphthalene I , NII = Naphthalene II , M = Melamine , P = Polycarboxylate

Table B-2 Mix proportions to be used in model formulation and verification tests for predicting bleeding and static segregation.

Mix. No.	Mix. Code	Cement (kg.)	Fly Ash (kg.)	Water (liter)	Sand (kg.)	Gravel 3/4"-#4 (kg.)	Type D (cc.)	Super-plasticizer (cc.)	Slump Flow (cm.)
Mix proportions prepared by the author									
1	γ1.4w/b0.25Dos1.0NI	594	-	149	890	890	-	5,940	20
2	γ1.4w/b0.25Dos1.0NII	594	-	149	890	890	-	5,940	20
3	γ1.4w/b0.25Dos2.0NII	594	-	149	890	890	-	11,880	28
4	γ1.8w/b0.25Dos0.5NI	764	-	191	760	760	-	3,820	20
5	γ1.8w/b0.25Dos0.5NII	764	-	191	760	760	-	3,820	20
6	γ1.8w/b0.25Dos1.0NI	764	-	191	760	760	-	7,640	33
7	γ1.4w/b0.45Dos1.0NI	440	-	198	890	890	-	4,400	64
8	γ1.4w/b0.45Dos1.0NII	440	-	198	890	890	-	4,400	62.5
9	γ1.4w/b0.45Dos2.0NI	440	-	198	890	890	-	8,800	68.5
10	γ1.4w/b0.45Dos2.0NII	440	-	198	890	890	-	8,800	70.5
11	γ1.4w/b0.45Dos2.0P	440	-	198	890	890	-	8,800	71.5
12	γ1.6w/b0.45Dos1.0P	502	-	226	830	830	-	5,020	57
13	γ1.4w/b0.29Dos0.9NI	260	260	150	770	940	-	4,700	72
14	γ1.4w/b0.28Dos0.9NI	260	260	145	770	940	-	4,500	71.5
15	γ1.4w/b0.28Dos0.8NI	260	260	145	770	940	-	4,200	55
16	γ1.6w/b0.29Dos1.0NI	260	260	150	770	940	-	5,000	47.5
17	γ1.8w/b0.28Dos1.2NI	315	315	176	760	760	1,200	6,300	74.5
18	γ1.6w/b0.29Dos1.2NI	275	275	160	830	830	1,200	5,500	72.5
19	γ1.6w/b0.29Dos1.2NI	275	275	160	804	830	1,200	5,500	69
20	γ1.8w/b0.28Dos1.0NI	315	315	176	760	760	1,200	5,040	79.5
21	γ1.8w/b0.28Dos1.0NI	315	315	176	736	760	1,200	5,040	79.5
22	γ1.6w/b0.28Dos1.3NI	413	177	165	804	830	1,200	6,195	61
23	γ1.6w/b0.28Dos1.3NI	413	177	165	778	830	1,200	6,195	55.5
24	γ1.8w/b0.26Dos1.2NI	476	204	180	712	760	1,200	7,140	71
25	γ1.8w/b0.26Dos1.2NI	324	324	170	760	760	1,200	6,455	77.5
26	γ1.8w/b0.26Dos1.5NI	324	324	170	760	760	1,200	8,390	79.5

Mix. No.	Mix. Code	Cement (kg.)	Fly Ash (kg.)	Water (liter)	Sand (kg.)	Gravel 3/4"-#4 (kg.)	Type D (cc.)	Super-plasticizer (cc.)	Slump Flow (cm.)
Mix proportions prepared by Thumasujarit (2006)									
27	F1-C1-B325	325	0	163	1,071	844	-	-	-
28	F1-C2-B319	287	32	159	1,071	844	-	-	-
29	F1-C3-B306	214	92	153	1,071	844	-	-	-
30	F1-C4-B294	147	147	147	1,071	844	-	-	-
31	F1-C5-B290	290	0	174	1,071	844	-	-	-
32	F1-C6-B284	256	28	171	1,071	844	-	-	-
33	F1-C7-B274	192	82	165	1,071	844	-	-	-
34	F1-C8-B264	132	132	159	1,071	844	-	-	-
35	F1-C9-B435	435	0	174	1,003	790	-	-	-
36	F1-C10-B424	382	42	170	1,003	790	-	-	-
37	F1-C11-B406	284	122	162	1,003	790	-	-	-
38	F1-C12-B388	194	194	155	1,003	790	-	-	-
39	F1-C13-B382	382	0	191	1,003	790	-	-	-
40	F1-C14-B373	336	37	187	1,003	790	-	-	-
41	F1-C15-B359	251	108	179	1,003	790	-	-	-
42	F1-C16-B344	172	172	172	1,003	790	-	-	-
43	F1-C17-B340	340	0	204	1,003	790	-	-	-
44	F1-C18-B333	300	33	200	1,003	790	-	-	-
45	F1-C19-B321	225	96	193	1,003	790	-	-	-
46	F1-C20-B310	155	155	186	1,003	790	-	-	-
47	F2-C22-B320	288	32	160	1,071	844	-	-	-
48	F2-C23-B308	216	92	154	1,071	844	-	-	-
49	F2-C24-B298	149	149	149	1,071	844	-	-	-
50	F2-C26-B286	257	29	171	1,071	844	-	-	-
51	F2-C27-B276	193	83	166	1,071	844	-	-	-
52	F2-C28-B268	134	134	161	1,071	844	-	-	-
53	F2-C30-B426	383	43	170	1,003	790	-	-	-
54	F2-C31-B409	286	123	164	1,003	790	-	-	-
55	F2-C32-B394	197	197	157	1,003	790	-	-	-
56	F2-C34-B374	337	37	187	1,003	790	-	-	-
57	F2-C35-B361	253	108	181	1,003	790	-	-	-
58	F2-C36-B350	175	175	175	1,003	790	-	-	-
59	F2-C38-B334	301	33	201	1,003	790	-	-	-
60	F2-C39-B324	227	97	194	1,003	790	-	-	-
61	F2-C40-B314	157	157	188	1,003	790	-	-	-

NI = Naphthalene I , NII = Naphthalene II , M = Melamine , P = Polycarboxylate

Table B-3 Mix proportions to be used in model formulation and verification tests for predicting passing ability through narrow openings

Mix. No.	Mix. Code	Cement (kg.)	Fly Ash (kg.)	Water (liter)	S_1 (FM.=3.24) (kg.)	S_2 (FM.=2.78) (kg.)	S_3 (FM.=2.89) (kg.)	Gravel (kg.)	Type D (cc.)	Superplas -ticizer (cc.)	Slump Flow (cm)	h (cm)
Mix proportions prepared by the author												
1	G-12.5mm(Round)-B570	345	230	170	-	820	-	820	1,200	5,250	71	52.2
2	G-12.5mm(Flaky)-B570	345	230	170	-	820	-	820	1,200	5,500	67.5	39
3	G-12.5mm(Elongated)-B570	345	230	170	-	820	-	820	1,200	5,250	69	6
4	G-12.5mm(Normal)-B570	345	230	170	-	820	-	820	1,200	5,500	70	51
5	G-12.5mm(Round)-B550	330	220	165	-	840	-	840	1,200	5,250	67	45
6	G-12.5mm(Flaky)-B550	330	220	165	-	840	-	840	1,200	5,500	65	6
7	G-12.5mm(Elongated)-B550	330	220	165	-	840	-	840	1,200	5,250	66.5	13.2
8	G-12.5mm(Normal)-B550	330	220	165	-	840	-	840	1,200	5,500	67	36
9	G-19mm(Round)-B560	335	225	170	-	830	-	830	1,200	4,750	70	49.8
10	G-19mm(Flaky)-B560	335	225	170	-	830	-	830	1,200	5,000	66.5	19.8
11	G-19mm(Normal)-B560	335	225	170	-	830	-	830	1,200	5,000	71.5	48
12	G-19mm(Round)-B540	325	215	165	-	850	-	850	1,200	5,000	65.5	43.2
13	G-19mm(Flaky)-B540	325	215	165	-	850	-	850	1,200	5,500	64.5	4.5
14	G-19mm(Normal)-B540	325	215	165	-	850	-	850	1,200	5,250	66.5	31.8
Mix proportions prepared by Tangtermsirikul, et al. (2002)												
15	G-25mm(Normal)-B562	281	281	166	954	-	-	648	-	4,569	65	47
16	G-25mm(Normal)-B562	281	281	166	922	-	-	680	-	4,569	62.5	50
17	G-25mm(Normal)-B564	282	282	165	875	-	-	729	-	4,585	64	39
18	G-25mm(Normal)-B568	284	284	164	716	-	-	891	-	4,156	62.5	6
19	G-25mm(Normal)-B490	245	245	147	958	-	-	706	-	6,175	62	19
20	G-25mm(Normal)-B436	218	218	149	1,022	-	-	754	-	5,317	58	5
21	G-19mm(Normal)-B554	277	277	182	-	779	-	794	-	5,855	64	52
22	G-19mm(Normal)-B514	257	257	180	-	880	-	734	-	5,641	62.5	51
23	G-19mm(Normal)-B554	277	277	182	-	904	-	667	-	11,035	65	52
24	G-19mm(Normal)-B544	272	272	175	-	872	-	727	-	8,403	62.5	52
25	G-19mm(Normal)-B436	218	218	149	-	1,022	-	754	-	5,317	53	3
26	G-12.5mm(Normal)-B466	233	233	154	-	-	1,206	527	-	6,820	62	54
27	G-12.5mm(Normal)-B533	267	267	171	-	-	1,132	494	-	6,933	67	55
28	G-12.5mm(Normal)-B494	247	247	148	-	-	991	731	-	7,631	62	42
29	G-12.5mm(Normal)-B558	279	279	151	-	-	945	697	-	7,712	68	55
30	G-12.5mm(Normal)-B603	302	302	157	-	-	788	803	-	5,883	67	55
31	G-12.5mm(Normal)-B559	280	280	151	-	-	733	913	-	7,272	68	13
32	G-12.5mm(Normal)-B595	298	298	155	-	-	716	891	-	5,805	66	14
33	G-12.5mm(Normal)-B618	309	309	161	-	-	698	869	-	9,546	66	55
34	G-12.5mm(Normal)-B638	319	319	153	-	-	465	1,106	-	9,337	63	6
35	G-19mm(Normal)-B470	235	235	169	-	-	1,178	514	-	6,496	63	52.8
36	G-19mm(Normal)-B602	301	301	187	-	-	1,048	458	-	6,852	67	52.2
37	G-19mm(Normal)-B460	230	230	147	-	-	1,014	748	-	5,236	55	9
38	G-19mm(Normal)-B506	253	253	162	-	-	961	709	-	6,993	63	51
39	G-19mm(Normal)-B536	268	268	172	-	-	930	686	-	5,229	65	50
40	G-19mm(Normal)-B512	256	256	159	-	-	835	851	-	6,244	65	9
41	G-19mm(Normal)-B538	269	269	161	-	-	815	830	-	6,561	63	34.2
42	G-19mm(Normal)-B624	312	312	168	-	-	762	776	-	7,102	66	52.8
43	G-19mm(Normal)-B612	306	306	153	-	-	710	884	-	5,971	66	15
44	G-19mm(Normal)-B700	350	350	168	-	-	656	817	-	8,537	66	13
45	G-25mm(Normal)-B473	237	237	166	-	-	1,178	514	-	5,384	55	37.8
46	G-25mm(Normal)-B515	258	258	155	-	-	1,169	510	-	7,955	59	51
47	G-25mm(Normal)-B508	254	254	157	-	-	968	714	-	7,021	64	9
48	G-25mm(Normal)-B573	287	287	178	-	-	899	663	-	7,454	69	52.2
49	G-25mm(Normal)-B613	307	307	178	-	-	755	770	-	9,469	73	4
50	G-25mm(Normal)-B684	342	342	150	-	-	755	770	-	6,673	64	20
51	G-25mm(Normal)-B701	351	351	154	-	-	742	756	-	5,699	62	40.2
52	G-25mm(Normal)-B652	326	326	163	-	-	680	846	-	6,891	72	4
53	G-25mm(Normal)-B773	387	387	162	-	-	626	780	-	6,285	58	25

Table B-4 Mix proportions to be used in the application of the proposed test method for water retainability of fine porous aggregate.

Mix. No.	Mix. Code	Cement (kg.)	Fly Ash (kg.)	Water (liter)	Sand (kg.)	Bottom Ash (kg.)	Expanded Clay (kg.)	Gravel 3/4"-#4 (kg.)	Type D (cc.)	Superplas-ticizer (cc.)	WR Test Method
1	γ1.2w/b0.55	210	90	166	810	0	-	1,155	630	-	ASTMC 128
2	γ1.2w/b0.55	210	90	166	810	0	-	1,155	630	-	ASTMC 128
3	γ1.2w/b0.55BAI10	210	90	166	730	50	-	1,155	630	-	ASTMC 128
4	γ1.2w/b0.55BAI10	210	90	166	730	50	-	1,155	630	-	New Method
5	γ1.2w/b0.55BAI20	210	90	166	650	100	-	1,155	630	-	ASTMC 128
6	γ1.2w/b0.55BAI20	210	90	166	650	100	-	1,155	630	-	New Method
7	γ1.2w/b0.61	210	90	183	795	0	-	1,130	630	-	ASTMC 128
8	γ1.2w/b0.61	210	90	183	795	0	-	1,130	630	-	ASTMC 128
9	γ1.2w/b0.61BAII10	210	90	183	715	65	-	1,130	630	-	ASTMC 128
10	γ1.2w/b0.61BAII10	210	90	183	715	65	-	1,130	630	-	New Method
11	γ1.2w/b0.61BAII20	210	90	183	635	135	-	1,130	630	-	ASTMC 128
12	γ1.2w/b0.61BAII20	210	90	183	635	135	-	1,130	630	-	New Method
13	γ1.3w/b0.4	280	120	160	755	0	-	1,130	-	4,000	ASTMC 128
14	γ1.3w/b0.4BAI10	280	120	160	680	45	-	1,130	-	4,000	ASTMC 128
15	γ1.3w/b0.4BAI10	280	120	160	680	45	-	1,130	-	4,000	New Method
16	γ1.3w/b0.4BAI20	280	120	160	605	90	-	1,130	-	4,000	ASTMC 128
17	γ1.3w/b0.4BAI20	280	120	160	605	90	-	1,130	-	4,000	New Method
18	γ1.3w/b0.4	280	120	160	755	0	-	1,130	-	4,000	ASTMC 128
19	γ1.3w/b0.4BAII10	280	120	160	680	65	-	1,130	-	4,000	ASTMC 128
20	γ1.3w/b0.4BAII10	280	120	160	680	65	-	1,130	-	4,000	New Method
21	γ1.3w/b0.4BAII20	280	120	160	605	125	-	1,130	-	4,000	ASTMC 128
22	γ1.3w/b0.4BAII20	280	120	160	605	125	-	1,130	-	4,000	New Method
23	γ1.5w/b0.29	384	164	158	880	0	-	875	-	6,300	ASTMC 128
24	γ1.5w/b0.29BAI10	384	164	158	790	55	-	875	-	6,300	ASTMC 128
25	γ1.5w/b0.29BAI10	384	164	158	790	55	-	875	-	6,300	New Method
26	γ1.5w/b0.29BAI20	384	164	158	700	105	-	875	-	6,300	ASTMC 128
27	γ1.5w/b0.29BAI20	384	164	158	700	105	-	875	-	6,300	New Method
28	γ1.5w/b0.29	384	164	158	880	0	-	875	-	6,300	ASTMC 128
29	γ1.5w/b0.29BAII10	384	164	158	790	75	-	875	-	6,300	ASTMC 128
30	γ1.5w/b0.29BAII10	384	164	158	790	75	-	875	-	6,300	New Method
31	γ1.5w/b0.29BAII20	384	164	158	700	150	-	875	-	6,300	ASTMC 128
32	γ1.5w/b0.29BAII20	384	164	158	700	150	-	875	-	6,300	New Method
33	γ1.7w/b0.27	448	192	172	810	0	-	815	-	7,300	ASTMC 128
34	γ1.7w/b0.27BAI10	448	192	172	730	50	-	815	-	7,300	ASTMC 128
35	γ1.7w/b0.27BAI10	448	192	172	730	50	-	815	-	7,300	New Method
36	γ1.7w/b0.27BAI20	448	192	172	650	100	-	815	-	7,300	ASTMC 128
37	γ1.7w/b0.27BAI20	448	192	172	650	100	-	815	-	7,300	New Method
38	γ1.7w/b0.27	448	192	172	810	0	-	815	-	7,300	ASTMC 128
39	γ1.7w/b0.27BAII10	448	192	172	730	70	-	815	-	7,300	ASTMC 128
40	γ1.7w/b0.27BAII10	448	192	172	730	70	-	815	-	7,300	New Method
41	γ1.7w/b0.27BAII20	448	192	172	650	135	-	815	-	7,300	ASTMC 128
42	γ1.7w/b0.27BAII20	448	192	172	650	135	-	815	-	7,300	New Method
43	γ1.5w/b0.29EC10	384	164	158	790	0	35	875	1,200	5,754	New Method
44	γ1.5w/b0.29EC20	384	164	158	700	0	70	875	1,200	5,754	New Method
45	γ1.7w/b0.27EC10	448	192	172	730	0	35	815	1,200	6,720	New Method
46	γ1.7w/b0.27EC20	448	192	172	650	0	65	815	1,200	6,720	New Method

BAI = Bottom Ash (Saraburi) , BAII = Bottom Ash (Mae Moh) , EC = Fine Expanded Clay

Table B-5 Mix proportions of SCC mixed with various percentages of bottom ash as partial replacement of fine aggregate.

Mix. No.	Mix. Code	Cement (kg.)	Fly Ash (kg.)	Water (liter)	Natural Sand (kg.)	Fine Sand (kg.)	Bottom Ash (kg.)	Gravel 3/4"-#4 (kg.)	Type D (cc.)	Superplasticizer (cc.)
1	SCC-BA 0% (Control)	385	165	170	765	85	-	850	1,200	5,800
2	SCC-BA 10%	385	165	170	765	-	58	850	1,200	5,800
3	SCC-BA 20%	385	165	170	680	-	117	850	1,200	5,800
4	SCC-BA 30%	385	165	170	595	-	175	850	1,200	5,800

Table B-6 Mix proportions of SCC mixed with various percentages of very-fine sand as partial replacement of fine aggregate.

Mix. No.	Mix. Code	Cement (kg.)	Fly Ash (kg.)	Water (kg.)	Normal Sand (kg.)	Very Fine Sand (kg.)	Gravel 3/4"-#4 (kg.)	Superplasticizer (cc.)
1	SCC-VFS 0%-B520 (Control)	260	260	150	770	0	940	4,240
2	SCC-VFS 10%-B520	260	260	150	693	77	940	4,240
3	SCC-VFS 20%-B520	260	260	150	616	154	940	4,240
4	SCC-VFS 30%-B520	260	260	150	539	231	940	4,240
5	SCC-VFS 0%-B540 (Control)	270	270	152	760	0	930	4,600
6	SCC-VFS 10%-B540	270	270	152	684	76	930	4,600
7	SCC-VFS 20%-B540	270	270	152	608	152	930	4,600
8	SCC-VFS 30%-B540	270	270	152	532	228	930	4,600

Table B-7 Mix proportion prepared by other researchers to be used in verification tests for predicting slump flow and 50-cm slump flow time.

Mix. No.	Mix. Code	Cement (kg.)	Fly Ash (kg.)	LSP (kg.)	Silica Fume (kg.)	Slag (kg.)	Water (liter)	Gravel 3/4"-#4 (kg.)	Sand (kg.)	Super-plasticizer (cc.)	Tested Slump Flow (cm)	Tested 50-cm Slump Flow Time (sec.)	Predicted Slump Flow (cm)	Predicted 50-cm Slump Flow Time (sec.)
Mix proportion prepared by Bui, V.K. et. al.														
1	γ1.6w/b0.39Dos0.3	349	163	-	-	-	199	853	780	1,367	58.6	2	60.4	1
2	γ1.6w/b0.39Dos0.3	349	163	-	-	-	199	853	780	1,625	66.7	2	69.7	1
3	γ1.6w/b0.39Dos0.5	349	162	-	-	-	199	852	779	2,333	73	1	76.7	1
4	γ1.6w/b0.39Dos0.5	349	162	-	-	-	199	852	779	2,608	76.2	1	77.6	1
5	γ1.5w/b0.38Dos0.4	350	133	-	-	-	183	884	816	1,900	58	5	61.3	6
6	γ1.5w/b0.38Dos0.4	350	133	-	-	-	183	884	816	2,033	63.5	4	65.8	5
7	γ1.5w/b0.38Dos0.5	350	133	-	-	-	184	884	816	2,392	65.7	4	69.3	5
8	γ1.5w/b0.38Dos0.6	350	133	-	-	-	184	884	816	2,683	70.5	3	72.2	3
9	γ1.5w/b0.38Dos0.6	350	133	-	-	-	184	883	815	3,017	72.4	3	75.2	2
10	γ1.5w/b0.39Dos0.4	350	111	-	-	-	179	901	832	1,875	54.8	4	58.4	5
11	γ1.5w/b0.39Dos0.4	350	111	-	-	-	179	901	832	1,958	60.6	4	64.1	5
12	γ1.5w/b0.39Dos0.5	350	111	-	-	-	180	901	831	2,317	64.8	4	66.6	5
13	γ1.5w/b0.39Dos0.6	350	111	-	-	-	180	901	831	2,575	68.6	3	72.2	2
14	γ1.5w/b0.39Dos0.6	350	111	-	-	-	180	900	831	2,892	71.1	3	72.1	2
15	γ1.6w/b0.38Dos0.3	250	257	-	-	-	192	854	788	1,733	59.1	4	60.1	5
16	γ1.6w/b0.36Dos0.4	427	115	-	-	-	195	844	779	2,300	69.9	3	72.3	3
17	γ1.4w/b0.39Dos0.5	350	90	-	-	-	171	924	853	2,092	64.3	3	63.2	3
18	γ1.4w/b0.39Dos0.5	350	90	-	-	-	171	923	852	2,208	68.6	2	66.7	2
19	γ1.4w/b0.39Dos0.6	350	90	-	-	-	171	923	852	2,717	68.6	1	68.7	2
20	γ1.5w/b0.35Dos0.7	327	173	-	-	-	175	803	902	3,433	66	3	68.2	3
21	γ1.5w/b0.35Dos0.7	327	173	-	-	-	175	803	902	3,683	67.3	2	71.0	3
22	γ1.4w/b0.39Dos0.6	350	88	-	-	-	171	714	1,070	2,650	66	4	62.5	4
23	γ1.4w/b0.39Dos0.7	350	88	-	-	-	171	713	1,070	2,900	69.2	3	69.9	3
24	γ1.4w/b0.39Dos0.8	350	88	-	-	-	171	713	1,069	3,317	71.1	3	70.2	3
25	γ1.6w/b0.39Dos0.3	350	163	-	-	-	200	654	980	1,742	55	3	57.5	2
26	γ1.6w/b0.39Dos0.4	350	163	-	-	-	200	653	980	1,917	60.6	2	62.9	2
27	γ1.6w/b0.39Dos0.4	350	163	-	-	-	200	653	980	2,092	66.7	2	69.4	2
28	γ1.6w/b0.39Dos0.4	350	163	-	-	-	200	653	980	2,275	68.3	2	70.0	2
29	γ1.6w/b0.39Dos0.5	350	163	-	-	-	200	653	979	2,550	70.8	2	72.4	2
30	γ1.6w/b0.35Dos0.3	380	145	-	-	-	184	854	788	1,833	70.6	7	71.8	8
31	γ1.6w/b0.33Dos0.4	350	186	-	-	-	178	851	786	2,000	73.1	6	76.5	6
32	γ1.6w/b0.35Dos0.5	380	145	-	-	-	184	659	988	2,475	71.3	6	74.5	7
33	γ1.7w/b0.35Dos0.3	380	192	-	-	-	200	621	931	1,892	72.8	4	74.8	4
34	γ1.6w/b0.37Dos0.5	346	171	-	-	-	193	836	772	2,417	81.3	1	83.9	1
35	γ1.7w/b0.36Dos0.5	343	186	-	-	-	192	830	766	2,733	73.7	1	75.5	1
36	γ1.6w/b0.38Dos0.4	516	0	-	-	-	197	859	793	1,908	66	3	66.9	3
37	γ1.6w/b0.38Dos0.4	516	0	-	-	-	197	859	792	2,025	74.3	2	73.6	1
Mix proportion prepared by Nehdi M., et al.														
38	γ1.6w/b0.33Dos0.4	187	107	-	-	239	176	805	826	2,275	67	-	66.5	-
39	γ1.6w/b0.39Dos0.6	300	200	-	-		195	819	778	2,899	63	-	66.7	-
40	γ1.6w/b0.37Dos0.4	330	0	-	-	200	195	750	870	1,987	70	-	69.2	-
Mix proportion prepared by Ghezal, et al.														
41	γ1.4w/b0.55Dos0.4	325	-	60	-	-	212	850	899	1,656	67	5	63.2	6
42	γ1.4w/b0.55Dos0.4	325	-	60	-	-	212	850	899	1,656	66.5	4	62.9	5
43	γ1.6w/b0.55Dos0.4	325	-	120	-	-	245	850	755	1,914	75.5	4	78.5	5
44	γ1.1w/b0.55Dos0.4	249	-	60	-	-	170	850	1,079	1,329	20.2	-	21.4	-
45	γ1.7w/b0.72Dos0.4	325	-	60	-	-	277	850	722	1,656	88.5	1	86.9	-
46	γ1.5w/b0.45Dos0.3	370	-	96	-	-	210	850	833	1,165	24	-	26.5	-
47	γ1.7w/b0.55Dos0.4	400	-	60	-	-	253	850	718	1,978	78.5	2	79.8	2
48	γ1w/b0.45Dos0.3	280	-	24	-	-	137	850	1,174	760	20	-	23.0	-
49	γ1.4w/b0.55Dos0.4	325	-	60	-	-	212	850	899	1,656	62.5	4	60.3	4
50	γ1w/b0.45Dos0.6	280	-	24	-	-	137	850	1,172	1,885	20.2	-	22.5	-
51	γ1.6w/b0.65Dos0.6	370	-	24	-	-	256	850	770	2,443	86	1	84.2	1
52	γ1.2w/b0.55Dos0.4	325	-	0	-	-	179	850	1,042	1,398	23	-	26.7	-
53	γ1.5w/b0.65Dos0.3	280	-	96	-	-	244	850	820	940	66	2	65.4	1
54	γ1.4w/b0.55Dos0.8	325	-	60	-	-	212	850	896	2,888	68	3	65.3	3
55	γ1.4w/b0.55Dos0.4	325	-	60	-	-	212	850	898	1,656	68.5	4	69.1	5
56	γ1.4w/b0.55Dos0.1	325	-	60	-	-	212	850	900	462	23	-	25.0	-
57	γ1.5w/b0.45Dos0.6	370	-	96	-	-	210	850	830	2,889	65.5	4	69.1	5
58	γ1.4w/b0.55Dos0.4	325	-	60	-	-	212	850	898	1,656	66	5	62.6	6
59	γ1.1w/b0.38Dos0.4	325	-	60	-	-	146	850	1,075	1,656	20.2	-	22.2	-
60	γ1.5w/b0.65Dos0.6	280	-	96	-	-	244	850	817	2,331	79.5	1	77.2	1
61	γ1.6w/b0.65Dos0.3	370	-	24	-	-	256	850	772	985	70.5	2	70.7	3
62	γ1.6w/b0.35Dos0.7	307	18	-	-	235	196	898	700	3,700	65	-	67.9	-
63	γ1.6w/b0.35Dos0.7	417	118	-	18	-	194	898	700	4,100	65	-	66.2	-
64	γ1.3w/b0.38Dos1.2	327	85	-	13	-	162	1,102	730	5,000	65	-	62.4	-
65	γ1.2w/b0.5Dos0.6	262	68	-	10	-	170	906	960	2,100	44	-	45.0	-
Mix proportion prepared by Patel, R., et al.														
66	γ1.3w/b0.39Dos0.4	220	180	-	-	-	156	900	916	1,400	59	-	58.6	-
67	γ1.3w/b0.39Dos0.4	220	180	-	-	-	156	900	916	1,400	59	-	58.6	-
68	γ1.3w/b0.39Dos0.4	160	240	-	-	-	156	900	886	1,400	63	-	66.4	-
69	γ1.1w/b0.39Dos0.4	193	158	-	-	-	137	900	1,024	1,229	41	-	40.4	-
70	γ1.4w/b0.45Dos0.4	220	180	-	-	-	180	900	850	1,400	76	-	76.2	-
71	γ1.4w/b0.36Dos0.2	198	232	-	-	-	153	900	874	860	54	-	57.4	-
72	γ1.5w/b0.39Dos0.4	248	203	-	-	-	176	900	808	1,579	68	-	71.4	-
73	γ1.1w/b0.35Dos0.2	237	133	-	-	-	131	900	1,034	740	33	-	29.3	-
74	γ1.3w/b0.39Dos0.4	220	180	-	-	-	156	900	916	1,400	57	-	57.3	-
75	γ1.2w/b0.42Dos0.5	237	133	-	-	-	157	900	960	1,850	65	-	65.8	-

Mix No.	Mix. Code	Cement (kg.)	Fly Ash (kg.)	LSP (kg)	Silica Fume (kg.)	Slag (kg.)	Water (liter)	Gravel 3/4"-#4 (kg.)	Sand (kg.)	Super-plasticizer (cc.)	Tested Slump Flow (cm)	Tested 50-cm Slump Flow Time (sec.)	Predicted Slump Flow (cm)	Predicted 50-cm Slump Flow Time (sec.)
76	γ1.4w/b0.43Dos0.5	275	155	-	-	-	183	900	827	2,150	81	-	81.9	-
77	γ1.3w/b0.39Dos0.4	280	120	-	-	-	156	900	946	1,400	51	-	48.0	-
78	γ1.3w/b0.42Dos0.2	170	200	-	-	-	157	900	830	740	60	-	60.5	-
79	γ1.3w/b0.39Dos0.6	220	180	-	-	-	156	900	916	2,400	77	-	73.5	-
80	γ1.3w/b0.39Dos0.4	220	180	-	-	-	156	900	916	1,400	60	-	59.3	-
81	γ1.3w/b0.39Dos0.1	220	180	-	-	-	156	900	916	400	38	-	41.6	-
82	γ1.4w/b0.36Dos0.5	198	232	-	-	-	153	900	872	2,150	71	-	72.7	-
83	γ1.3w/b0.39Dos0.4	220	180	-	-	-	156	900	916	1,400	58	-	58.0	-
84	γ1.2w/b0.33Dos0.4	220	180	-	-	-	132	900	982	1,400	35	-	35.5	-
85	γ1.3w/b0.42Dos0.5	170	200	-	-	-	157	900	928	1,850	76	-	73.5	-
86	γ1.4w/b0.43Dos0.2	275	155	-	-	-	183	900	830	860	48	-	51.3	-